DETERMINING A ROLE FOR THE CALCIUM-SENSING RECEPTOR (CaR) IN NEURONAL DEVELOPMENT

A thesis submitted to Cardiff University for the degree of PhD

2006

Thomas N. Vizard

Cardiff School of Biosciences
Cardiff University

ProQuest LLC
789 East Eisenhower Parkway
P.O. Box 1346
Ann Arbor, MI 48106-1346

DECLARATION

This work has not been accepted in substance for any degree and is not concurrently submitted in candidature for any degree.

Signed....Thomas N. Hazard..... (candidate) Date..14-12-06.....

STATEMENT 1

This thesis is being submitted in partial fulfilment of the requirements for the degree of.....PhD.....

Signed.....Thomas N. Hazard..... (candidate) Date..14-12-06.....

STATEMENT 2

This thesis is the result of my own independent work/investigation, except where otherwise stated. Other sources are acknowledged by footnotes giving explicit references.

Signed...Thomas N. Hazard..... (candidate) Date..14-12-06.....

STATEMENT 3

I hereby give consent for my thesis, if accepted, to be available for photocopying and for inter-library loan, and for the title and summary to be made available to outside organisations.

Signed....Thomas N. Hazard..... (candidate) Date..14-12-06.....

STATEMENT 4

I hereby give consent for my thesis, if accepted, to be available for photocopying and for interlibrary loans **after expiry of a bar on access** approved by the Graduate Development Committee.

Signed....Thomas N. Hazard..... (candidate) Date..14-12-06.....

ABSTRACT

The calcium-sensing receptor (CaR) is expressed in neurons of the adult central and peripheral nervous systems (PNS). There are currently no data describing the expression or function of the CaR during neuronal development. CaR mRNA expression was detected in sympathetic and sensory mouse ganglia at a number of embryonic (E) and postnatal (P) ages where, in superior cervical ganglia (SCG), CaR mRNA expression peaked at E18. At this age CaR protein was localised to the cell soma of dissociated neurons and throughout the neurite field.

When compared to neurons grown in low (0.7mM) extracellular Ca^{2+} concentration ($[Ca^{2+}]_o$), high (2.3mM) $[Ca^{2+}]_o$ increased SCG neurite outgrowth within a specific developmental window, E18-P0, correlating with a time when these neurons are exposed to a systemic $[Ca^{2+}]_o$ of 1.7mM *in vivo*. SCG neurite outgrowth within this window was susceptible to pharmacological modulation of the CaR by calcimimetic and calcilytic compounds, increasing and decreasing neurite growth, respectively. Expression of a dominant negative CaR (R185Q) reduced outgrowth of E18 neurite arbors, whereas overexpression of a wild-type CaR re-introduced $[Ca^{2+}]_o$ sensitivity of neurons outside the developmental window. Consistent with these data, *Car*$^{-/-}$ SCG neurons displayed impaired neurite arborisation *in vitro* and sympathetic target innervation *in vivo* when compared to *Car*$^{+/-}$ and *Car*$^{+/+}$ neurons. This role for the CaR is not limited to the PNS. Overexpression of the dominant negative CaR in P4 hippocampus reduced neurite outgrowth of CA2 and CA3 pyramidal neurons.

Preliminary data also suggest a role for the CaR in neuronal survival, where increasing $[Ca^{2+}]_o$ from 0.7 to 2.3mM increased E18 SCG survival in a dose-dependent manner. Further, high $[Ca^{2+}]_o$ enhances NGF-dependent survival, an effect that can be reduced using the calcilytic compound. These data are the first to show that $[Ca^{2+}]_o$ modulates neurite growth and neuronal survival during development and that these effects of $[Ca^{2+}]_o$ are mediated though the CaR.

CONTENTS

LIST OF FIGURES

LIST OF TABLES

ACKNOWLEDGMENTS

I would like to thank Daniela Riccardi for her supervision throughout the last 3 years and for her committent to members of her group.

I must sincerely thank Alun Davies for welcoming me in his laboratory for the last 2 years and for his supervision throughout this period.

I have to express my enormous gratitude and thanks to Gerard O' Keeffe for his input throughout this project and for the drinks after work.

Thanks also to Humberto Gutierrez for his work on the calcium-sensing receptor in the hippocampus, Claudine Kos for the knock out mice, Ed Nemeth and NPS Pharmaceuticals for the NPS compounds, Geoff Lloyd and the Biochemisty lab at the University Hospital for use of the radiometer 125 and Stephen Brazier for his advice on site-directed mutagenesis.

Thanks to my friends in the lab, especially Ger, Katja, Melita and David for their support and all the guys in both labs who have made it fun.

I must express a special thanks to Alex for her unconditional support over the last 3 years and for understanding and to Dad, Kate and Jotham for their continual encouragement.

DEDICATION

For my parents.

ABBREVIATIONS

ADH	Autosomal dominant hypercalcaemia
Akt	Protein kinase B
AMPA	α-amino-3-hydoxy-5-methyl-4-isoxazolepropioic acid
BDNF	Brain-derived neurotrophic factor
BMP	Bone morphogenic protein
Bp	Base pair
BSA	Bovine serum albumin
Ca^{2+}	Calcium ion
Ca^{2+}_i	Intracellular calcium ion
Ca^{2+}_o	Extracellular calcium ion
$[Ca^{2+}]_o$	Extracellular ionised calcium concentration
CA1	Cornu ammonis field 1
CAKC	Ca^{2+}-activated potassium channel
cAMP	Cyclic adenosine monophosphate
CaR	Calcium sensing receptor
cDNA	Complementary DNA
CNS	Central nervous system
CNTF	Ciliary neurotrophic factor
CREB	cAMP responsive element-binding protein
Ct	Threshold cycle
CT	Calcitonin
CT-1	Cardiotrophin-1
DAG	Diacylglycerol
DMSO	Dimethylsulphoxide

DN CaR	Dominant negative calcium sensing receptor
DRG	Dorsal root ganglion
E18	Embryonic day 18
EC_{50}	Effective concentration
ECD	Extracellular domain
EGTA	Ethylene glycol tetraacetic acid
ERK1/2	Extracellular signal-regulated kinase 1/2
$^{exon5(-)}CaR$	Exon 6-less calcium sensing receptor
FAM	Carboxyfluorscein
FHH	Familial hypocalciuric hypercalcaemia
GABA	γ-aminobutyric acid
$GABA_B$-R1	Type B γ-aminobutyric acid receptor 1
GAPDH	Glyceraldehyde 3-phosphate dehydrogenase
GPCR	G protein coupled receptor
HEK-293	Human embryonic kidney-293
HET	Heterozygous
HEX	6-carboxy-2',4,7,7'-tetrachlorofluorscein
HGF	Hepatocyte growth factor
IC_{50}	Half-maximal inhibition
IL-6	Interleukin-6
IP_3	Inositol-1,4,5-triphosphate
JNK	c-jun N-terminal kinase
KO	Knock out
Mg^{2+}_o	Extracellular magnesium ion
mRNA	Messenger RNA

MSP	Macrophage-stimulating protein
NCC	Non-selective cation channel
NF-κB	Nuclear factor-κB
NGF	Nerve growth factor
NT-3 (4/5)	Neurotrophin-3 (4/5)
NTC	No template control
NSHPT	Neonatal severe hyperparathyroidism
OSM	Oncostatin-M
LIF	Leukaumia-inhibitory factor
LTP	Long-term potentiation
mGluR	Metabotropic glutamate receptor
MSP	Macrophage-stimulating protein
NMDA	N-methyl-D-aspartate
PI_3K	Phophatidylinositol-3-kinase
PBS	Phosphate buffered saline
PCR	Polymerase chain reaction
PKC	Protein kinase C
PLC	Phospholipase C
PLD	Phospholipase D
PNS	Peripheral nervous system
PTH	Parathyroid hormone
PTHrP	Parathyroid hormone-related peptide
P1	Postnatal day 1
$p75^{NTR}$	p75 neurotrophin receptor
RT-PCR	Reverse transcriptase polymerase chain reaction

SCG	Superior cervical ganglion
SDM	Site directed mutagenesis
SFO	Subfornical organ
TH	Tyrosine hydroxylase
TNF	Tumour necrosis factor
Trk	Tropomycin-related kinase
WT	Wild type
WT CaR	Wild type calcium sensing receptor

CHAPTER 1

INTRODUCTION

1.1 Organisation of the Peripheral Nervous System (PNS)

The peripheral nervous system (PNS) consists of neurons and nerves that reside, or extend outside the central nervous system (CNS) (the brain and spinal cord) and comprises two divisions; the somatic and autonomic systems.

1.1.1 The Somatic PNS

The somatic division consists of the motor and sensory axons of the spinal and cranial nerves. The cell bodies of somatic motoneurons lie within the spinal cord and brainstem and their axons innervate skeletal muscle, controlling voluntary muscle contraction. Somatic sensory axons convey sensory information from skin, muscles, joints and viscera in the periphery and convey this to the CNS. The cell bodies of these sensory fibers are found within the dorsal root ganglia (DRG) and cranial sensory ganglia.

1.1.2 The Autonomic PNS

The autonomic division of the PNS consists of three subdivisions; the sympathetic, parasympathetic and enteric nervous systems. The cell bodies of preganglionic neurons of the autonomic nervous system reside within the brainstem and spinal cord and their axons synapse with postganglionic neurons in sympathetic and parasympathetic ganglia. The sympathetic ganglia are further divided into the paravertebral and prevertebral ganglia. The paravertebral ganglia comprise the ganglia of the sympathetic chain which innervate targets in the head and neck, heart, lungs, other thoracic viscera and blood vessels in the rest of the body (Fig. 1). Extensive work has been carried throughout this study on the superior cervical ganglion (SCG) which is found at the most rostral aspect lies of the sympathetic chain and innervates salivary, lacrimal and sweat glands, as well as blood vessels and hair follicles of the head and neck. Prevertebral sympathetic ganglia innervate

organs of the digestive and urogenital tracts. The parasympathetic ganglia are found close to their target organs and are supplied by 3 of the 12 cranial nerves and preganglionic fibers from sacral nerves S2, S3 and S4.

The enteric nervous system is largely autonomous from the rest of the nervous system, although its function is regulated by innervation from the sympathetic and parasympathetic nervous systems.

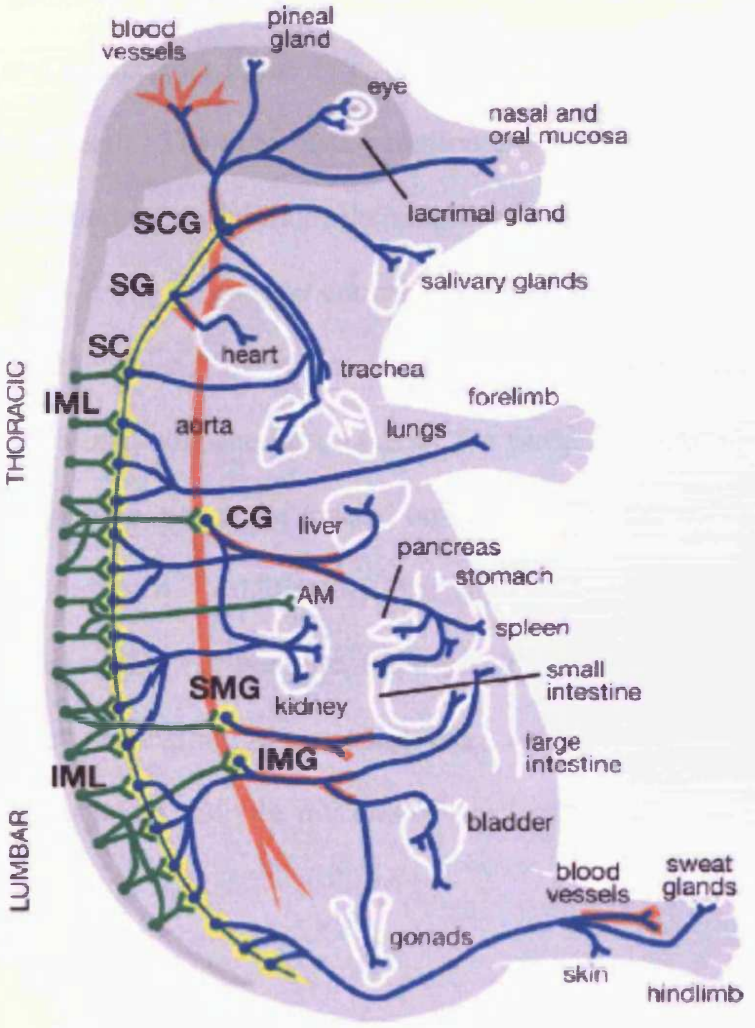

Figure 1: The Mouse Sympathetic Nervous System. The cell bodies of preganglionic sympathetic neurons (in green) located in the intermediolateral column (**IML**) at thoracic and lumbar levels of the spinal cord synapse on to postganglionic neurons in sympathetic ganglia (in yellow). Paravertebral ganglia include the **SCG**, superior cervical ganglion; **SG**, stellate ganglion; **SC**, sympathetic chain. Prevertebral ganglia include the **CG**, celiac ganglion; **SMG**, superior mesenteric ganglion and the **IMG**, inferior mesenteric ganglion. The **AM**, adrenal medulla receives preganglionic input. Taken from [1].

1.1.2 Cranial Sensory Ganglia

The 12 pairs of cranial nerves (Fig. 2), with the exception of nerves X and XI, primarily serve the motor and sensory systems of the head and neck. Cranial nerves, I, II and VIII are sensory; III, IV, VI, XI and XII are motor while V, VII, IX and X are mixed sensory-motor. Cranial nerves III, VII, IX and X also contain parasympathetic fibers.

Eight pairs of sensory ganglia exist and are found on 5 of the 12 pairs of cranial nerves. The trigeminal ganglion is located on cranial nerve V and its neurons innervate thermoreceptors and nociceptors in the face, oral cavity and nasal cavity and periodontal mechanoreceptors of teeth. The geniculate ganglion, on cranial nerve VII, innervates the taste buds from the anterior two thirds of the tongue and skin from the external ear. The vestibulocochlear and spiral ganglia, on cranial nerve VIII, innervate the hair cells of the organs of hearing and balance. The petrosal ganglion is located on cranial nerve IX and innervates the carotid body and the taste buds of the posterior third of the tongue. The jugular and nodose ganglia, which are located on cranial nerve X, innervate the pharynx, larynx, thorax and abdomen. Additionally, the superior glossopharyngeal ganglion is situated on cranial nerve IX. Furthermore, the trigeminal mesencephalic nucleus, located in the midbrain, but originating from neural crest cells, contains the cell bodies of proprioceptive neurons innervating the muscles of mastication.

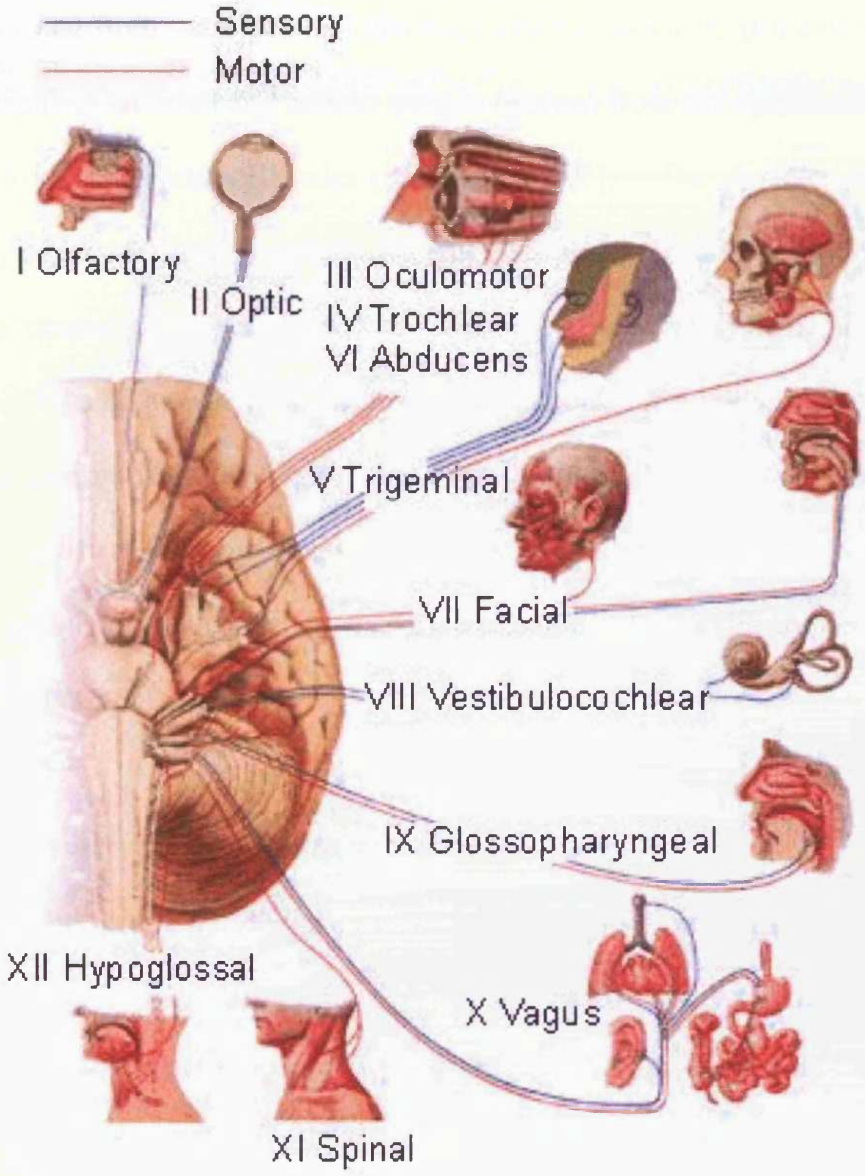

Figure 2: The Cranial Nerves. Seven cranial sensory ganglia are located on the twelve pairs of cranial nerves, including; the trigeminal ganglion (cranial nerve V), the geniculate ganglion (cranial nerve VII, facial), the vestibulocochlear ganglion (cranial nerve VIII), the petrosal ganglion (cranial nerve IX, glossopharyngeal), the nodose/jugular ganglion (cranial nerve X, vagus) and the superior glossopharyngeal ganglion (cranial nerve IX, glossopharyngeal). Taken from [2].

1.1.5 Origins of the PNS

Sensory neurons arise from progenitors derived from specialised regions of embryonic ectoderm; either the neural crest, formed by migration of cells from the neural tube; or neurogenic placodes, transient embryonic thickenings of head ectoderm. The ventolateral trigeminal (formed from the trigeminal placode), vestibulocochlear (formed from the otic placode), geniculate, petrosal and nodose ganglia (formed from the epibranchial placodes) are derived from neurogenic placodes (reviewed by [3]). The dorsolateral trigeminal ganglion [4], trigeminal mesencephalic nucleus [5], jugular ganglion and the DRG are derived from cranial neural crest. Of the autonomic nervous system, neurons of the parasympathetic ganglia arise from mesencephalic neural crest cells, while sympathetic neurons are generated from the trunk neural crest (reviewed by [6]). The enteric nervous system is formed from the vagal and lumbosacral neural crest [6]. Glia (Schwann cells and satellite cells) associated with all sensory and autonomic ganglia are derived entirely from the neural crest [4].

1.2 The Neurotrophins and Their Receptors

The neurotrophins are a family of low molecular weight proteins that includes the prototypical neurotrophin nerve-growth factor (NGF) as well as brain-derived neurotrophic factor (BDNF), neurotrophin-3 (NT-3) and NT-4/5. Neurotrophins are secreted as pro-neurotrophins, 30-35 kDa in size, that are cleaved by extracellular proteases to produce mature 12-13 kDa proteins [7]. The cleaved, mature neurotrophins mediate their effects through two kinds of membrane glycoprotein; the tropomysin-related kinase (Trk) family of receptor tyrosine kinases (TrkA, TrkB and TrkC) which bind specific neurotrophins and p75 neurotrophin receptor ($p75^{NTR}$), a common receptor for all neurotrophins.

TrkA is a receptor for NGF, TrkB for BDNF and NT-4/5, and TrkC a receptor for NT-3 (Fig. 3). However, NT-3 can also bind and signal via TrkA and TrkB. Ligand binding induces Trk receptor dimerisation and autophosphorylation within the cytoplasmic domain, causing a cascade of protein phosphorylations within the cell and ultimately leading to cell survival. The $p75^{NTR}$ receptor, belonging to the tumour necrosis factor (TNF) receptor superfamily, can bind all mature neurotrophins with equally low affinity. Furthermore, $p75^{NTR}$ also has the ability of altering the affinity of a Trk receptor for its cognate ligand. Another function of $p75^{NTR}$ is to mediate the biological activity of the pro-neurotrophins. Both pro-NGF and pro-BDNF have been shown to bind with high affinity to $p75^{NTR}$ which, in opposition to the mature neurotrophins, leads to neuronal apoptosis [8, 9].

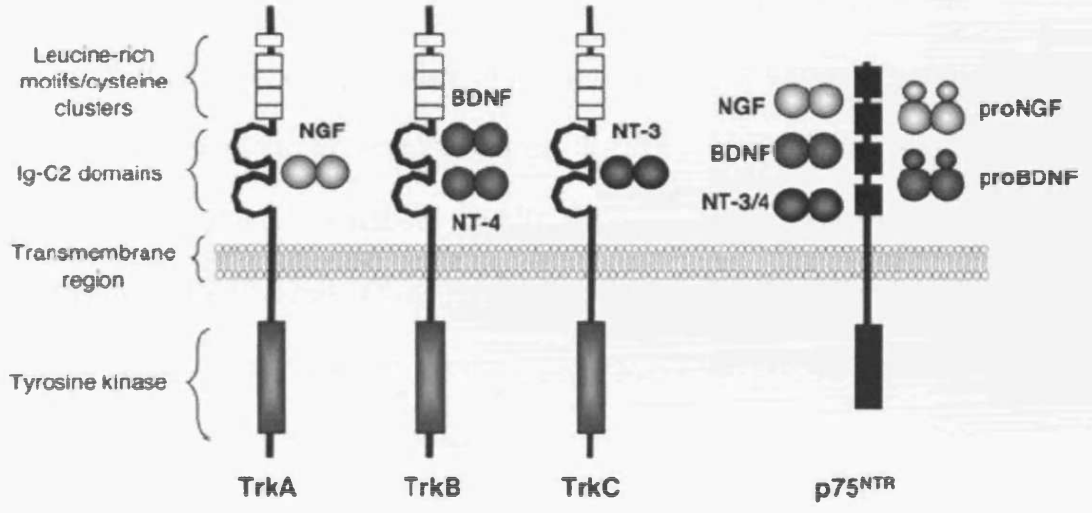

Figure 3: The Neurotrophin Receptors and their Cognate Ligands. See text for details. Taken from [10].

Neurotrophic factor family	Neurotrophic factor	Preferred receptor
Neurotrophins	Nerve growth factor (NGF)	TrkA, $p75^{NTR}$
	Brain-derived neurotrophic factor (BDNF)	TrkB, $p75^{NTR}$
	Neurotrophin-3 (NT-3)	TrkC, $p75^{NTR}$
	Neurotrophin-4 (NT-4)	TrkB, $p75^{NTR}$
GDNF family	Glial cell-derived neurotrophic factor (GDNF)	Ret, GFRα-1
	Neurturin	Ret, GFRα-2
	Artemin	Ret, GFRα-3
	Persephin	Ret, GFRα-4
Neurotrophic cytokines	Ciliary neurotrophic factor (CNTF)	gp130, LIFRβ, CNTFRα
	Leukaemia-inhibitory factor (LIF)	gp130, LIFRβ
	Cardiotrophin 1 (CT-1)	gp130, LIFRβ
	Oncostatin-M (OSM)	gp130, OSMRβ
	Interleukin-6 (IL-6)	gp130, IL6Rα
HGF family	Hepatocyte growth factor (HGF)	Met
	Macrophage-stimulating protein (MSP)	Ron

Table 1: Families of Structurally Related Neurotrophic factors and their Receptors. Taken from [11].

1.2.1 Additional Neurotrophic Factors

In addition to the NGF family of structurally related neurotrophic factors, the neurotrophins, several other families of proteins have been shown to promote the survival of various populations of neurons during development. These include the glial-cell derived neurotrophic factor (GDNF) family, the neurotrophic cytokines and the hepatocyte growth factor (HGF) family (Table 1). Furthermore, it has become clear that members of the neurotrophic factor families promote the survival of various populations of neurons during defined periods of development.

1.3 Regulation of Neuronal Survival and Number in the Developing PNS

1.3.1 Neurogenesis

Neurogenesis studies suggest that neurons of the trigeminal ganglia are born from a pool of proliferating precursors over E9.5-E13.5 in the rat (E9-E11.5 in the mouse) with a peak over E11-E12 (E9.5-E10.5 in the mouse) when the majority of neurons are supported by

BDNF and NT-3 [12, 13]. Furthermore, the nodose/petrosal ganglion is formed from migration of placode-derived cells during E10.5 in the mouse [14] and neurogenesis occurs between E11 and E15 in the rat, corresponding to E9-E13 in the mouse [12]. Both NT-3 and NT-4 are required at the earliest stages of nodose/petrosal ganglion formation, at the height of neurogenesis and differentiation at E12-13 in the mouse, before neurons of this ganglion become dependent on target-derived BDNF [15]. At E12.5 paravertebral sympathetic ganglia consist predominantly of proliferating neuroblasts. In the SCG, neurons are generated from a proliferating population until E14-E15 when the first neurons start responding to NGF [16]. Andres *et al* (2001) [17] showed that the GDNF family member artemin promotes the proliferation of sympathetic neuroblasts and increases the generation of new neurons in cultures established from E12 to E14 ganglia. Furthermore, HGF enhances the survival and differentiation of sympathetic neuroblasts but does not affect proliferation [18].

1.3.2 Neurotrophin Independence

In vitro studies of several populations of PNS neurons from the earliest ages of development suggest that many neurons initially survive independently of neurotrophins at an age where their axons start growing to their targets (reviewed by [19]). For example, in the embryonic mouse trigeminal system, where NGF-responsive cutaneous sensory neurons innervate the facial region [20], the commencement of NGF production and NGF receptor expression are both related to the arrival of sensory axons to their target field, the maxillary process [21]. NGF protein is detectable in the maxillary process only when the earliest trigeminal axons begin to reach their target (E11), the onset of which is not dependent on innervation [22]. Similarly, the expression of NGF receptors and

neurotrophin dependence of trigeminal neurons coincides with target innervation, events which are independent of neuron-target contact [21].

Comparative survival studies of sensory neurons from chick vestibulo-acoustic, geniculate, petrosal and nodose ganglia (Fig. 4) determined that the duration of neurotrophin independence is matched with target distance [23]. These ganglia are derived from ectodermal placodes and are born over the same period of embryogenesis (E2-E5) but differ in their distances their axons have to grow to reach their peripheral and central targets and becoming dependent on target-derived BDNF [23, 24].

Figure 4: *Camera lucida* Drawing of a Wholemount Stage 22 Chick Embryo. G, geniculate ganglion; **V**, vestibular ganglion; **P**, petrosal ganglion; **N**, nodose ganglion. Taken from [24].

When cultured in low density, in the absence of neurotrophins and at a time when their earliest axons would be extending to their target *in vivo*, these neurons die at different rates; vestibulo-acoustic rapidly, geniculate and petrosal intermediate, and nodose slowly [23]. The timing of these intrinsic survival effects is correlated with target distance; vestibular neurons have the closest targets, geniculate and petrosal have more distant

targets, and nodose neurons have the furthest targets [24]. Therefore, neurons which have more distant targets that are innervated later in development have a more protracted period of intrinsic neurotrophin independence [19].

In addition, measurement of nerve lengths of sensory neurons in single-cell cultures has revealed that axonal growth rate is also matched with distance from their common central target, the hindbrain. The axonal growth rate of the vestibular neurons was slowest, geniculate and petrosal neurons two to three-fold faster and nodose neurons five-fold faster [24]. Therefore, neurons with more distant target fields have fastest growth rates, yet despite this it takes longer for the faster growing neurons to reach their targets compared to the slower growing neurons with near-by targets [19, 24].

1.3.3 The Ca^{2+} Set Point Hypothesis

The mechanism by which neurons survive during this period of neurotrophin independence is largely unknown. However, much later in development when neurons have become dependent on NGF for survival, Koike *et al* (1989) [25] demonstrated that depolarising levels of K^+ prevented the death of NGF-deprived E21 rat SCG neurons *in vitro*. This protection by high K^+ was abolished by withdrawal of free ionised extracellular Ca^{2+} (Ca^{2+}_o) or loading the cells with a Ca^{2+} chelator. Furthermore, blockers of L-type Ca^{2+} channels also ablated the pro-survival effects of high K^+, suggesting that Ca^{2+} influx promoted the survival effect in the absence of NGF [25]. Activation of nicotinic cholinergic receptors also rescued NGF-deprived neurons which was unaffected by removal of Ca^{2+}_o but was abolished by chelation of intracellular Ca^{2+} (Ca^{2+}_i), indicating possible involvement of intracellular stores [25]. Koike *et al* (1989) [25] proposed a "Ca^{2+} set-point hypothesis" which states that an optimal level of $[Ca^{2+}]_i$ exists which allows for

neuronal survival in the absence of neurotrophic factors, and at levels below this neurons become dependent on a supply of neurotrophin.

In line with this, Larmet *et al* (1992) [26] using the embryonic chick system showed that depletion of Ca^{2+}-regulated or IP_3-regulated intracellular stores caused the death of early neurotrophic factor independent nodose neurons, but had little effect on older neurotrophin dependent neurons growing in the presence of BDNF [26]. Furthermore, chick nodose neurons begin expressing L-type Ca^{2+} channels shortly before they become dependent on BDNF *in vitro* and *in vivo*, correlating with a time when axons begin to reach their targets *in vivo* [23, 26]. Interestingly, Larmet *et al* (1992) [26] further demonstrated that the pro-survival effect of BDNF is dependent neither on Ca^{2+} influx nor intracellular Ca^{2+} stores.

1.3.4 The Neurotrophic Hypothesis

During normal development, neurons are generated in quantities exceeding that required to form a functional nervous system. Final neuronal number is determined by a subsequent phase of naturally occurring cell death where 20-80% of neurons with long projecting axons undergo apoptosis [11, 27]. A series of studies in the chick embryo demonstrated that altering target field size prior to innervation by either ablation or transplantation of supernumerary wing buds resulted in either death or increased numbers of innervating brachial spinal motor neurons, respectively [28]. These findings have lead to the neurotrophic hypothesis, which specifies that to ensure the optimal amount of target innervation, neurons are overproduced during development and compete for limiting amounts of target-derived neurotrophic factor [29]. Evidence for the neurotrophic hypothesis emerged from a series of studies on nerve growth factor (NGF), the first neuron survival factor to be identified [30], revealing that populations of developing sympathetic and sensory nociceptive neurons depend on a supply of NGF *in vitro*, also

depend on NGF *in vivo*. For example, Levi-Montalcini (1987) [31] demonstrated that these neurons could be eliminated by administering function-blocking anti-NGF antibodies during target field innervation. Furthermore, these neurons are also lost in mice that lack either NGF or its cognate receptor, TrkA [32, 33]. Conversely, naturally occurring cell death during this period of innervation can be prevented by the administration of excess NGF [31].

NGF is synthesised in the target fields of these neurons in limiting amounts [34] and binds TrkA on axon terminals initiating local as well as retrograde signalling to cell bodies. This results in the retrograde transport of NGF from the target field by endocytosis of an NGF-TrkA complex with the subsequent formation of signalling endosomes which are consequently transported to the cell soma [35]. Activated TrkA accumulates in the cell soma, resulting in the activation of signal cascades that support neuronal survival and gene expression.

1.3.5 $p75^{NTR}$ -Induced Survival and Death

The receptor $p75^{NTR}$ possesses an intracellular death domain which is responsible for the activation of apoptotic signalling pathways. However, due to the receptor's activation by numerous pro- and mature neurotrophins, the influence of $p75^{NTR}$ on cell survival and death depends on the cellular context in which it is expressed. For example, the receptor enhances the survival effects of NGF in TrkA expressing neurons, but in conditions of absent or reduced Trk signalling $p75^{NTR}$ can induce cell death (reviewed by [36]).

ProNGF has a greater affinity for $p75^{NTR}$ than NGF and is more potent in the induction of cell death [8]. Therefore, as a death receptor, $p75^{NTR}$ may be used by neurotrophins to

eliminate neurons that innervate inappropriate targets. Furthermore, other members of the TNF receptor superfamily, Fas and TNFα, have been shown to induce apoptotic cell death in neurons which do not receive an adequate supply of neurotrophic factor (reviewed by [11]).

1.4 Neurotrophic Requirements of Developing Sensory and Sympathetic Ganglia

1.4.1 Trigeminal Ganglia

Neurons of the mouse trigeminal ganglia are dependent on BDNF and NT-3 for their survival at the earliest stages of ganglion formation, at E10 in the mouse when the first trigeminal axons begin growing to their targets [37]. However, by E12 very few are BDNF dependent, with NGF being their preferred survival factor [13]. The early survival response to BDNF and NT-3 is mediated predominantly via TrkB; the number of apoptotic neurons is increased in *trkB*$^{-/-}$ embryos and *nt3*$^{-/-}$ embryos during this period and later in development during NGF dependency apoptosis is increased in *trkA*$^{-/-}$ embryos [37, 38].

This switch in neurotrophin dependency is partly due to the sequential generation of BDNF-responsive and NGF-responsive neurons in the trigeminal ganglion, but also that BDNF-dependent neurons switch to become dependent on NGF [39]. Interestingly, these neurons also have a dependency on the hepatocyte growth factor (HGF) family member macrophage-stimulating protein (MSP) when at birth the majority of these neurons can be supported by MSP or NGF *in vitro* [40]. Further, trigeminal neurons can be supported by the cytokines ciliary neurotrophic factor (CNTF), leukaemia inhibitory factor (LIF), oncostatin M (OSM) and cardiotrophin-1 (CT-1) at E17, several days after acquiring

NGF-dependence [41]. The peripheral axons of sensory neurons that switch neurotrophic factors are exposed to BDNF and NT-3 en route to their targets, suggesting that these factors provide intermediate neurotrophic support before axons reach their final target where NGF is synthesised [42]. It is important to note that sensory neurons which do not show a switch in neurotrophin dependence have a more protracted period of neurotrophin-independence *in vitro*, and are perhaps not dependent on intermediate trophic support before reaching their targets [42].

1.4.2 Nodose Ganglia

Neurons of the mouse nodose ganglion retain dependence on BDNF throughout foetal development, from E11 onwards [41]. Furthermore, a range of neurotrophic cytokines, including CNTF, LIF, OSM and CT-1 can support the survival of a subpopulation of nodose neurons as early as E11, during ganglion formation. Neurons also show a marked survival response to these cytokines throughout development [41]. The nodose ganglion also contains a population of neurons, distinct from the subset of catacholaminergic neurons, which have a survival requirement for NGF, peaking at E12 and E13 in the mouse [43]. In addition, nodose neurons also respond to the GDNF family member neurturin during development [44].

1.4.3 Superior Cervical Ganglia (SCG)

In the SCG Andres *et al* (2001) [17] revealed that, in addition to its effects on proliferating neuroblasts, GDNF family member artemin promotes the survival of newly generated sympathetic neurons that have undergone terminal differentiation, a response that is lost by E16. The HGF family member MSP also promotes the survival of a subset of E14 SCG neurons, an effect which is lost at E17 [40]. SCG neurons begin responding to the

classical target-derived growth factor, NGF, at E14 and by E18 the majority of the neurons of these ganglia are dependent on NGF for their survival [16]. Embryonic sympathetic neurons also have a survival requirement for NT-3; with a subset of neurons becoming dependent on NT-3 *in vivo*, between E16 and E18 [45, 46]. While postnatal SCG neurons retain dependency on NGF for survival until adulthood, NT-3 has also been shown to be required for postnatal sympathetic neuron survival [45, 46]. Sympathetic neurons also become responsive to artemin at P12, correlating with a time when SCG neurons begin to acquire neurotrophin-independent survival, which continues into adulthood promoting survival as effectively as NGF [17]. Postnatal SCG neurons also acquire survival responses to CNTF, LIF, and HGF [44, 47].

1.5 Regulation of Axon Extension, Dendrite Formation and Target Innervation in the PNS

In addition to their effects on survival, neurotrophins can promote neurite growth and influence synaptic function. For example, NGF influences the extent of terminal axonal branching and dendritic complexity *in vivo* and enhances neurite extension *in vitro* [48, 49]. However, it has not been possible to determine the precise physiological relevance of neurotrophins in neurite growth as either blocking neurotrophin function, or deletion of the gene encoding the neurotrophin or its cognate receptor, results in neuronal death. The difficulty in separating these survival- and neurite-outgrowth promoting effects has been overcome by using pharmacological agents or transgenic mice to prevent apoptosis and allow neurons to survive *in vitro* or *in vivo* in the absence of neurotrophic support [50-52].

1.5.1 Axon Extension

Axonal growth depends on the dynamics and structure of actin filaments and microtubules within the axon and growth cone. Neuronal growth cones are rich in filamentous actin (F-actin) and continuously extend lamellipodia and filopodia, two highly motile structures located at the leading edge of the growth cone which expand and retract according to growth and guidance cues derived from intermediate and final target fields (reviewed by [53]). Patel *et al* (2000) [52] developed mice deficient in either NGF or TrkA and the pro-apoptotic protein Bax, a member of the Bcl-2 family which has been shown to be required for naturally occurring cell death in the peripheral nervous system [51]. The *bax*$^{-/-}$*trkA*$^{-/-}$ and *bax*$^{-/-}$*ngf*$^{-/-}$ mice displayed a reduction in cutaneous innervation; central axons from the DRG of these mice showed normal projection into dorsal roots and spinal cord but the peripheral axons were absent [52]. Consistent with a role for NGF in the promotion of neurite growth of DRG neurons, E11-E13 *Bax*$^{-/-}$ DRG neurons become bipolar and exhibit neurite outgrowth in the presence of NGF, NT-3 or BDNF [54]. Furthermore, Tucker *et al* (2001) [55] revealed that in organotypic slice cultures mouse DRG axons were targeted to ectopically placed beads containing NGF, BDNF, NT-3 or NT-4/5. Conversely, function-blocking antibodies to NGF, BDNF and NT-3 inhibited elongation of DRG axons [55]. Neurotrophins are thought to stimulate axonal growth by mediating polymerisation or accumulation of F-actin in growth cones or along axon shafts. In line with this NGF, BDNF and NT-3 induce increases in the amount of F-actin in the growth cones of rat embryonic DRG neurons [56].

HGF is thought to be involved in the initiation of sympathetic axon growth during sympathetic ganglia formation, via a local autocrine growth factor loop [18, 57]. Proximal axon extensions from several sympathetic ganglia en route to final target organs occur

along arterial vasculature. Artemin, which is expressed by smooth muscle cells and stimulates sympathetic axon growth *in vitro* and attracts sympathetic axons *in vitro* and *in vivo*, is a candidate molecule for controlling proximal axon extension *in vivo* [58, 59]. NT-3 is also another candidate for promoting proximal axon extension; it is expressed in blood vessels and induces sympathetic axon growth *in vitro* [60, 61]. In line with this, proximal axon projections along blood vessels and into final targets is reduced for pre- and paravertebral ganglia in $nt3^{-/-}$ mice [61].

1.5.2 Target Innervation

The innervation of trigeminal and nodose target fields has been considered in sections 1.3 and 1.4. However, NGF mediates sympathetic axon extension toward peripheral targets where it is produced. Analysis of $bax^{-/-}ngf^{-/-}$ mice suggest it is not required for proximal axon extension from sympathetic ganglia [62]. Furthermore, some targets show a complete lack of innervation in the $bax^{-/-}ngf^{-/-}$ mice, however, others showed partial defects, indicating other factors are also involved in target innervation; HGF [47], GDNF [59] and NT-3 [61] are all potential candidates.

1.5.3 Dendrite Growth

Dendrites begin to grow *in vivo* before sympathetic axons reach their targets; preganglionic activity and postganglionic spontaneous activity are thought to control dendrite initiation [63]. Members of the bone morphogenic protein (BMP) family are thought also to be involved; BMP-5, -6 and -7 are produced by sympathetic neurons and glia [64] and stimulate dendrite formation from sympathetic neurons in the presence of NGF *in vitro* [65, 66]. BMP-mediated induction of gene expression can be modulated by neuronal activity *in vitro*, suggesting that activity and BMPs may work together to initiate

dendrite growth [67]. Size and complexity of sympathetic dendritic arbors is also influenced by target-derived signals and target size; NGF, for example, promotes dendritic growth in neonatal and adult mice [68, 69]. However, *in vitro* studies indicate that NGF alone is not sufficient to initiate sympathetic dendritic growth [63, 70]. Evidence for a role for BDNF and NT-3 in the promotion of dendritic growth has emerged from studies on central neurons [71-73]. However, in cortical neurons these factors have reported to be mutually antagonistic [74].

1.6 Intracellular Signalling Pathways and the Regulation of Neuronal Survival and Neurite Outgrowth in the Developing PNS

On binding of neurotrophin, Trk receptors dimerise and tyrosine residues undergo phoshorylation in the Trk receptor cytoplasmic domain. Adaptor proteins, including Shc and FRS2, are then recruited coupling Trk receptors to intracellular signalling cascades, which include the Ras-ERK (extracellular signal-regulated kinase) pathway, the PI_3K (phosphatidylinositol-3-kinase)-Akt pathway and the phospholipase C (PLC)-γ -protein kinase C (PKC) pathway (reviewed by [36, 75]).

Although Trk receptors and $p75^{NTR}$ do not bind to each other directly, there is evidence that complexes may form between the two types of receptor, allowing $p75^{NTR}$ to confer greater ligand sensitivity on Trk receptors [76]. Signal transduction through independent $p75^{NTR}$ activation results in JNK (c-jun N-terminal kinase), NF-κB (nuclear factor κB) and ceramide [77].

1.6.1 Signalling Pathways Associated with Neuronal Survival and Death

When neurotrophic factors are withdrawn from neurons dependent upon neurotrophin for survival, these cells initiate a series of apoptotic signalling events which includes the translocation of Bax to the mitochondria, release of cytochrome *c*, activation of the apoptosome and caspase-mediated death [50, 78, 79]. Neurotrophic factors can initiate local as well as retrograde signalling to cell bodies to impinge on these apoptotic pathways. For example, NGF can be retrogradely transported from sympathetic axon terminals by endocytosis of an NGF-TrkA complex, formation of signalling endosomes and the transportation and accumulation of phosphorylated TrkA in the cell soma (reviewed by [75]). This results in the induction of signalling events (Fig. 5), including increased activity of PI_3K-Akt, which suppresses cell death by inhibiting the apoptotic activities of forkhead and Bcl 2-associated death protein (BAD), and ERK5 which indirectly activates the transcription factor CREB (cAMP responsive element-binding protein) [75]. Furthermore, the local axonal Trk signalling leads to the activation of the Ras-ERK and PI_3K-Akt pathways [75].

The functions of $p75^{NTR}$ are diverse and complex and it exerts its effects via a number of interacting proteins (Fig. 6), including; NRIF (neurotrophin receptor interacting protein), NRAGE (neurotrophin receptor-interacting MAGE homolog), NADE ($p75^{NTR}$ associated cell death executioner) and SC-1 (Schwann cell-1) (reviewed by [10]). The function of $p75^{NTR}$ is dependent upon the cellular context, yet $p75^{NTR}$ can promote pro-survival (via NF-κB) as well as pro-death effects (via NRIF, NRAGE, NADE, SC-1 and TRAF6) [10].

1.6.2 Signalling Pathways Associated with Neurite Growth

Downstream of Trk receptor activation, local Ras-ERK and PI_3K-Akt signalling contributes to axonal growth by regulating the stability of microtubules and actin [53]. Furthermore, a number of pathways signal to transcription factors which also contribute to axonal growth, including CREB and NFAT (nuclear factor of activated T cells) and Trk receptor signalling may also promote *de novo* expression of transcription factors [80-82]. $p75^{NTR}$ activation may also exert an effect on neurite growth via the GTP-binding protein RhoA. In the absence of neurotrophins, a constitutive interaction between $p75^{NTR}$ and RhoA maintains RhoA activation and inhibits axon growth, however, dissociation of RhoA from $p75^{NTR}$ by neurotrophin binding leads to axonal growth.

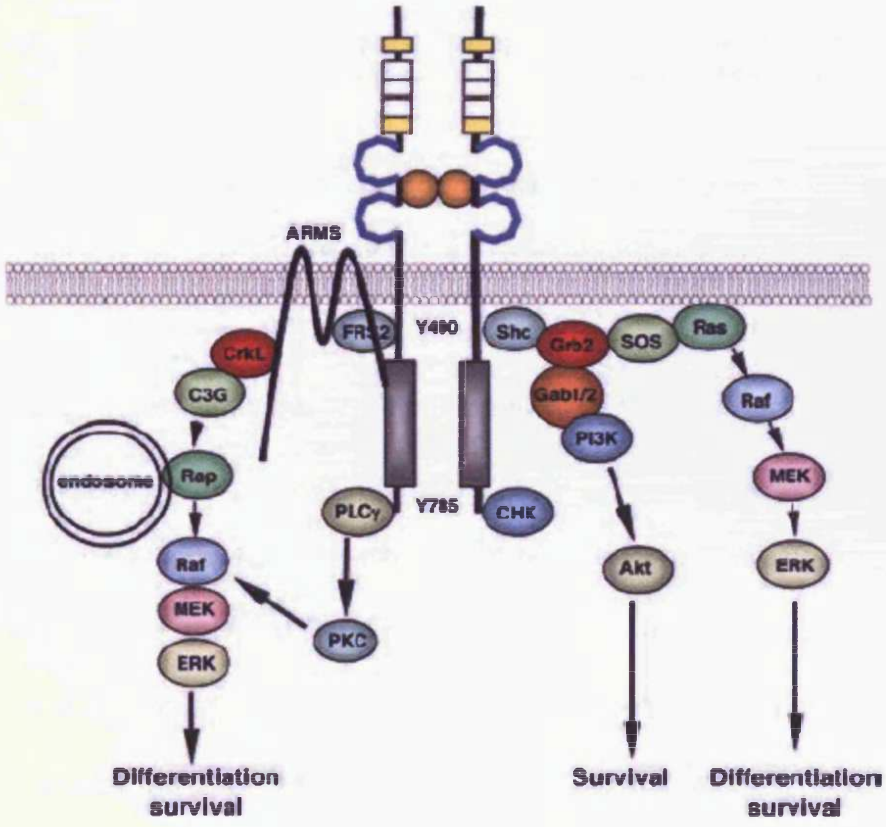

Figure 5: Trk Receptor Mediated Signal Pathways. On binding of neurotrophin, Trk receptors dimerise and tyrosine residues undergo phoshorylation in the Trk receptor cytoplasmic domain. Adaptor proteins are then recruited coupling Trk receptors to intracellular signalling cascades including Ras, Rap, PI_3K and PLCγ pathways. Taken from [10].

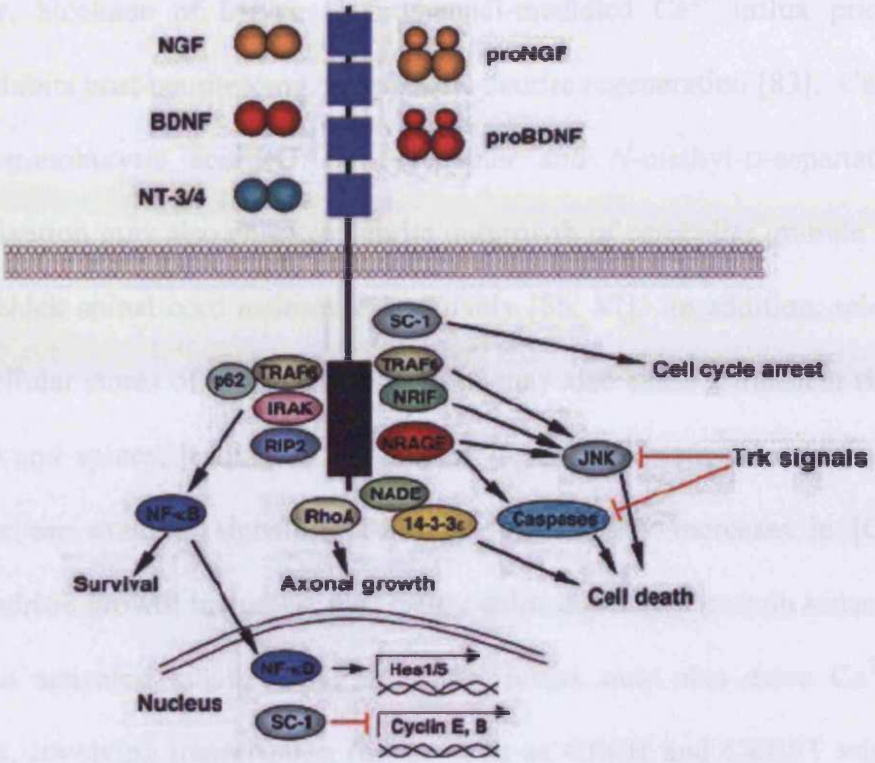

Figure 6: p75^{NTR} Receptor Mediated Signal Pathways. The functions of p75^{NTR} are diverse and complex and exerts its effects via a number of interacting signalling proteins which may either promote cell death (NRIF, NADE, NRAGE, SC-1), survival (NF-κB) or changes in the actin cytoskeleton (RhoA). From [10].

1.7 Extracellular Calcium (Ca^{2+}_o), Neuronal Survival and Neurite Growth

In addition to the role for Ca^{2+}_o in the "Ca^{2+} set-point hypothesis" and neurotrophic factor independence via influx through L-type Ca^{2+} channels, Ca^{2+}_o can affect the outgrowth of neuritic processes from numerous different populations of neurons, with the general premise that neurons grown in conditions of low Ca^{2+}_o concentration ($[Ca^{2+}]_o$) have a reduction in neurite arborisation. A significant body of work reveals that Ca^{2+} influx through Ca^{2+} channels is essential for neurite outgrowth [83-87]. Indeed, blockers of Ca^{2+} permeability (Co^{2+}, Mn^{2+}, La^{3+} and nitrendipine) decreased the fraction of chick retinal neurons that extend neurites and rate of neurite growth, without influencing cell-substratum adhesion or survival capacity [85]. Mattson and Kater (1987) [84] proposed a "Ca^{2+}-set point" for neurite outgrowth, where a critical Ca^{2+}_i concentration ($[Ca^{2+}]_i$) is required for optimal outgrowth and deviation above or below this attenuates outgrowth.

Interestingly, blockade of L-type Ca^{2+} channel-mediated Ca^{2+} influx prior to injury markedly inhibits post-neuritotomy sympathetic neurite regeneration [83]. Ca^{2+} influx via type A γ-aminobutyric acid ($GABA_A$) receptor and *N*-methyl-D-aspartate (NMDA) receptor activation may also enhance neurite outgrowth of cerebellar granule neurons and embryonic chick spinal cord neurons, respectively [86, 87]. In addition, release of Ca^{2+} from intracellular stores of hippocampal neurons may also cause a transient rise of $[Ca^{2+}]_i$ in dendrites and spines, leading to an increase in size of existing dendritic spines [88]. Indeed there are multiple signalling pathways affected by increases in $[Ca^{2+}]_i$ which regulate dendritic growth including, Ca^{2+}/calmodulin-dependent protein kinases (CaMKs) and mitogen activated kinase (MAPK). Ca^{2+} influx may also drive Ca^{2+}-dependent transcription, involving transcription factors such as CREB and CREST which mediate activity-dependent dendritic outgrowth (reviewed by [89]).

In contrast, however, activation of Ca^{2+} permeable AMPA receptors reduces neurite outgrowth from embryonic chick retinal neurons [90]. Furthermore, Campenot and Draker (1989) [91] showed that distal neurites from newborn rat sympathetic neurons readily grew into a fluid environment, separate from the cell bodies, which was substantially deprived of Ca^{2+}, as long as Ca^{2+} was supplied to the cell bodies. The Ca^{2+}-deprived neurites extended at rates 20-35% slower than that of their controls, arguing that neither Ca^{2+}_o nor Ca^{2+} influx at or near the growth cone is required for sustained neurite growth [91].

1.8 A Calcium-sensing Receptor (CaR)

The extracellular calcium-sensing receptor (CaR) is a 121kDa G-protein coupled receptor (GPCR), cloned initially from bovine parathyroid cells and was demonstrated to have a

key role in the regulation of systemic free ionised extracellular Ca^{2+} concentration ($[Ca^{2+}]_o$). The CaR is comprised of 1085 amino acids with three predicted structural domains (Fig. 7) [92]. A large N-terminal extracellular domain (ECD), containing a 21 residue signal peptide and a 24 residue hydrophobic segment [92], is *N*-glycosylated at multiple sites, which is believed to be essential for efficient cell surface expression [93].

Until recently, the ECD alone was believed to confer specificity to its low affinity physiological ligand, Ca^{2+}_o, the binding of which involving clusters of acidic amino acids conserved within this region [94, 95]. However, it is now apparent that the junction between transmembrane helices 6 and 7, proximal to the plasma membrane, is critical for CaR activation by Ca^{2+}_o [96]. The receptor also contains a 250 residue central core with seven transmembrane α-helices, a characteristic of the GPCR superfamily. The 216 residue C-terminus transduces CaR activation by coupling to various G-proteins. The CaR is believed to be expressed at the cell surface as a homodimer; an interaction mediated by disulphide bonding between the ECDs, and a non-covalent, hydrophobic interaction between the transmembrane domains of each CaR monomer [97-99].

1.8.1 CaR and Systemic Ca^{2+} Homeostasis

Systemic calcium homeostasis in mammals is a complex mechanism involving the parathyroid glands, kidney, bone and intestine [100]. Small but physiologically relevant changes in $[Ca^{2+}]_o$ are sensed by cells of the parathyroid gland, which subsequently regulates the secretion of parathyroid hormone (PTH) into the systemic circulation, a process now known to be mediated by the CaR [92, 101, 102]. Indeed, a steep inverse sigmoidal relationship exists between PTH secretion and Ca^{2+}_o (Fig. 8), allowing the maintenance of systemic $[Ca^{2+}]_o$ between 1.1-1.3mM, correlating with the CaR's EC_{50}

from Ca^{2+}_o [103]. Furthermore, $[Ca^{2+}]_o$ has an IC_{50} (half-maximal inhibition) over PTH release correlating with the physiological range of free ionised Ca^{2+} in blood [103]. Therefore, slight decreases in systemic $[Ca^{2+}]_o$ (i.e. hypocalcaemia) promote PTH secretion. Targets of circulating PTH, a so-called 'calciotropic' hormone, then modify the level of Ca^{2+} in the extracellular fluid, thereby ensuring normocalcaemia [103].

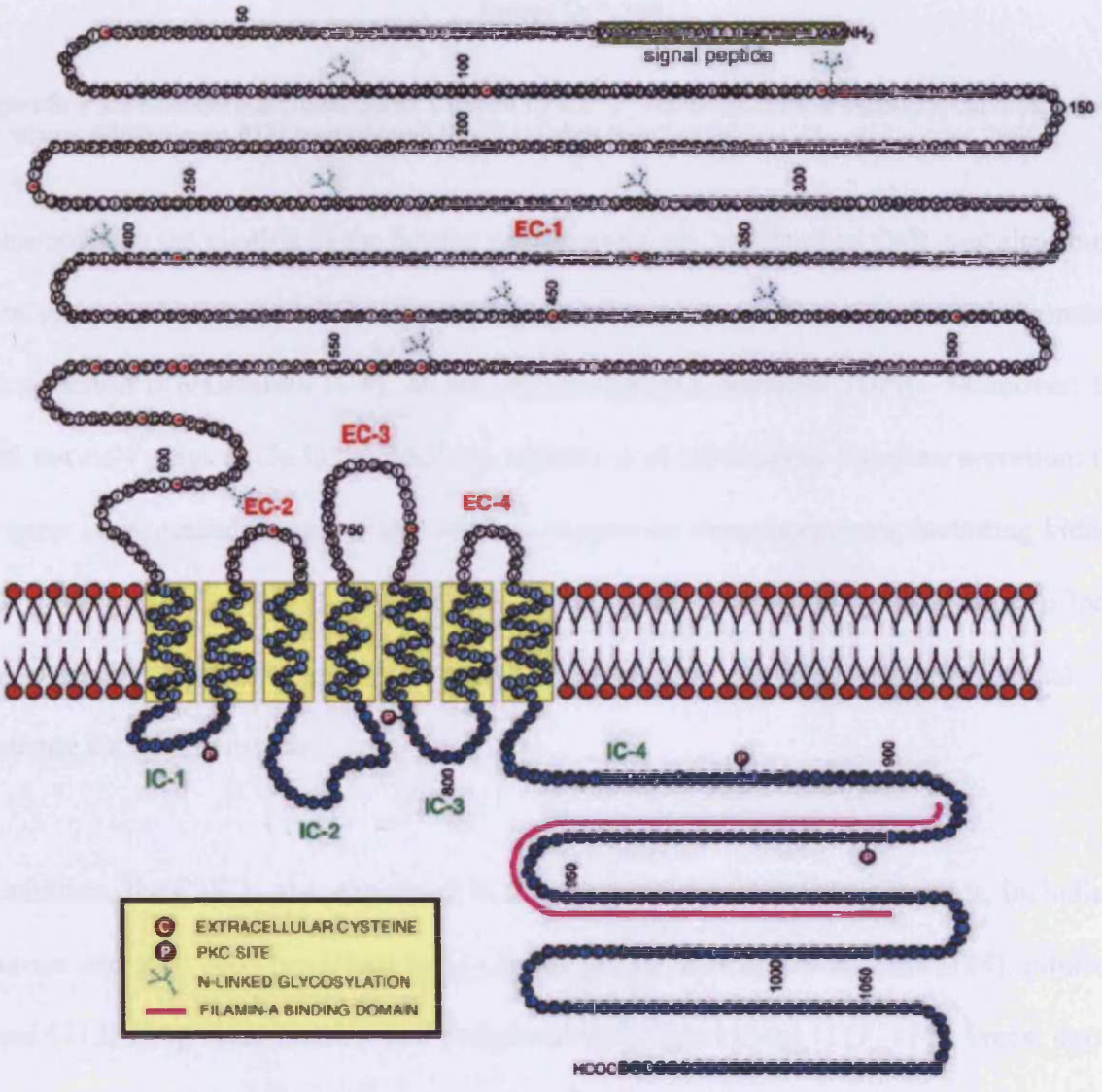

Figure 7: The Predicted Structure of the CaR. **EC-1**, N-terminal extracellular domain; **EC2-4**, extracellular loops 2-4; **IC-1-3**; intracellular loops 1-3; **IC-4**, C-terminal tail; showing putatative **PKC**, protein kinase C concensus phosphorlyation sites. The yellow boxes highlight the seven transmembrane domain. Taken from [104].

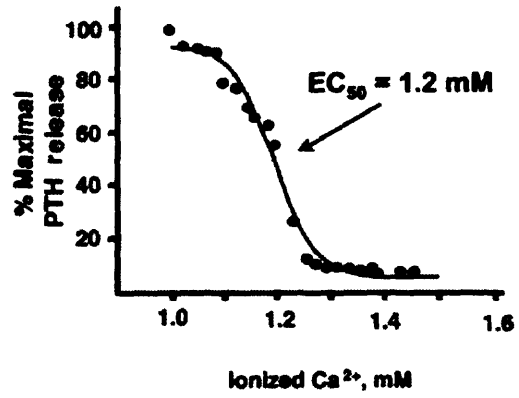

Figure 8: PTH Secretion is Under Strict Control by Ca^{2+}_o. The steep, inverse sigmoidal curve describing the relationship between PTH secretion and $[Ca^{2+}]_o$. Taken from [105].

Subsequent to the cloning of the bovine parathyroid CaR, an identical CaR was also found to be expressed in thyroidal C-cells, the high $[Ca^{2+}]_o$-evoked activation of which promotes the secretion of calcitonin (CT), an anti-hypercalcaemic hormone [106]. Moreover, the CaR not only plays a role in the feedback regulation of calciotropic hormone secretion; the receptor is expressed in tissues that serve as targets for these hormones, including kidney [107, 108], intestine [109] and bone [110, 111], where the receptor participates in local Ca^{2+}_o-sensing, regulating local calciotropic processes that contribute towards maintaining systemic Ca^{2+} homeostasis.

In addition, the CaR is also expressed in tissues unrelated to Ca^{2+} homeostasis, including, neurons and glial cells (reviewed by [112] and [113]), lens epithelial cells [114], pituitary gland [115, 116], bone marrow and peripheral blood monocytes [117, 118], breast ductal cells [119], keratinocytes (reviewed by [120]), gastrointestinal tract [109], pancreas [121], where in many of these cases the 'non-homeostatic' role of the receptor is still to be elucidated. However, it is emerging that within these tissues the CaR may regulate

numerous cellular processes including, gene expression, hormone secretion, control of local ionic homeostasis and regulation of cell fate (reviewed by [100]).

1.8.2 Other Receptors with Homology to the CaR

The CaR belongs to Group II of family C GPCRs, together with putative odorant and pheromone receptors. Group I contains the metabotropic glutamate receptors (mGluRs), whereas $GABA_B$ (or metabotropic) receptors and the leucine-isoleucine-valine (LIV) bacterial periplasmic binding protein reside within Group III (reviewed by [104]).

The human CaR shares 18-24% amino acid homology with various rat mGluRs, with strongest conservation seen between human CaR and rat mGluR1 [122]. Furthermore, a region of 280 amino acids in the human CaR N-terminal domain shows a low level of homology to mouse and rat NMDA receptor subunits [122].

The cysteine residues that mediate intra- or inter-molecular disulphide bonds in the ECD are highly conserved throughout the family C GPCRs. This has implications for overlapping pharmacologies; glutamate and other L-amino acids can activate the CaR and, conversely, high $[Ca^{2+}]_o$ can activate certain mGluRs with potencies similar to the CaR [123]. Furthermore, a number of family C members have been shown to physically interact with the CaR; $GABA_B$-R1, which also functions as a homo- or heterodimer, has recently been shown to interact with the CaR in mouse growth plate chondrocytes [124]. The two receptors co-immunoprecipitate and *in vitro* knockout of the $GABA_B$-R1 genes resulted in an upregulation of the CaR and a greater sensitivity to high $[Ca^{2+}]_o$ [124]. However, these findings have now been refuted. The CaR has also been shown to heterodimerise with mGluR1α or mGluR5 *in vitro* and with mGluR1α in bovine brain,

where CaR and mGluR1α co-localise throughout the hippocampus and cerebellum [125]. These heterodimers appear to be functional as both receptors internalised upon activation by glutamate when co-expressed in HEK293 cells [113, 125].

The CaR also shares family C with six orphan receptors including GPRC6a, a GPCR with a long amino-terminal domain which has conserved Ca^{2+} and calcimimetic (a selective CaR allosteric agonist) binding sites [126]. In addition, CaR agonists dose-dependently activate GPRC6a when expressed in HEK293 cells, but at concentrations significantly higher (>5mM Ca^{2+}_o) than those required to activate the CaR [126]. Interestingly, the Ca^{2+}-binding protein osteocalcin also activated GPRC6a in the presence of Ca^{2+}_o, but inhibits CaR activation by Ca^{2+}_o. These effects can be blocked by inhibition of $G\alpha_i$ and $G\alpha_q$ signalling [126]. Furthermore, GPRC6a is widely expressed in many tissues including bone, lung, liver, spleen, kidney, skeletal muscle, testis and brain [126].

1.9 Inherited Disorders of Ca^{2+} Metabolism Associated with the CaR

The discovery of inherited mutations in the *Car* gene coding for the human CaR, reducing or enhancing receptor sensitivity to Ca^{2+}_o, has established the central role of CaR as a mediator in the regulation of calciotropic hormone secretion and the 'setting' of both Ca^{2+}_o and Mg^{2+}_o.

1.9.1 Human Disorders Due to CaR Loss of Function

Familial Hypocalciuric Hypercalcaemia (FHH), or Familial Benign Hypercalcaemia, is rare autosomal dominant disorder characterised by mild, asymptomatic hypercalcaemia [127]. Patients present with hypophosphataemia, mild to moderate hypermagnesemia, but normal or mildly elevated serum [PTH] despite their hypercalcaemia [127]. FHH

individuals have an elevated set point for Ca^{2+}_o (i.e. the IC_{50} of Ca^{2+}_o over PTH release) as well as PTH-independent excessive renal tubular reabsorption of Ca^{2+}_o, suggesting a reduced response to Ca^{2+}_o in the parathyroid glands and kidney, respectively [128].

Neonatal Severe Hyperparathyroidism (NSHPT) is the homozygous phenotype of FHH; an autosomal recessive life threatening disorder characterised by markedly elevated serum $[Ca^{2+}]$ and [PTH] due to primary parathyroid hyperplasia [128]. Bony demineralisation, multiple fractures and rib cage deformity are common among NSHPT patients; moreover, the disorder is generally lethal unless parathyroidectomy is carried out within the first few weeks of life [129].

1.9.2 Mouse Models of CaR Loss of Function

Ho *et al*, (1995) generated hetero- and homozygous murine models of inactivating mutations of the *Car* gene by targeted disruption [130]. Mice heterozygous ($Car^{+/-}$) and homozygous ($Car^{-/-}$) for the *Car* allele demonstrated symptoms, serum and urine profiles near those of FHH and NSHPT, respectively [130]. Heterozygous and wild-type ($Car^{+/+}$) mice were indistinguishable throughout life in physique, body weight or physical activity [130]. The growth of null mice, however, was markedly reduced by second postnatal day of life compared to wild-type mice, exhibiting reduced bone mass, bowing of the long bones and parathyroid gland hyperplasia [130]. Null mice became progressively lethargic and usually died between 3 and 30 days of life [130]. Furthermore, null mice often failed to exhibit normal extension of digits, elbows or knee joints [130]. However, it proved difficult to discriminate between the direct effects of CaR deficiency with those of severe hyperparathyroidism and hypercalcaemia in these mice [130].

More recently, Kos *et al* (2003) and Tu *et al* (2003) have independently developed murine models null for both CaR and PTH, producing viable fertile mice that live into adulthood [131, 132]. Mice subject to this 'molecular parathyroidectomy' do not exhibit the rickets and osteomalacia seen in the earlier model and associated with NSPHT. This suggests, therefore, that hyperparathyroidism and severe hypercalcaemia, rather than CaR deficiency, are directly responsible for the NSHPT phenotype [131, 132].

1.9.3 $Car^{-/-}$ Mice and Foetal $Ca^{2+}{}_o$ Metabolism

Interestingly, Kovacs *et al* (1996) demonstrated that, like in humans, murine foetal blood ionised $[Ca^{2+}]_o$ is raised above maternal, an increase that is dependent on PTH-related peptide (PTHrP) [133]. Within litters resulting from mating $Car^{-/+}$ females to $Car^{-/+}$ males, a normal blood ionised $[Ca^{2+}]$ of 1.69mM was observed in wild-type embryos, a level which is set by the CaR independently of the ambient maternal $[Ca^{2+}]_o$ [133]. However, this was modestly increased to 1.8-1.9mM in $Car^{+/-}$ and $Car^{-/-}$ embryos due to severe hyperparathyroidism (>80pg.ml^{-1} $PTH_{1\text{-}34}$ in $Car^{-/-}$ compared with <20pg.ml^{-1} in $Car^{+/-}$ and $Car^{+/+}$ mice), increase in 1,25-dihydroxyvitamin D levels and an increase in collagen resorption from the foetal skeleton, parameters chronically elevated in the $Car^{-/-}$ embryo [133]. However, some aspect of the intrauterine environment prevents the $Car^{-/-}$ embryo from reaching a higher blood Ca^{2+} level, possibly via suppression of PTHrP-mediated placental Ca^{2+} transfer [133]. Therefore, the role of the foetal parathyroid CaR maybe to keep PTH suppressed, and through it 1,25-dihydroxyvitamin D as well. In $PTHrP^{-/-}$ embryos, foetal blood $[Ca^{2+}]_o$ falls to a level which allows increased PTH secretion and where blood $[Ca^{2+}]$ is maintained at the adult level possibly as the CaR responds in the same way as in the adult [133].

1.9.4 Human Disorders Related to CaR Gain of Function

Autosomal dominant hypocalcaemia (ADH) or a form of sporadic hypocalcaemia are typically caused by activating missense mutations located within the CaR ECD or, rarely, within its transmembrane domain [134]. Functional analysis of the mutant receptor reveals that these polymorphisms cause a reduction in the EC_{50} for high Ca^{2+}-evoked CaR activation, consistent with a gain-in-function [135]. These disorders resemble hypoparathyroidism with $Ca^{2+}{}_o$ reset downward; patients have a high level of urinary Ca^{2+} excretion due to activated renal CaR which leads to a reduction in tubular Ca^{2+} reabsorption. Individuals are generally asymptomatic, however, seizures can occur [134].

1.9.5 Mouse Models of CaR Gain of Function

Until recently, a model for an activating mutation of the CaR was not available, however, Hough *et al* (2004), developed a model bearing the *Gprc2a*^{Nuf} (*Nuf*) mutation which was generated by screening animals that had been treated with a mutagenic alkylating chemical. The *Nuf* mice displayed cateracts, ectopic calcification, hypocalcaemia, hyperphosphatemia, and inappropriately raised levels of PTH. The homozygous missense mutation (L723Q) was mapped to the fourth transmembrane domain of the CaR [136]. Furthermore, the recombinant L723Q CaR evoked a leftward shift in the $Ca^{2+}{}_o$-dose response when compared to wild-type CaR in HEK-293 cells [136].

1.10 Pharmacological Characterisation of the CaR

Extracellular Ca^{2+} represents the physiologically relevant CaR ligand *in vivo*, effective within the range of 1-1.5mM. However, other ligands have shown to activate the receptor directly or potentiate its sensitivity to other physiological agonists. Ligands that mimic or potentiate the effects of Ca^{2+}_o on the CaR have been termed calcimimetics, of which two classes exist.

1.10.1 Class I Calcimimetics

Class I calcimimetics, including Ca^{2+}_o, are 'true' or orthosteric CaR agonists. These are organic or inorganic polycations which do not require the presence of Ca^{2+}_o to activate the CaR. Class I calcimimetics are believed to act predominantly within the CaR ECD, although Ca^{2+}_o is now known to also act at the junction of CaR transmembrane helices 6 and 7 [96]. Members of the class I calcimimetics include a number of di- and trivalent cations, polyamines, aminoglycosides and polybasic amino acids (Table 2).

The inorganic cations can be classed according to their potency in CaR activation into strong agonists, typically ions of the Lanthanide series (e.g. La^{3+}, Gd^{3+}), which activate the CaR at micromolar levels; medium agonists (Ca^{2+}, Ba^{2+}, Sr^{2+}), which activate the CaR at millimolar and sub-millimolar levels; and weak agonists (e.g. Mg^{2+}, Fe^{2+}, Na^{+}), which activate the CaR at high millimolar levels [104]. Potency in receptor activation is thought to be related to positive charge number and cationic radius; ions with small cationic radii are, in general, less potent CaR agonists, however the potency of cations with radii $\geq$0.84Å increases with their charge number [104]. For example, in order of potency La^{3+} (1.06Å) > Gd^{3+} (0.94 Å) > Ca^{2+} (0.99Å) = Ba^{2+} (1.34 Å) > Mg^{2+} (0.66Å) [104].

Type I Calcimimetics	Positive Charges	EC_{50}
Inorganic Ions		
Calcium	2	1.2 mM
Magnesium	2	5.2 mM
Lanthanum	3	33 μM
Gadolinium	3	20 μM
Aluminium	3	4 mM
Barium	2	-
Cadmium	2	-
Nickel	2	-
Cobalt	2	-
Iron	2	-
Lead	2	100 μM
Polyamines		
Spermine	3	150 μM
Spermidine	4	2 mM
Pentaethylenehexamine	6	500 μM
Hexacyclin	6	21 μM
Aminoglycosides		
Streptomycin	3	600 μM
Bekanamycin	5	200 μM
Gentamycin	5	150 μM
Neomycin	6	30 μM
Polybasic Amino Acids		
Polylysine (38kD)	55	3 nM
Polyarginine (100kD)	640	4 nM

Table 2: A Summary of Class I Calcimimetics Described to Date. Relative positive charge and EC_{50} of CaR activation are shown. Adapted from [137].

Polyamines are also potent CaR agonists due to their multiple positively charged amino groups. Spermine is an endogenous polyamine with four free amino groups, with an EC_{50} of 200-300μm for CaR activation [138]. A possible physiological role for this organic cation may exist in the gastrointestinal tract where the activation of the CaR by polyamines may promote gut cell differentiation and in the brain, where spermine reaches these levels [138]. Aminoglycoside antibiotics (e.g. neomycin) and polybasic amino acids (e.g. polylysine) also mimic the effect of $Ca^{2+}{}_o$ on CaR activation. Interestingly, amyloid β-peptides, $A\beta_{1\text{-}25}$ and $A\beta_{1\text{-}40}$, elicit the activity of a non-selective cation channel (NCC) in CaR-transfected, but not in non-transfected, HEK-293 cells [139]. Furthermore, Ye *et al* (1997) demonstrated NCC activation by $A\beta_{1\text{-}40}$ in wild-type hippocampal pyramidal neurons, but not from neurons null for CaR [139]. This suggests that amyloid β-peptide aggregates may inappropriately activate the CaR, stimulating NCC and causing neuronal

dysfunction in this cell type via sustained increases in Ca^{2+}_i, contributing to the pathogenesis of Alzheimer's disease [139].

1.10.2 Class II Calcimimetics

The class II calcimimetics are endogenous allosteric modulators which potentiate CaR sensitivity to Ca^{2+}_o, shifting the concentration-response curve to the left, without altering the maximal response. The class II calcimimetics, therefore, require the presence of Ca^{2+}_o for biological activity and are thought to act largely within the CaR transmembrane domain, a mechanism distinct to that of the class I calcimimetics [94].

The aromatic amino acids tyrosine, phenylalanine and tryptophan act as positive allosteric modulators that activate CaR in the presence of at least 1mM Ca^{2+}_o in CaR-transfected HEK-293 cells [140]. Aromatic residues were found to act stereoselectively, with L-amino acids several times more potent than D-isomers [140].

The affinity of the CaR for Ca^{2+}_o may also be modulated by ionic strength; Quinn et al [141] reported changes in $[NaCl]_o$ lead to inverse alterations in CaR activation by Ca^{2+}_o and spermine, an effect specific to the receptor [141]. Furthermore, alterations in extracellular pH (pH_o) may potentiate CaR sensitivity to its agonists, including the AGAs; elevations in pH_o (pH 7.4-8.5) increase CaR sensitivity, while reducing pH_o (pH 7.4 to 6.5) does the converse [141, 142].

1.11 Pharmacological Modulation of the CaR

Due to a key role in the control of PTH secretion and urinary Ca^{2+} excretion, small organic compounds have been developed to manipulate the parathyroid CaR, a suitable molecular target for the treatment of primary and secondary hyperparathyroidism. Polycationic ligands lack specificity and potency and are clearly unsuitable candidates for the pharmaceutical modulation of the CaR.

1.11.1 "Calcimimetic" Compounds

First generation class II calcimimetics, typified by NPS-467R and NPS-568R (Fig. 9A), are low molecular weight phenylalkylamine compounds structurally derived from fendiline and other drugs that block voltage-gated Ca^{2+} channels [143]. The so-called pharmacological "calcimimetic" compounds act as positive allosteric modulators, increasing the sensitivity of the CaR to activation by Ca^{2+}_o and are, therefore, inactive in the absence of Ca^{2+}_o [144]. NPS-568R, for example, demonstrated an inhibition of PTH secretion from both human adenomatous and bovine parathyroid cells and showed a leftward shift in the $[Ca^{2+}]$ response curve in CaR-expressing *Xenopus* oocytes (Fig. 9B) [145].

Importantly, the observation that these compounds do not induce cellular responses at $[Ca^{2+}]_o$ below 0.1mM or above 3mM, in other words, ineffective at minimal and maximal levels of the physiological ligand, further confirmed their allosteric mechanism of action [143].

These drugs possess one chiral carbon and exhibit stereoselectivity both *in vitro* and *in vivo*, where the *R*-enantiomer demonstrates a 10- to 100-fold increase in potency

compared to the *S*- enantiomer [144]. This is a phenomenon that can be used to distinguish CaR-specific from non-specific effects of these drugs which, due to derivation from channel-blocking compounds, block a variety of ion channels at concentrations that maximally activate the CaR [143]. However, these phenylalkylamine compounds lack activity at receptors for thrombin, bradykinin, and ATP [144]. Furthermore, 100nM NPS-568 fails to elicit responses from receptors sharing significant homology to the CaR, including the Group I GPCR mGluR1a, Group II mGluR2 and Group III mGluR8 [144].

In animal models NPS-R568 induce a rapid decrease in serum PTH and Ca^{2+} levels in a dose dependent manner [146] and effectively reduce parameters of primary and secondary hyperparathyroidism when used in clinical trial [137, 147]. The requirement for a compound with improved bioavailability and a longer half-life led to the development of the second generation calcimimetic, AMG-073 [146]. AMG-073, or Cinacalcet HCl, is now in clinical use as a safe and efficacious means of lowering serum [PTH] and calcium-phosphorous product in dialysis patients with secondary HPT [148]. Furthermore, evidence suggests calcimimetic compounds reduce cardiovascular complications associated with secondary HPT [137] and recently Odenwald *et al* (2006) demonstrated an antihypertensive action of NPS-568R by using the compound to decrease blood pressure in uremic rats [149]. Furthermore, clinical trials also suggest a potential use for the drug as treatment for primary HPT [150, 151].

In addition to their therapeutic potential, the allosteric stereoselective nature of the calcimimetic compounds makes them valuable tools for studying CaR function. In the current study the calcimimetic NPS-467R was used.

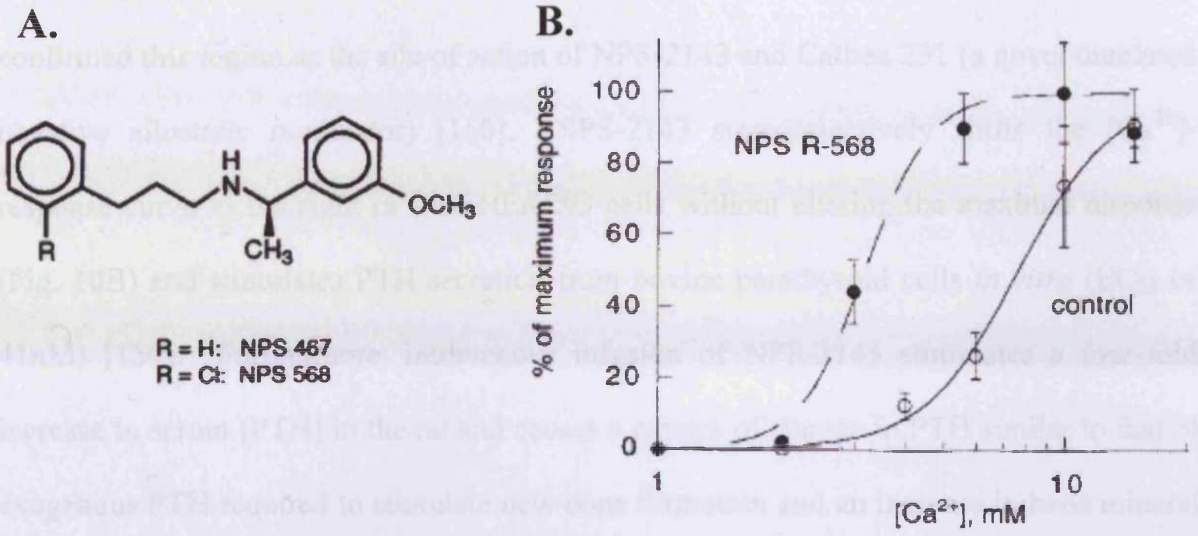

Figure 9: The Calcimimetics NPS-467 and NPS-568 A. The structure of calcimimetics NPS-467 / NPS-568. **B.** NPS-568 exhibits a stereoselective leftward shift in the $[Ca^{2+}]_o$ dose response curve in CaR-expressing *Xenopus laevis*. Taken from [144, 145].

1.11.2 "Calcilytic" Compounds

The small molecules NPS-2143 (Fig. 10A) and NPS-89636 are orally active 'calcilytic' compounds developed as CaR antagonists. Rational design of NPS-2143 was encouraged by the discovery of the nature of transient increases in serum [PTH] to increase bone strength and mineral density [152-154]. Therefore, a compound that could produce pulsatile changes in endogenous PTH would be suitable as a novel therapeutic for osteoporosis or osteopenia [150].

Pre-treatment of CaR-HEK293 cells with NPS-2143 blocks Ca^{2+}_o-induced increases in $[Ca^{2+}]_i$ (IC_{50} = 43nM) [150, 155, 156]. However, NPS-2143 did not affect PLC-mediated responses by purinergic, thrombin and bradykinin receptors to their cognate ligands nor did it affect mGluRs or $GABA_BRs$, other members of family C GPCR which are structurally homologous to the CaR [150].

Homology models of the CaR transmembrane domain utilising bovine rhodopsin, confirmed this region as the site of action of NPS-2143 and Calhex 231 (a novel unrelated negative allosteric modulator) [150]. NPS-2143 stereoselectively shifts the $[Ca^{2+}]$-response curve to the right in CaR-HEK293 cells without altering the maximal response (Fig. 10B) and stimulates PTH secretion from bovine parathyroid cells *in vitro* (EC_{50} of 41nM) [150]. Furthermore, intravenous infusion of NPS-2143 stimulates a four-fold increase in serum [PTH] in the rat and causes a pattern of change in PTH similar to that of exogenous PTH required to stimulate new bone formation and an increase in bone mineral density [157]. Further, when administered orally to osteopenic ovarectomised rats, NPS-2143 caused a sustained increase in serum [PTH] with subsequent increase in bone turnover, yet bone resorption and formation remained in balance [157]. Moreover, concurrent administration of NPS-2143 and 17β-estradiol increased bone turnover and increased bone mass, due to the antiresorptive action of estrogen [158].

Calcilytic compounds may be a valuable alternative to PTH as an anabolic therapeutic for bone diseases such as osteoporosis. In addition, they provide an excellent pharmacological tool to study CaR function. In this study, the calcilytic compound NPS-89636 was used.

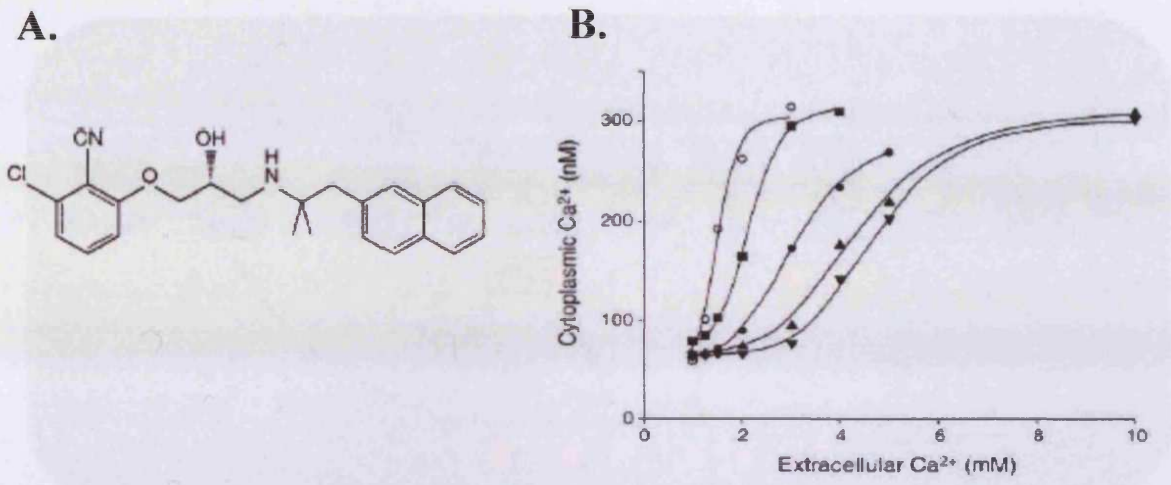

Figure 10: The Calcilytic NPS-2143. **A.** Structure of the calcilytic NPS-2143. **B.** NPS-2143 shifts the $[Ca^{2+}]_o$ dose-response to the right in CaR-transfected HEK293 cells; clear circle, Ca^{2+}_o only; others NPS-2143 30, 200, 300 or 1000nM. Taken from [150].

1.11.3 Signal Transduction Pathways Coupled to CaR Activation

The CaR intracellular C-terminal domain couples to the α-subunits of $G_{q/11}$ heterotrimeric G-proteins involved in the activation of phosphatidylinositol-specific phospholipase C (PLC) (Fig. 11) [159]. The efficiency of coupling to and activation of PLC is modulated by the PKC-dependent phosphorylation of 5 predicted PKC sites in the human CaR C-terminus, of which Thr-888 is believed to be the most critical for PKC-mediated regulation [160, 161]. The C-terminal tail may also couple to the PLCβ isoform by liberation of βγ-subunits from G_i, the generation of inositol-1,4,5-triphosphate (IP_3) and diacylglycerol by PLC subsequently mediates intracellular Ca^{2+} release and PKC activation. The CaR is also believed to couple to $G_{\alpha i}$, resulting in the inhibition of adenylate cyclase and reduction of cellular cAMP levels [162]. Interestingly, CaR has recently been shown to couple to $G_{12/13}$ and activate PLD via a Rho-dependent mechanism [159, 163], a pathway which had been shown to induce CaR-mediated changes in actin stress fiber assembly and cell morphology [164].

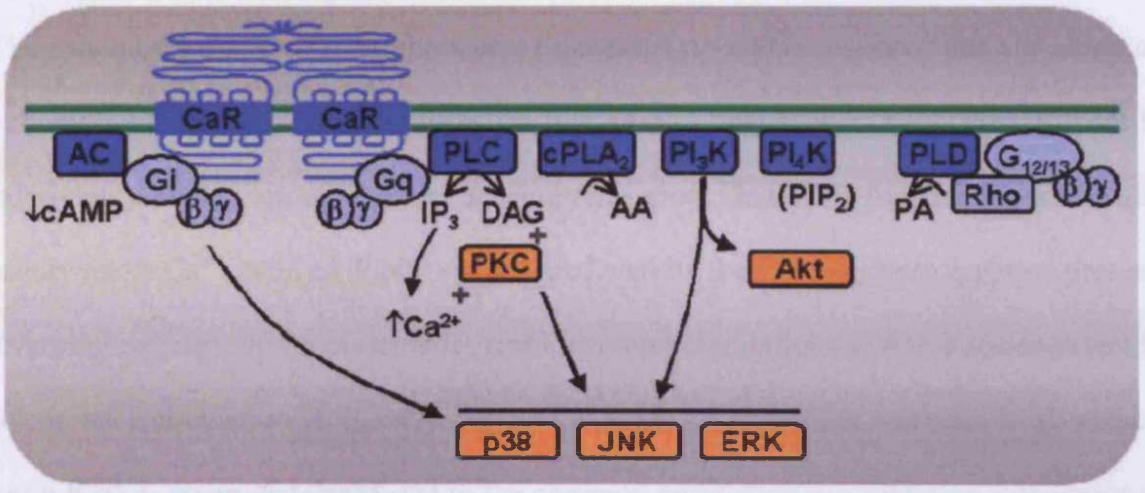

Figure 11: Overview of CaR-mediated Intracellular Signalling. The CaR C-terminus couples to the α-subunits of $G_{q/11}$ leading to the activation of **PLC** (phospholipase C) and the formation of **DAG** (diacylglycerol) and **IP_3** (inositol triphosphate) leading to intracellular Ca^{2+} release and **PKC** (protein kinase C) activation. CaR may also couple to Gi leading to the activation of **AC** (adenylate cyclase), and G12/13 leading to the activation of **PLD** (phospholipase D) and **PA** (phosphatidic acid) production. Other CaR effectors include; **PLA_2** (phospholipase A_2) activation, liberating **AA** (arachidonic acid); **PI_3K** (phosphatidyl inositol-3 kinase)-mediated **Akt** (protein kinase B) activation; and activation of the MAPKs p38, **JNK** (Jun amino-terminal kinase) and **ERK1/2** (extracellular-signal-regulated kinases 1/2). Taken from [161].

In addition, CaR also activates phospholipase A_2 (PLA_2), liberating arachidonic and its metabolites [165]. CaR activation may also evoke PI_3K-mediated Akt (protein kinase B) phosphorylation in a number of systems (reviewed by [161]). Furthermore, the receptor activates downstream MAPK cascades, including ERK1/2, p38 and JNK (Fig. 11) [166].

1.12 CaR Expression in Peripheral and Central Nervous Systems

1.12.1 Perivascular Sensory Nerves

Bukoski *et al* (1997) revealed CaR mRNA to be expressed in rat DRG and CaR protein localised to perivascular nerves of rat mesenteric resistance arteries [167]. Interestingly, Bukoski *et al* (1997) showed expression of CaR mRNA in DRG neurons using RT-PCR yet failed to detect CaR mRNA in mesenteric artery [167]. The detection of CaR protein in the perivascular adventitia of mesenteric arteries lead Bukoski *et al* (1997) to propose

that CaR message is processed and transported from the DRG to the perivascular network of peripheral arteries [167]. Furthermore, Bukoski *et al* (1997) proposed that Ca^{2+} binding to the perivascular nerve CaR induces the release of a vasodilator which then diffuses to underlying vascular smooth muscle, causing relaxation. Indeed, a functional perivascular sensory nerve Ca^{2+}-induced dilator system mediated by the CaR has been reported present, in varying degrees, in the mesenteric, renal, cerebral circulations and to a lesser extent in the coronary circulation [168, 169]. Further, significant relaxation was seen in all vessels over a $[Ca^{2+}]_o$ range of 1-3mM, yet in the coronary circulation a contraction was observed [168].

1.12.2 The Brain and CNS

The brain CaR was initially cloned by Ruat *et al* (1996) [170] and subsequent studies have revealed a wide distribution of the receptor in the CNS. The majority of these regions expressing high levels of the CaR are implicated in fluid and mineral homeostasis.

The subfornical organ (SFO), for example, exhibits the highest region of CaR expression in the adult brain [112, 171]. The SFO is exposed to systemic fluid and thus a candidate for sensing Ca^{2+}_o. Moreover, the SFO is a primary site for angiotensin II regulation of drinking behaviour and is known to have roles in the regulation of electrolyte and cardiovascular function [112]. Such a role may be accomplished by its metabotropic actions on non-selective cation channels or by potentiating sub-threshold hyperpolarisation-activated inward current and subthreshold Na^+ current [172].

The CaR is expressed on the soma and nerve terminals of hippocampal pyramidal neurons, exhibiting a distribution similar to that of mGluRs and ionotropic GluRs (iGluRs) both of

which having roles in long-term potentiation (LTP), an *in vitro* analogue of memory [173]. Indeed, Chattopadhyay *et al* (1997) observed that CaR mRNA and protein was expressed at low levels in rat hippocampus from 5 days postnatally (P5) increasing markedly at P10. This level persisted until P30 when it decreased 3-fold to adult level of expression (P45) [173]. The large increase in CaR expression during hippocampal development coincides with the time LTP can first be induced in the rat, suggesting a role for the receptor. In addition, amyloid β (Aβ) peptides, which are involved in both trophic and toxic functions in the hippocampus and contribute to the deterioration of long term memory in Alzheimer's disease, modulate the probability of opening (P_o) of nonselective cation channels (NCCs) via the CaR and may play a cognitive role as well as a neurodegenerative one [139].

The CaR is expressed in neurons of the olfactory bulb in the rat where it is speculated that the receptor may play a role in the differentiation of olfactory neurons to gonadotropin-releasing hormone (GnRH) secreting neurons during CNS development in rats [112]. More recently, Chattopadhyay *et al* (2006) demonstrated that the CaR promotes migration of post-mitotic GnRH neurons from the anterior nasal compartment to the basal forebrain to become components of the hypothalamic-pituitary-gonadal axis [174]. CaR is believed to exert this effect via controlling the secretion of the chemokine monocyte chemoattractant protein-1 (MCP-1) [174].

In addition, the CaR is also expressed in other brain regions including Purkinje cells of the cerebellum, in neurons of striatum, basal ganglia and cingulate cortex where its biological role is currently unknown.

1.12.3 Regulation of Neuronal Function by the CaR

CaR activation increases the probability of opening (P_o) of NCCs [175] and alters the activity of a Ca^{2+}-activated K^+ channel (CAKC) in hippocampal pyramidal neurons [176], where CaR may mediate alterations in $[Ca^{2+}]_i$ thought to be involved in the regulation of synaptic plasticity and to affect neuronal excitability, respectively [112]. Furthermore, Vassilev *et al* (1997), using a biophysical model of Ca^{2+}_o fluctuations during synaptic terminal stimulation, hypothesised that presynaptic terminal CaRs sense the transient frequency-dependent increase in synaptic cleft $[Ca^{2+}]_o$, thereby enabling Ca^{2+}_o to serve as a retrograde messenger [177]. In line with this, brief trains of synaptic transmission in the hippocampal CA1 region have been shown to induce a transient depletion of local $[Ca^{2+}]_o$ [178]. Furthermore, physiological reductions in cleft $[Ca^{2+}]_o$ have also been shown to activate NCCs in neocortical nerve terminals, channels which are directly inhibited by the CaR agonists Gd^{3+}, Ca^{2+} and Mg^{2+} (but not NPS-467R), consistent with a retrograde messenger role for Ca^{2+}_o in modulating the excitability of the presynaptic terminal [179]. Heterodimerisation of the CaR with mGluRs 1 and 5 in neurons also provide alternative means of modifying transmission or plasticity through sensing $[Ca^{2+}]_o$ at synapses [113, 125].

1.12.4 Glial Cells

The CaR is present in oligodendroglia, microglia, human primary astrocytes and astrocytoma cell lines in all of which, with the exception of U373 astrocytoma cells, where it activates an NCC, CaR agonists stimulate CAKC. Indeed, CaR expression in myelin-forming oligodendrocytes exhibits a pattern similar to that observed in hippocampus, and activation of CaR by Ca^{2+}_o results in proliferation of immature oligodendrocytes [180]. Furthermore, astrocytes also functionally express the CaR where a role in regulating

mitogenesis has been speculated [181]. In these cells CaR regulates PTHrP secretion, raising the possibility that high $[Ca^{2+}]_o$ and CaR regulate proliferation and differentiation indirectly via PTHrP [182]. Microglia, the resident macrophages within the CNS, also express the CaR where the receptor may mediate the effects of high $[Ca^{2+}]_o$ in reducing the activity of an inward rectifying K^+ current in these cells [183].

1.13 Aims and Objectives

The CaR is developmentally expressed in mouse sensory and sympathetic neurons

The CaR is expressed in both peripheral and central neurons including DRG and hippocampal pyramidal neurons, a brain region which also displays developmentally regulated postnatal CaR expression (section 1.12). To determine the developmental profile of CaR expression in experimentally tractable populations of mouse neurons CaR mRNA expression will be characterised in three populations of mouse neurons that can be dissected from mice at different stages of development, including; superior cervical ganglia (SCG), nodose ganglia and trigeminal ganglia.

The CaR mediates neurite outgrowth in vitro and target innervation in vivo

A number of studies using several different populations of neurons have shown that Ca^{2+}_o is required for neurite outgrowth (section 1.7). In addition, CaR activation is known to induce cytoskeletal changes by coupling to $G_{12/13}$ with the activation of PLD via a Rho-dependent mechanism (section 1.11.3). To determine whether increasing $[Ca^{2+}]_o$ over the range to which the CaR is sensitive increases neurite outgrowth *in vitro*, neurons will be grown in culture medium containing low (i.e. 0.7mM) and high (i.e. 2.3mM) $[Ca^{2+}]_o$ followed by quantification of morphological parameters. Furthermore, cultures will be set up from animals of different developmental ages to reveal any changes in the effects of $[Ca^{2+}]_o$ on neurite arborisation over developmental time.

Pharmacological manipulation of the CaR using calcimimetic (NPS-467R) and calcilytic (NPS-89636) compounds will be used to determine whether the CaR mediates the effects of $[Ca^{2+}]_o$ on neurite outgrowth. CaR function will also be manipulated by overexpressing dominant negative (R185Q) and wild-type CaR proteins. In addition, the neurite arbors

from dissociated neurons in cultures established from $Car^{+/+}$, $Car^{+/-}$ and $Car^{-/-}$ animals will be compared. The physiological relevance of CaR in regulating target field innervation *in vivo* will be addressed by comparison of target organ innervation in $Car^{+/+}$, $Car^{+/-}$ and $Car^{-/-}$ animals.

The CaR regulates neuronal survival during a period of naturally occurring cell death

CaR activation may evoke ERK and Akt phosphorylation, signals associated with differentiation and survival (section 1.11.3), yet the CaR may also induce apoptosis in some cell types. This hypothesis will be addressed initially by Ca^{2+}-dose response using dissociated cultures established from ganglia at their peak of naturally occurring neuronal death. Analyses will then be extended to include a neurotrophic factor-dose response in the presence of low, EC_{50} and high $[Ca^{2+}]_o$ values taken from the Ca^{2+}-dose response. The pharmacological agents NPS-467R and NPS-89636 will then be used to determine whether shifts in the dose response induced by varying $[Ca^{2+}]_o$ are mediated by the CaR, once their optimal working concentrations are established.

CHAPTER 2

MATERIALS AND METHODS

2.1 Breeding and Maintainance of Wild-type CD1 Mice

Wild-type CD1 females were used for routine experiments; overnight matings of wild-type CD1 mice were carried out by Joint Services technical staff. All mice were fed on Rodent Global Diet pellets (Harlan) and given water *ad libidum*.

2.2 Isolation of Mouse Embryos

Pregnant CD1 females were killed at the required stage of gestation by exposure to a rising concentration of CO_2, followed by cervical dislocation in line with the regulations of the Home Office Animals (Scientific Procedures) Act 1986. Death was confirmed by pedal reflex. Embryos were isolated by laparotomy as follows; scissors that had been sterilised in 70% ethanol were used to make a small incision across the front of the abdomen. The skin lying above and below the incision was then pulled manually in opposing directions, exposing the underlying abdominal muscles. A pair of toothed forceps was used to hold the anterior abdominal muscle whilst making an incision using scissors, allowing air to enter the peritoneal cavity. The incision was then extended across the abdominal muscles without the hazard of cutting the intestines and contaminating the dissection with gut bacteria [184]. Each gravid uterine horn was removed from the abdomen using toothed forceps cutting tissue free with a pair of scissors, and transferring to a 50ml Falcon tube (Greiner) containing sterile L-15 medium (Gibco, Invitrogen). Embryos were then transferred to a 90mm Petri dish (Greiner) containing L-15 medium where one continuous incision was made along the anti-mesometrial border of each uterine horn, exposing the embryos enclosed within their membranes [184]. Embryos were detached from their uterine horns using a pair of scissors and finally removed from the chorion and amnios using watchmaker's forceps and transferred to a fresh 90mm Petri

dish containing L-15 medium [184]. Embryos were carefully staged according to the criteria set by Theiler (1989) [185].

2.3 Dissection of Superior Cervical and Nodose Ganglia

Embryos were killed by decapitation (as were neonatal pups from P0 to P5) using a pair of scissors. The top of the skull and underlying forebrain was removed and the head was cut in half along the sagittal plane. The jugular foramen was opened up by deflection of the occipital bone using watchmaker's forceps, revealing the nodose and superior cervical ganglia at the mouth of the foramen (Fig. 12) [184]. The nodose ganglion was identifiable due to its spherical appearance and prominent vagus nerve attached to its distal aspect [184]. The SCG is a more elongated structure which was found lying above the carotid artery, attached caudally to the sympathetic chain [184]. Ganglia were then cleaned of adherent tissue using tungsten needles (see section 2.6, below).

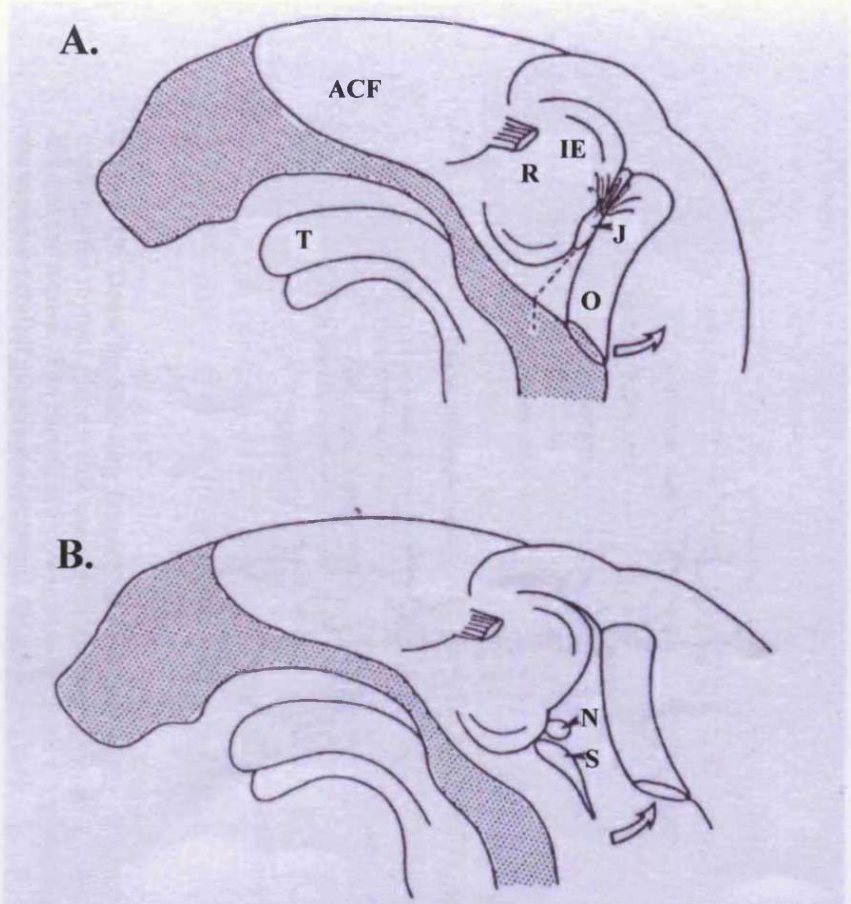

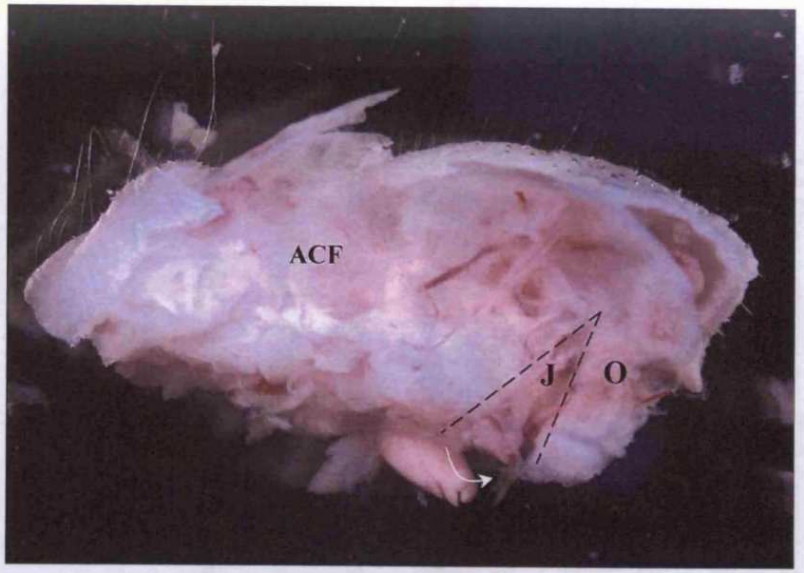

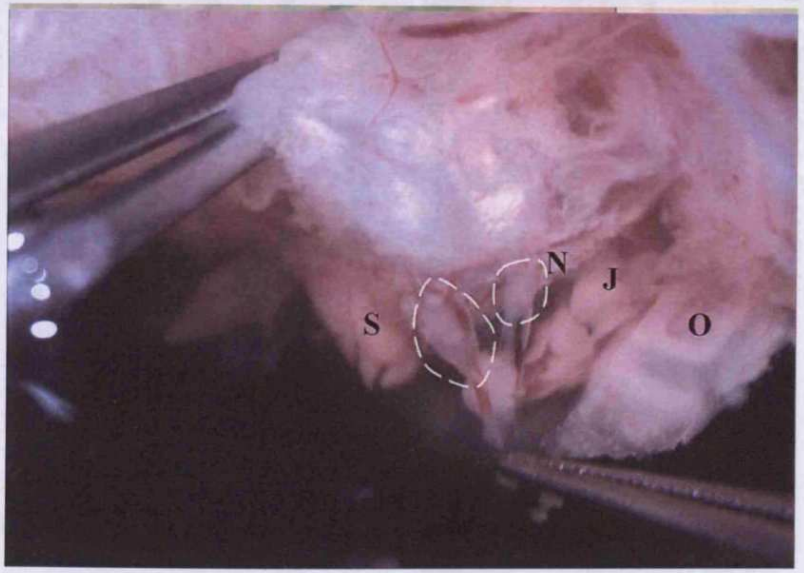

Figure 12: Dissection of Superior Cervical and Nodose Ganglia from the Right Half of a Mouse Head. **A.** The intended opening of the jugular foramen (**J**) by deflection of the occipital bone (**O**) is indicated by the dashed line. **B.** The jugular foramen is opened revealing nodose (**N**) and the superior cervical ganglion (**S**). **C.** the right half of a P4 mouse head showing the deflected occipital bone (**O**) and opening of the jugular foramen (**J**), indicated by a dashed line. **D.** Opened jugular foramen (**J**) revealing the nodose ganglion (**N**), with its prominent vagus nerve attached, and superior cervical ganglion (**S**) lying above the carotid artery. **T**, tongue; **ACF**, anterior cranial fossa; **R**, root of the trigeminal nerve; **IE**, inner ear. **A** and **B** taken from [184].

2.4 Dissection of P20 Superior Cervical Ganglia

Due to the formation of bone in later postnatal ages, P20 SCG were accessed through the neck of adult mice. P20 mice were sacrificed by exposure to a rising concentration of CO_2 without cervical dislocation, avoiding the destruction of tissue around this region. The front of the neck was prepared by squirting the area with 70% ethanol before making a small incision. The skin lying above and below the incision was then pulled manually in opposing directions exposing the thymus gland and the underlying neck muscles. These were pulled away using watchmaker's forceps to reveal the submaxillary glands and the trachea (Fig. 13), the latter was further exposed, cut using forceps and pinned back towards the head of the mouse. The carotid artery was then followed along each side of the neck towards the head until the superior cervical ganglia was reached and removed using forceps. Ganglia were then cleaned of adherent tissue using tungsten needles (see section 2.6).

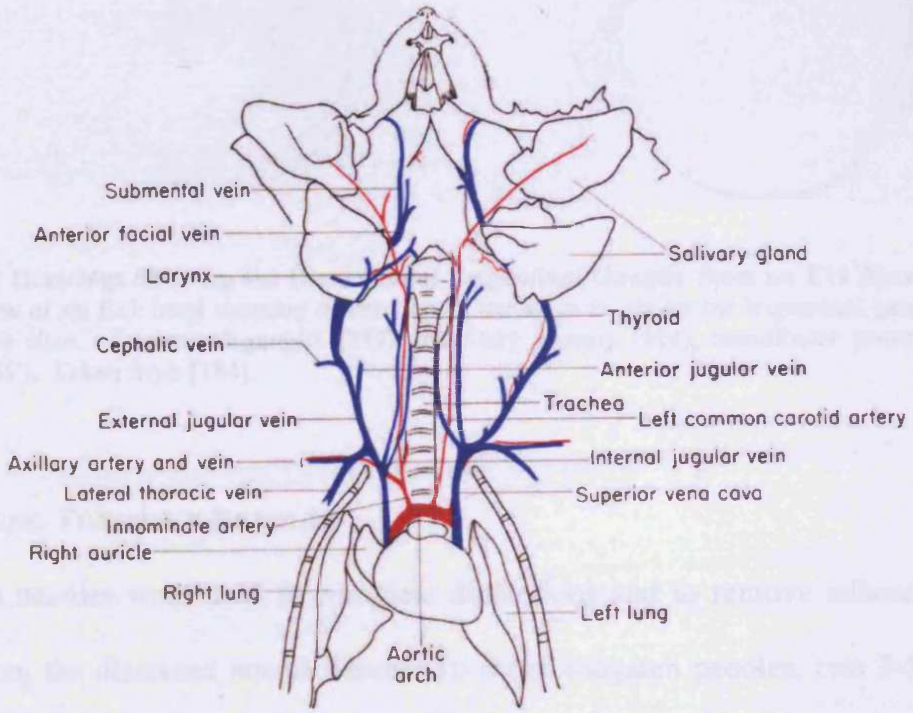

Figure 13: Drawing Showing Dissection of Adult SCG. A small incision was made across the neck exposing the thymus gland. This was pulled away to reveal the trachea which was pinned back, towards the head of the mouse. The carotid artery was then followed along each side of the neck towards the head until the superior cervical ganglia was reached. Taken from [186].

2.5 Dissection of Trigeminal Ganglia

Using a pair of forceps to steady the embryo, a pair of fine scissors was used to cut off the top of the skull in a plane above the eyes and the whisker pads (Fig. 14) [184]. A second cut was made parallel to the first but just passing the mouth [184]. The tissue slices were transferred to a fresh 90mm Petri dish containing L-15 medium and two further cuts were made in front of and behind the trigeminal ganglia which could then be freed using fine watchmakers forceps. Ganglia were then cleaned of adherent tissue using tungsten needles (see section 2.6, below).

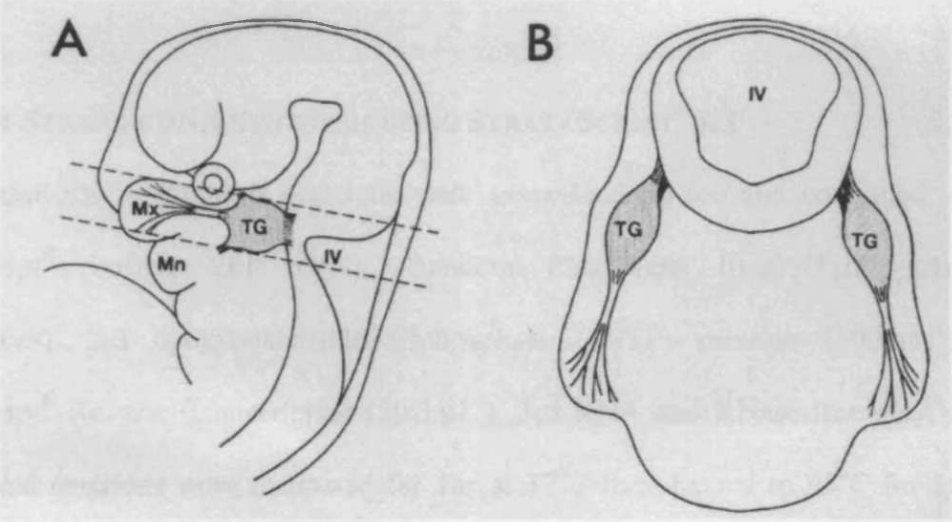

Figure 14: Drawings Showing the Dissection of Trigeminal Ganglia from an E11 Mouse Embryo. A. Lateral view of an E11 head showing orientation of incisions to obtain the trigeminal ganglia. **B.** Rostral view of the slice. Trigeminal ganglia (**TG**), maxillary process (**Mx**), mandibular process (**Mn**), fourth ventricle (**IV**). Taken from [184].

2.6 Making Tungsten Needles

Tungsten needles were used to complete dissections and to remove adherent connective tissue from the dissected neural tissue. To make tungsten needles, two 3-5cm pieces of 0.5mm diameter tungsten wire (Goodfellows, Cambridge) were cut and the end 1cm of each bent by an angle between 60 to 90° [184]. This end was immersed in 1M KOH and a 3-12V AC current was passed through the wire and a second electrode immersed in the

solution [184]. The tungsten is etched away, forming a taper from the bend to the tip of the needle. The needles are then held in chuck-grip platinum wire holders and sterilised using either a Bunsen flame or 70% ethanol.

2.7 Isolation of RNA for Reverse Transcriptase (RT)-PCR

Six to eight ganglia from mice at different developmental ages were collected for each RNA isolation, pelleted and stored at -80°C until required. Isolation of total RNA was achieved using an RNeasy Mini Kit (Qiagen) and carried out according to manufacturer's instructions and stored in RNase-free dH_2O at -70°C until required.

2.8 First Strand cDNA Synthesis using StrataScript® RT

First strand cDNA synthesis reactions were assembled on ice and contained; 4µl 10X StrataScript® buffer, 2µl $pd(N)_6$ Random Hexamers ($0.005U.\mu l^{-1}$; Amersham Biosciences), 2µl deoxynucleoside triphosphate (dNTP) mixture (100mM), 0.38µl StrataScript® Reverse Transcriptase ($50U.\mu l^{-1}$), 3µl RNA and RNase-free dH_2O to 40µl. First strand reactions were incubated for 1hr at 37°C then heated to 95°C for 10mins to inactivate the reverse transcriptase (RT) enzyme. The subsequent cDNA was then stored at -20°C for long periods or 4°C if to be used immediately.

2.9 PCR using *Ex Taq*™ DNA Polymerase (TakaRa)

2.9.1 Calcium-sensing Receptor (GPRC2a) PCR from Murine Ganglia cDNAs

The forward primer CaRmousertFd (5'-ACC TGC TTA CCC GGA AGA GGG CTT T-3'; MWG Biotech) and the reverse primer CaRmousertRv (5'-GCA CAA AGG CGG TCA GGA AAA TGC C-3', MWG Biotech) were designed to amplify a 584bp region of the extracellular domain and 1st transmembrane region encoded by exons 4, 5, 6 and 7

(13.8Kb predicted product from genomic DNA). PCR reactions were assembled in thin walled 0.2ml PCR tubes (Axygen Scientific, Inc.) on ice and contained 5µl 10X *Ex Taq*™ Buffer (TaKaRa), 4µl dNTP mix (2.5mM each; TaKaRa), 0.5µl Forward Primer (100mM), 0.5µl Reverse Primer (100mM), 4µl cDNA template, 0.25µl *Ex Taq*™ DNA Polymerase (5U/µl; TaKaRa) and PCR-grade dH_2O (Gibco, Invitrogen) to 50µl. Samples were amplified using a Geneamp PCR System 9700 thermocycler (Perkin Elmer Applied Biosystems) with an initial denaturing period of 94°C for 2min, followed by 35 cycles of; denaturing at 94°C for 30sec, annealing at 56°C for 30sec and extension at 72°C for 1min. The PCR reaction was ended with a final extension at 72°C for 8min. 6µl of each PCR product was then electrophoretically separated on a 0.8% TAE (Tris Acetate EDTA, see appendix) agarose gel with ethidium bromide ($0.5mg.ml^{-1}$) against 1Kb DNA ladder markers (Bioline). The remaining RT-PCR reaction products were run on a 0.8% TAE agarose gel with ethidium bromide ($0.5mg.ml^{-1}$) and the 584bp CaR-specific band excised with a clean scalpel blade and gel extracted using a Qiaquick Gel Extraction Kit (Qiagen). The purifed DNA was sent to be sequenced (LARK Technologies, Inc.) using the forward primer, CaRmousertFd and sequencing products were then aligned with the GPRC2a sequence using the computer package BioEdit, ensuring the amplification of CaR sequences.

2.9.2 β-Actin PCR from Murine Ganglia cDNAs

The house-keeping gene β-actin was amplified from the same cDNAs as the CaR PCR using the forward primer MouseBActFd (5'-TCC TAG CAC CAT GAA GAT C-3'; MWG Biotech) and the reverse primer MouseBActRv (5'-AAA CGC AGC TCA GTA ACA G-3'; MWG Biotech). The PCR reactions were set up as described in section 2.9.1, however the thermocycling conditions were as follows; an initial denaturing period of

94°C for 2min, followed by 30 cycles of; denaturing at 94°C for 30sec, annealing at 50°C for 30sec and extension at 72°C for 1min. The PCR reaction was ended with a final extension at 72°C for 8min. 6µl of each PCR product was then run on a 0.8% TAE agarose gel with ethidium bromide (0.5mg.ml^{-1}) against 1Kb DNA ladder markers (Bioline) with the expected band size of 189bp for β-actin PCR (314bp product from genomic DNA).

2.10 Quantitative PCR using SYBR® Green (Molecular Probes, Inc.)

2.10.1 SYBR Green I Dye

The fluorescent reporter molecule SYBR Green I is a high affinity double stranded DNA (dsDNA) minor groove binding dye which excites at 497nm and emits at 520nm. The dye exhibits little fluorescence in the unbound state, but increases to over 1000-fold when bound to dsDNA [187]. During denaturation phases of PCR amplification, all DNA becomes single-stranded and at this stage SYBR Green is unbound and not fluorescing. During the annealing step, however, the primers hybridise to the target sequence generating a dsDNA target to which SYBR Green can bind. As the primers are extended by the DNA polymerase the DNA becomes double-stranded, and a maximum incorporation of SYBR Green is reached [187]. This property of SYBR Green I allows the monitoring of PCR product accumulation [187]. However, due to its non-specific binding to dsDNA specificity is determined solely by the oligonucleotide primers, but it is possible that measured fluorescence contains non-specific products (e.g. primer dimers) giving false threshold cycle (Ct) values (see section 2.10.2) [187]. Non-specific signals were detected in PCR reactions by examining the melting curve for each PCR product. The melting temperature of a product is dependent on length; therefore, a single thermal transition in fluorescence intensity would suggest PCR products of the same length [187].

However, multiple thermal transitions would suggest the presence of a mixed population of products [187].

2.10.2 Real-time Quantification

SYBR Green I was used to monitor the progress of each amplification reaction, the fluorescence of which was quantified in real-time through the comparison of threshold cycle values with a standard curve [187]. The threshold cycle (Ct) (Fig. 15) is the first cycle at which the PCR instrument can distinguish amplification-generated fluorescence from background signal [187]. By running a standard curve dilution series with the unknown samples, the Ct value of the unknowns were compared to the standard curve, allowing the determination of the quantity of initial starting material.

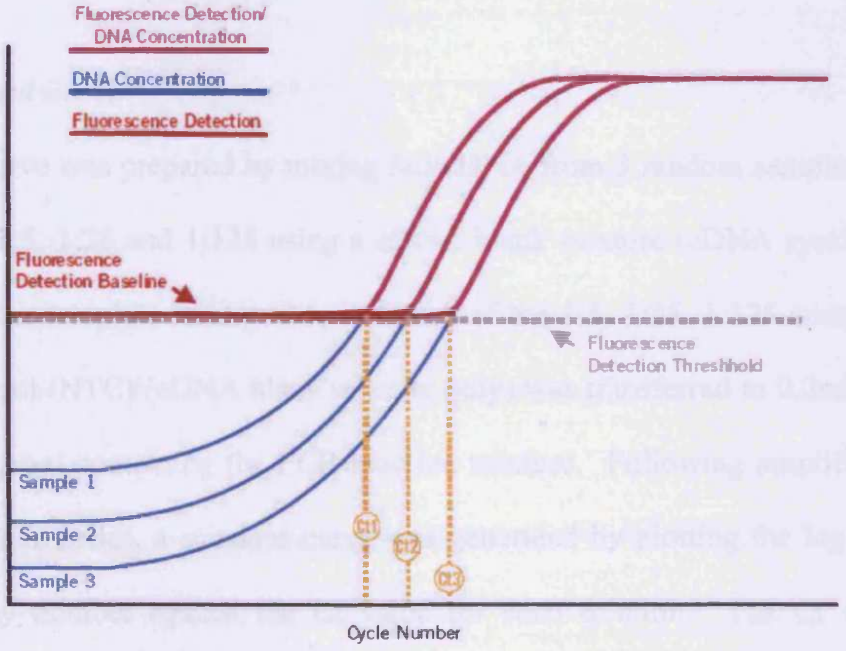

Figure 15: Diagram Showing Fluorescence Detection Threshold and Threshold Cycle (Ct). The threshold cycle is the first cycle detectable above background fluorescence [187].

2.10.3 Preparing Real-time PCR Reactions

Real-time PCR reactions using Brilliant Core QPCR Reagent Kit (Stratagene) were carried out in final volumes of 25µl. However, for convenience and consistency a PCR mastermix was assembled on ice containing; 2.5µl 10X Buffer, 1.5µl 50mM $MgCl_2$ (3mM final), 0.5µl forward / reverse 15µM primer mix, 0.4µl Rox reference dye (2µM; Stratagene), 0.25µl Sybr Green (diluted 1:4000 in dH_2O; Molecular Probes), 0.33µl SureStart *Taq* DNA Polymerase (Stratagene), 1µl dNTPs (20mM; Stratagene) and 15.8µl dH_2O per reaction. The mastermix was mixed well before transferring 22.5µl to 0.2ml optical PCR tubes (Stratagene) where 2.5µl of the appropriate cDNA template was added. For each developmental age, cDNAs from 3 separate RNA isolations were used as template and the entire developmental series was carried out in the same PCR run in either duplicate or triplicate.

2.10.4 Standard Curve

A standard curve was prepared by mixing 5µl cDNA from 3 random samples and serially diluting this 1:5, 1:25 and 1:125 using a cDNA blank mixture (cDNA synthesis reaction mixture without template RNA). 2.5µl of each of the 1:5, 1:25, 1:125 controls and a no template control (NTC) (cDNA blank mixture only) was transferred to 0.2ml optical PCR tubes (Stratagene) containing the PCR reaction mixture. Following amplification of the standard dilution series, a standard curve was generated by plotting the log of the initial template copy number against the Ct value for each dilution. The Ct values of the unknown samples were then compared with the standard curve and the initial template quantities determined.

2.10.5 Calcium-sensing Receptor (GPRC2a) Quantitative PCR

The forward primer (MsCaRPCRFd) 5'-ACC TGC TTA CCC GGA AGA GGG CTT T-3' and the reverse primer (MsCaRPCRRv) 5'-AAT TCA GGT GCC GTA GGT GTT TCA G-3' were designed to amplify a 99bp region of the extracellular domain, encoded by exons 4 and 5. Samples were amplified using a MX3000P real-time spectrofluorimetric thermal cycler (Stratagene) with an initial denaturing period of 95°C for 10min, followed by 40 cycles of denaturing at 95°C for 30sec, annealing at 58°C for 1min, an extension period of 72°C for 30sec. These cycles were then followed by 95°C for 1min, 65°C for 30sec and 95°C for 30sec.

2.10.6 Normalisation Using GAPDH Quantitative PCR

CaR quantitative PCR data were normalised to the reference gene GAPDH [188-190], which was amplified using the forward primer 5'-TCC CAC TCT TCC ACC TTC-3' and the reverse primer 5'-CTG TAG CCG TAT TCA TTG TC-3' from the same cDNA samples. The thermocycling protocol for GAPDH PCR was as described for the *Car* PCR but with modification of the annealing temperature to 51°C. The data were normalised by expressing initial template quantities of the CaR samples as a ratio of GAPDH initial template quantities.

2.11 Immunolocalisation of the CaR in E18 SCG Neurons

E18 SCG neurons grown in 4-well 35mm dishes (Greiner) were fixed after 24hrs using ice cold methanol. Cells were then washed twice with PBS before blocking with 5% [v/v] bovine serum albumin (BSA), 0.02% [v/v] Triton-X100 in phosphate buffered saline (PBS) (Sigma) for 1hr or 4°C overnight. The primary antibody, either an anti-CaR polyclonal raised to an amino acid sequence in the rat CaR carboxy-terminus (a kind gift

from Dr D Shoback), or an anti-CaR polyclonal raised to an amino acid sequence in the human CaR N-terminus (Imgenex) were used 1:100 and 1:200, respectively, in 1% [v/v] BSA, 0.02% [v/v] Triton-X in PBS, together with a monoclonal β-III tubulin antibody (R&D Systems) (used at 1:1000) as a neuronal marker and incubated overnight at 4°C.

The cells were then washed three times with PBS before applying the secondary antibodies, Alexa 488-conjugated anti-rabbit IgG (Molecular Probes) and Alexa 594-conjugated anti-mouse IgG (Molecular Probes) diluted 1:500 in 1% [v/v] BSA, 0.02% [v/v] Triton-X in PBS for 90mins at room temperature, protected from light. The secondary antibodies were removed and the cells washed a further three times with PBS. Immunofluorescence was visualised using a Zeiss laser scanning microscope LSM 510 and images were acquired and processed using LSM 510 software.

2.12 Breeding and Maintenance of Transgenic Mice

Experiments requiring CaR-deficient or Bax-deficient animals were mated and genotyped as described in section 2.13. All mice were fed on Rodent Global Diet pellets (Harlan) and given water *ad libidum*. The CaR mice were derived from the mice heterozygous at the *Pth* and *Car* loci, generously provided by Dr Claudine Kos, Tufts University, Boston, Massachusetts. USA. Lines were kept on a C57Bl6 background and maintained by breeding $Car^{+/-}$ males to $Car^{+/+}$ females. Mice wild-type, heterozygous and deficient for the CaR required for experiments were generated by overnight matings of $Car^{+/-}$ males with $Car^{+/-}$ females. Furthermore, Bax-deficient embryos required for experiments were generated from overnight matings of $Bax^{+/-}$ CD1 males with $Bax^{+/-}$ CD1 females. Breeding was confirmed by the presence of a vaginal plug and the period of gestation was considered to be embryonic day (E) 0.5.

2.13 GENOTYPING

2.13.1 Genomic DNA isolation

Genomic DNA was isolated from tail tips for routine colony maintenance using Nucleospin® Tissue kit (Macherey-Nagel) according to the manufacturer's instructions. For rapid genomic DNA extraction from embryonic or early post-natal tissue, a Maxwell™ 16 Blood Purification Kit (Promega) was used in combination with a Maxwell™ 16 Instrument and carried out according to the manufacturer's instructions.

2.13.2 CaR/Pth Genotyping PCR

To determine the genotype at the *Car* locus, two PCR amplification reactions were required for each animal. To detect the wild-type *Car* allele samples were amplified with the *Car* forward primer CaR6h-'5 (Table 3) and the CaR reverse primer CaR6h-'3. To detect the presence of the null CaR allele, Neo forward primer r-Neo-2 was used with the *Car* reverse primer CaR6h-'3. The wild type *Pth* allele was detected using PTH forward primer PTHF2 and the *Pth* reverse primer PTHR2. The null *Pth* allele was detected using the Neo forward primer r-Neo-2 and the PTH reverse primer PTHR2.

Primer	Sequence	Supplier
CaR6h-'5	5'-TCT GTT CTC TTT AGG TCC TGA AAC A-'3	MWG Biotech
CaR6h-'3	5'-TCA TTG ATG AAC AGT CTT TCT CCC T-'3;	MWG Biotech
r-Neo-2	5'-TCT TGA TTC CCA CTT TGT GGT TCT A-'3	MWG Biotech
PTHF2	5'-GAT GTC TGC AAA CAC CGT GGC TAA-'3	MWG Biotech
PTHR2	5'-TCC AAA GTT TCA TTA CAG TAG AAG-'3	MWG Biotech

Table 3: Primer and Molecular Beacon Sequences Used for the Genotyping of CaR- and PTH-Deficient Animals.

Car/Pth genotyping reactions carried out as a modified method of Kos *et al* (2003) [131]. Reactions were assembled in thin walled 0.2ml PCR tubes (Axygen Scientific, Inc.) on ice and contained 2µl 10X ExTaq Buffer (TaKaRa), 1.6µl dNTP mix (2.5mM each), 0.2µl Forward Primer (100mM), 0.2µl Reverse Primer (100mM), 1µl cDNA template, 0.1µl *Ex Taq*™ DNA Polymerase (5U/µl; TaKaRa) and PCR-grade dH_2O to 20µl. Samples were amplified using a Geneamp PCR System 9700 thermocycler (Perkin Elmer Applied Biosystems) with an initial denaturing period of 94°C for 2mins, then 35 cycles of 94°C for 30sec, 55°C for 30sec, 72°C for 45sec followed by a final amplification step of 72°C for 7min. PCR products were then run on a 1% TAE agarose gel with ethidium bromide ($0.5mg.ml^{-1}$) (see Appendix) against 1Kb DNA ladder markers (Bioline) with the following expected band sizes; wild-type *Car* allele ~220bp, null *Car* allele ~270bp, wild-type PTH allele ~650bp and null PTH allele ~250bp.

2.13.3 Bax Genotyping Real-time PCR Using Molecular Beacons

Bax embryos were genotyped using molecular beacons (Fig. 16); probes consisting of a hairpin loop structure where the central loop sequence is complementary to the target and the stem arms are complementary to each other [187]. The 5' end of the beacon is modified with a reporter fluorophore and the 3' end carries a quenching compound which, in the absence of target DNA, absorbs the energy of the reporter proximal to it when in the hairpin conformation. In the presence of target DNA, however, annealing of the central loop sequence to its target is the preferred conformation, where the reporter and quencher are separated and reporter fluorescence can be detected.

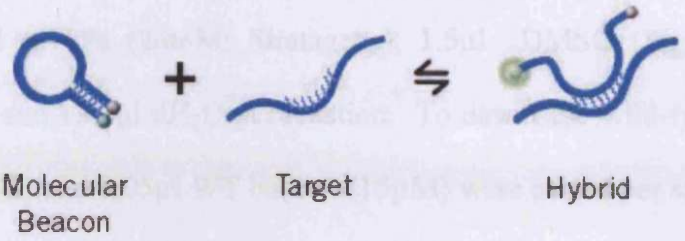

Figure 16: Molecular Beacon Chemistry. The probe consists of a hairpin loop structure where the central loop sequence is complementary to the target and the stem arms are formed by internal sequences complementary to each other. On binding the target, the reporter and quencher are separated and reporter fluorescence can be detected. Taken from [187].

To determine the genotype at the *Bax* locus two real-time PCR amplification reactions were required for each animal. To detect the wild-type *Bax* allele samples were amplified with the forward primer Baxwt F2 (Table 4) with the common primer, BaxCommon, and the WT beacon. To detect the null allele, samples were amplified with the forward primer BaxKO F2 with the BaxCommon primer and the KO beacon.

Primer / Beacon	Sequence	Supplier
BaxwtF2	5'-CTA GAG GGT GCT GAG GAG TC-3'	MWG Biotech
BaxKO F2	5'-CGG TGG ATG TGG AAT GTG-3'	MWG Biotech
BaxCommon	5'-AGG AAG GTC TCA AGT ATA GC-3'	MWG Biotech
WT beacon	5'-FAM-CGC GAT CCG GAG GAA GTC CAG TGT CCA GCG ATC GCG-BlackholeQuencher1-3'	MWG Biotech
KO beacon	5'-HEX-CGC GAT CCA TGC TCC AGA CTG CCT TGG GAA AGA TCG CG-BlackholeQuencher1-3'	MWG Biotech

Table 4: Primer and Molecular Beacon Sequences Used for the Genotyping of Bax-Deficient Animals.

Real-time genotyping PCR reactions using Brilliant Core QPCR Reagent Kit (Stratagene) were carried out in final volumes of 25µl. A PCR mastermix was assembled on ice containing; 2.5µl 10X Buffer, 2.5µl 50mM $MgCl_2$ (5mM final), 1µl ROX (carboxy-X-

rhodamine) reference dye (2μM; Stratagene), 0.6μl Sure Start *Taq* DNA Polymerase (Stratagene), 1μl dNTPs (20mM; Stratagene), 1.5μl DMSO (Sigma), 0.1μl common primer (150μM) and 13.3μl dH_2O per reaction. To detect the wild-type *Bax* allele 0.15μl WT primer (15μM) and 0.05μl WT beacon (15μM) were added per sample. To detect the null *Bax* allele instead 0.25μl KO primer (15μM) and 0.025μl KO beacon (15μM) were added per sample. The mastermix was mixed well before transferring 22.5μl to 0.2ml optical PCR tubes (Stratagene) where 2.5μl of the appropriate cDNA template was added. Samples were amplified using a MX3000P real-time PCR machine (Stratagene) with an initial denaturing period of 95°C for 10min, followed by 40 cycles of denaturing at 95°C for 30sec, annealing at 52°C for 1min, an extension period of 72°C for 30sec. These cycles were then followed by 95°C for 10min, 65°C for 30sec and 95°C for 30sec. The presence of a wild-type or null *Bax* allele was detected by an increase in fluorescence of the (FAM) (carboxyfluorscein) (WT) or HEX (6-carboxy-2',4,7,7'-tetrachlorofluorscein) (KO) fluorophores. The isolation of Bax-deficient neurons was further confirmed by setting up neuronal cultures from *Bax* heterozygous and *Bax* null embryos, in the absence of NGF, and assessing neuronal survival after 24hrs in culture.

2.14 Preparing Dissociated Neuronal Cultures

2.14.1 Preparation of Culture Substratum

Neurons were grown on a laminin/poly-ornithine substratum. Dishes were prepared by transferring either 1ml poly-DL-ornithine (Sigma) / borate solution (see Appendix) to 35mm tissue culture dishes (Greiner), or 250µl to each well of a 4-well dish (Greiner), and left overnight at room temperature [184]. The poly-ornithine solution was aspirated the following morning and the dishes were washed twice with sterile distilled water before being allowed to air dry in the laminar flow hood. Two to three hours prior to use, 100µl of a 20mg.ml^{-1} solution of laminin (Sigma) in Hank's Balance Salt Solution (HBSS) (Gibco, Invitrogen) was transferred to the center of each dish and subsequently spread over the dish surface [184]. The dishes were then placed in a tissue culture incubator for 2-3hrs. The dishes were then removed from the incubator and washed twice with sterile distilled water, taking care not to allow the dishes to dry out, and then 1ml of medium added immediately after washing.

2.14.2 Preparation of Culture Medium

Ham's Modified F-14 (JRH Biosciences) was obtained in powered form where a 10X concentrate would be made, including the antibiotics penicillin G (Sigma) and streptomycin sulphate (Sigma) (final concentrations in 1X F-14; 179.4µM and 68.6µM, respectively) and stored as 25ml aliquots at -20°C [184]. To make 1X F-14, 500mg sodium hydrogen carbonate (BDH) was dissolved in 250ml tissue culture-grade distilled water (Gibco, Invitrogen), 25ml of this was then replaced with the 10X F-14 concentrate. The 1X F-14 solution was then supplemented with 2.5ml 200mM glutamine (Gibco, Invitrogen) (2mM final) and 5.5ml of an Albumax I solution containing Albumax I (Gibco, Invitrogen), progesterone, putrescine, L-thyroxine, sodium selenite and tri-

iodothyronine (all Sigma) (see Appendix) [184]. The supplemented F-14 medium was then filter sterilised using a 0.2μm Acrocap filter unit (Pall Corporation) and stored at 4°C for up to a month.

2.14.3 Dissociation of Neurons

Ganglia were resuspended in 950μl HBSS (Gibco, Invitrogen) and 50μl 1% trypsin (See Appendix; Worthington) was added and mixed [184]. The trypsin-HBSS mixture was then incubated at 37°C for a period of time suitable for that developmental age (see Table 5).

Dev. age	Time in 0.05% trypsin
E15	10mins
E16	15mins
E18	20mins
P0	25mins
P1	25mins

Table 5: The Incubation Time Required in 0.05% Trypsin at 37°C for Ganglia of Different Developmental Ages.

The trypsin-HBSS mixture was then aspirated and the ganglia were washed twice with 1ml F-12 (Gibco, Invitrogen) with 10% [v/v] heat inactivated horse serum (HIHS), to inactivate any residual trypsin [184]. The F-12/10% HIHS was then aspirated and replaced with a suitable volume (0.5-1ml) of F-14. A single cell suspension was made by trituration using a siliconised pipette (see Appendix; Fisher Scientific), the end of which had been polished to a fine bore using a bunsen burner. The tissue was taken up into the pipette slowly and expelled with firm pressure, avoiding over-trituration and the introduction of bubbles. Trituration was monitored by pipetting 10μl of the cell suspension onto a lid of a 35mm dish and examined under a phase contrast Nikon Diaphot inverted microscope [184]. Trituration was complete when only connective tissue

fragments were present in the cell suspension and single neurons, with fairly long processes, were visible under the microscope [184].

2.15 Experimental Treatments

2.15.1 7S mNGF

Murine 7S nerve growth factor (mNGF 7S) (Calbiochem), isolated from mouse submaxillary glands, was used throughout this study. The 7S mNGF holoenzyme is a 130kDa complex consisting of five subunits ($\alpha_2\beta\gamma_2$), the α-subunit is an inactive serine protease and the γ-subunit is an active serine protease capable of processing the β-NGF precursor protein [191]. 7S mNGF was used throughout this study to support the survival and growth of sympathetic neurons in culture.

2.15.2 $Ca^{2+}{}_o$ and NPS Pharmacological Compounds

The effects of $[Ca^{2+}]_o$ and the calcimimetic NPS-467R and the calcilytic NPS-89636 compounds on neurite outgrowth and neuronal survival were studied. The $[Ca^{2+}]_o$ in the cell culture medium was adjusted by either chelation with EGTA (ethylene glycol tetraacetic acid) (Sigma) (using 1mM EGTA to lower $[Ca^{2+}]_o$ by 1mM to give a predicted value) or by supplementing with $CaCl_2$ (BDH). Actual free $[Ca^{2+}]_o$ after the addition of EGTA or $CaCl_2$ was determined by use of a radiometer ABL system 625 and corrected to 37°C, pH 7.4 (Table 6). The compounds NPS-467R and NPS-89636 were made to 10mM stocks in DMSO and diluted to 1mM with sterile tissue culture grade dH_2O (Gibco, Invitrogen). Further dilution of these compounds to micromolar working stocks was achieved using sterile tissue culture grade dH_2O (Gibco, Invitrogen).

Predicted $[Ca^{2+}]_o$	Actual $[Ca^{2+}]_o$*	0.5M EGTA to add	1M $CaCl_2$ to add
0.5mM	0.73mM	5.72µl	-
1.2mM	1.07mM	2.92µl	-
1.9mM	1.42mM	-	-
2.6mM	1.98mM	-	1.34µl
3mM	2.28mM	-	2.14µl
3.5mM	2.63mM	-	3.14µl
5mM	4.15mM	-	6.14µl

Table 6: Predicted and actual $[Ca^{2+}]_o$ at 37°C, pH 7.4 determined using a radiometer ABL system 625 after the addition of EGTA or $CaCl_2$. * = Actual concentration at 37°C, pH 7.4

2.15.3 Caspase Inhibitors and Bax-Deficient Neurons

Caspases are cysteine-dependent, aspartate-dependent proteases which exist as latent precursors and when activated by limited proteolysis, initiate a cell death program by cleaving key components of the cell infrastructure and activate additional apoptotic mechanisms [192]. Caspase activation can occur by either the receptor mediated (Fas ligand / TNFα-mediated) apoptotic pathway, leading to the activation of pro-caspase 8, or the mitochondrial apoptotic pathway, resulting in the association of Bcl-2 family members with the mitochondria, release of cytochrome c and activation of pro-caspase 9 [192]. The broad spectrum caspase inhibitor III (Boc-D-FMK) (Calbiochem), used in this study, acts by binding irreversibly to the caspase active site, directed by a peptide recognition sequence bound to a functional group (fluromethylketone, FMK).

Neurons deficient in Bax were used as an alternative means of preventing apoptosis in the absence of neurotrophic support. Bax is a death promoting member of the Bcl-2 family of proteins, involved in the permeabilisation of the outer mitochondrial membrane and release of cytochrome c after its activation and the induction of apoptosis (reviewed by [193]). Targeted disruption of the *Bax* gene has shown that Bax is required for naturally

occurring cell death of different populations of peripheral and CNS neurons during normal development [50, 51].

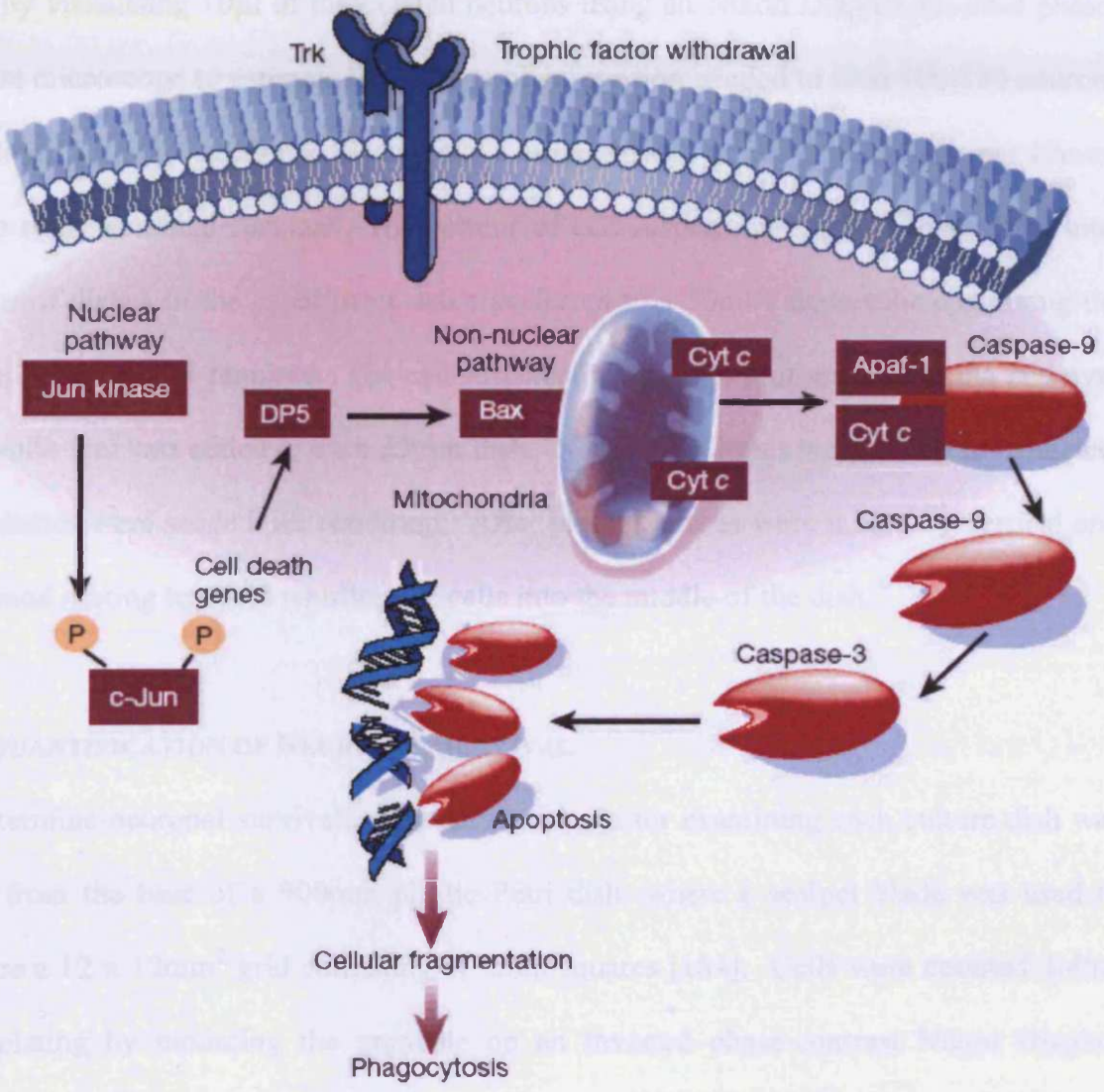

Figure 17: Activation of Apoptosis in Sympathetic Neurons by Trophic Factor Withdrawal. Trophic factor withdrawl normally induces JNK activation, activating c-Jun and inducing the expression of DP-5 which may activate Bax. Neurotrophin withdrawal also induces a non-nuclear pathway, resulting in the association of Bcl-2 family members with the mitochondria, release of cytochrome c and activation of pro-caspase 9. Taken from [194].

2.16 Seeding Neurons

Neurons were seeded in laminin-coated 35mm dishes already containing 1ml F-14 with twice the final concentration of NGF (Calbiochem) and the experimental treatment (EGTA, $CaCl_2$, NPS-467R or NPS-89636) where appropriate. A cell suspension was made by visualising 10µl of dissociated neurons using an Nikon Diaphot inverted phase-contrast microscope to estimate the volume of suspension needed to seed 100-150 neurons per $12mm^2$ grid (see section 2.17) to study neurite growth, or 200-250 neurons per $12mm^2$ grid to study neuronal survival. The volume of cell suspension required to seed the total number of dishes in the experiment was transferred to a 50ml Falcon tube containing the total volume of F-14 required. The cell suspension was kept uniform by mixing end over end, while 1ml was added to each 35mm dish. Neuronal cultures were set up in triplicate; three dishes were seeded per condition. After plating, dishes were mixed by vertical and horizontal mixing to avoid whirling the cells into the middle of the dish.

2.17 Quantification of Neuronal Survival

To determine neuronal survival, a standard graticule for examining each culture dish was made from the base of a 900mm plastic Petri dish, where a scalpel blade was used to inscribe a 12 x $12mm^2$ grid consisting of 2mm squares [184]. Cells were counted 3-4hrs after plating by mounting the graticule on an inverted phase-contrast Nikon Diaphot microscope [184]. Each dish was then placed over the graticule and the number of neurons present in the $12mm^2$ grid was then counted [184]. Neurons which had not attached to the substratum were ignored. The number of phase-bright neurons in all dishes was counted at 24hr intervals until necessary. The number of phase-bright neurons at 24hr or 48hrs was then expressed as a percentage of the initial cell count. For each survival experiment, the mean percentage survival from three dishes per condition was determined.

2.18 Analysis of Neurite Outgrowth

Neurons, on which neurite outgrowth was to be studied, were plated at a density of 100-150 neurons per 12mm^2 grid in 35mm dishes. In preliminary experiments neurons were fixed after 24hrs in culture by aspirating the culture medium and adding 1ml ice-cold methanol and leaving for 10mins at room temperature. The methanol was removed and the cells washed twice with PBS. Cells were then blocked with 5% [w/v] BSA, 0.02% [v/v] Triton-X100 in PBS for 1hr or 4°C overnight. A mouse monoclonal βIII-tubulin antibody (Abcam) diluted 1:1000 in 1% [w/v] BSA, 0.02% [v/v] Triton-X100 in PBS was transferred to the dishes and incubated overnight at 4°C. The cells were then washed three times with PBS before applying the Alexa 488-conjugated anti-mouse IgG secondary antibody (Molecular Probes) (1:500 in 1% [w/v] BSA, 0.02% [v/v] Triton-X in PBS) for 90mins at room temperature in the dark. The secondary antibody was removed and the cells washed a further 3 times with PBS.

Alternatively neurons were fluorescently labelled using calcein-acetoxymethyl ester (AM) fluorogenic esterase substrate (Molecular Probes, Invitrogen). Calcein-AM (1mg.ml^{-1} in dry DMSO) was added to cell culture medium to 1µg.ml^{-1} and incubated for 10-30mins. The dye is retained in cells that have intact membranes but does not label dead cells. For every condition studied, 40 to 70 neurons were digitally captured using either a Zeiss laser scanning microscope LSM 510 or Zeiss Axiovert 200 inverted fluorescent microscope using SimplePCI software on which Sholl analysis [195] was carried out. Neuron images were analysed using a customised Matlab script for the automatic counting of number of primary dendrites, the number of branch points, total dendritic length and other morphological parameters. Concentric, digitally generated rings 30µm apart, were centered on the cell soma of each neuron, and the neurites intersecting each ring were

counted and neurite terminals marked. These data were then shown as the number of intersections with distance from the cell soma, total neurite length and number of branch points.

2.19 Ballistic Transfection

Transfection of dissociated neurons was carried out using a hand held Helios Gene gun (Biorad Hercules, USA). Gold particle cartridges were prepared using the manufacturer's protocol. 15mg of 1.6μm gold particles (Biorad) (to prepare 10 cartridges) were suspended in 100μl 50mM spermidine and 2.5μg pYFP (Clontech) alone or with 10μg CaR- or DNCaR-pcDNA3.1 constructs. The gold particles were then precipitated in 100μl 2mM $CaCl_2$ for 15mins at room temperature. During this time a 20cm length of Teflon tubing was dried using nitrogen gas in a tubing prep station (Biorad) (Model PDS-1000/HE Biolistic Particle Delivery System). The gold particles were then spun down briefly, the supernatant removed and replaced with 1ml of 100% ethanol and vortexed well. The gold particles were washed a further two times with 100% ethanol, resuspended in 300μl 100% ethanol and transferred to a fresh microfuge tube. Remaining gold particles were resuspended with a further 300μl 100% ethanol and then finally pooled. The gold particles were loaded into Teflon tubing by drawing the suspension into the tubing using a syringe and leaving for 3mins for the gold to settle. The ethanol was removed using a syringe and the tubing dried for 5-10mins using nitrogen gas. The gold-coated tubing was cut into 13mm lengths using a tubing cutter (Biorad) and used either immediately or stored at 4°C for up to 4-5 weeks until required.

For transfecting dissociated neurons, high density cultures were established from 20-28 ganglia where 1000-3000 neurons were plated in a 50μl droplet in the centre of each

35mm culture dish. Neurons were incubated at 37°C / 5% CO_2 for 2-3hrs to allow the cells to adhere before removing the culture medium from each dish prior to transfection. The coated gold microcarriers were shot into the cultured neurons at a pressure of 140pSi. A 70μm nylon mesh screen was placed between the gun and the culture to protect the cells from the pressure wave. Immediately after transfection, 1ml (to limit the use of expensive pharmacological agents) of defined medium was added to the culture dishes.

2.20 Quantification of Neuronal Survival and Neurite Outgrowth within Transfected Cultures

Fluorescent images were taken after 24hrs in culture using a Zeiss Axiovert 200 inverted fluorescent microscope and neurite outgrowth quantified according to methods described in section 2.18. YFP-labelled neurons were counted 24hrs after plating using a Zeiss Axiovert 200 inverted fluorescent microscope and again at 48hrs. The number of neurons surviving at 48hrs was then expressed as a percentage of the initial number of neurons counted at 24hrs.

2.21 Organotypic Hippocampal Slice Cultures

Hippocampal slice cultures were prepared by Dr. Humberto Gutierrez. Hippocampi of P4 pups were dissected and 300μm slices were cut in a coronal plane using a McIlwain Tissue Chopper vibrotome (The Mickle Laboratory Engineering Co. Ltd.) in cold (4°C) artificial cerebrospinal fluid (160mM NaCl, 200mM KH_2PO_4, 5mM KCl, 1mM $MgSO_4$, 33mM glucose, 10mM HEPES, 1mM $CaCl_2$). Hippocampal slices were transfected with two triple transfections, combined within the same cartridge; pYFP, Bcl-X_L and pcDNA3.1 (control) and pRFP, Bcl-X_L and DN CaR-pcDNA3.1. The slices were cultured in 35mm Petris dishes (Greiner) on 0.4μm Millicel inserts (Millipore) floating on 1ml of

culture medium (50% Dulbecco's Minimal Essential Medium, 25% heat-inactivated horse serum, 25% Hanks Balanced Salt Solution, 6.5mg.ml^{-1} glucose and 100U.ml^{-1} streptomycin and penicillin). The cultures were incubated in a humidified 5% CO_2 atmosphere at 37°C. Fluorescent images were acquired and analysed according to methods described in section 2.18.

2.22 Generating a Dominant Negative (R185Q) CaR Construct using Site-Directed Mutagenesis (SDM)

Site-directed mutagenesis was carried out using Quikchange II XL Site-Directed Mutagenesis Kit (Stratagene) to introduce the G to A point mutation in the second position of the 185 codon of the human parathyroid CaR sequence [135]. This procedure relies on a methylated supercoiled double-stranded DNA plasmid and two oligonucleotide primers containing the desired mutation (Fig. 18). The oligonucleotide primers, complementary to opposite strands of the plasmid, are incorporated and extended using a high fidelity DNA polymerase. Extension of the oligonucleotide primers generates a mutated plasmid containing staggered nicks. Following thermocycling, the reaction product is treated with *Dpn* I restriction enzyme which is specific for methylated and hemi-methylated DNA and digests the parental (i.e. non-mutated) supercoiled dsDNA, selecting for the mutated, un-methylated nicked plasmid DNA.

Primers were designed to introduce the required point mutation to generate the R185Q polymorphism in the human parathyroid CaR sequence using PrimerX, a computer package to aid the design of mutagenic primers for site-directed mutagenesis (SDM). The forward primer R185Qfd (5'-CAA TTC AAG TCT TTC CTC CAA ACC ATC CCC AAT GAT GAG -3'; Sigma Genosys) and reverse primer R185Qrv (5'-CTC ATC ATT

GGG GAT GGT TTG GAG GAA AGA CTT GAA TTG-3'; Sigma Genosys) were PAGE purified to reach the required mutation efficiency.

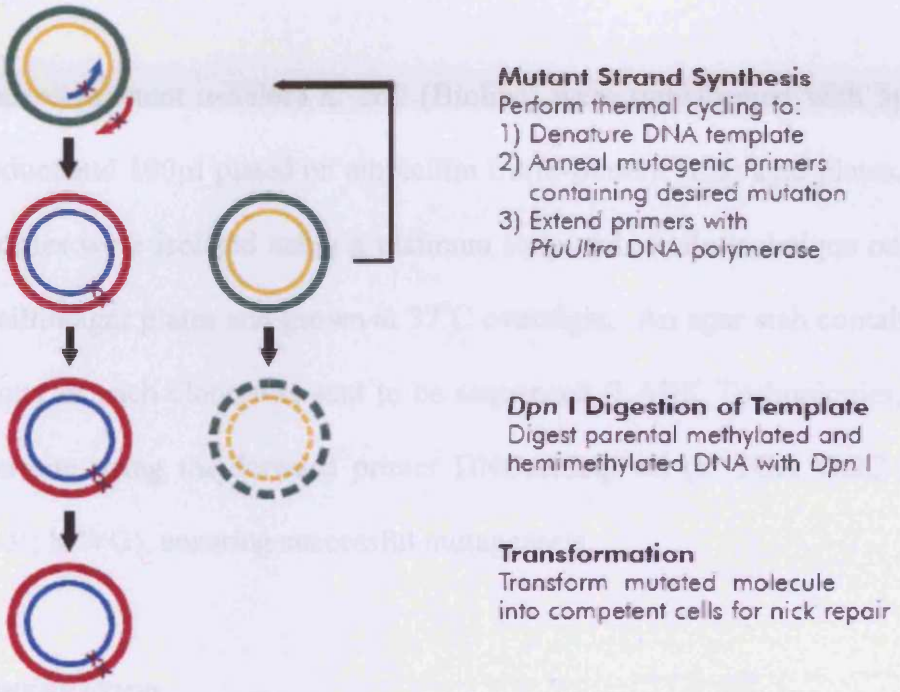

Figure 18: Diagram Showing the Principle of Site Directed Mutagenesis using Quikchange II XL Site-Directed Mutagenesis Kit. Taken from [196].

The site-directed mutagenesis reaction was assembled on ice using a thin walled 0.2ml PCR tube (Axygen Scientific, Inc.) and contained 5µl 10X reaction buffer (Stratagene), 1µl template (10ng HuPCaR-pcDNA3.1), 1µl forward primer (125ng.µl $^{-1}$), 1µl reverse primer (125ng.µl^{-1}), 1µl dNTP mixture (Stratagene), 3µl QuikSolution (Stratagene) and PCR-grade dH_2O (Gibco, Invitrogen) to 50µl. Finally, 1µl *PfuUltra* High Fidelity DNA Polymerase (2.5U/µl; Stratagene) was then added. The sample was amplified using a Geneamp PCR System 9700 thermocycler (Perkin Elmer Applied Biosystems) with an initial denaturing period of 95°C for 1min followed by 18 cycles of denaturing at 95°C for 50secs, annealing at 60°C for 50secs, extension at 68°C for 9mins (1min/kb of plasmid)

and a final extension of 68°C for 7mins. Following thermocycling the reaction was placed on ice for 2min to cool the reaction to ≤37°C. 1µl *Dpn* I restriction enzyme (10U.µl^{-1}; Stratagene) was then added and the mixture centrifuged for 1min at 16,000xg. The mixture was then immediately incubated at 37°C for 1hr to digest the parental DNA.

100µl of supercompetent α-Select *E. coli* (Bioline) were transformed with 5µl of SDM reaction product and 100µl plated on ampicillin Luria-Bertani (LB)/agar plates. Five well isolated colonies were isolated using a platinum loop and sterile technique on individual plates ampicillin/agar plates and grown at 37°C overnight. An agar stab containing a well isolated colony of each clone was sent to be sequenced (LARK Technologies, Inc.) over the mutation site using the forward primer DNCaRSeqFwd (5'-TCA GGC GTC TCC ACG GCA-3'; MWG), ensuring successful mutagenesis.

2.23 Iris Innervation

Tyrosine hydroxylase (TH), the first enzyme in catecholamine synthesis which catalyses the conversion of L-tyrosine to L-DOPA (Fig. 19), is highly localised to noradrenergic neurons of the SCG [197]. The SCG innervates multiple targets in the head and neck, including the iris, which is supplied by the external carotid nerve. Moreover, a 99% decrease in TH activity in the iris can be seen after bilateral ganglionectomy of the SCG [198], indicating sympathetic innervation of the iris is almost entirely from the SCG.

The eyes from P1 and P2 pups were dissected out and fixed in formalin (BDH) overnight at 4°C. Eyes were then transferred to 25% [w/v] sucrose in PBS and left overnight, or until required, at 4°C. Serial 15µm coronal sections were taken by mounting the eye in Tissue Tek® O.C.T.™ compound (SAKURA) on a cryostat chuck with the lens facing

upwards and fixed in position by freezing to -30°C. Coronal sections were taken from the cornea to the bottom of the lens using a Bright 5030 microtome (Bright Instrument Company Ltd.) and transferred to superfrost slides (BDH).

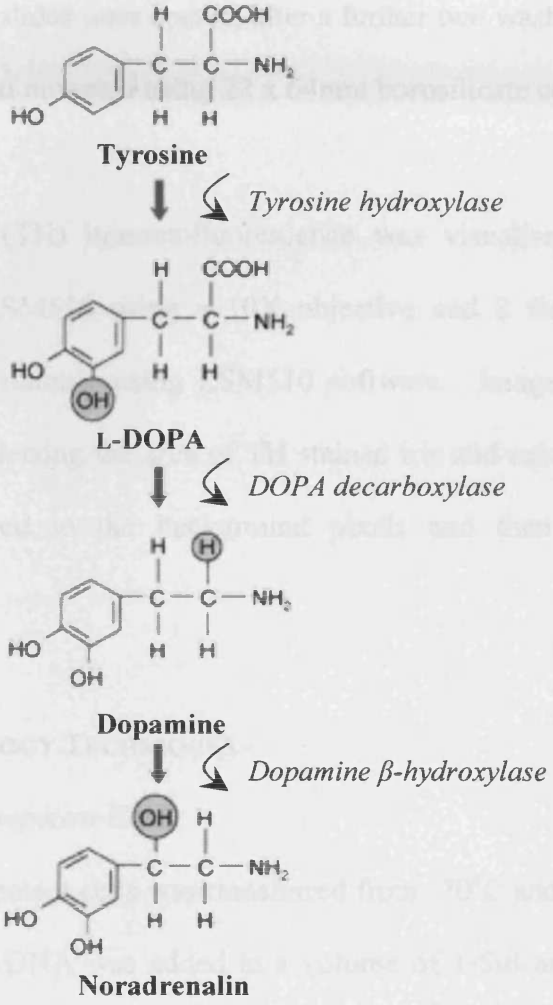

Figure 19: The Noradrenalin Biosynthetic Pathway. Tyrosine hydroxylase catalyses the conversion of tyrosine to dihydroxyphenylalanine (DOPA), the rate limiting step in this pathway. DOPA decarboxylase converts DOPA to dopamine, which is subsequently converted to noradrenalin by dopamine β-hydroxylase.

The slides were covered in aluminium foil, dried overnight before blocking in 10% [v/v] normal goat serum (NGS) (Sigma), 0.1% [v/v] Triton-X100 (Sigma) in PBS for 1hr at room temperature. An anti-tyrosine hydroxylase polyclonal antibody (Chemicon) was used 1:200 in 2% [v/v] NGS, 0.02% [v/v] Triton-X100 (Sigma) in PBS overnight at 4°C.

The sections were washed three times with PBS before incubation with an Alexa 594-conjugated secondary antibody (Molecular Probes) diluted 1:500 in 2% [v/v] NGS, 0.02% [v/v] Triton-X100 (Sigma) in PBS for 2hrs at room temperature. The sections were further stained using DAPI (Molecular Probes) diluted 1:1000 [v/v] in PBS for 5min at room temperature. The slides were coated, after a further two washes with PBS, with 50% glycerol [v/v] in PBS and mounted using 22 x 64mm borosilicate coverglass (BDH).

Tyrosine Hydroxylase (TH) immunofluorescence was visualised using a Zeiss laser scanning microscope LSM510 using a 10X objective and 2 fields were captured per section displaying TH staining using LSM510 software. Images were analysed using Adobe Photoshop by selecting the area of TH stained iris and calculating the ratio of TH specific pixels compared to the background pixels and then expressing this as a percentage.

2.24 Molecular Biology Techniques

2.24.1 Transforming Competent Cells

A 100µl aliquot of competent cells was transferred from -70°C and thawed on ice. To the competent cells 5-20ng DNA was added in a volume of 1-5µl and incubated on ice for 30mins. Competent *E. coli* were heat shocked at 42°C for 30secs and returned to ice for 2min before adding 800µl LB and shaking at 37°C for 45mins. A 100µl aliquot of transformation reaction was subsequently spread onto selective LB/agar plates before pelleting remaining cells at 2500 x g in an Eppendorf 5417C centrifuge, resuspending in 100µl LB and spreading as before.

2.24.2 Plasmid DNA Preparations

Plasmid DNA was obtained from *E. coli* cells either by QIAprep Spin Miniprep Kit (Qiagen) or Plasmid Midi Kit (Qiagen) depending on application and carried out according to manufactures instructions. Plasmid DNA was eluted or resuspended in either 10mM Tris.Cl pH 8.5 or molecular biology grade dH_2O.

2.24.3 Restriction Endonuclease Digests

All restriction endonuclease digests were assembled on ice, in 1.5ml microfuge tubes according to manufacturer's instructions. Analyses of recombinant plasmid DNA were carried out separately in total volumes of 25µl, however, volumes of 30-40µl were used in reactions utilising larger amounts of DNA, including those required for gel band extraction. Digests were incubated for either 1-3hrs or overnight, according to manufacturer's instructions.

2.24.4 Agarose Gel Electrophoresis

Agarose gels were prepared according to the size of DNA fragments to be separated. In general, 0.8% [w/v] agarose gels prepared by melting agarose (Bioline) in 1X TAE buffer (see Appendix) and cooled prior to the addition of ethidium bromide to 0.5mg/ml. Gels were poured and allowed to set before transferring to the gel tank, containing 1X TAE running buffer. DNA samples were prepared with 5X DNA loading buffer (Bioline) added to 1X, loaded and separated against 5µl Hyperladder I DNA markers (Bioline) at 65V for 30-60mins, depending on application.

2.25 Statistical Analyses

The sample number (n) shown for each experiment describes either the total number of neurons sampled (for neurite growth experiments), the total number of fields sampled per genotype (for innervation experiments) or the number of separate cultures carried out (for neuronal survival experiments). Where data is shown from more than one replicate, the number of separate cultures, irides sampled or number of mice is indicated.

Data are presented as means ± SEM, and statistical significance was determined by the Unpaired T-test or, if there were more than two sets of data to compare, then the one-way analysis of variance (ANOVA) with Tukey post hoc test was used. The significance was accepted for $P<0.05$.

CHAPTER 3

DEVELOPMENTAL CaR EXPRESSION IN SYMPATHETIC AND SENSORY MOUSE NEURONS

3.1 RT-PCR Analysis of CaR (GPRC2a) Expression in Sympathetic and Sensory Mouse Neurons

In order to confirm the expression of CaR mRNA in sensory and sympathetic mouse neurons, specific intron-spanning primers were designed to amplify a 584bp fragment from the extracellular domain and first transmembrane region of the mouse CaR (GPRC2a) sequence by RT-PCR, incorporating nucleotides 1830-2415 (Fig. 20). The primers were designed to span exon 5, therefore, ensuring amplification from full-length CaR, rather than the alternatively spliced exon 5-missing CaR cDNA [199]. In order to assess CaR expression quantitatively over developmental age, quantitative PCR primers were designed to amplify a 99bp region spanning exon 5, incorporating nucleotides 1830-1929 (Fig. 20). The RT-Fd primer was used as the forward primer and a reverse primer (QPCR-Rv) was designed downstream of exon 5.

3.1.1 The CaR is Developmentally Expressed in Murine SCG

CaR-specific products were amplified from sympathetic (SCG) and sensory (trigeminal and nodose) ganglia in a developmental manner. In the SCG, the 584bp fragment was clearly amplified from E15, E18 and P1 but not earlier (E13) or later (P5) developmental ages (Fig. 21A). A faint band is detectable in the whole E13 embryo positive control but not in the no-template 'H_2O' control. Furthermore, 189bp products were amplified from β-actin in all samples (Fig. 21B), with the exception of the no-template control, indicating the presence of viable cDNA template.

3.1.2 The CaR is Developmentally Expressed in Murine Trigeminal Ganglia

In the trigeminal ganglia, 584bp products were amplified from E15, E18 and P5 cDNAs, but were not detected in either E12 or P1 (Fig. 22A). The presence of β-actin product in

all samples (excluding the no-template control) indicates the presence of intact cDNA template (Fig. 22B). However, the lack of 584bp CaR-specific product from P1 may be attributed to the quality or quantity of the cDNA in this sample, as the intensity of the 189bp β-actin product from P1 appears to be considerably lower than samples from the other developmental ages.

3.1.3 The CaR is Developmentally Expressed in Murine Nodose Ganglia

Amplification of CaR from nodose ganglia reveals a developmental profile, where expression increases with developmental age, similar to CaR expression in trigeminal ganglia. CaR PCR products were detected from at the earliest age of E18 and were present in P1 and P5 cDNA preparations (Fig. 23A). The presence of intact cDNA was demonstrated by the amplification of an 189bp β-actin product from all samples, excluding the no-template control (Fig. 23B).

3.1.4 Alignment of RT-PCR products from SCG, Trigeminal and Nodose Ganglia with GPRC2a and GPRC6a Sequences

The E18 and P1 SCG, and P5 584bp CaR PCR products from trigeminal and nodose ganglia were sequenced after purification by gel extraction. The obtained sequences were aligned with the mouse GPRC2a (CaR) and GPRC6a sequences (Fig. 24). The sequenced products from all three ganglia align with GPRC2a but show many clear differences with GPRC6a. Furthermore, all PCR product sequences span across exons 5 and 6 indicating that the RT-PCR products have been amplified from genuine CaR mRNA transcripts rather than GPRC6a mRNA or genomic DNA.

3.2 Quantitative PCR Analysis of CaR (GPRC2a) Expression in Sympathetic and Nodose Mouse Neurons

3.2.1 Quantitative CaR Expression Profile in SCG over Developmental Age

CaR expression was studied quantitatively in the SCG from early embryonic (E13) to early adulthood (P20) (Fig. 25). The CaR has a biphasic expression profile; showing significant expression at E13 and E15, and a second larger peak later in development at E18 (n=5-6; $P<0.001$). CaR expression then declines during early postnatal life (P1-P5) to a low basal level in early adulthood (P20).

3.2.2 Quantitative CaR Expression Profile in Nodose Ganglia over Developmental Age

CaR expression shows a more linear profile in nodose ganglia; the CaR is expressed from E18 and the number of transcripts expressed dramatically increases from E18 to P5 (n=9; $P<0.001$) (Fig. 26).

3.3 CaR Immunolocalisation in Dissociated E18 SCG Neurons

The localisation of CaR protein in dissociated E18 SCG neurons was determined using polyclonal antibodies raised to the C- (Fig. 27) or N-terminus (Appendix 3) of the receptor and visualised using laser-scanning confocal microscopy. The CaR was shown to be strongly expressed in the cell body but with detectable signal throughout the neurite field of permeablised neurons (Fig. 27A). The neuronal marker β-III tubulin (Fig. 27B) is expressed throughout the cell and overlaps with CaR signal throughout the processes and the cell body (Fig. 27C). At higher magnification CaR localisation is shown to be evenly distributed throughout the cell body and is detectable within proximal processes (Fig. 27D), where it co-localises with β-III tubulin (Fig. 27E-F). Furthermore, no CaR signal is detectable when the primary anti-CaR antibody is omitted (Fig. 27G-I).

tacagccccgctgaagcaacgctggagtctagcagaacgcctaagagtgtttattatactgtgagttctggatctttactaggaaaaaagtgccccatcctctggcacagttgccttgtgatcct
ctttccatctccagggaggagcgggaagcgtgtgtgctgcggggaaggaggggttgtatcttcccagaccaacagcaggagcaggatcggaagcctgggatggctagagcctcatcg
cacacaggaggactccagcgctagacctcggtctctcagaaaacatctcgggcagtctctacatgatgtcacttctcaggactcgaggaccaaccaccctacacctctgcatcggagaagg
cagaaatggacacagaagggccatgacttctcttctgtcattaaccactctgtagacatgtatccccatcagaaggcgtgaaccacaccgagggctgtggagttctcgggcccccaaaccac
taacacctttaactgtcccctggagagaaggcagagcc

atggcatggtttggctactgtttggccctcctggctctcacctggcactcctctgcctatgggcctgaccagcgagcccaaaag

aaggggacattatcctaggaggtctctttcctatccatttggagtagcagccaaagatcaagatctgaagtcaagaccagagtctgtggagtgcatcaggtataacttccgtggattccgatg

gttacaagccatgatctttgccatagaggagataaacagcagccccgcccttcttcccaacatgactctgggatataggatattcgacacctgtaacaccgtctccaaggctctggaggccacc

ttgagttttgttgcccagaacaaaatcgattctctgaacctggatgagttctgcaactgctccgagcacatcccttcaaccatcgcagtggtgggagcaaccggctccggtgtctccacagcgg

tagccaacctgctgggacttttctatatccccccaggtgagctacgcctcctctagcaggcttctcagcaataagaaccagttcaagtccttcctccgcaccattcccaacgacgaacaccaggc

caccgcgatggctgacattatcgagtatttccgttggaactgggtgggcacaattgcagccgacgacgactatggcaggcctggcattgagaagttccgagaggaagccgaggagaggg

acatctgcattgacttcagcgagctcatctcccagtactctgatgaggaagagatccagcaggtggtggaagtgatccagaactctacagccaaggtcattgtcgttttctccagcggcccag

acctagaacctctcatcaaggagattgtgcgccgtaacatcacaggcaggatctggctggccagcgaggcctgggccagttcctccctgattgctatgcctgagtacttccatgtagtcgggg

gtaccattgggttcggtctgaaggctgggcagattccaggcttccgagaattcctacagaaagtccatcccaggaagtctgtccacaatggttttgccaaagagttttgggaagaaacatttaat

tgccacctgcaagacggcgcaaaaggacctttacccgtggacaccttcgtgagaagtcacgaggaaggcggcaacaggttactcaatagctccactgccttccgacccctctgcacgggg

gatgaaaacatcaatagtgtcgagaccccttacatgggctacgaacatttacggatatcctacaacgtgtacttagccgtctactccattgcgcacgccctgcaagatatatac***acctgcttacc***

RT-Fd Primer **QPCR-Rv Primer**

cggaagagggctttt*caccaacgggtcctgtgcagacatcaagaaggttgaggcctggcaggtc*[redacted]tcaccaacaacatgggggagcaggtg

accttcgatgagtgcggtgacctggtggggaactactccatcatcaactggcacctctccccagaggacggctccattgtgttcaaggaagttgggtactacaatgtgtatgccaa

gaagggagaaagactgttcatcaatgaggggaagatcttgtggagtgggttctccagagaggtgcccttctccaactgcagccgggactgtcaggcagggaccaggaagggca

tcattgagggagagcccacctgctgtttttgagtgtgtggagtgtcctgacggcgagtacagtggtgagacagatgcgagtgcctgtgacaagtgcccggatgacttctggtccaat

RT-Rv Primer

gagaactacacttcctgcattgccaaggagattgagttcctggcgtggactgagccctttggaatcgctctcactctctttgcggtgctgggcattttcctgaccgccttttgtgctggg

TM1

cgtcttcatcaagttccgaaacacgcccattgtcaaggccaccaaccgagagctgtcctacctcctgctcttctcactcctctgctgcttctccagctccctgttcttcattggggagccccagga

TM2

ctggacctgccgcctgcgacagcccgccttcggcatcagcttcgtgcttttgtatctcgtgcatcttggtgaagaccaatcgagtcctcctggtatttgaggccaaaatacccaccagcttccacc

TM3

ggaagtggtggggactcaacctgcagttcctgctggttttcctctgcaccttcatgcagattgtcatctgcatcatctggctctacacggcaccccccctccagctaccgcaaccacgagctgga

TM4

agacgaaatcatcttcatcacgtgccatgagggctcactcatggcgctcggctccctgatcggctacaccttcctcctggctgccatcttcttcttttgccttcaagtctcggaagctgccag

TM5

agaacttcaacgaagccaagttcattaccttcagcatgctcatcttcttcatcgtctggatctccttcattccagcctatgccagcacctacggcaagtttgtctctgccgtggaggtgatcgccat

TM6

cctggcagccagctttggcttgctagcctgcatcttcttcaacaaggtctacatcatcctcttcaagccttcacggaacaccatcgaggaggtgcgctccagcactgcggctcatgctttcaaag

TM7

tggcagcccgcgccactctacgccgccccaacatctcccggaagcggtccagcagcctcggaggctccactgggtccaatccctcctcctccatcagcagcaaaagcaacagcgaagac

cggttcccacagccggagaggcagaagcaacagcaaccactggccctgacccagcaagaacagcagcagccccctgactctccagccgcagcaacagcaacagccacagcagcc

gagatgcaaacagaaggtcatcttcggcagtggcacagtcaccttctctctgagctttgatgagcctcagaagaatgctatggcccacaggaactccatgcgccagaactccctggaggccc

agaagagcaatgacactttgaacagacaccaggccctgcttcccctacagtgtgcagaggcggactcagaaatgaccattcaggagacgggcttgcaagggccaatggtgggggaccac

cagccagaaatagaaagcccagatgaaatgtccccagctctggtcgtgtccacctctcggagcttcgtcatcagcggtggaggtagctctgtgacggaaaacatactgcactcctaa

tggag

ggagaggttacccggttgagagtttttcttagagtcccaggaaaaaggatgggtcttcccaggaagccagggatagtgggtgcatcaaagcctgtactcggctgcactgctttgaatgacag
tgaactgactggtgggctctttacaagttagaagagccatgttttggggatcgttttccagagctcagtgtcatacctggatttgctgaaatcttttcctctgctccatccaccaccagctcggatg
aaagcaaggctataagctacccacctgcttcccctcaaaaacgcttatatccagaaatccctacccgaggcacagtccagatacagatggatgggacatcagatctgccaccattaaagttg
agtctaaaagccagatagtcaccaggactgtctatcacattgacagtggacagaactgtacatttgcaagacatcaggcagacatgtcctctcctatttataaagaccttaagaagtgtggcctt
tttatcctccctgttgctgctactgtgtaacatctgttccatctgcatcctttcctgtgacgtcatgcatggatgtatccagaacctgaaggcaatgccacatttagatcttaggatcataagtatcacc
tccaagcaccgggaaaggactgactcaacccaacgagctgtctctgtagctaatatcaatgtacatagcgtaatccttaagaaactgcttctgttgtaatagtccatgggcgattataaactgaa
aaatgtcgcagtctaaaaaaaaaaaaaaaa

Figure 20: Mouse CaR (GPRC2a) Sequence (Accession: NM 013083). The segments in bold denote the 584bp amplicon of GPRC2a amplified by the RT-PCR oligonucleotide primers (shown in yellow). The sequence in bold italics denotes the 99bp amplicon amplified by the quantitative PCR primers (RT-Fd in yellow and QPCR-Rv shown in blue). The start and stop codons are shown in red. The intron-exon boundaries are shown by a backslash.

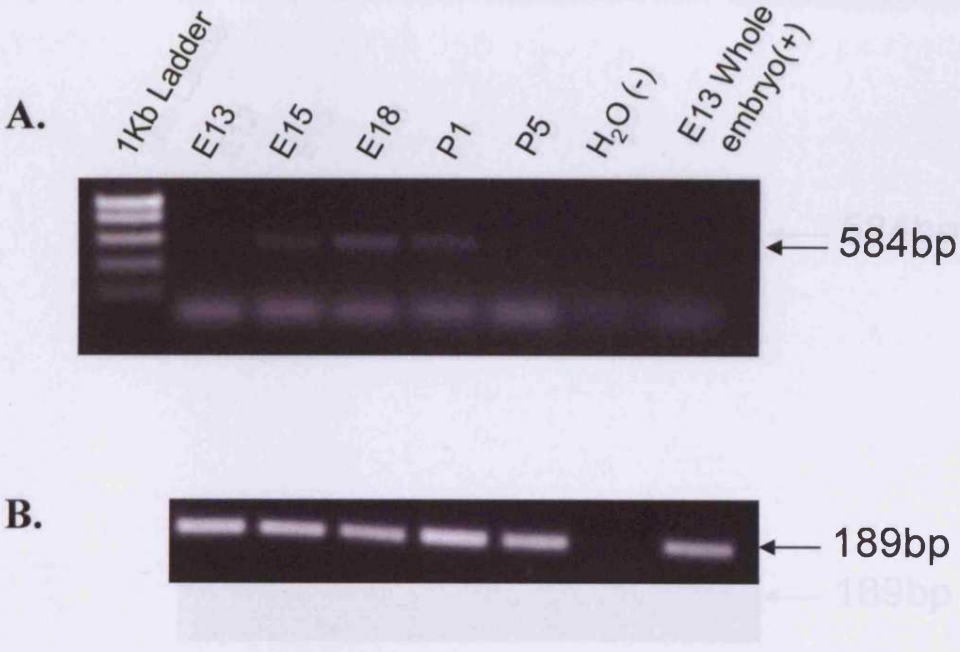

Figure 21: The CaR is Developmentally Expressed in Murine SCG. cDNAs were prepared from SCG RNA as described in the Methods section and were used in CaR-specific PCR reactions. **A.** A 584bp fragment of the CaR extracellular domain and 1st transmembrane segment was amplified from SCG cDNA. **B.** A 189bp β-actin fragment was amplified from the same cDNAs. Whole E13 embryo and water served as positive and negative controls, respectively.

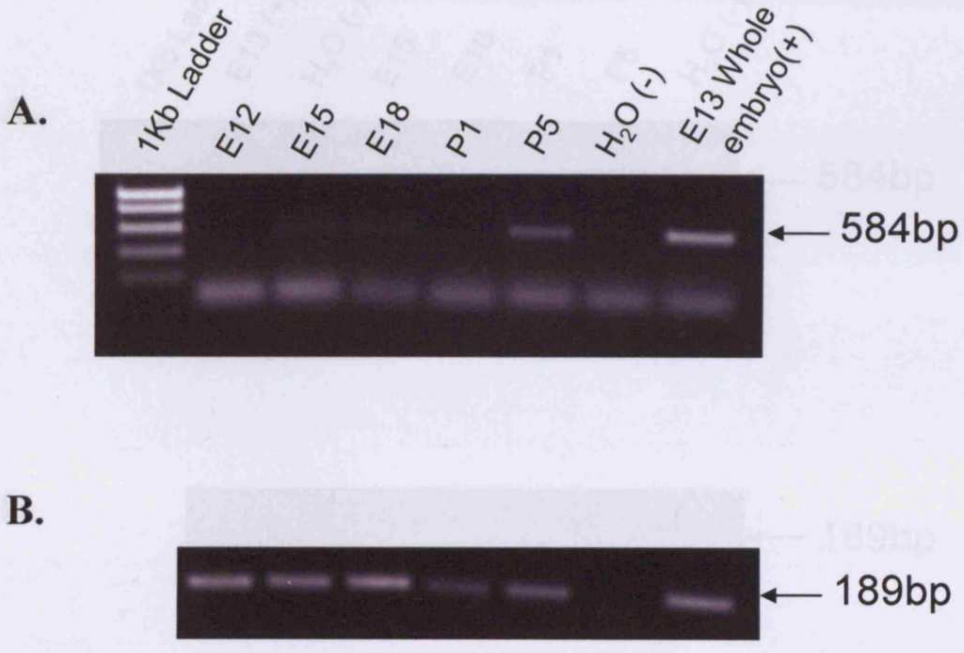

Figure 22: The CaR is Developmentally Expressed in Murine Trigeminal Ganglia. cDNAs were prepared from trigeminal ganglia RNA as described in the Methods section and were used in CaR-specific PCR reactions. **A.** A 584bp fragment of the CaR extracellular domain and 1st transmembrane segment was amplified from trigeminal ganglia cDNA. **B.** A 189bp β-actin fragment amplified from the same cDNAs. Whole E13 embryo and water served as positive and negative controls, respectively.

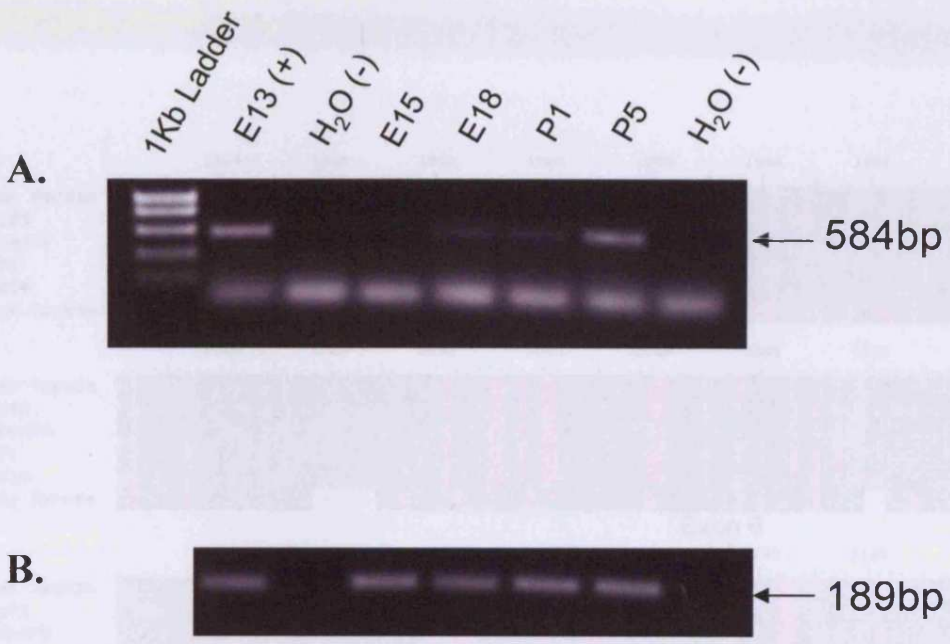

Figure 23: The CaR is Developmentally Expressed in Murine Nodose Ganglia. cDNAs were prepared from nodose ganglia RNA as described in the Methods section and were used in CaR-specific PCR reactions. **A.** A 584bp fragment of the CaR extracellular domain and 1st transmembrane segment was amplified from nodose ganglia cDNA. **B.** A 189bp β-actin fragment amplified from the same cDNAs. Whole E13 embryo and water served as positive and negative controls, respectively.

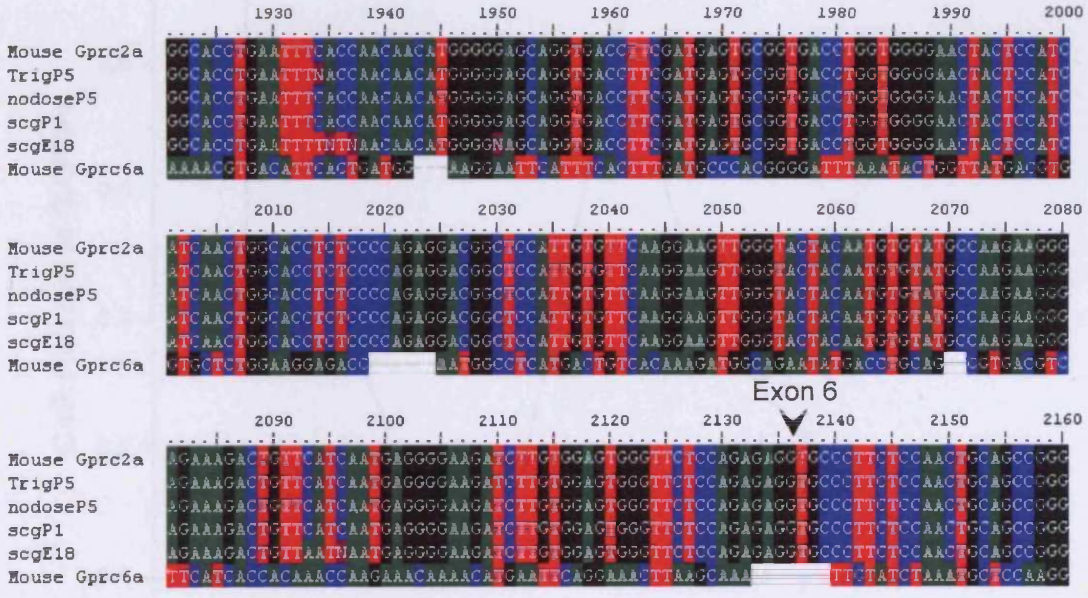

Figure 24: Alignment of RT-PCR products from Trigeminal, Nodose and SCG ganglia with Mouse GPRC2a (Mouse CaR; Accession: NM 013083) and GPRC6a (Accession: NM 153071) sequences. The location of exon 6 junction is shown, indicating amplification from spliced, mature CaR transcripts rather than genomic DNA. Nucleotides are colour coded as follows; A, green; T, red; G, black; C, blue.

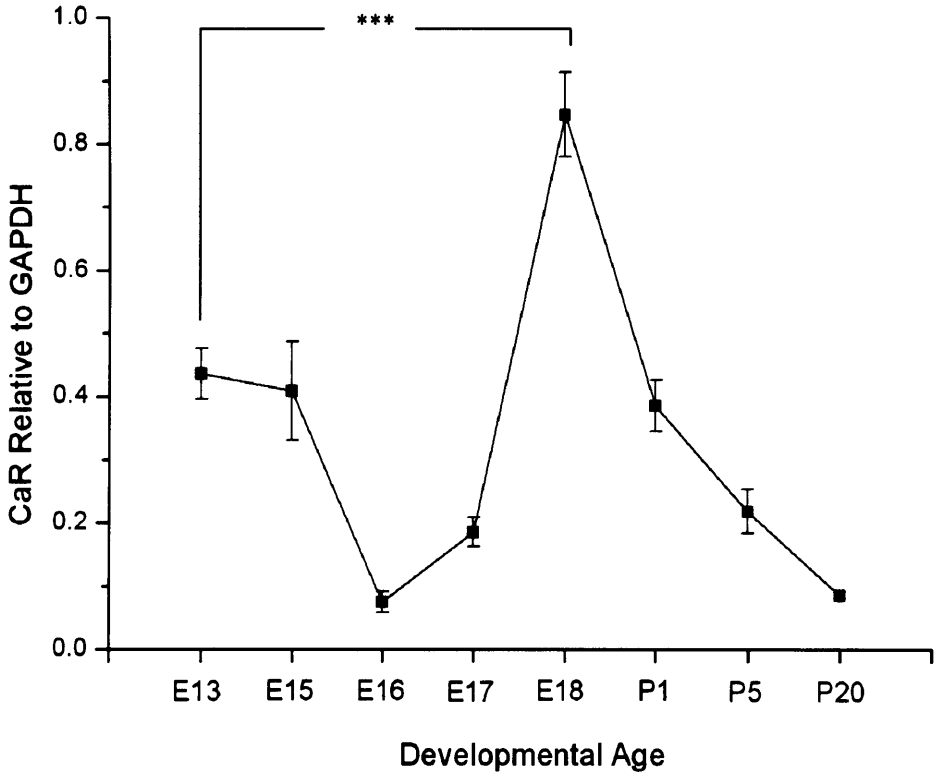

Figure 25: Quantitative CaR Expression Profile in SCG Over Developmental Age. Three separate RNA isolations were carried out per age and the series of 24 cDNA samples was carried out in duplicate for both the CaR and GAPDH PCR. CaR reactions which had a melting peak different to 87°C were removed. The ratio of CaR:GAPDH was calculated as described in the Methods section. N=3, ***$P<0.001$ One-way ANOVA with Tukey post hoc test. Data are presented as the mean ± SEM.

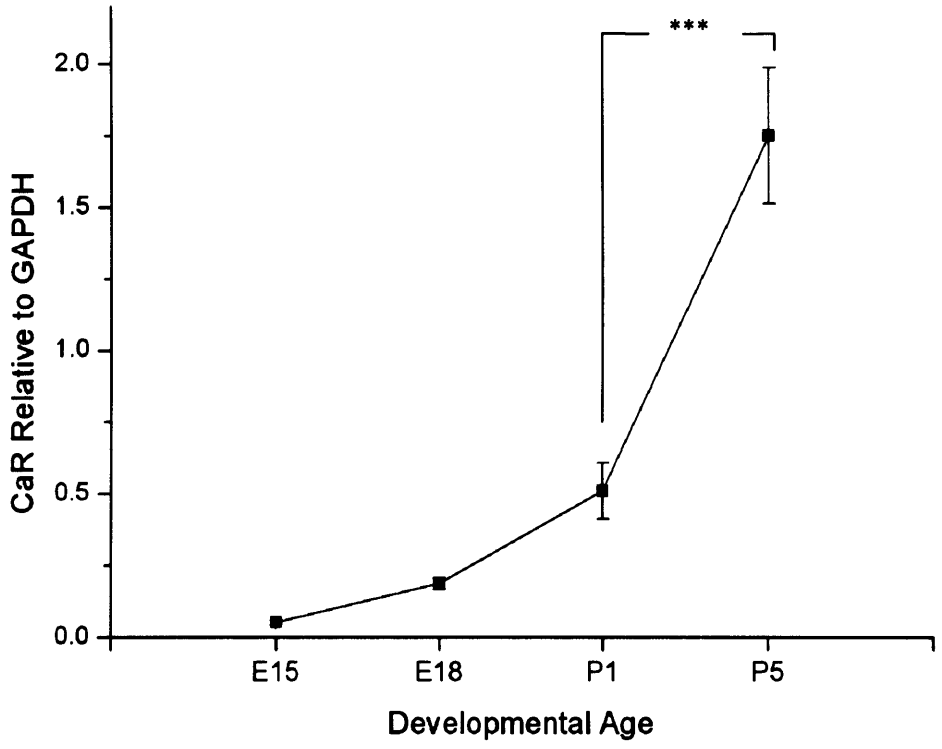

Figure 26: Quantitative CaR Expression Profile in Nodose Ganglia Over Developmental Age. Three separate RNA isolations were carried out per age and the series of 12 cDNA samples was carried out in triplicate for both the CaR and GAPDH PCR. The ratio of CaR:GAPDH was calculated as described in the Methods section. N=3, ***$P<0.001$ One-way ANOVA with Tukey post hoc test. Data are presented as the mean ± SEM. Reproduced courtesy of Dr. G. W. O'Keeffe.

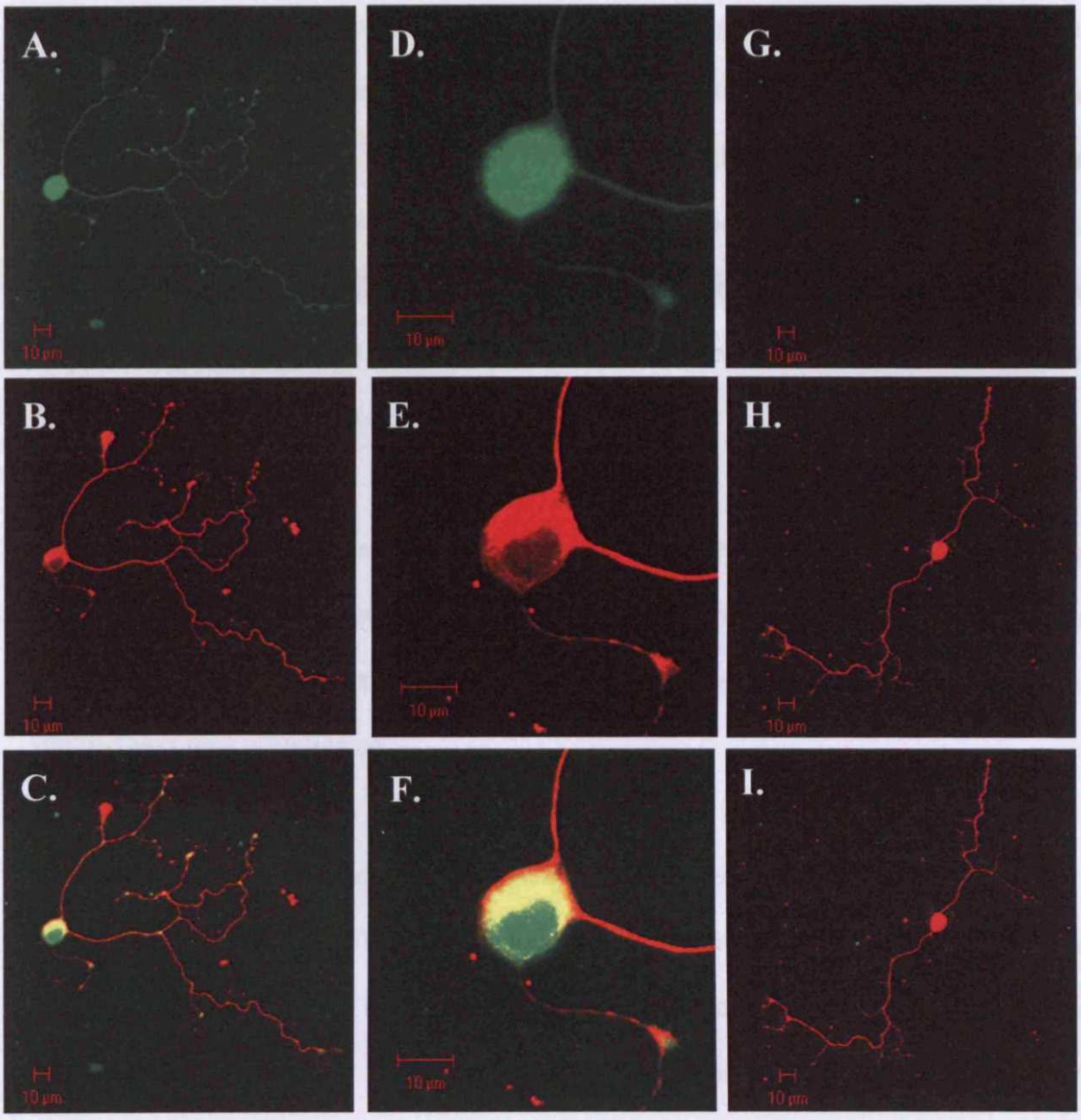

Figure 27: CaR Immunolocalisation in Dissociated E18 SCG Neurons. E18 SCG neurons were dissociated and cultured in 4 well dishes in the presence of 0.4ng.ml^{-1} NGF using F-14 medium at the standard $[Ca^{2+}]_o$ (1.4mM) for 24hrs. Low (**A**, **B**, **C**, **G**, **H** and **I**) and high magnification (**D**, **E** and **F**) images were taken using a 40X water immersion objective. **A.** and **D.** Anti-CaR polyclonal antibody raised to an amino acid sequence in the CaR C-terminus, **G.** Negative control (anti-CaR antibody omitted), **B**, **E** and **H.** β-III tubulin, **C**, **F** and **I** Merge.

3.4 Discussion

Current knowledge of the role of the CaR in the developing peripheral and central nervous systems is limited to information derived from expression studies of the receptor in postnatal and adult tissues. Despite the identification of functional CaR in a number of primary and established cell culture models, many studies only speculate as to the biological significance of CaR expression in neurons. In this study the developmental expression of the CaR has been characterised in well established models of neuronal development and its *in vitro* expression confirmed.

Subsequently, using three independent approaches, namely pharmacological modulators, overexpression of dominant negative and wildtype CaR and transgenic models, a functional role for the receptor in the regulation of sympathetic neurite outgrowth and survival was then investigated.

3.4.1 The CaR is Developmentally Expressed in SCG, Nodose and Trigeminal Ganglia

My results demonstrate that the CaR is expressed significantly in superior cervical ganglia at E13-E15, at a time when the ganglia consist predominantly of proliferating neuroblasts *in vivo*. Furthermore, E15 nears the end of the proliferative period in the SCG, when immature sympathetic neurons are becoming responsive to NGF [16]. CaR transcription decreases at E16 and E17 only to peak at E18, correlating with a time of naturally occurring cell death *in vivo*, when axons from an almost entirely NGF-dependent neuronal population [16] are reaching their targets and competing for limiting amounts of target derived neurotrophic factor, suggesting a role for the CaR in the regulation of neuronal survival or apoptosis. CaR expression then declines at P1, to a level comparable to that at

E13 and E15, and decreases further to a low basal level in early adulthood (P20) where 40% of SCG neurons survive in culture in the absence of NGF [47].

The nodose ganglion is formed from the migration of placode-derived cells during E10.5 in the mouse [14], and neurogenesis occurs between E9-E13 [12]. Both NT-3 and NT-4 act at early stages of nodose ganglion formation during E12-E13, at a time when most of the neurons are born [200]. The majority of nodose neurons are supported *in vitro* by the target-derived neurotrophin, BDNF, from E12 onwards [201, 202] and at E13 small numbers of vagal nerves have begun to innervate the muscle walls of the abdominal esophagus and stomach *in vivo* [203]. During the period of development E14-E18, NGF can enhance the survival of a subset of TrkA-expressing nodose neurons supported by BDNF *in vitro* [43]. CaR transcripts were identified using RT-PCR from E18 and P1, correlating with an approximate 4.5-fold increase in TrkA expression from E15 in the nodose ganglion [43] and with a period where GDNF is required for survival [204]. Furthermore, CaR expression increased even further by P5 in this ganglion when compared to earlier timepoints, consistent with quantitative PCR data which showed a more linear CaR expression profile when compared to sympathetic ganglia, suggesting a role for the receptor later on in development during target innervation, for example.

The earliest axons emerge from the trigeminal ganglion at E9.5 and these grow to their targets and come into contact with the epithelium by E10.5 in the mandibular process and E11 in the maxillary process [20]. The earliest developmental age CaR-specific products were detected from trigeminal cDNA preparations was E15. Trigeminal neurons undergo naturally occurring cell death during E12 to E18, peaking at E14 *in vivo* [20]. A gap of CaR expression occurs at P1, however this may be due to either poor cDNA quantity or

quality as, although the RT-PCR product from β-actin is present, it appears to be at a lower intensity than the other β-actin products. However, a strong CaR-related band was detected at P5 in trigeminal ganglia, correlating with a period of dental pulp innervation *in vivo* [205], suggesting a role for the receptor in the innervation of trigeminal targets.

CaR transcription can be modified by vitamin D ($1,25(OH)_2D_3$) due to the presence of vitamin D response elements in both known CaR promoter sequences [206]. Rats treated with $1,25(OH)_2D_3$ show a modest increase in CaR mRNA in the kidney and parathyroid [207] and $1,25(OH)_2D_3$ levels in blood are known to vary during development [208, 209] and thus may account for the increases observed in CaR expression in this study. Furthermore, the CaR is also under transcriptional regulation by NF-κB [210], the activation of which can be mediated by high $[Ca^{2+}]_o$ via the CaR [211]. Indeed, elevated levels of $Ca^{2+}{}_o$ increased CaR mRNA levels 2-fold in pituitary-derived AtT-20 cells [116]. Therefore, CaR activation by Ca^{2+}, or other CaR agonists, and the subsequent increase in NF-κB activity provides a possible mechanism where by the CaR regulates and may increase its own level of transcription.

A number of transcripts, closely related to the CaR, are also expressed in a number of tissues. These include several CaR splice variants, including an exon 5-less splice variant [$^{(exon5(-))}$CaR] [199] which retains ligand-sensing ability [212] and a novel putative cation-sensing receptor GPRC6a [126, 213]. This orphan GPCR has recently been shown to retain conserved binding sites for Ca^{2+} and calcimimetic compounds and is activated by these agonists, but has distinct apparent affinities for extracellular cations and differences in ligand specificity [126]. Further, the putative novel cation-sensing receptor has been shown to be expressed in multiple mouse tissues, including brain, where it is speculated

that GPRC6a may have overlapping functions with the CaR [126]. The sequenced RT-PCR products amplified from the sympathetic and sensory ganglia aligned with the mouse CaR sequence GPRC2a, spanning exons 4, 5 and 6. Many sequence discrepancies were observed when the products were aligned with the putative novel cation-sensing GPCR, GPRC6a [126]. Taken together, these observations demonstrate that RT-PCR products were amplified from *bona fide* full-length CaR transcripts, rather than the exon 5-less splice variant [199], GPRC6a [126] or genomic DNA. Although the presence of GPRC6a has not been investigated, a role for this receptor may be ruled out due to its lower affinity to $[Ca^{2+}]_o$ (5mM $Ca^{2+}{}_o$ consistently fails to activate GPRC6a) [126], yet possible heterodimerisation with the CaR cannot be ruled out.

It should be noted that cDNAs were prepared from whole ganglia which are known to contain satellite cells, in which expression of the CaR is currently unknown. The CaR has been shown to be expressed in glia within the CNS, including; oligodendrocytes [180], microglia [214] and astrocytes [215]. It is possible, therefore, that these glial cells may express the CaR and contribute to the transcripts detected from whole ganglia cDNA. However, when detecting CaR transcripts by *in situ* hybridisation in rat DRG, Ferry *et al* (2000) report that satellite cells surrounding the cell bodies of DRG neurons were left unlabelled [216], suggesting these glial cells do not express the CaR.

3.4.2 E18 SCG Neurons Express the CaR in Vitro

CaR protein was detected in dissociated E18 SCG neurons using antibodies raised to the N- or C-terminus of the receptor where CaR staining was strongly localised to the cell body, consistent with expression of the CaR in DRG neurons and pyramidal neurons of the hippocampus [173, 217]. However, this finding is in contrast to that reported by Ruat

et al (1996) who localised the CaR to nerve terminals in the rat brain, but not to the cell bodies of either neurons or astrocytes [170]. This disparity may be attributed to the nature of the antibody used; a polyclonal anti-CaR antibody raised to the C-terminus of the receptor was used in this study, further, Wang *et al* (2003) and Chattopadhyay *et al* (1997) used an antibody raised to the CaR N-terminus [173, 217]. However, Ruat *et al* (1996) used a polyclonal anti-CaR antiserum that had been raised to a sequence overlapping with the CaR 21 amino acid signal peptide [170]. The design of this antibody could account for loss of plasma membrane signal due to cleavage of the signal peptide, which is required for proper expression at the plasma membrane [100, 218]. Therefore, the CaR immuno-staining reported by Ruat *et al* (1996) may not reflect the true nature of CaR expression throughout the CNS [170].

Considerable intracellular CaR-related staining was observed within the cell body, which is consistent with other cells endogenously expressing the CaR, including; proximal tubular kidney cells [219], chondrocytes [220], keratinocytes [221] and astrocytes [181]. The significance of the intracellular staining is likely to be due to receptor trafficking and maturation.

3.4.3 Summary

In the current study the developmental expression of the CaR has been characterised in three well established models of neuronal development. Quantitative PCR data are in agreement with RT-PCR analyses, demonstrating a predominantly embryonic expression profile in sympathetic ganglia compared to the expression of the CaR in the sensory ganglia, where the emphasis is more postnatal. Furthermore, the RT-PCR products were shown to be amplified from *bona fide* full-length CaR transcripts, showing clear

disparities between the putative cation-sensing receptor, GPRC6a. In addition, CaR protein was localised to the cell body and neurite field of sympathetic neurons *in vitro*. Taken together, these observations demonstrate a developmentally regulated expression of the CaR in sympathetic and sensory ganglia.

CHAPTER 4

DETERMINING A ROLE FOR THE CaR IN THE REGULATION OF NEURITE OUTGROWTH AND TARGET FIELD INNERVATION

4.1 Effects of $[Ca^{2+}]_o$ on Neurite Outgrowth of Sympathetic Neurons

4.1.1 E18 SCG Neurons are Dependent on NGF for Survival

To investigate the role of $Ca^{2+}{}_o$ in the regulation of NGF-dependent neurite outgrowth and neuronal survival, the optimal concentration of NGF with which to use in culture for all subsequent experiments had to be determined. An NGF dose response was carried out using E18 SCG dissociated neurons to determine a concentration of NGF which would not mask the effects of $[Ca^{2+}]_o$ on neurite outgrowth and neuronal survival in subsequent experiments. Percentage neuronal survival is shown after 24hrs in culture (Fig. 28); the optimal level of NGF was considered to be $0.4ng.ml^{-1}$.

4.1.2 Neurite Outgrowth of E18 SCG Neurons is Dependent on $[Ca^{2+}]_o$: Pilot Experiment I

A pilot experiment was conducted to determine whether $Ca^{2+}{}_o$ plays a role in neurite outgrowth of E18 SCG neurons. These neurons were used as CaR mRNA expression appears to peak at this age in the SCG. The arborisation of E18 SCG neurons cultured in 1.1, 1.4 and 2.3mM $Ca^{2+}{}_o$ was compared. Fig. 29A shows that increasing $[Ca^{2+}]_o$ from 1.1 to 2.3mM in the culture medium increases the Sholl profile (n=23 neurons). This increase in arborisation can be attributed to an increase in the number of branch points with increasing $[Ca^{2+}]_o$ from 1.1mM (2.5±0.6; n=25 neurons) to 1.4mM (5.2±0.78; n=25 neurons) and 2.3mM (7.2±0.78; n=23 neurons) (Fig. 29B) rather than total neurite length (Fig. 29C). However, due to the absence of survival data for this experiment the increase in arborisation with increasing $[Ca^{2+}]_o$ may have been biased due to a potential negative effect of low $[Ca^{2+}]_o$ on neuronal survival.

4.1.3 Neurite Outgrowth of E18 SCG Neurons is Dependent on $[Ca^{2+}]_o$: Pilot Experiment II

To ensure sampling from an unbiased population of neurons, a second pilot experiment was conducted using the same $[Ca^{2+}]_o$ including a larger sample size and neuronal survival data at 24hrs. Importantly, neurons were sampled from cell groups with differences in survival that were ≤5% and that were not statistically significant. Fig. 30A shows there to be no difference between cell groups in terms of neuronal survival. However, increasing $[Ca^{2+}]_o$ from 1.1mM to 2.3mM increases the Sholl profile significantly (Fig. 30B), an effect which is already maximal at 1.4mM Ca^{2+}. Surprisingly, however, the branching of neurite arbors remained unaffected by variations in $[Ca^{2+}]_o$ (Fig. 30C), in contrast to the earlier E18 SCG pilot experiment. Furthermore, the total length of neurite arbors grown in 2.3mM Ca^{2+} (3019.2±177.9μm; n=64 neurons) were increased compared to those grown in 1.1mM Ca^{2+} (2222.2±156.1μm; n=65 neurons) (Fig. 30D).

4.1.4 Neurite Outgrowth of P1 SCG Neurons is Not Dependent on $[Ca^{2+}]_o$: Pilot Experiment III

To investigate whether the effect of $Ca^{2+}{}_o$ on neurite outgrowth was present in postnatal as well as late embryonic SCG neurons, the effect of changes in $[Ca^{2+}]_o$ on P1 SCG neurite arborisation was studied. Despite a clear effect of high $[Ca^{2+}]_o$ on neuronal survival (n=65 neurons) (Fig. 31A), there was no difference in the Sholl profile between neurons cultured in different Ca^{2+} concentrations (n=65 neurons) (Fig. 31B). Similarly, no difference was seen between cell groups in either branching or length parameters (Fig. 31C and D).

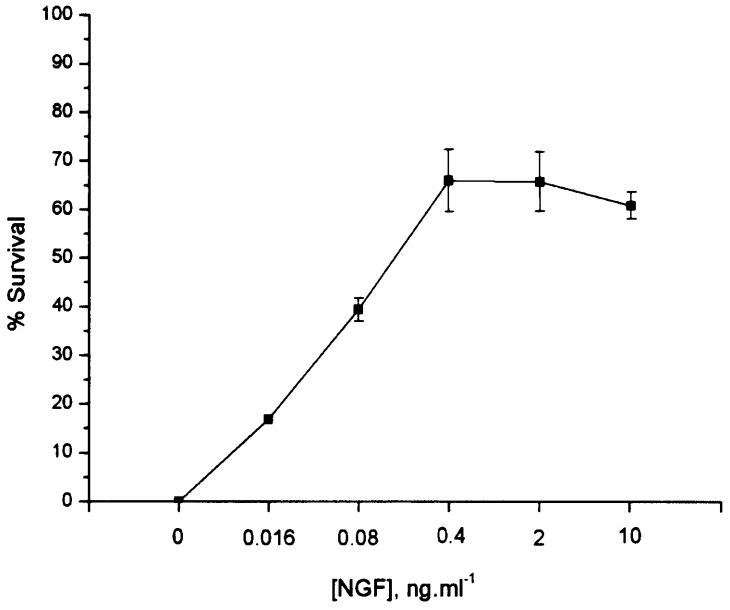

Figure 28: E18 SCG Neurons are Dependent on NGF for Survival. E18 SCG neurons were cultured in 35mm dishes in the presence of a range of NGF concentrations, serially diluted 1:5 in the standard $[Ca^{2+}]_o$ present in the medium (1.4mM). This figure shows that 0.4ng.ml^{-1} NGF represents a maximal but non-saturating concentration of NGF with which to use in subsequent survival experiments. Percentage survival is shown here after 24hrs in culture (n=1). Neuronal survival was determined as described in the Methods section. Data are presented as the mean ± SEM.

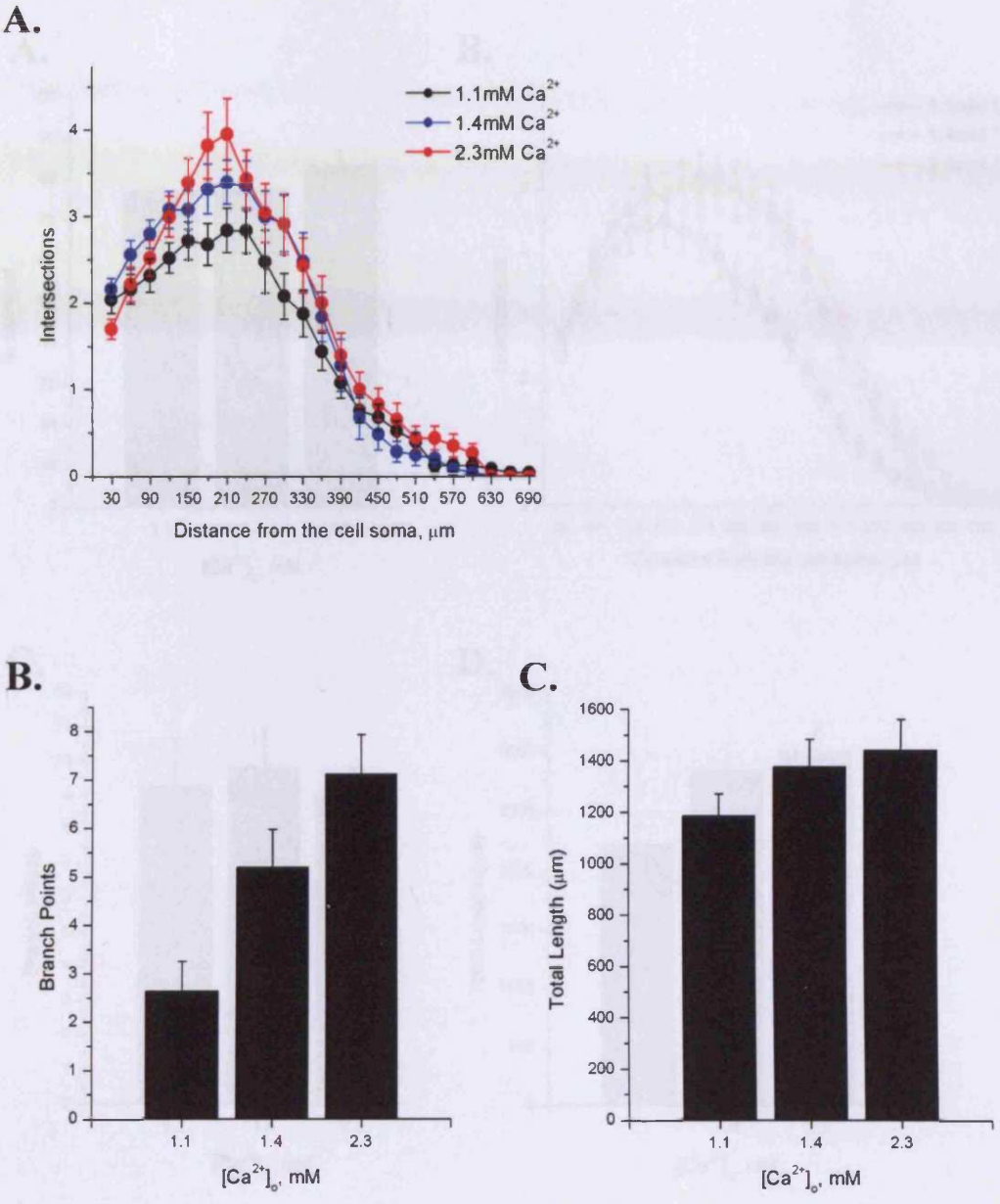

Figure 29: Neurite Outgrowth of E18 SCG Neurons is Dependent on $[Ca^{2+}]_o$: Pilot Experiment I. Neurons were cultured in 0.4ng.ml^{-1} NGF in 1.1, 1.4 or 2.3mM $[Ca^{2+}]_o$ for 24hrs before fixing and labelling with antibodies to β-III tubulin. **A.** Sholl analysis reveals an increase in number of intersections with increasing $[Ca^{2+}]_o$. **B.** Increasing $[Ca^{2+}]_o$ caused an increase in branch points, **C.** but not an increase in total neurite length. No survival data was recorded for this experiment (n=23-25 neurons per condition). Data are presented as the mean ± SEM.

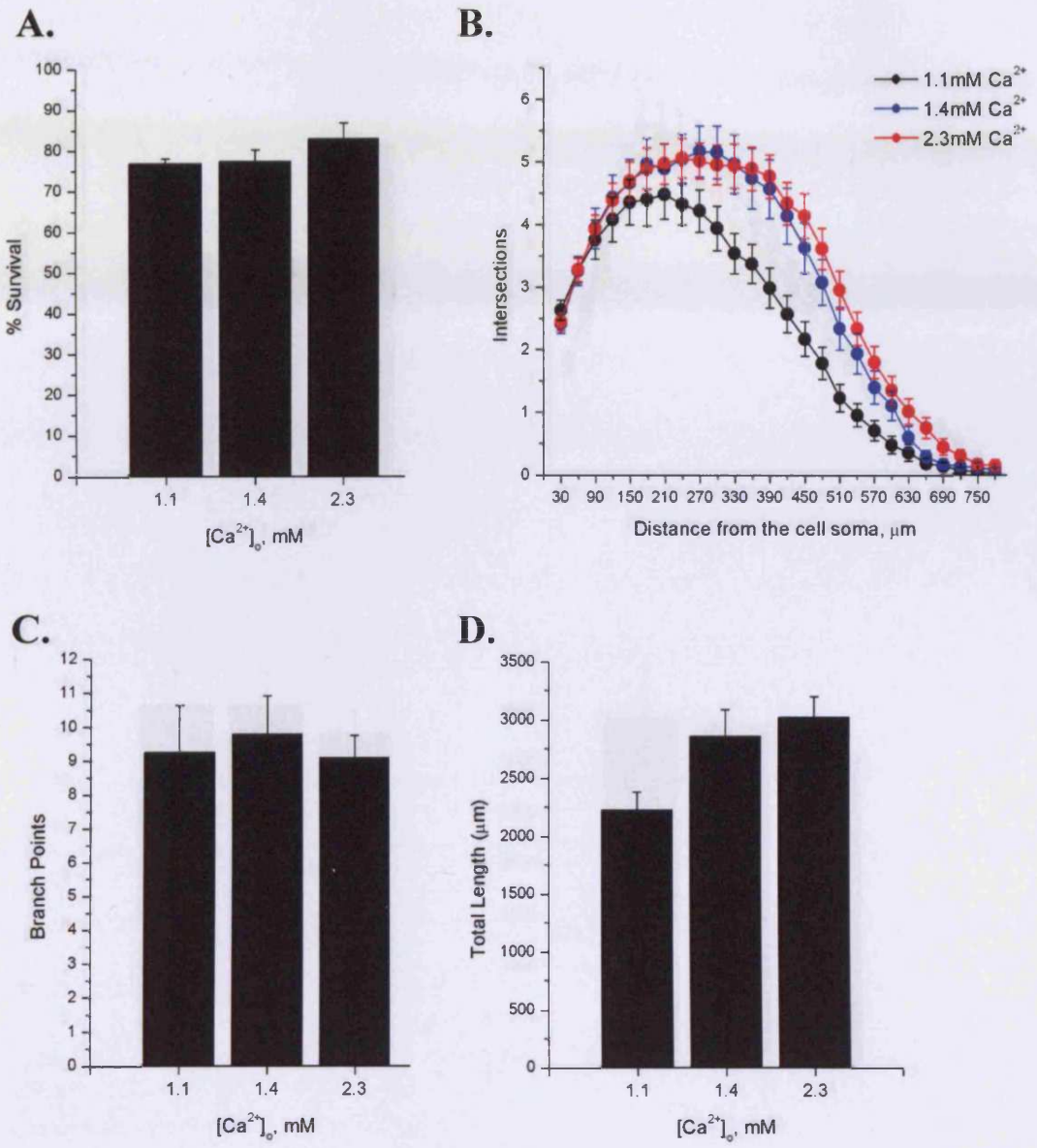

Figure 30: Neurite Outgrowth of E18 SCG Neurons is Dependent on $[Ca^{2+}]_o$: Pilot Experiment II. Neurons were cultured in 0.4ng.ml^{-1}NGF in 1.1, 1.4 or 2.3mM $[Ca^{2+}]_o$ for 24hrs before determining survival, fixing and labelling with antibodies to β-III tubulin and then capturing fluorescent images. **A.** No difference in percentage survival at 24hrs was seen between cell groups. **B.** Sholl analysis reveals the effect of increasing intersections with increasing $[Ca^{2+}]_o$ and is maximal at 1.4mM Ca^{2+} (statistical significance between 2.3mM and 1.1mM Ca^{2+} is shown). **C.** Increasing $[Ca^{2+}]_o$ had no effect on the number of branch points, **D.** but increased total neurite length (n=65 neurons per condition). Data are presented as the mean ± SEM.

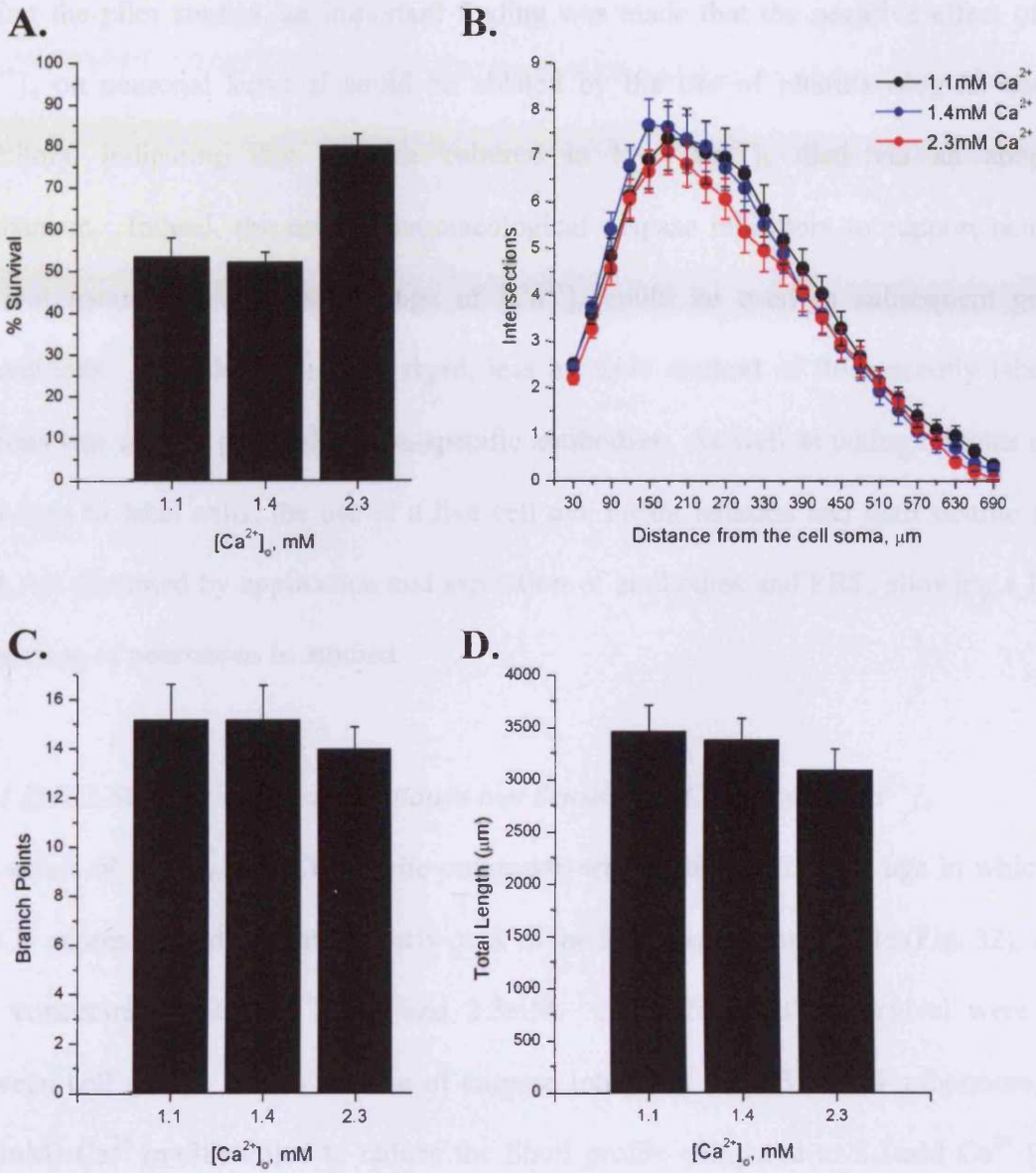

Figure 31: Neurite Outgrowth of P1 SCG Neurons is Not Dependent on $[Ca^{2+}]_o$: Pilot Experiment III. Neurons were cultured in 0.4ng.ml^{-1}NGF in 1.1, 1.4 or 2.3mM $[Ca^{2+}]_o$ for 24hrs before fixing and labelling with antibodies to β-III tubulin. **A.** No difference in survival was observed between 1.1mM and 1.4mM $[Ca^{2+}]_o$, yet a significant increase in survival is seen with 2.3mM Ca^{2+}. **B.** Sholl analysis reveals there is no effect of increasing $[Ca^{2+}]_o$ on neurite outgrowth, despite the differences seen in neuronal survival. Increasing $[Ca^{2+}]_o$ had no effect on the number of branch points (**C.**) and total neurite length (**D.**) (n=65 neurons per condition). Data are presented as the mean ± SEM.

4.2 Effects of $[Ca^{2+}]_o$ on Neurite Outgrowth over Developmental Age

During the pilot studies, an important finding was made that the negative effect of low $[Ca^{2+}]_o$ on neuronal survival could be ablated by the use of pharmacological caspase inhibitors, indicating that neurons cultured in low $[Ca^{2+}]_o$ died via an apoptotic mechanism. Indeed, the use of pharmacological caspase inhibitors to support neuronal survival meant that a broader range of $[Ca^{2+}]_o$ could be used in subsequent growth experiments. In addition, a more rapid, less invasive method of fluorescently labelling neurons was used in place of neuron-specific antibodies. As well as taking minutes rather than days to label cells, the use of a live cell dye meant neurons and their neurite fields were not disrupted by application and aspiration of antibodies and PBS, allowing a larger population of neurons to be studied.

4.2.1 I) E15 SCG Neurite Arborisation is Not Sensitive to Changes in $[Ca^{2+}]_o$

The effect of $[Ca^{2+}]_o$ on SCG neurite outgrowth was studied at E15, an age in which the CaR is expressed and exhibits an early peak in the SCG expression profile (Fig. 32), using two concentrations of $Ca^{2+}{}_o$; 0.7 and 2.3mM. No differences in survival were seen between cell groups due to the use of caspase inhibitors (Fig. 32A). Furthermore, low (0.7mM) Ca^{2+} (n=38) failed to reduce the Sholl profile compared to 2.3mM Ca^{2+} (n=48 neurons) (Fig. 32B) and, in places, increased the Sholl profile (n=38 neurons). However, an insensitivity to $[Ca^{2+}]_o$ at this age is suggested by a lack of differences in branching (Fig. 32C) and total neurite length (Fig. 32D) between E15 SCG neurite arbors grown in 0.7mM and 2.3mM Ca^{2+}.

4.2.2 IIa) E18 SCG Neurite Arborisation is Sensitive to Changes in $[Ca^{2+}]_o$

Pilot E18 SCG outgrowth experiments suggested that neurite arborisation was sensitive to changes in $[Ca^{2+}]_o$ (Fig. 33), a comparison of outgrowth in 0.7 and 2.3mM $[Ca^{2+}]_o$ in the presence of caspase inhibitors was consistent with this observation. Fig. 33A demonstrates that a broad population of neurons was studied in this experiment, rather than a population of neurons selected for by low or high $[Ca^{2+}]_o$, due to the use of caspase inhibitors. However, the Sholl analysis reveals a dramatic increase in the number of intersections with distance from the cell soma by increasing $[Ca^{2+}]_o$ from 0.7 to 2.3mM (Fig. 33B). Fig. 33C and D demonstrate that both the number of branch points (13.5±1.1; n=41 neurons) and total neurite length (2899.5±172.9μm; n=41 neurons) of neurite arbors grown in 2.3mM $[Ca^{2+}]_o$ are both increased compared to neurons cultured in 0.7mM $[Ca^{2+}]_o$ (branch points, 7.9±0.8; total neurite length, 2051±152.4μm; n=48 neurons).

4.2.3 IIb) $[Ca^{2+}]_o$ Sensitivity of E18 SCG Neurite Arborisation Using Caspase Inhibitors can be Reproduced using Bax-Deficient Neurons

As the effect of $[Ca^{2+}]_o$ on neurite outgrowth has been established using caspase inhibitors, this effect was reproduced in an alternative system for preventing apoptotic cell death. E18 SCG neurons deficient in Bax were established from $Bax^{+/-}$ x $Bax^{+/-}$ matings and cultures were set up using the genotyped embryos. Fig. 34A shows there to be no difference in survival between cultures grown in low or high $[Ca^{2+}]_o$ due to Bax deficiency. Fig. 34B reveals that a sensitivity to $[Ca^{2+}]_o$ is still present in these neurons as 2.3mM $[Ca^{2+}]_o$ significantly increases the number of intersections with distance from the cell soma when compared to the 0.7mM $[Ca^{2+}]_o$ profile. Furthermore, the branching (Fig. 34C) and length parameters (10.1±0.5; 1572.2±63.4μm; n=98 neurons from two $Bax^{-/-}$ embryos) (Fig. 34D) were increased in populations of neurons cultured in 2.3mM $[Ca^{2+}]_o$

compared to 0.7mM Ca^{2+} (7.5±0.5; 1218.4±69.1μm; n=101 neurons from two *Bax*$^{-/-}$ embryos). Representative examples of Bax-deficient neurons grown in 0.7mM and 2.3mM $[Ca^{2+}]_o$ are shown in Fig. 34E-F; where a reduction in neurite arbor size and complexity can be seen in the neuron grown in 0.7mM $[Ca^{2+}]_o$ when compared to the neuron grown in 2.3mM $[Ca^{2+}]_o$.

4.2.4 III) P0 SCG Neurite Arborisation is Sensitive to Changes in $[Ca^{2+}]_o$

Fig. 35 demonstrates the sensitivity of neurite outgrowth to $[Ca^{2+}]_o$ is retained in SCG neurons from newborn mouse (P0). Caspase inhibitors protect neurons from apoptosis (Fig. 35A); moreover, the effect of increasing $[Ca^{2+}]_o$ from 0.7 to 2.3mM on the Sholl profile is remarkably similar to that observed for E18 SCG neurons (Fig. 33). Furthermore, both branching (14.3±1.9; n=50 neurons) (Fig. 35C) and length (3428.4±242.1μm; n=50 neurons) (Fig. 35D) parameters are increased with 2.3mM $[Ca^{2+}]_o$, when compared to 0.7mM $[Ca^{2+}]_o$ (6.42±0.8; 2317.5±137.5μm; n=52 neurons).

4.2.5 IV) P1 SCG Neurite Arborisation is Not Sensitive to Changes in $[Ca^{2+}]_o$

An age with comparable levels of CaR expression to E15, the pilot experiment had suggested that neurite arborisation of P1 SCG neurons were not sensitive to changes in $[Ca^{2+}]_o$ (Fig. 31). There is no effect of $[Ca^{2+}]_o$ on survival due to the use of caspase inhibitors (Fig. 36A), moreover, the effect of increasing $[Ca^{2+}]_o$ on the Sholl profile is significantly different at this age (Fig. 36B). Neurons cultured in 0.7mM paradoxically had a small increase in the Sholl profile, (n=116 neurons from two separate cultures).

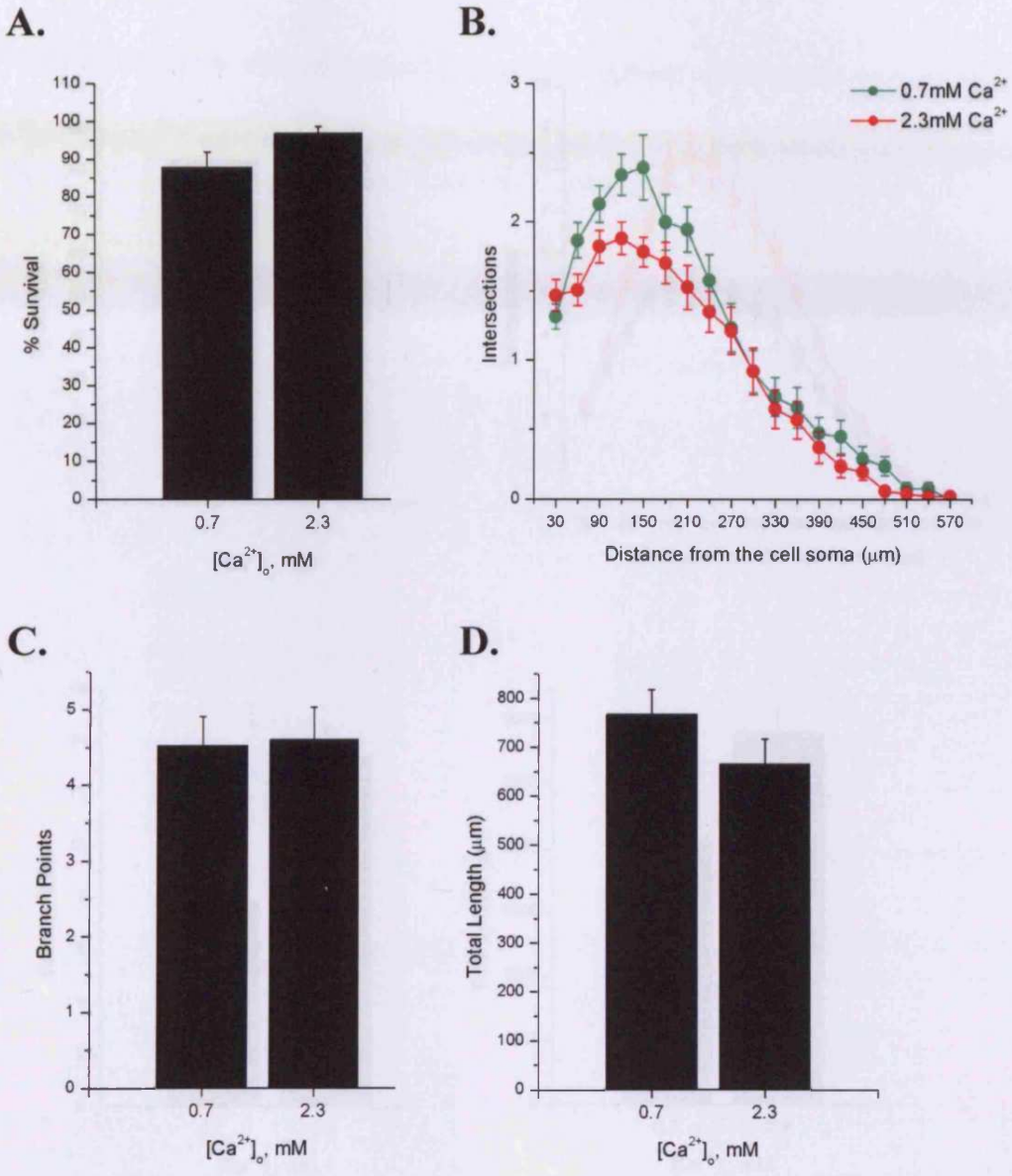

Figure 32: Developmental Effect of $[Ca^{2+}]_o$ on SCG Neurite Outgrowth I: E15 SCG Neurite Arborisation is Not Sensitive to Changes in $[Ca^{2+}]_o$. E15 SCG neurons were cultured in the presence of 0.4ng.ml^{-1} NGF and 100μM caspase inhibitor III in either 0.7mM or 2.3mM $[Ca^{2+}]_o$. Neurons were grown for 24hrs before determining percentage survival, labelling with calcein-AM and capturing fluorescent images. **A.** No differences in neuronal survival were seen between cell groups due to the use of caspase inhibitors, **B.** Sholl analysis, **C.** the number of branch points and **D.** total neurite length show there to be no effect of altering $[Ca^{2+}]_o$ on the arborisation of E15 SCG neurons (n=38-48 neurons per condition). Data are presented as the mean ± SEM.

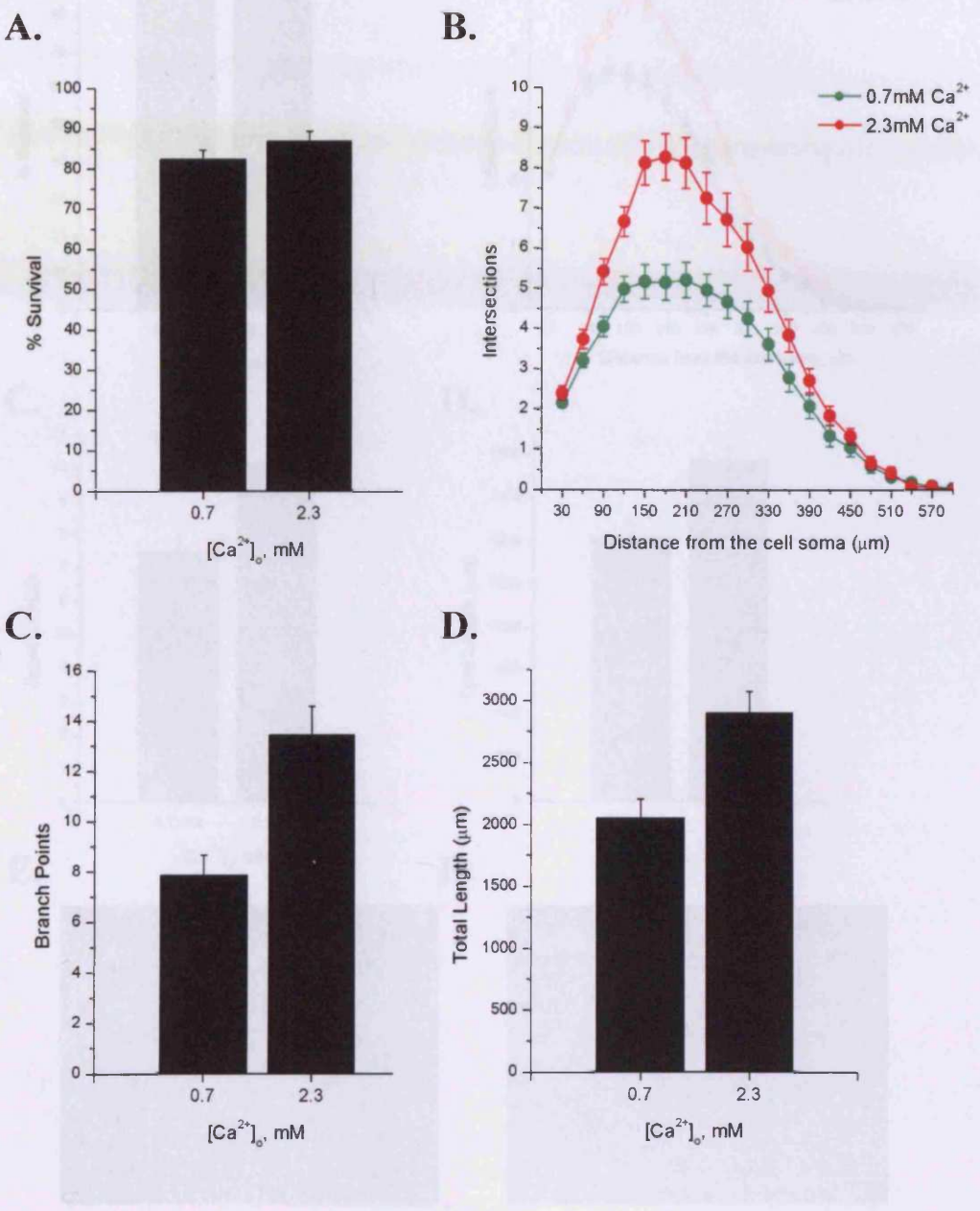

Figure 33: Developmental Effect of $[Ca^{2+}]_o$ on SCG Neurite Outgrowth IIa: E18 SCG Neurite Arborisation is Sensitive to Changes in $[Ca^{2+}]_o$. E18 SCG neurons were cultured in the presence of 0.4ng.ml^{-1} NGF and 100μM caspase inhibitor III in either 0.7mM or 2.3mM $[Ca^{2+}]_o$. Neurons were grown for 24hrs before determining percentage survival, labelling with calcein-AM and capturing fluorescent images. **A.** No differences in neuronal survival were seen between cell groups due to the use of caspase inhibitors, **B.** Sholl analysis, **C.** the number of branch points and **D.** total neurite length reveal a reduction in arborisation of neurons cultured in low (0.7mM) $[Ca^{2+}]_o$ compared to high (2.3mM) $[Ca^{2+}]_o$ (n=41-48 neurons per condition;. Data are presented as the mean ± SEM.

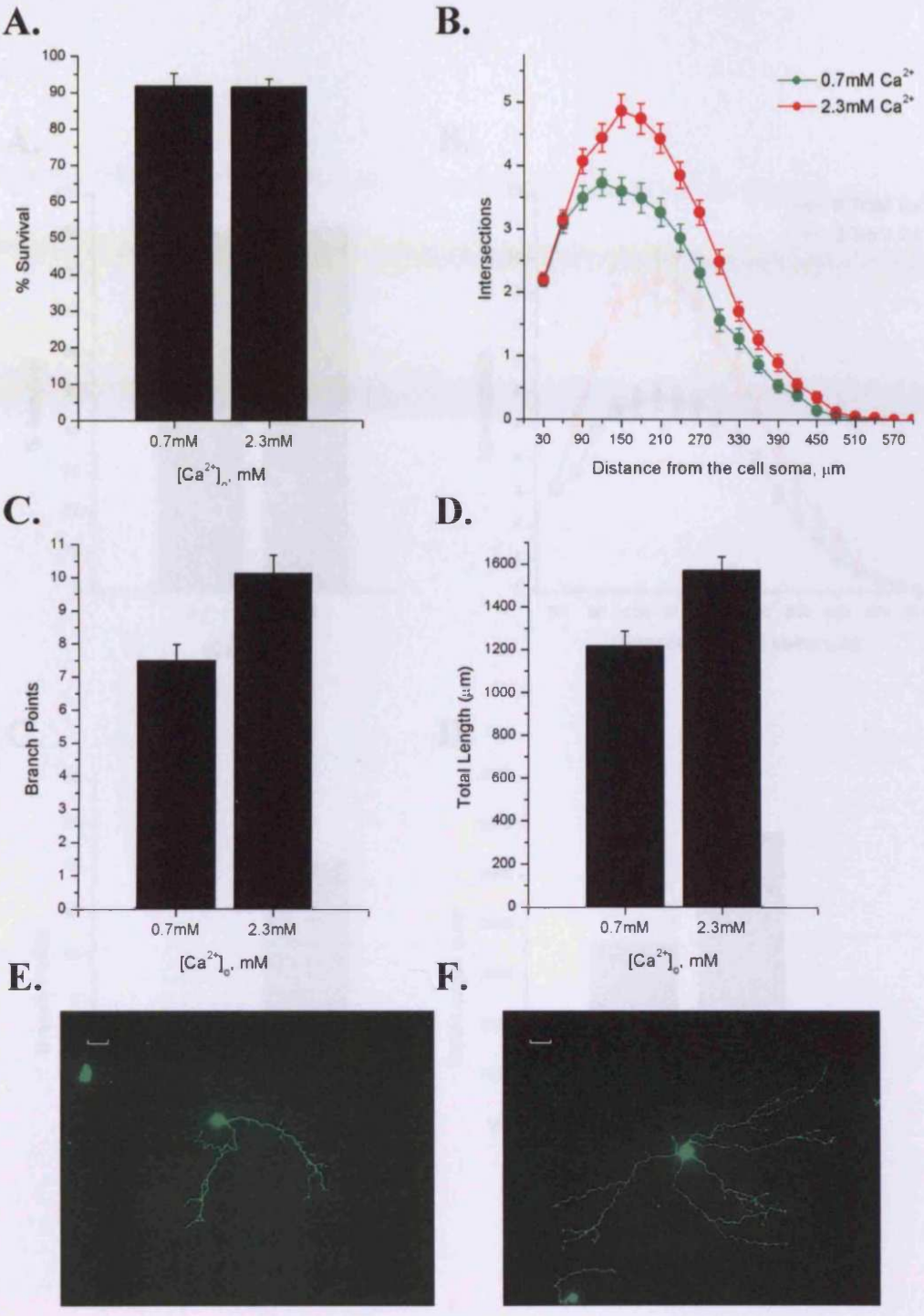

Figure 34: Developmental Effect of $[Ca^{2+}]_o$ on SCG Neurite Outgrowth IIb: $[Ca^{2+}]_o$ Sensitivity of E18 SCG Arborisation Using Caspase Inhibitors to Support Survival can be Reproduced using Neurons Deficient in Bax. *Bax*$^{-/-}$ neurons were cultured in the presence of 0.4ng.ml^{-1} NGF and either 0.7mM or 2.3mM $[Ca^{2+}]_o$. Neurons were grown for 24hrs before determining percentage survival, and capturing fluorescent images. **A.** No differences were seen in survival due to the Bax deficiency. **B.** Sholl analysis, **C.** Number of branch points and **D.** Total neurite length of neurons grown at 0.7mM $[Ca^{2+}]_o$ are significantly reduced compared to those in 2.3mM $[Ca^{2+}]_o$ (n=98-101 neurons from two *Bax*$^{-/-}$ embryos per condition). Data are presented as the mean ± SEM. **E.** An example of a calcein-stained Bax-deficient neuron grown in 0.7mM Ca^{2+} and **F.** an example of a calcein-stained Bax-deficient neuron grown in 2.3mM Ca^{2+}. Scale bar = 50µm.

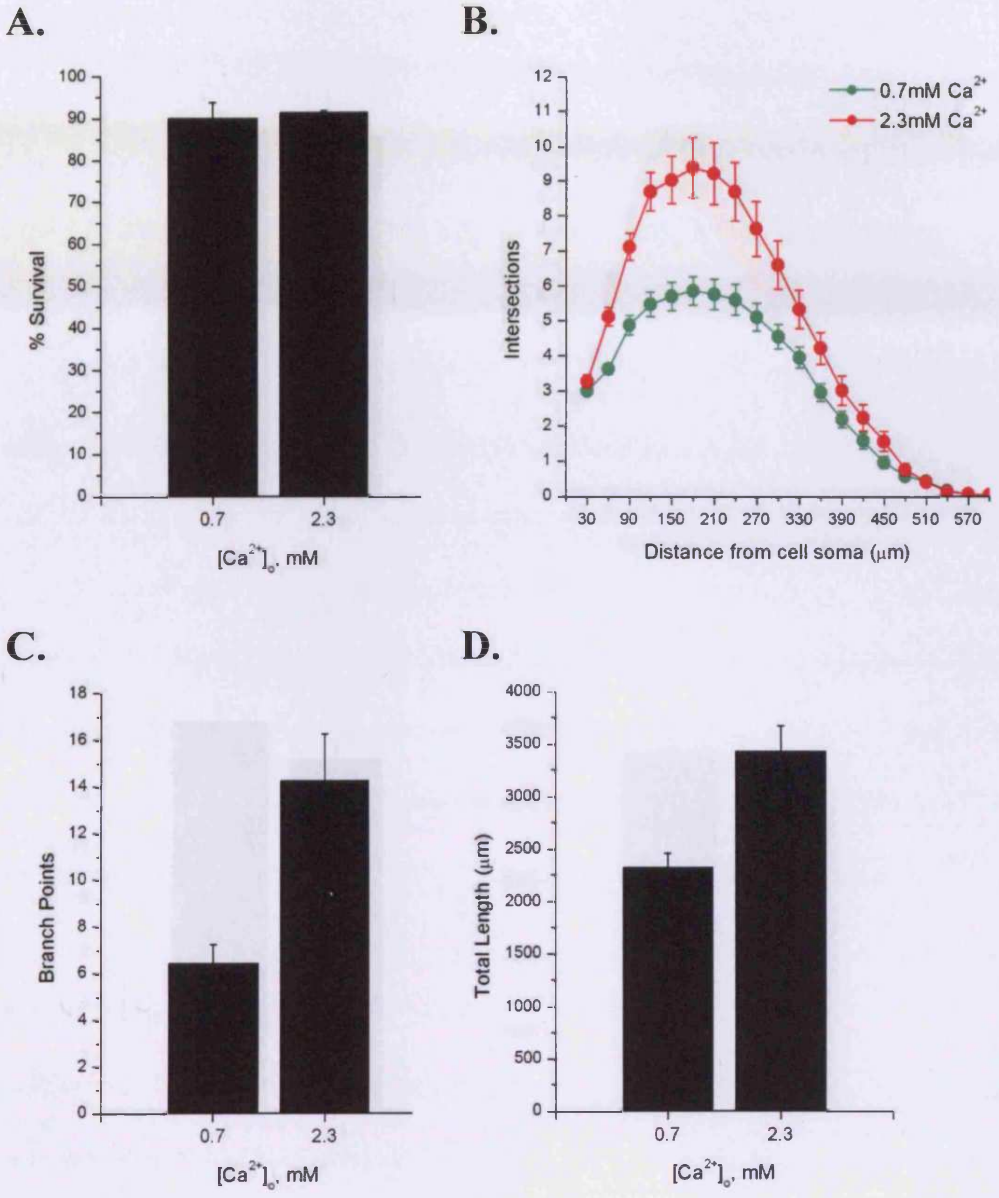

Figure 35: Developmental Effect of $[Ca^{2+}]_o$ on SCG Neurite Outgrowth III: P0 SCG Neurite Arborisation is Sensitive to Changes in $[Ca^{2+}]_o$. P0 SCG neurons were cultured in the presence of 0.4ng.ml^{-1} NGF and 100μM caspase inhibitor III in either 0.7mM or 2.3mM $[Ca^{2+}]_o$. Neurons were grown for 24hrs before determining percentage survival, labelling with calcein-AM and capturing fluorescent images. **A.** No differences in neuronal survival were seen between cell groups due to the use of caspase inhibitors, **B.** Sholl analysis, **C.** the number of branch points and **D.** total neurite length reveal a reduction in arborisation of neurons cultured in low (0.7mM) $[Ca^{2+}]_o$ compared to high (2.3mM) $[Ca^{2+}]_o$ (n=50-51 neurons per condition). Data are presented as the mean ± SEM.

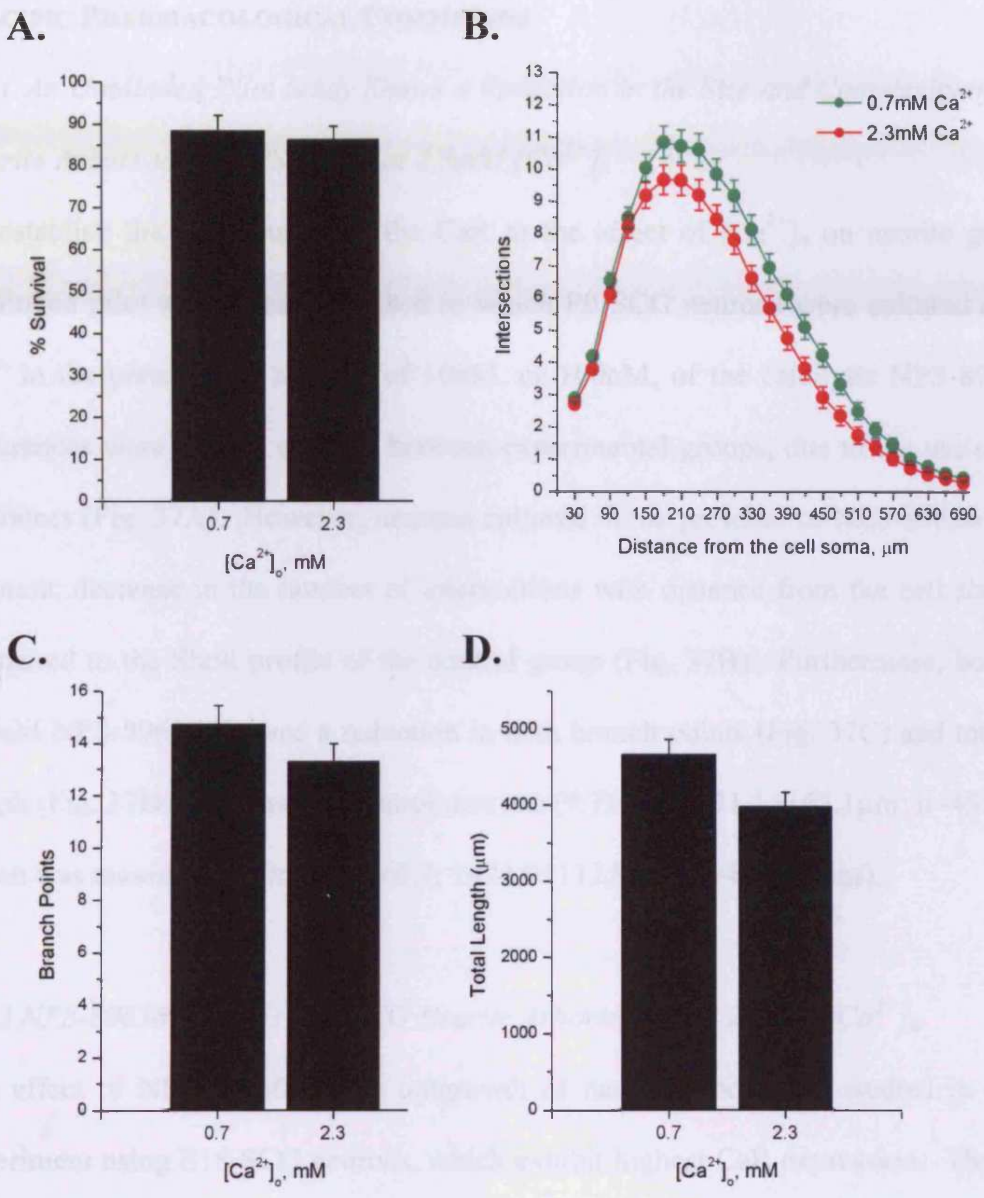

Figure 36: Developmental Effect of $[Ca^{2+}]_o$ on SCG Neurite Outgrowth IV: P1 SCG Neurite Arborisation is Not Sensitive to Changes in $[Ca^{2+}]_o$. P1 SCG neurons were cultured in the presence of 0.4ng.ml^{-1} NGF and 100μM caspase inhibitor III in either 0.7mM or 2.3mM $[Ca^{2+}]_o$. Neurons were grown for 24hrs before determining percentage survival, labelling with calcein-AM and capturing fluorescent images. **A.** No differences in neuronal survival were seen between cell groups due to the use of caspase inhibitors, **B.** Sholl analysis, **C.** the number of branch points and **D.** total neurite length show there to be no effect of altering $[Ca^{2+}]_o$ on the arborisation of P1 SCG neurons (n=116-120 neurons per condition from two separate cultures). Data are presented as the mean ± SEM.

4.3 Determining a Role for the CaR in Neurite Outgrowth Using CaR-Specific Pharmacological Compounds

4.3.1 An Unblinded Pilot Study Shows a Reduction in the Size and Complexity of P0 SCG Neurite Arbors using NPS-89636 at 2.3mM $[Ca^{2+}]_o$

To establish the contribution of the CaR to the effect of $[Ca^{2+}]_o$ on neurite growth, an unblinded pilot study was conducted in which P0 SCG neurons were cultured at 2.3mM Ca^{2+} in the presence or absence of 10nM, or 100nM, of the calcilytic NPS-89636. No differences were seen in survival between experimental groups, due to the use of caspase inhibitors (Fig. 37A). However, neurons cultured in the presence of NPS-89636 showed a dramatic decrease in the number of intersections with distance from the cell soma, when compared to the Sholl profile of the control group (Fig. 37B). Furthermore, both 10 and 100nM NPS-89636 showed a reduction in both branch points (Fig. 37C) and total neurite length (Fig. 37D) compared to control neurons (9.7±0.8; 2371.1±163.1μm; n=45 neurons), which was maximal at 10nM (6.2±0.7; 1424.9±112.9μm; n=45 neurons).

4.3.2 NPS-89636 Reduces E18 SCG Neurite Arborisation at 2.3mM $[Ca^{2+}]_o$

The effect of NPS-89636 on the outgrowth of neurite arbors was studied in a blinded experiment using E18 SCG neurons, which exhibit highest CaR expression. The effect of NPS-89636 on E18 neurons was very similar to the effect at P0. The culture was carried out using caspase inhibitors so no effect on survival was apparent (Fig. 38A) and both 10 and 100nM NPS-89636 reduced the Sholl profile when compared to the control group (Fig. 38B), 10nM reaching $P<0.001$ at 210μm from the cell soma (n=81 neurons from two separate cultures). As seen at P0, the calcilytic reduced both branching (Fig. 38C) and length (Fig. 38D) parameters significantly (n=80-90 neurons from two separate cultures) with a maximal effect seen using 10nM.

Representative examples of neurons grown in 0nM (control), 10nM and 100nM NPS-89636 are shown in Fig. 38E-G, respectively. A reduction in the size and complexity of neurite arbors is apparent with 10 and 100nM NPS-89636 when compared to the control.

4.3.3 NPS-89636 Does Not Affect P1 SCG Neurite Arborisation at 2.3mM $[Ca^{2+}]_o$

To determine whether the effects of NPS-89636 were non-specific, adverse effects on neuronal morphology, P1 SCG neurons, which have been shown to be insensitive to changes in $[Ca^{2+}]_o$, were grown in the presence of 100nM NPS-89636 at 2.3mM Ca^{2+}. Fig. 39A reveals no survival effect between experimental groups, due to the inclusion of caspase inhibitors in the culture medium. The Sholl profile (Fig. 39B), and both the number of branch points (Fig. 39C) and total neurite length (Fig. 39D) show there to be no difference in the size and complexity of neurite arbors grown in the presence (n=52 neurons) and absence (n=57 neurons) of 100nM NPS-89636.

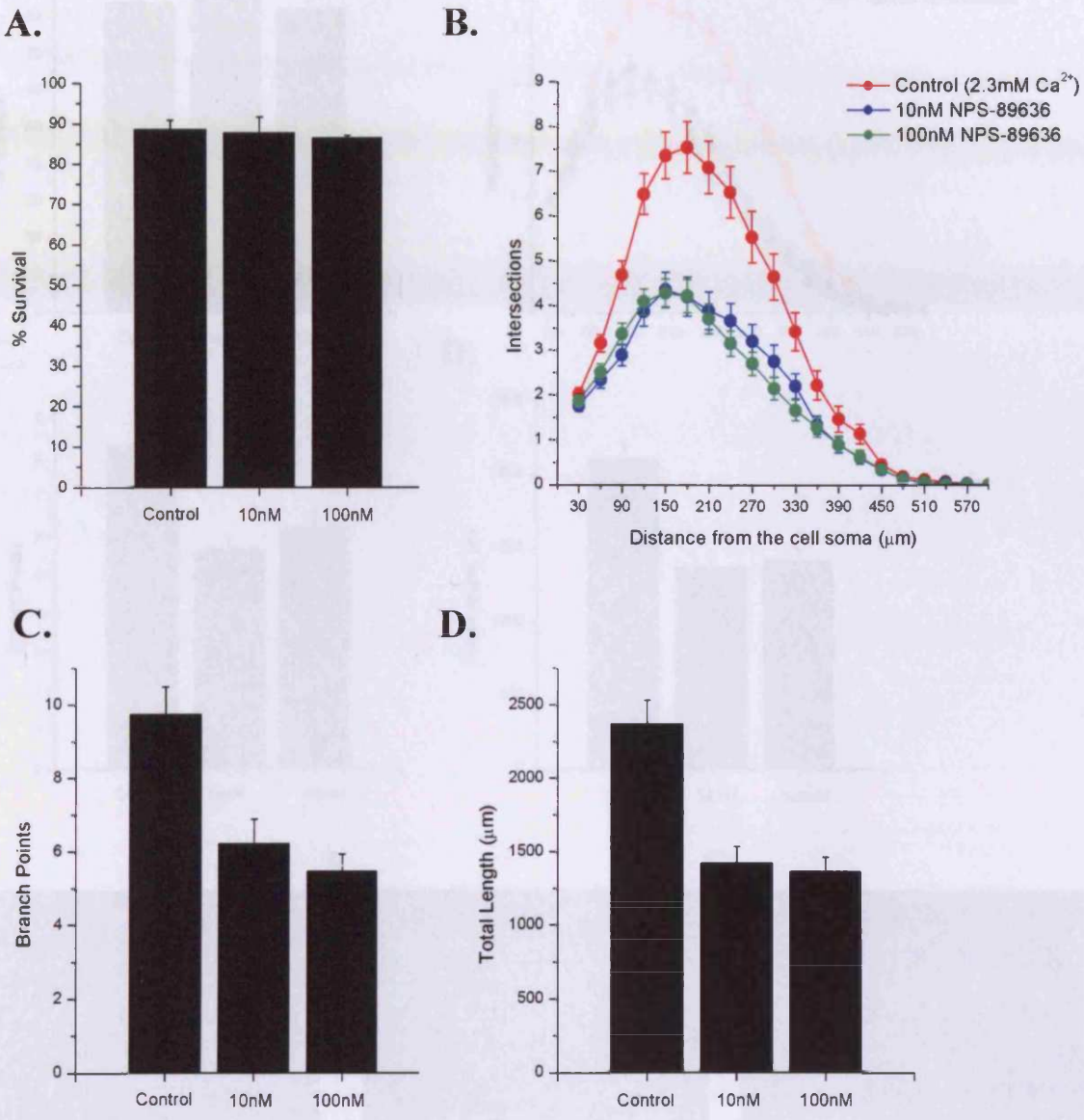

Figure 37: An Unblinded Pilot Experiment shows a Reduction in the Size and Complexity of P0 SCG Neurite Arbors using NPS-89636 at 2.3mM $[Ca^{2+}]_o$. P0 SCG neurons were cultured in the presence of 0.4ng.ml^{-1} NGF, 100μM Caspase Inhibitor III at 2.3mM $[Ca^{2+}]_o$. Neurons were grown for 24hrs before determining percentage survival and capturing fluorescent images for the quantification of neurite length and branching. **A.** No differences in neuronal survival were seen between cell groups due to the use of caspase inhibitors, **B.** Sholl analysis reveals a reduction in size and complexity of P0 SCG arbors with 10 and 100nM NPS-89636 (statistical significance for both 10 and 100nM NPS-89636 versus control is shown), **C.** the number of branch points and **D.** total neurite length demonstrate a reduction P0 SCG neurite arborisation with NPS-89636, which is maximal at 10nM (n=45-47 neurons per condition). Data are presented as the mean ± SEM.

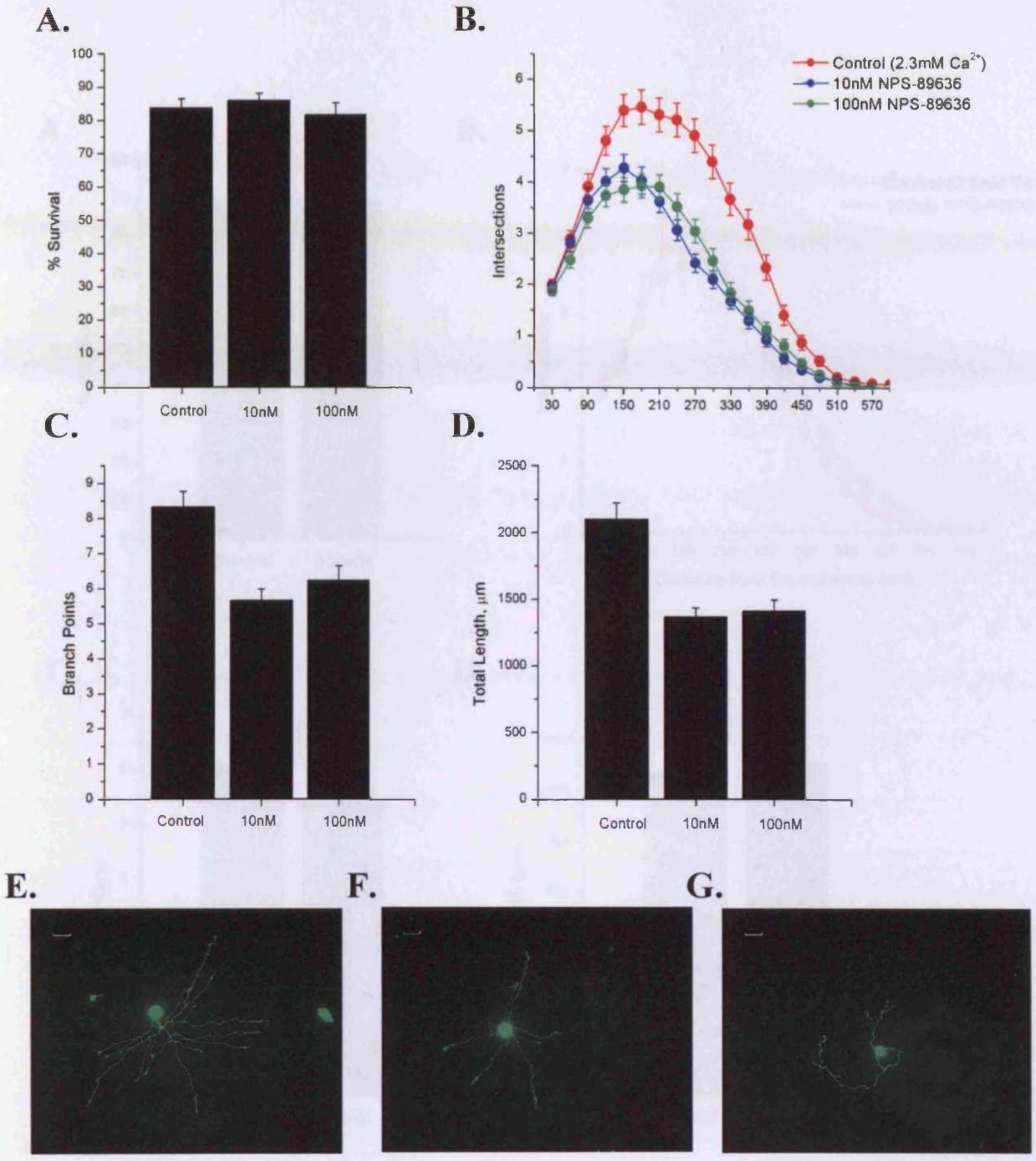

Figure 38: NPS-89636 Reduces E18 SCG Neurite Arborisation at 2.3mM $[Ca^{2+}]_o$: E18 SCG neurons were cultured in the presence of 0.4ng.ml^{-1} NGF, 100µM Caspase Inhibitor III at 2.3mM $[Ca^{2+}]_o$. Neurons were grown for 24hrs before determining percentage survival, and capturing fluorescent images. **A.** No differences in neuronal survival were seen between cell groups due to the use of caspase inhibitors, **B.** Sholl analysis shows a reduction in size and complexity of neurite arbors with 10nM and 100nM NPS-89636 (statistical significance is shown for both 10 and 100nM NPS-89636 versus control). **C.** the number of branch points and **D.** total neurite length also demonstrate a reduction in neurite arborisation of E18 SCG neurons with NPS-89636 (n=80-90 neurons per condition from two separate cell isolations). Data are presented as the mean ± SEM. Examples of calcein-stained neurons grown in **E.** 0nM (control), **F.** 10nM and **G.** 100nM NPS-89636. Scale bar = 50µm.

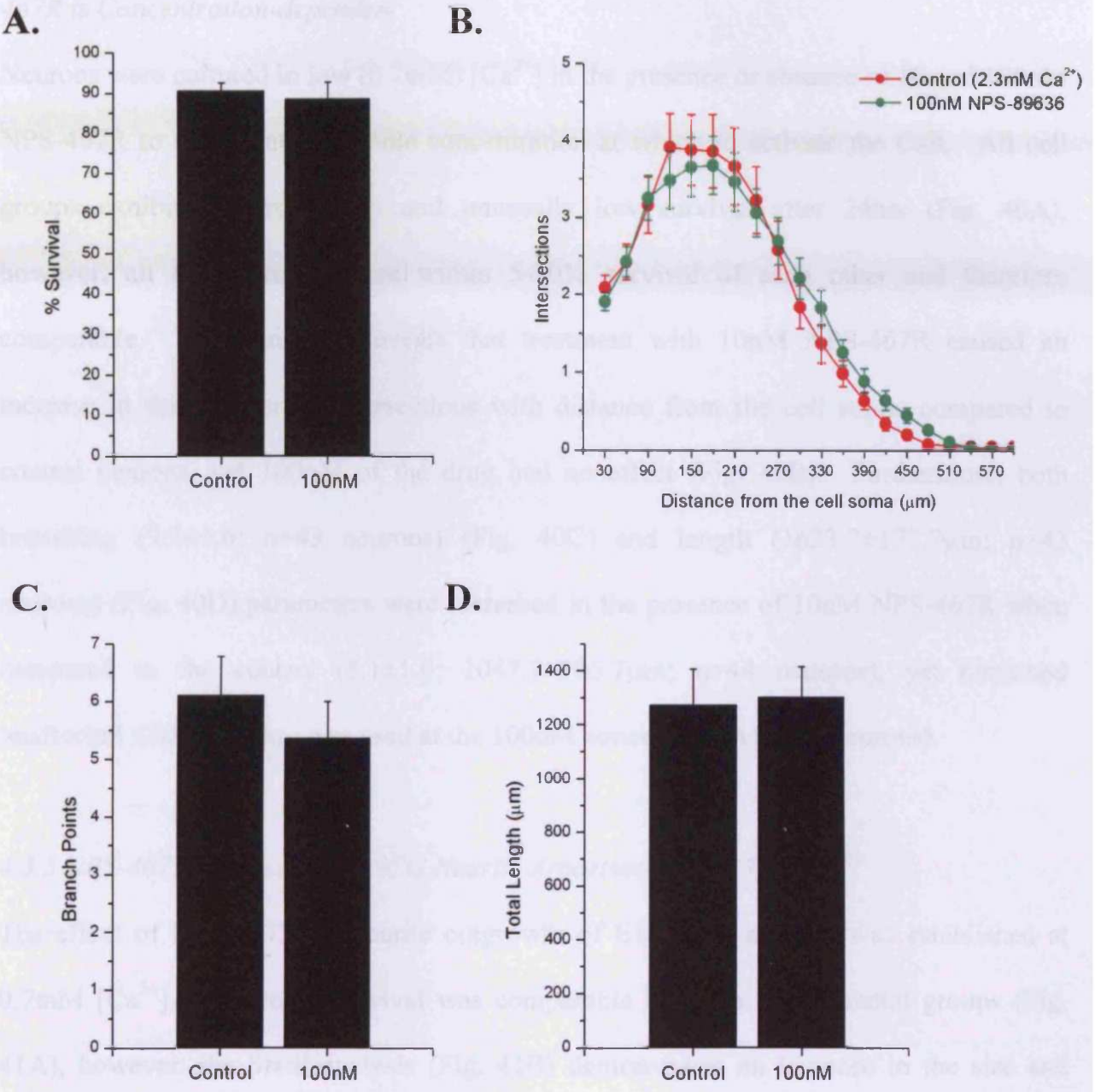

Figure 39: NPS-89636 Does Not Affect P1 SCG Neurite Arborisation at 2.3mM $[Ca^{2+}]_o$: P1 SCG neurons were cultured in the presence of 0.4ng.ml^{-1} NGF, 100μM Caspase Inhibitor III at 2.3mM $[Ca^{2+}]_o$. Neurons were grown for 24hrs before determining percentage survival, and capturing fluorescent images. **A.** No differences in neuronal survival were seen between cell groups due to the use of caspase inhibitors, **B.** Sholl analysis reveals there to be no difference in size and complexity of neurite arbors grown in the presence or absence of 100nM NPS-89636. **C.** the number of branch points and **D.** total neurite length also show there to be no difference in the neurite arborisation of P1 SCG neurons grown in the presence or absence of 100nM NPS-89636 (n=52-75 neurons per condition). Data are presented as the mean ± SEM.

4.3.4 The Effect of Increasing E18 SCG Neurite Arborisation at 0.7mM $[Ca^{2+}]_o$ with NPS-467R is Concentration-dependent

Neurons were cultured in low (0.7mM) $[Ca^{2+}]$ in the presence or absence of 10 and 100nM NPS-467R to determine a suitable concentration at which to activate the CaR. All cell groups exhibited unexpectedly and unusually low survival after 24hrs (Fig. 40A), however, all three groups were within 5-10% survival of each other and therefore comparable. Sholl analysis reveals that treatment with 10nM NPS-467R caused an increase in the number of intersections with distance from the cell soma, compared to control neurons, yet 100nM of the drug had no effect (Fig. 40B). Furthermore, both branching (9.5±1.6; n=43 neurons) (Fig. 40C) and length (1623.7±177.7μm; n=43 neurons) (Fig. 40D) parameters were increased in the presence of 10nM NPS-467R when compared to the control (5.1±1.0; 1047.7±105.7μm; n=44 neurons), yet remained unaffected when the drug was used at the 100nM concentration (n=42 neurons).

4.3.5 NPS-467R Increases E18 SCG Neurite Arborisation at 0.7mM Ca^{2+}

The effect of NPS-467R on neurite outgrowth of E18 SCG neurons was established at 0.7mM $[Ca^{2+}]_o$. Neuronal survival was comparable between experimental groups (Fig. 41A), however, the Sholl analysis (Fig. 41B) demonstrates an increase in the size and complexity of neurite arbors of neurons grown in the presence of 10nM NPS-467R at 0.7mM (reaching $P<0.001$ at 150μm from the cell soma) compared to the control group. Furthermore, both the number of branch points (10.8±0.86; n=134 neurons from 3 independent cultures; $P<0.001$) (Fig. 41C) and total neurite length (1988.8±114.7μm; n=134 neurons from 3 independent cultures; $P<0.001$) (Fig. 41D) were increased by NPS-467R treatment, compared to the control (7.3±0.6; 1513.4±80.8μm; n=134 neurons from 3 separate cultures).

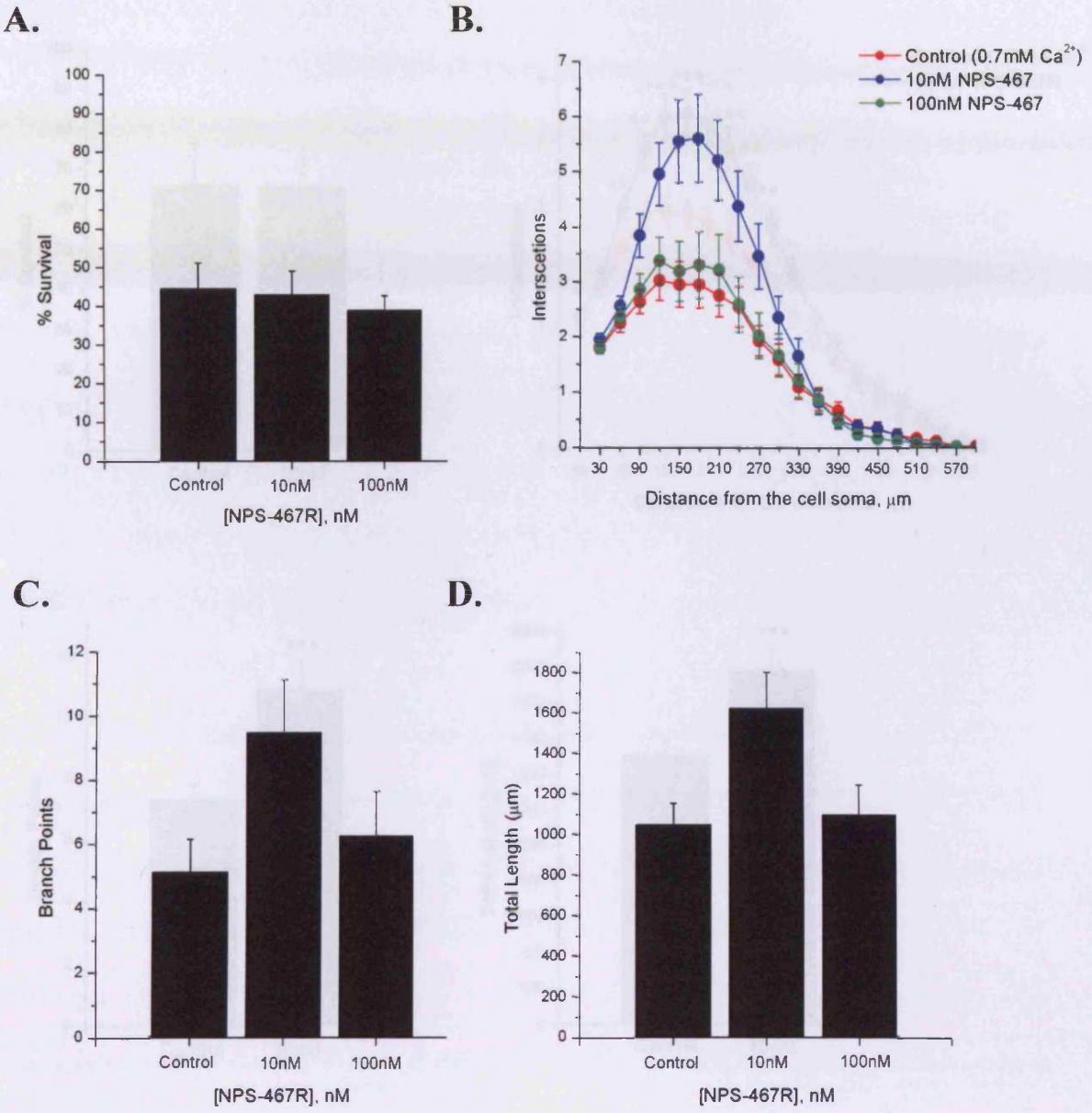

Figure 40: The Effect of Increasing E18 SCG Neurite Arborisation at 0.7mM $[Ca^{2+}]_o$ Using NPS-467R is Concentration Dependent: E18 SCG neurons were cultured in the presence of 0.4ng.ml^{-1} NGF, 100μM Caspase Inhibitor III at 0.7mM $[Ca^{2+}]_o$. Neurons were grown for 24hrs before determining percentage survival, and capturing fluorescent images. **A.** Although unusually low % survival was seen using caspase inhibitors, no differences in neuronal survival were seen between cell groups, **B.** Sholl analysis, **C.** the number of branch points and **D.** total neurite length demonstrate an increase in arborisation of E18 SCG neurons with 10nM, but not with 100nM NPS-467R (n=42-44 neurons per condition). Data are presented as the mean ± SEM.

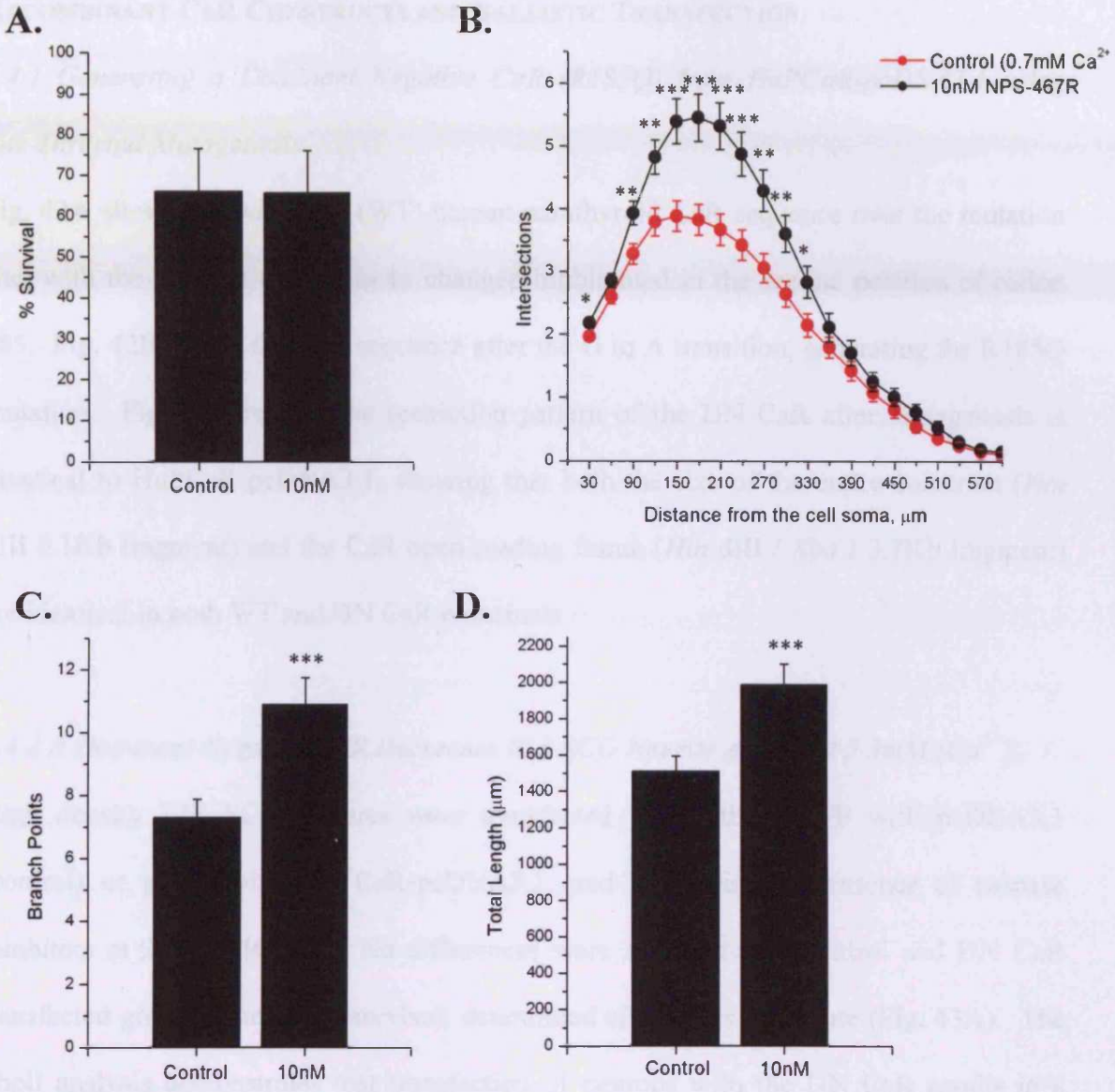

Figure 41: NPS-467R Increases E18 SCG Neurite Arborisation at 0.7mM $[Ca^{2+}]_o$: E18 SCG neurons were cultured in the presence of 0.4ng.ml^{-1} NGF, 100μM Caspase Inhibitor III at 0.7mM $[Ca^{2+}]_o$. Neurons were grown for 24hrs before determining percentage survival, and capturing fluorescent images. **A.** No differences in neuronal survival were seen between cell groups due to the use of caspase inhibitors, **B.** Sholl analysis, **C.** the number of branch points and **D.** total neurite length demonstrates an increase in arborisation of E18 SCG neurons with NPS-467R (n=133 neurons per condition from three separate cultures; *P<0.05, **P<0.01, ***P<0.001, Unpaired T-test). Data are presented as the mean ± SEM.

4.4 Determining a Role for the CaR in Neurite Outgrowth Using Recombinant CaR Constructs and Ballistic Transfection

4.4.1 Generating a Dominant Negative CaR (R185Q) from HuPCaR-pcDNA3.1 using Site-Directed Mutagenesis

Fig. 42A shows the wild-type (WT) human parathyroid CaR sequence over the mutation site, with the guanine residue to be changed highlighted in the second position of codon 185. Fig. 42B shows the CaR sequence after the G to A transition, generating the R185Q mutation. Fig. 42C reveals the restriction pattern of the DN CaR after mutagenesis is identical to HuPCaR-pcDNA3.1, showing that both the size of the entire construct (*Hin* dIII 9.1Kb fragment) and the CaR open reading frame (*Hin* dIII / *Xba* I 3.7Kb fragment) are identical in both WT and DN CaR constructs.

4.4.2 A Dominant Negative CaR Decreases E18 SCG Neurite Arbors at 2.3mM $[Ca^{2+}]_o$

High density E18 SCG cultures were transfected with either pYFP with pcDNA3.1 (control) or pYFP with DN CaR-pcDNA3.1, and grown in the presence of caspase inhibitors at 2.3mM $[Ca^{2+}]_o$. No differences were seen between control and DN CaR transfected groups in terms of survival, determined after 48hrs in culture (Fig. 43A). The Sholl analysis demonstrates that transfection of neurons with the DN CaR results in a dramatic reduction in the size and complexity of E18 SCG neurite arbors when compared to control transfected neurons (Fig. 43B). Consistent with previous data using the NPS-89636 compound, transfection with the DN CaR construct reduced both the number of branch points (3.4±0.4; n=138 neurons from three separate cultures; $P<0.001$) and total length (562.1±58.3μm; n=138 neurons from three separate cultures; $P<0.001$) of E18 SCG neurite arbors when compared to the control group (9.2±0.8; 1083.1±68.4μm; n=204 neurons from three separate cultures) (Fig. 43C and D).

Representative examples of control- and DN CaR-transfected neurons grown in 2.3mM $[Ca^{2+}]_o$ in caspase inhibitors are shown in Fig. 43E and F. The example of control-transfected neurons exhibits a much larger and more complex neurite arbor compared to the DN CaR-transfected example.

4.4.3 Over-expressing Wild-type CaR (WT CaR) has No Effect on E18 SCG Neurite Arbors at 2.3mM $[Ca^{2+}]_o$

Expressing the WT human parathyroid CaR at E18 was not only a control for the effects of overexpressing the DN CaR at this age, but would also establish whether the size and complexity of neurite arbors could be increased further with overexpression of the WT CaR. No differences in survival were seen between control and WT CaR transfected groups, determined after 48hrs in culture (Fig. 44A). Sholl analysis of transfected neurons showed that there was no difference in arborisation between WT CaR-expressing (n=44 neurons) and control neurons (n=57 neurons) (Fig. 44B). Furthermore, there are no significant differences in the number of branch points and total neurite length of WT CaR transfected arbors when compared to the control (Fig. 44C-D).

4.4.4 A Dominant Negative (R185Q) CaR has No Effect on the $Ca^{2+}{}_o$ Sensitivity of P1 SCG Neurite Arbors at 2.3mM $[Ca^{2+}]_o$

To establish whether the effect of the DN CaR on E18 SCG neurite arborisation was due to a knock-down of SCG CaR function or a non-specific, adverse effect of overexpressing the construct, the DN CaR was expressed at an age where neurite arborisation is insensitive to changes in $[Ca^{2+}]_o$. P1 SCG neurons were transfected with pYFP with pcDNA3.1 (control) or pYFP with DN CaR-pcDNA3.1 and cultured in the presence of caspase inhibitors at 2.3mM $[Ca^{2+}]_o$. No differences were seen between control (n=60

neurons) and DN CaR-transfected (n=53 neurons) groups in terms of survival determined after 48hrs in culture (Fig. 45A). Furthermore, the DN CaR failed to affect the arborisation of P1 SCG neurons as determined by Sholl analysis (Fig. 45B). The branching and length parameters also remained unaffected (Fig. 45C-D).

4.4.5 Over-expressing Wild-type CaR (WT CaR) Increases the Size and Complexity of P1 SCG Neurite Arbors at 2.3mM $[Ca^{2+}]_o$

To determine whether sensitivity to $[Ca^{2+}]_o$ could be re-introduced at an age where neurite arborisation is normally unaffected by changes in $[Ca^{2+}]_o$, P1 SCG neurons were transfected with pYFP alone (control) or pYFP with WT CaR-pcDNA3.1 and cultured at 2.3mM $[Ca^{2+}]_o$ in caspase inhibitors. Under these conditions, no differences in survival were seen between groups at 48hrs, due to the use of caspase inhibitors (Fig. 46A). However, over-expression of the WT CaR caused a significant increase in the Sholl profile when compared to the control group (n=127-157 neurons; WT CaR reaching $P<0.01$ at 60μm from the cell soma) (Fig. 46B). Furthermore, the number of branch points (12.51±0.81; n=127 neurons from three separate cultures; $P<0.01$) and total neurite length (1649.2±118.8μm; n=127 neurons from three separate cultures; $P<0.001$) of WT CaR transfected neurons was increased when compared to control neurons (9.3±0.6; 916.5±62.9μm; n=157 neurons from three separate cultures) (Fig. 46C and D).

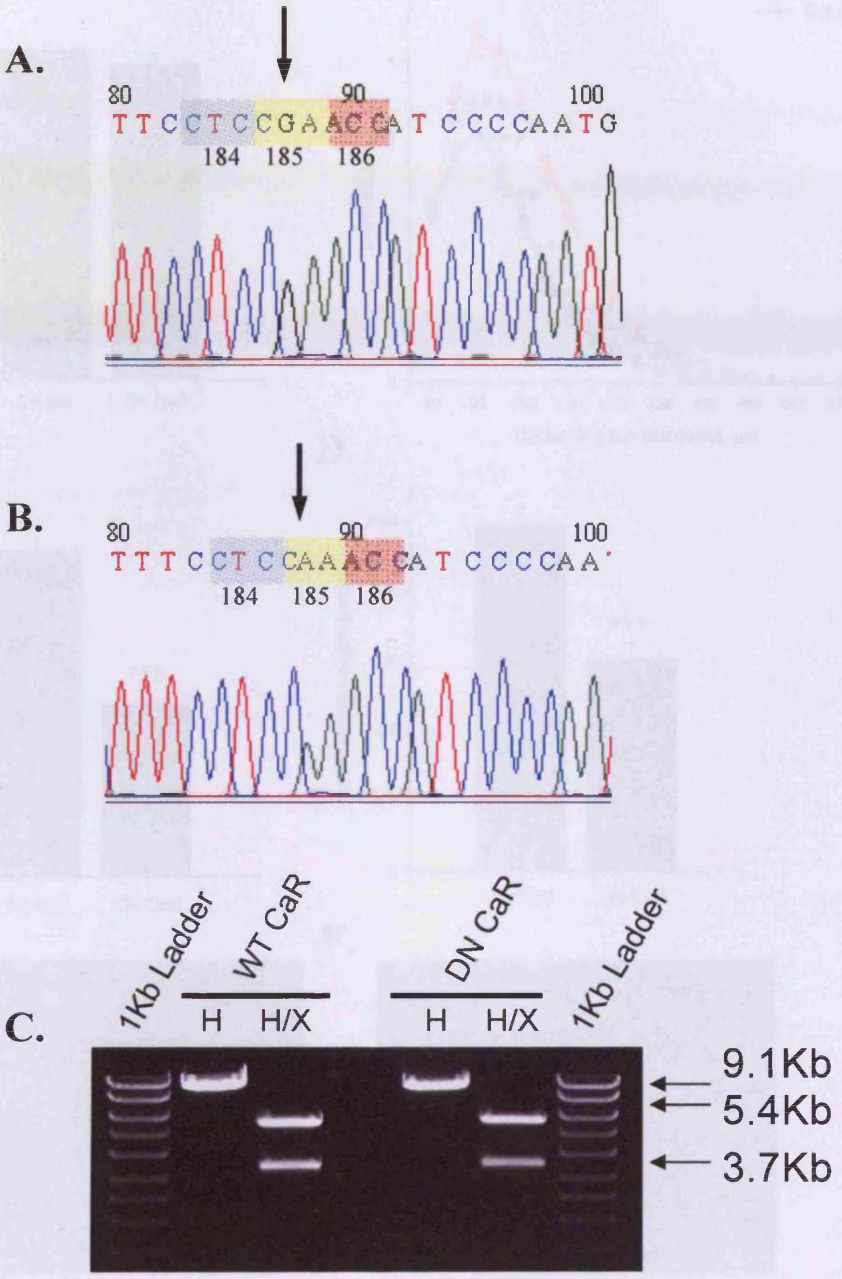

Figure 42: Generating a Dominant Negative CaR (R185Q) from HuPCaR-pcDNA3.1 using Site-Directed Mutagenesis. **A.** Wild-type CaR sequence highlighting the G to be mutated in the second position of codon 185 **B.** The dominant negative CaR sequence after the G to A transition, generating the R185Q mutation. **C.** *Hin* dIII (H) and *Hin* dIII / *Xba* I (H/X) restriction enzyme digests of the HuPCaR- and DN CaR-pcDNA3.1 constructs. The digests show the DN CaR construct (*Hin* dIII 9.1Kb fragment) and the CaR open reading frame (*Hin* dIII / *Xba* I 3.7Kb fragment) to be the correct size after mutagenesis.

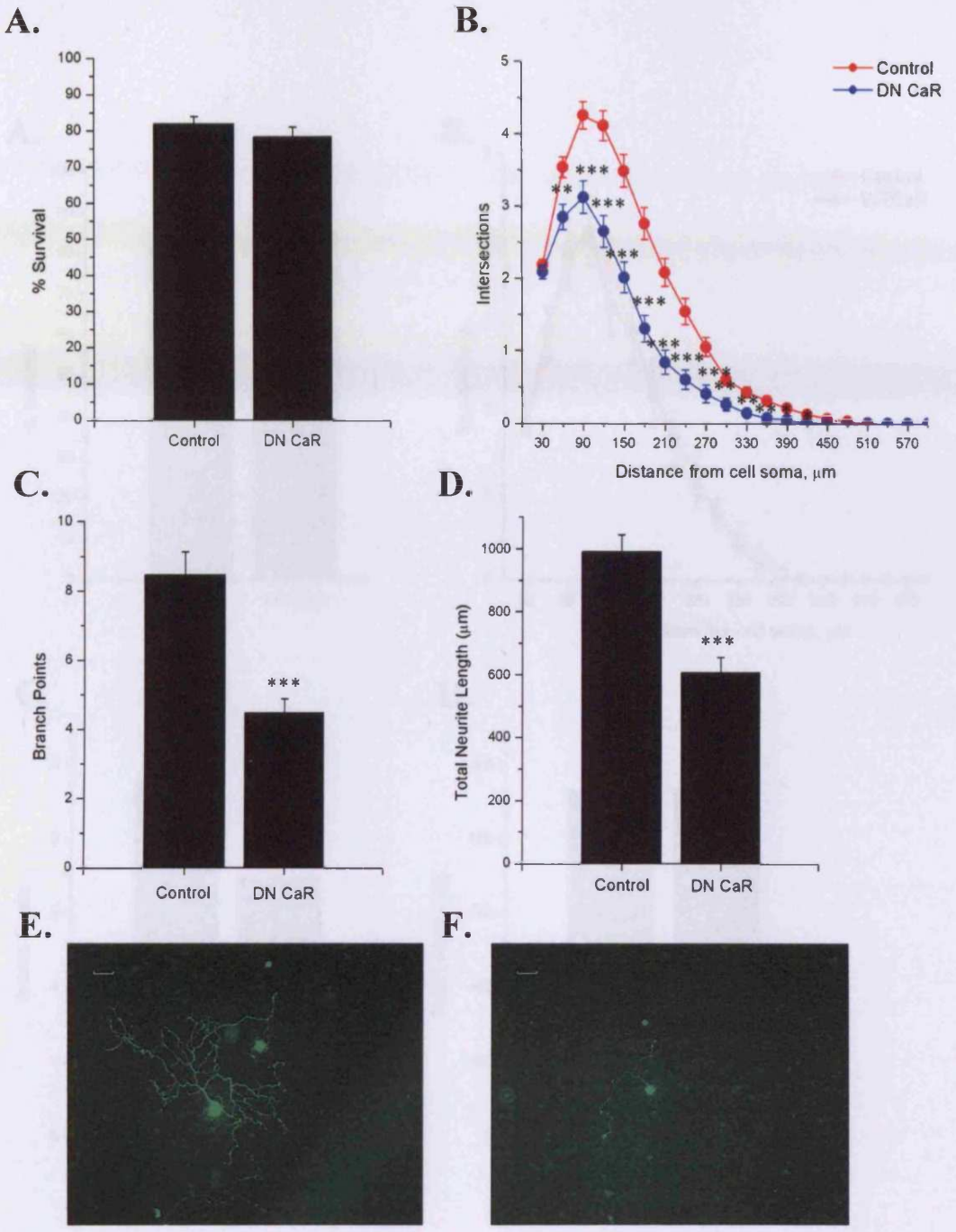

Figure 43: A Dominant Negative CaR (R185Q) Decreases E18 SCG Neurite Arbors at 2.3mM $[Ca^{2+}]_o$. Neurons were grown in high density cultures for 1-3hrs before ballistic transfection with pYFP alone (control) or pYFP with DN CaR-pcDNA3.1. Neurons were grown in the presence of caspase inhibitor III and 0.4ng.ml^{-1} NGF at 2.3mM $[Ca^{2+}]_o$. Fluorescent images were captured at 24hrs and estimates of survival were made at 48hrs, as described in the Methods section. **A.** No differences in neuronal survival were seen between cell groups due to the use of caspase inhibitors, **B.** Sholl analysis, **C.** the number of branch points and **D.** total neurite length demonstrate a decrease in arborisation of E18 SCG neurons with overexpression of the DN CaR (n=138-204 neurons per condition from three separate cultures; *P<0.05, **P<0.01, ***P<0.001, Unpaired T-test). Data are presented as the mean ± SEM. Representative pictures showing neurons that had been grown in high density cultures for 1-3hrs before ballistic transfection with **E.** pYFP alone (control) or **F.** pYFP with DN CaR-pcDNA3.1 Scale bar = 50μm.

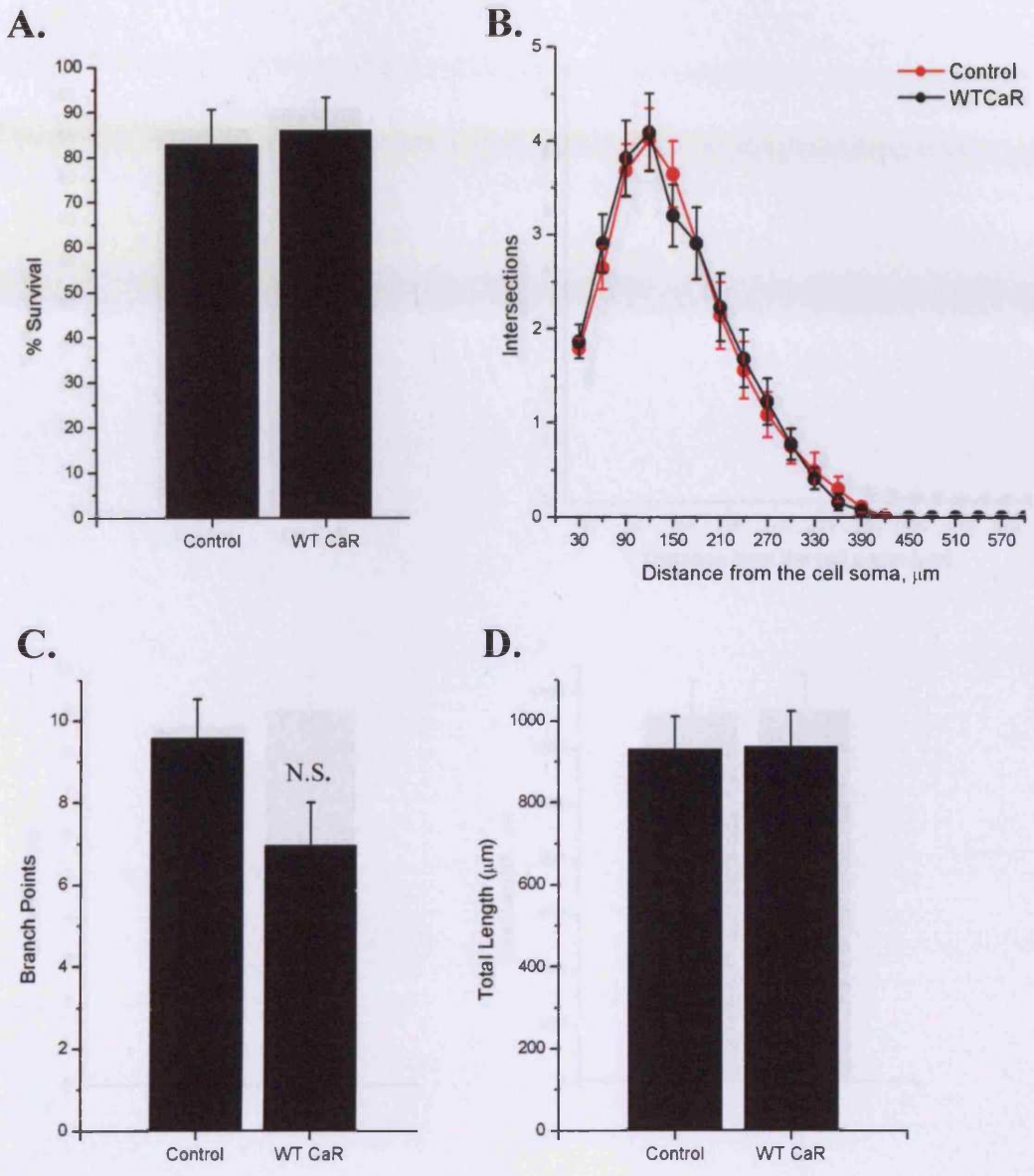

Figure 44: Over-expressing Wild-type CaR (WT CaR) Has No Effect on E18 SCG Neurite Arbors at 2.3mM $[Ca^{2+}]_o$. Neurons were grown in high density cultures for 1-3hrs before ballistic transfection with pYFP alone (control) or pYFP with DN CaR-pcDNA3.1. Neurons were grown in the presence of Caspase Inhibitor III and 0.4ng.ml^{-1} NGF at 2.3mM $[Ca^{2+}]_o$. Fluorescent images were captured at 24hrs and estimates of survival were made at 48hrs, as described in the Methods section. **A.** No differences in neuronal survival were seen between cell groups due to the use of caspase inhibitors, **B.** Sholl analysis, **C.** the number of branch points and **D.** total neurite length show there to be no effect of overexpressing the WT CaR on the arborisation of E18 SCG neurons (n=44-57 neurons per condition; Unpaired T-Test; N.S., not statistically significant). Data are presented as the mean ± SEM.

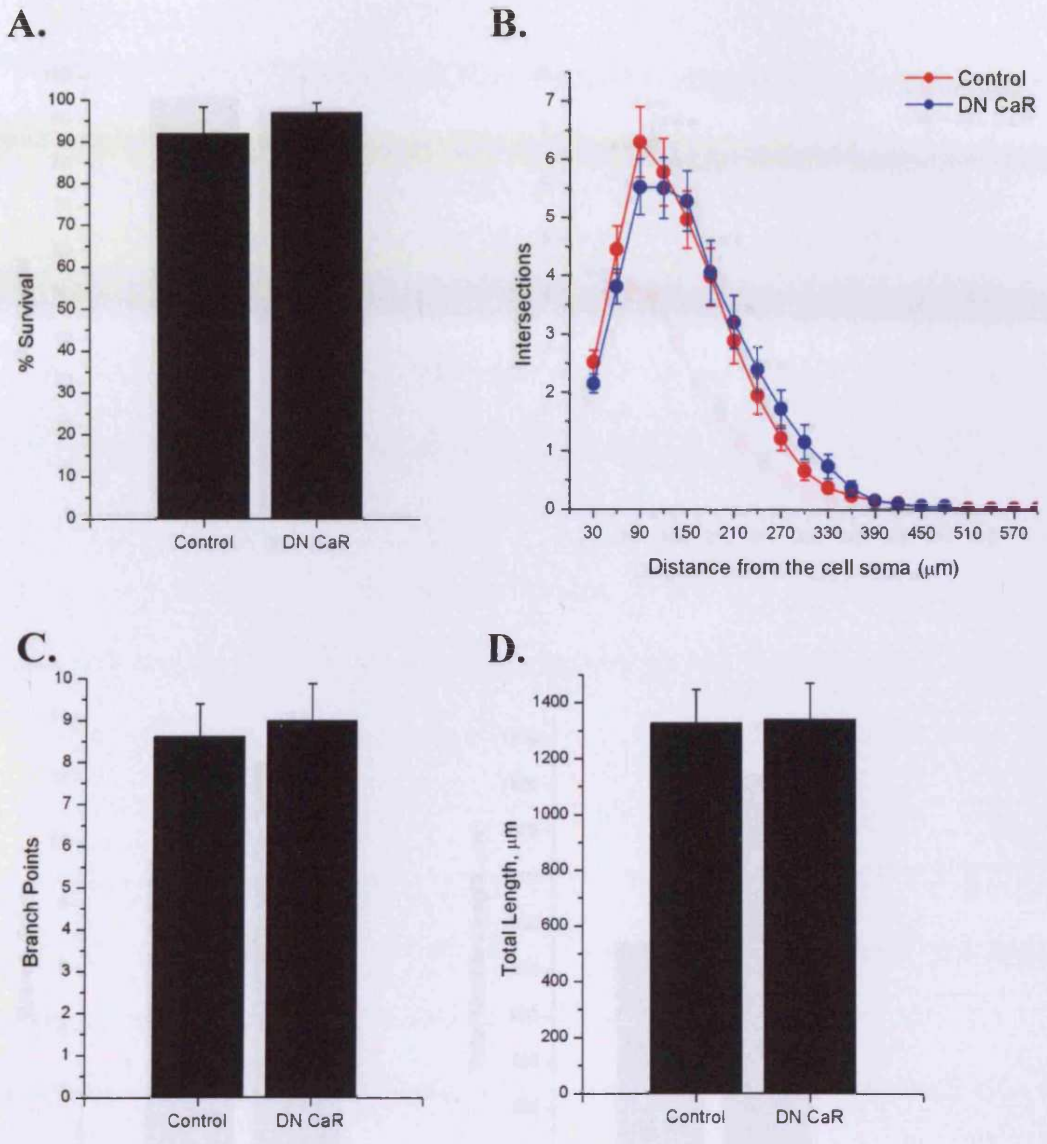

Figure 45: A Dominant Negative CaR (R185Q) Has No Effect on Ca^{2+}_o-Sensitivity of P1 SCG Neurite Arbors at 2.3mM $[Ca^{2+}]_o$. Neurons were grown in high density cultures for 1-3hrs before ballistic transfection with pYFP alone (control) or pYFP with DN CaR-pcDNA3.1. Neurons were grown in the presence of caspase inhibitor III and 0.4ng.ml^{-1} NGF at 2.3mM $[Ca^{2+}]_o$. Fluorescent images were captured at 24hrs and estimates of survival were made at 48hrs, as described in the Methods section. **A.** No differences in neuronal survival were seen between cell groups due to the use of caspase inhibitors, **B.** Sholl analysis, **C.** the number of branch points and **D.** total neurite length show there to be no effect of overexpressing the DN CaR on the arborisation of P1 SCG neurons (n=50-60 neurons per condition). Data are presented as the mean ± SEM.

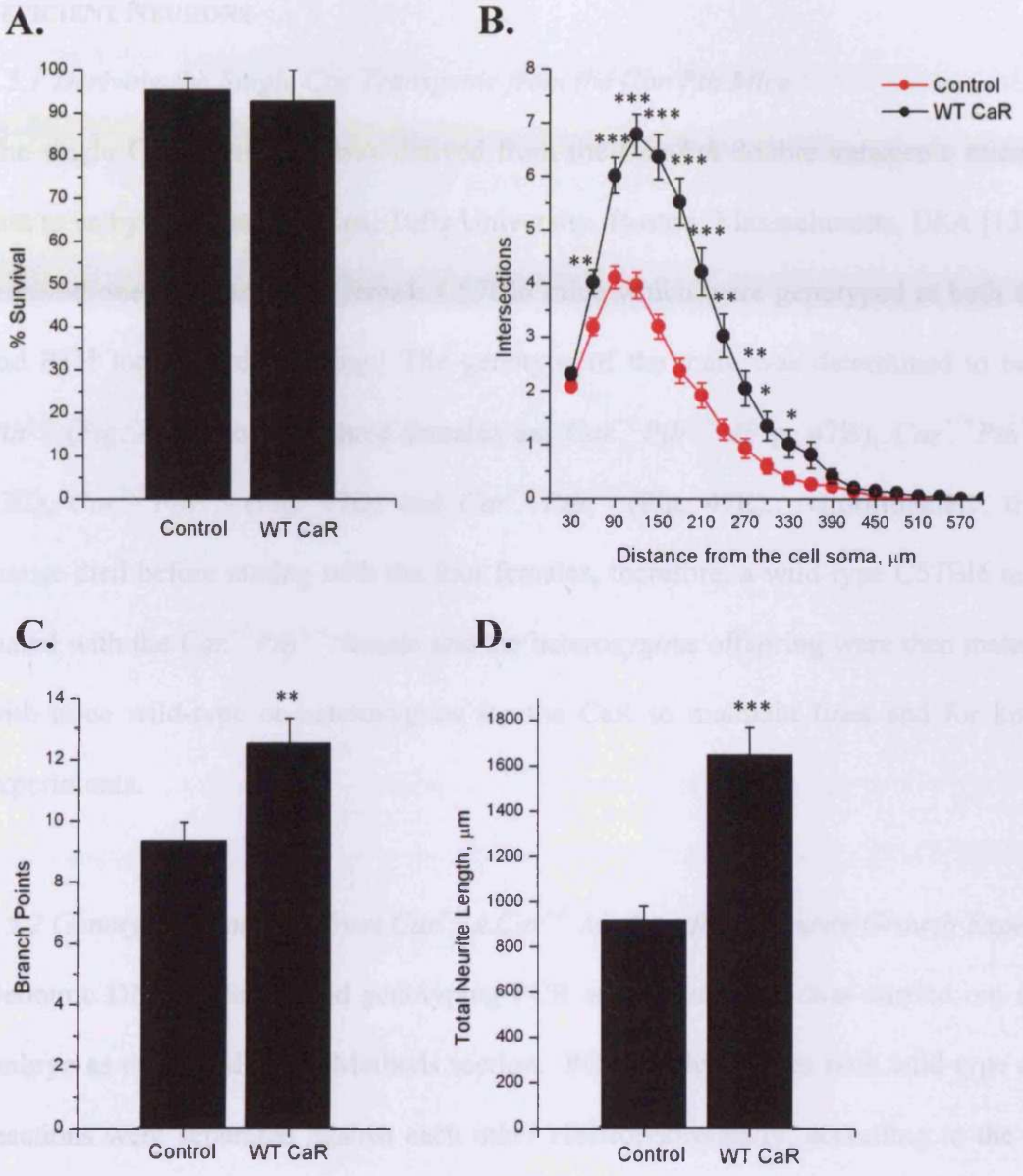

Figure 46: Over-expressing Wild-type CaR (WT CaR) Increases the Size and Complexity of P1 SCG Neurite Arbors at 2.3mM $[Ca^{2+}]_o$. Neurons were grown in high density cultures for 1-3hrs before ballistic transfection with pYFP alone (control) or pYFP with DN CaR-pcDNA3.1. Neurons were grown in the presence of caspase inhibitor III and 0.4ng.ml^{-1} NGF at 2.3mM $[Ca^{2+}]_o$. Fluorescent images were captured at 24hrs and estimates of survival were made at 48hrs, as described in the Methods section. **A.** No differences in neuronal survival were seen between cell groups due to the use of caspase inhibitors, overexpressing the WT CaR increases the Sholl profile (**B.**) but branching remains unaffected (**C.**) while total neurite length is significantly increased (**D.**) (n=127-157 neurons per condition from three separate cultures; *P<0.05, **P<0.01, ***P<0.001 Unpaired T-test). Data are presented as the mean ± SEM.

4.5 Determining a Role for the CaR in Neurite Outgrowth Using CaR-deficient Neurons

4.5.1 Deriving the Single Car Transgenic from the Car/Pth Mice

The single CaR transgenic was derived from the *Car/Pth* double transgenic mice kindly sent to us by Dr. Claudine Kos, Tufts University, Boston, Massachusetts, USA [131]. We received one male and four female C57Bl6 mice which were genotyped at both the CaR and PTH loci before breeding. The genotype of the male was determined to be $Car^{+/-}$ $Pth^{+/-}$ (Fig. 47A) and the three females as; $Car^{+/-}Pth^{+/+}$ (Fig. 47B), $Car^{+/+}Pth^{+/-}$ (Fig. 47C), $Car^{+/+}Pth^{+/+}$ (Fig. 47D) and $Car^{+/+}Pth^{+/-}$ (Fig. 47E). Unfortunately, the male mouse died before mating with the four females, therefore, a wild-type C57Bl6 male was mated with the $Car^{+/-}Pth^{+/+}$ female and the heterozygous offspring were then mated either with mice wild-type or heterozygous for the CaR to maintain lines and for knock-out experiments.

4.5.2 Genotyping Embryos from $Car^{+/-}$ x $Car^{+/-}$ Matings for a Neurite Growth Experiment

Genomic DNA isolation and genotyping PCR at the *Car* locus was carried out for each embryo as described in the Methods section. PCR products from both wild-type and null reactions were separated against each other electrophoretically, according to the embryo number. Fig. 48 shows a typical result from a genotyping gel for E18 embryos from a $Car^{+/-}$ x $Car^{+/-}$ mating. Embryos 1, 3 and 8 were genotyped as $Car^{-/-}$ as they were positive for the null allele alone; embryos 2, 4, 5 and 6 were identified as $Car^{+/-}$ as they were positive for both wild-type and null alleles; and embryo 7 ($Car^{+/+}$) positive for the wild-type allele only.

4.5.3 E18 SCG $Car^{-/-}$ Neurite Arbors have Decreased Size and Complexity Compared to $Car^{+/+}$ and $Car^{+/-}$ Arbors at 2.3mM $[Ca^{2+}]_o$

E18 SCG neurons deficient, heterozygous and wild-type for the CaR were plated after genotyping and grown at 2.3mM $[Ca^{2+}]_o$ in the presence of caspase inhibitors. No differences were seen between cell groups in terms of survival, determined after 24hrs in culture due to the addition of caspase inhibitors (Fig. 49A).

However, CaR-deficient neurons exhibited a marked reduction in the number of intersections with distance from the cell soma (n=254 neurons from 4 separate cultures set up from 4 $Car^{-/-}$ embryos; reaching $P<0.001$ at 30μm from the cell soma), compared to neurons heterozygous (n=188 neurons from 4 separate cultures set up from 4 $Car^{+/-}$ embryos) and wild-type (n=94 neurons from 3 separate cultures set from 3 $Car^{+/+}$ embryos) for the receptor (Fig. 49B). Furthermore, CaR null neurons also demonstrated a reduced number of branch points (6.2±0.3; n=254 neurons from 4 separate cultures from 4 $Car^{-/-}$ embryos; $P<0.001$) and a reduction in total neurite length (1486.8±56.4μm; n=254, neurons from 4 separate cultures from 4 $Car^{-/-}$ embryos; $P<0.001$) when compared with neurons from heterozygous (9.3±0.5; 1980.9±75.2μm; n=188 neurons from 4 separate cultures from 4 $Car^{+/-}$ embryos) and wild-type (8.7±0.6; 2109.8±116.2μm; n=94 neurons from 3 separate cultures from 3 $Car^{+/+}$ embryos) littermates (Figs. 49C-D).

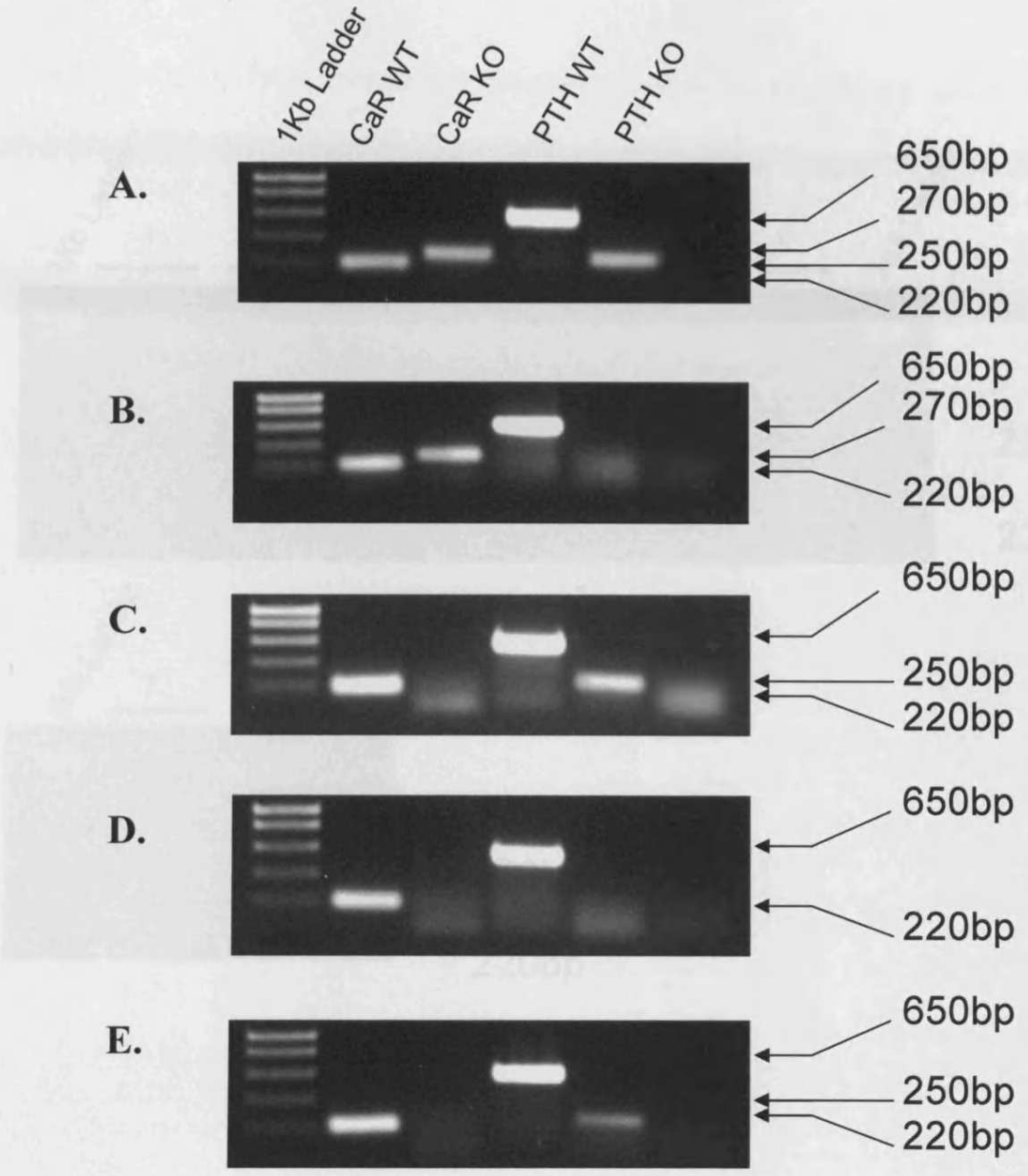

Figure 47: Deriving the Single CaR Mouse from CaR/PTH Mice: Genomic DNA was isolated from tissue taken from each tail tip and used as template in 4 PCR reactions per animal; to determine the genotype at both the $Car^{+/+}$ and $Car^{-/-}$ alleles. Products from both reactions were then separated against each other on a 1% TAE agarose gel in the following order; $Car^{+/+}$ allele product (220bp), $Car^{-/-}$ allele product (270bp), $Pth^{+/+}$ allele product (650bp), $Pth^{-/-}$ allele product (250bp). Mice positive for both alleles were considered to be heterozygous for the CaR. Genotypes were determined as follows; **A.** 6490male, $Car^{+/-}Pth^{+/-}$; **B.** 9416 female, $Car^{+/-}Pth^{+/+}$; **C.** 9418 female, $Car^{+/+}Pth^{+/-}$; **D.** 9420 female $Car^{+/+}Pth^{+/+}$; **E.** 9421 female $Car^{+/+}Pth^{+/-}$.

Figure 48: Genotyping Embryos from *Car*$^{+/-}$ x *Car*$^{+/-}$ Matings for a Neurite Growth Experiment: Genomic DNA was isolated from tissue taken from each embryo and used as template in 2 PCR reactions per animal, determining the genotype at both the CaR wild-type and null alleles. Products from both reactions were then separated against each other according to the embryo, on a 1% TAE agarose gel. A typical genotyping result is shown; *Car*$^{+/+}$ allele products (270bp) shown in the left lane of each embryo and *Car*$^{-/-}$ allele products (220bp) in the right-hand lane. Embryos positive for both alleles were considered to be heterozygous for the CaR. Genotypes were determined as follows; *Car*$^{+/+}$: embryo 7; *Car*$^{+/-}$: embryos 2, 4, 5 and 6; *Car*$^{-/-}$: embryos 1, 3 and 8. Non-specific bands appear in the lefthand lane for *Car*$^{-/-}$ embryos.

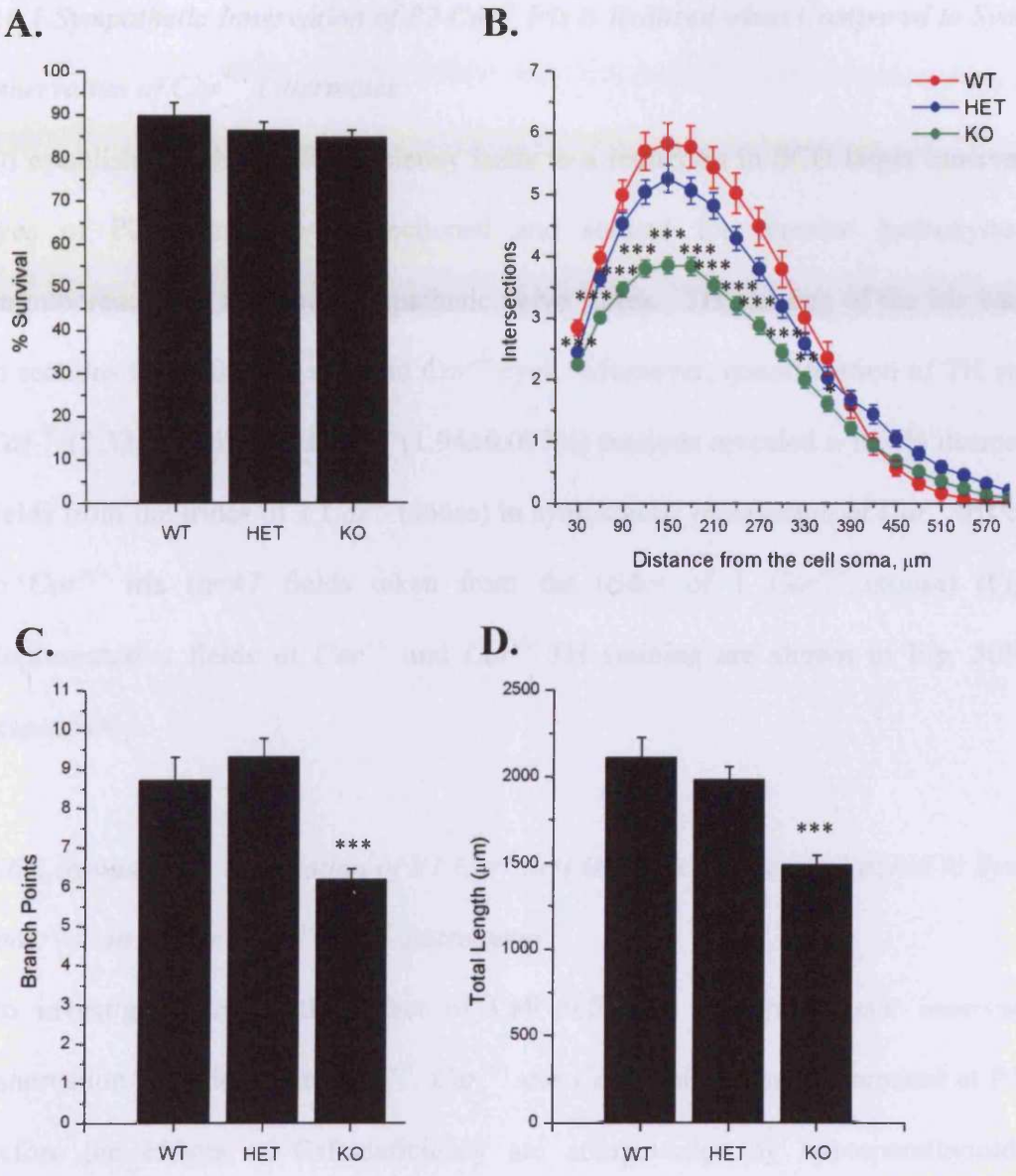

Figure 49: E18 SCG *Car*$^{-/-}$ Neurons Have Decreased Neurite Arbors at 2.3mM $[Ca^{2+}]_o$ When Compared to *Car*$^{+/+}$ and *Car*$^{+/-}$ Neurons. Genotyped neurons were cultured in 100μM Caspase Inhibitor III and 0.4ng.ml^{-1} NGF at 2.3mM $[Ca^{2+}]_o$. **A.** No differences in neuronal survival were seen between cell groups due to the use of caspase inhibitors, **B.** Sholl analysis, **C.** the number of branch points and **D.** total neurite length demonstrate a decrease in the arborisation of E18 SCG neurons with CaR deficiency compared to heterozygous and wild-type neurons (n=94-254 neurons per condition from 3-4 separate cultures from three *Car*$^{+/+}$ and four *Car*$^{+/-}$, *Car*$^{-/-}$ embryos; **P*<0.05, ***P*<0.01, ****P*<0.001, One Way ANOVA with Tukey post hoc test). Data are presented as the mean ± SEM.

4.6 Determining a Role for the CaR in Sympathetic Target Innervation *in Vivo*

4.6.1 Sympathetic Innervation of P2 $Car^{-/-}$ Iris is Reduced when Compared to Sympathetic Innervation of $Car^{+/-}$ Littermates

To establish whether CaR deficiency leads to a reduction in SCG target innervation, the eyes of P2 animals were sectioned and stained for tyrosine hydroxylase (TH)-immunoreactivity to detect sympathetic nerve fibres. TH staining of the iris was present in sections taken from $Car^{+/-}$ and $Car^{-/-}$ eyes. Moreover, quantification of TH staining in $Car^{+/-}$ (2.32±0.136%) and $Car^{-/-}$ (1.94±0.097%) sections revealed a 16.4% decrease (n=47 fields from the irides of 1 $Car^{-/-}$ mouse) in sympathetic innervation of $Car^{-/-}$ iris compared to $Car^{+/-}$ iris (n=47 fields taken from the irides of 1 $Car^{+/-}$ mouse) (Fig. 50A). Representative fields of $Car^{+/-}$ and $Car^{-/-}$ TH staining are shown in Fig. 50B and C, respectively.

4.6.2 Sympathetic Innervation of P1 $Car^{-/-}$ Iris is Reduced when compared to Sympathetic Innervation of $Car^{+/-}$ and $Car^{+/+}$ Littermates

To investigate further the effect of CaR-deficency on sympathetic innervation, the innervation of irides from $Car^{+/+}$, $Car^{+/-}$ and $Car^{-/-}$ animals was compared at P1; an age before the effects of CaR-deficiency are compounded by hyperparathyroidism and hypercalcaemia. Quantification of TH immunoreactivity in sections from $Car^{+/+}$ (2.24±0.06%; n=160 fields from the irides of 6 $Car^{+/+}$ mice), $Car^{+/-}$ (2.14±0.07%; n=156 fields from the irides of 6 $Car^{+/-}$ mice) and $Car^{-/-}$ (1.72±0.04%; n=167 fields from the irides of 6 $Car^{-/-}$ mice) (Fig. 51A) reveal a 23.2% decrease in the sympathetic innervation of $Car^{-/-}$ iris compared to $Car^{+/+}$ ($P<0.001$) and a 19.6% decrease compared to $Car^{+/-}$ iris ($P<0.001$). Representative fields of $Car^{+/+}$, $Car^{+/-}$ and $Car^{-/-}$ iris TH staining revealing a reduction in sympathetic innervation of the $Car^{-/-}$ iris are shown in Fig. 51B-D.

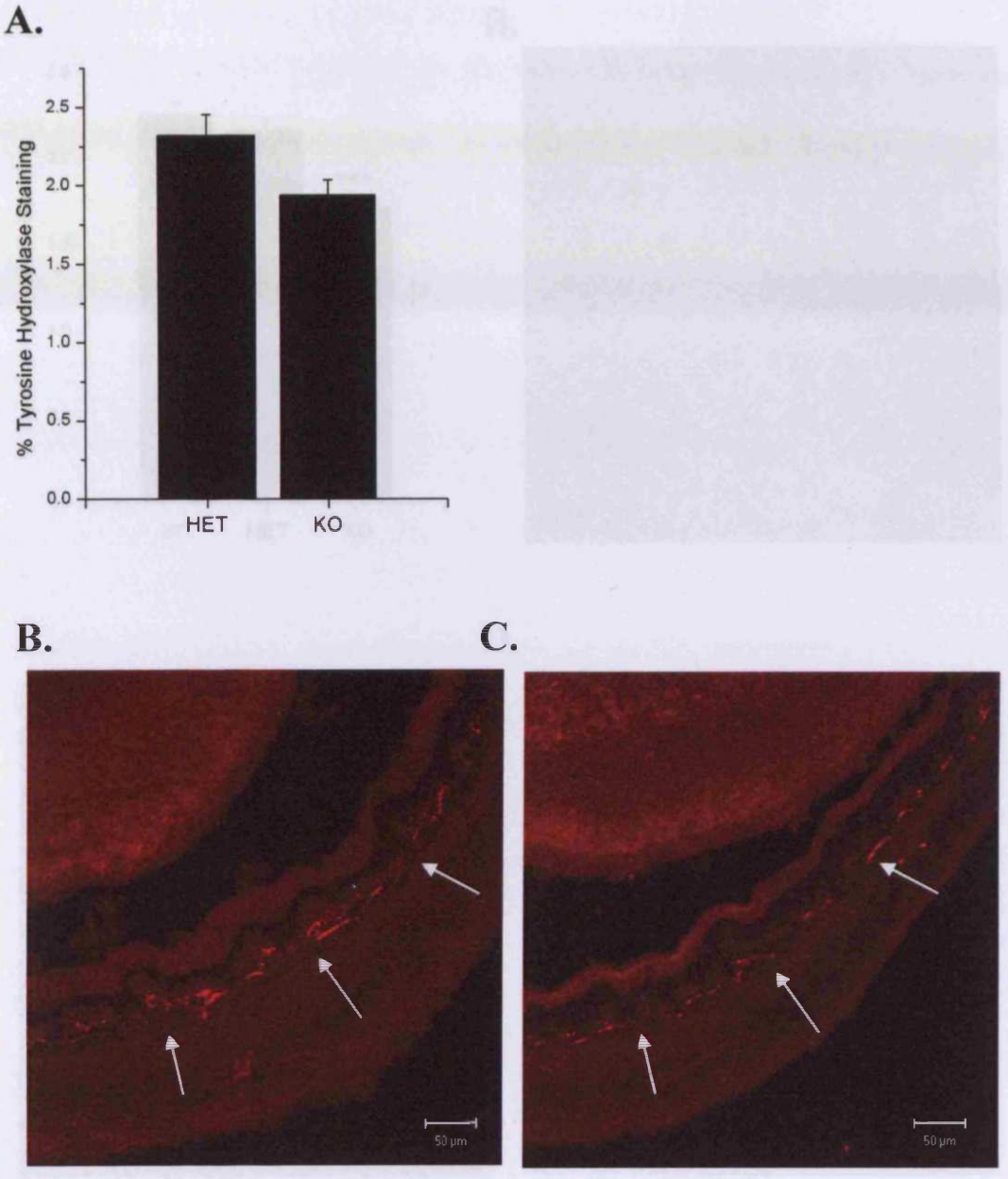

Figure 50: Sympathetic Innervation of P2 *Car*$^{-/-}$ Iris is Reduced When Compared to Sympathetic Innervation of *Car*$^{+/-}$ Littermates. The eyes from P2 *Car*$^{+/-}$ and *Car*$^{+/+}$ littermates were dissected, sectioned, stained for tyrosine hydroxylase (TH) before capturing fluorescent images. The ratio of TH staining : background staining of the iris was then determined from images of both *Car*$^{+/-}$ and *Car*$^{-/-}$ sections. **A**. Comparison of TH staining between *Car*$^{+/-}$ and *CaR*$^{-/-}$ using densitometry (n=47 fields per genotype taken from the irides of 1 mouse of each genotype). **B.** Representative field of *Car*$^{+/-}$ iris TH staining. **C.** Representative field of *Car*$^{-/-}$ iris TH staining. Scale bar = 50µm. Data are presented as the mean ± SEM.

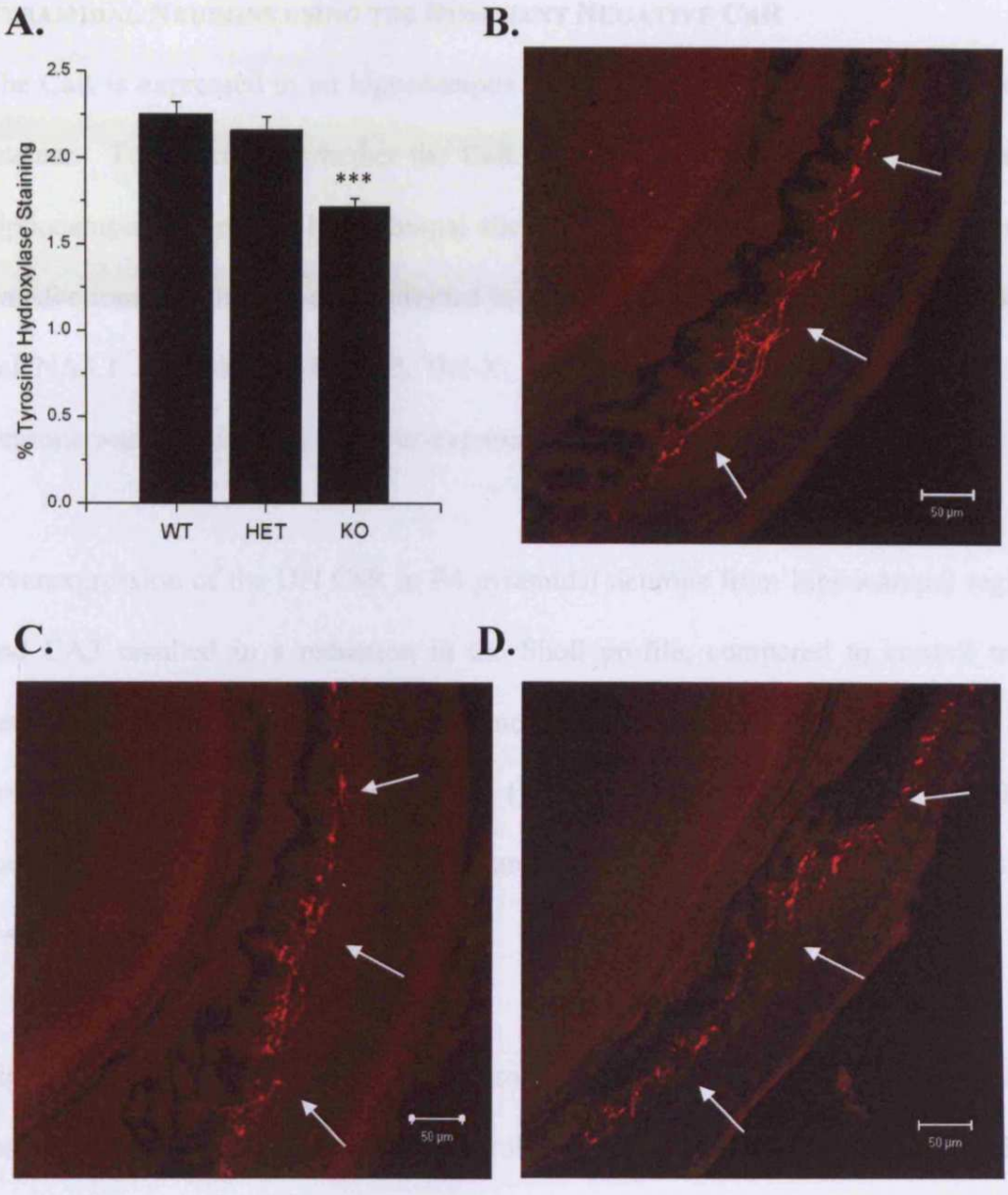

Figure 51: Sympathetic Innervation of P1 *Car*$^{-/-}$ Iris is Reduced When Compared to Sympathetic Innervation of *Car*$^{+/-}$ and *Car*$^{+/+}$ Littermates. The eyes from P1 *Car*$^{+/+}$, *Car*$^{+/-}$ and *Car*$^{-/-}$ littermates were dissected, sectioned, stained for tyrosine hydroxylase (TH) before capturing fluorescent images. The ratio of TH staining : background staining of the iris was then determined from images of both *Car*$^{+/-}$ and *Car*$^{-/-}$ sections. **A.** Comparison of TH staining between *Car*$^{+/+}$, *Car*$^{+/-}$ and *Car*$^{-/-}$ using densitometry (n=156-167 fields per genotype taken from the irides of 3 mice of each genotype; ***P<0.001, One way ANOVA with Tukey post hoc test). **B.** Representative field of *Car*$^{+/+}$ iris TH staining. **C.** A representative field of *Car*$^{+/-}$ iris TH staining. **D.** A representative field of *Car*$^{-/-}$ iris TH staining. Scale bar = 50µm. Data are presented as the mean ± SEM.

4.7 Determining a Role for the CaR in Neurite Outgrowth of Hippocampal Pyramidal Neurons using the Dominant Negative CaR

The CaR is expressed in rat hippocampus from P5 in the rat [173] yet its function here is unclear. To determine whether the CaR regulates neurite outgrowth in the developing hippocampus, P4 mouse hippocampal slices were ballistically transfected with two triple transfections which had been combined in the same gene-gun cartridge; pYFP, Bcl-X_L and pcDNA3.1 (control), and pRFP, Bcl-X_L and DN CaR-pcDNA3.1. Survival of these neurons was supported by the over-expression of Bcl-X_L.

Overexpression of the DN CaR in P4 pyramidal neurons from hippocampal regions CA2 and CA3 resulted in a reduction in the Sholl profile, compared to control transfected neurons (n=36-39) (Fig. 52A). Furthermore, both the number of branch points (7.4±0.8; n=39 neurons) and total neurite length (1763.7±137.4μm; n=39 neurons) of DN CaR-tranfected neurons were reduced compared to the control (11.9±1.0; 2614.7±242.5μm; n=36 neurons) (Fig. 52B and C).

Fig. 52D and E show examples of control- and DN CaR-transfected pyramidal neurons, respectively. Fig. 52F shows a control-transfected neuron (green) and a DN CaR-transfected neuron (red) within the same field.

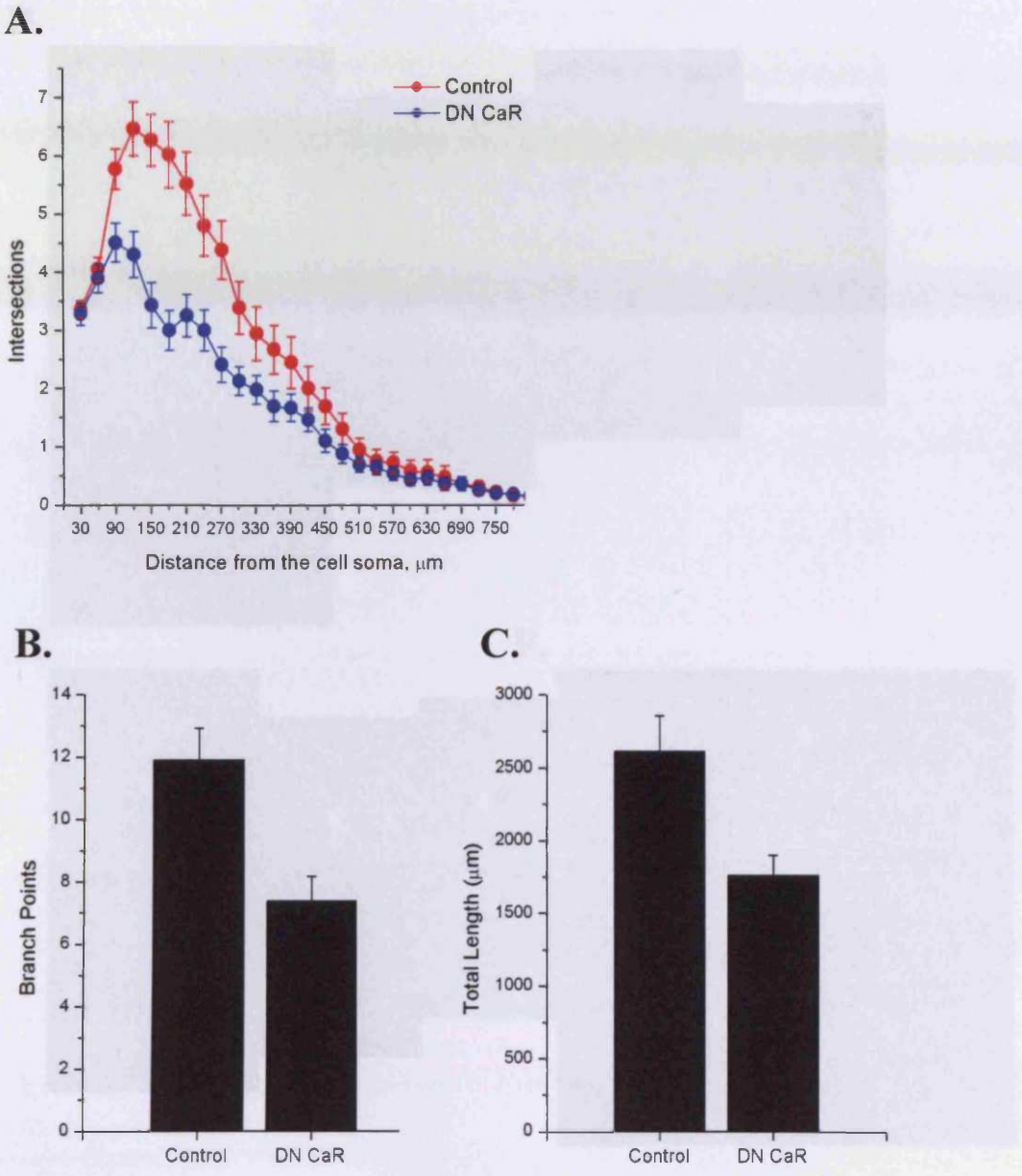

Figure 52: The Dominant Negative (R185Q) CaR Reduces Neurite Arborisation of Pyramidal Neurons from CA2 and CA3 Regions of P4 Hippocampal Slices. 300μm hippocampal slices were transfected with two triple transfections combined in the same cartridge; pYFP, Bcl-X_L and pcDNA3.1 (control) and pRFP, Bcl-X_L and DN CaR-pcDNA3.1. The slices were cultured in 50% DMEM, 25% heat-inactivated horse serum, 25% HBSS and 6.5mg.ml^{-1} glucose and images of fluorescent CA2 and CA3 pyramidal neurons were captured 48hrs post-transfection. **A.** The Sholl profile of dominant negative-transfected neurons is considerably reduced compared to the control-transfected profile. Both the number of branch points (**B**) and total neurite length (**C**) of DN CaR-transfected pyramidal neurite arbors are reduced when compared to the control-transfected group (n=36-41 neurons per condition; $*P<0.05$, $**P<0.01$, $***P<0.001$, Unpaired T-test). Reproduced courtesy of Dr. H. Gutierrez. Data are presented as the mean ± SEM.

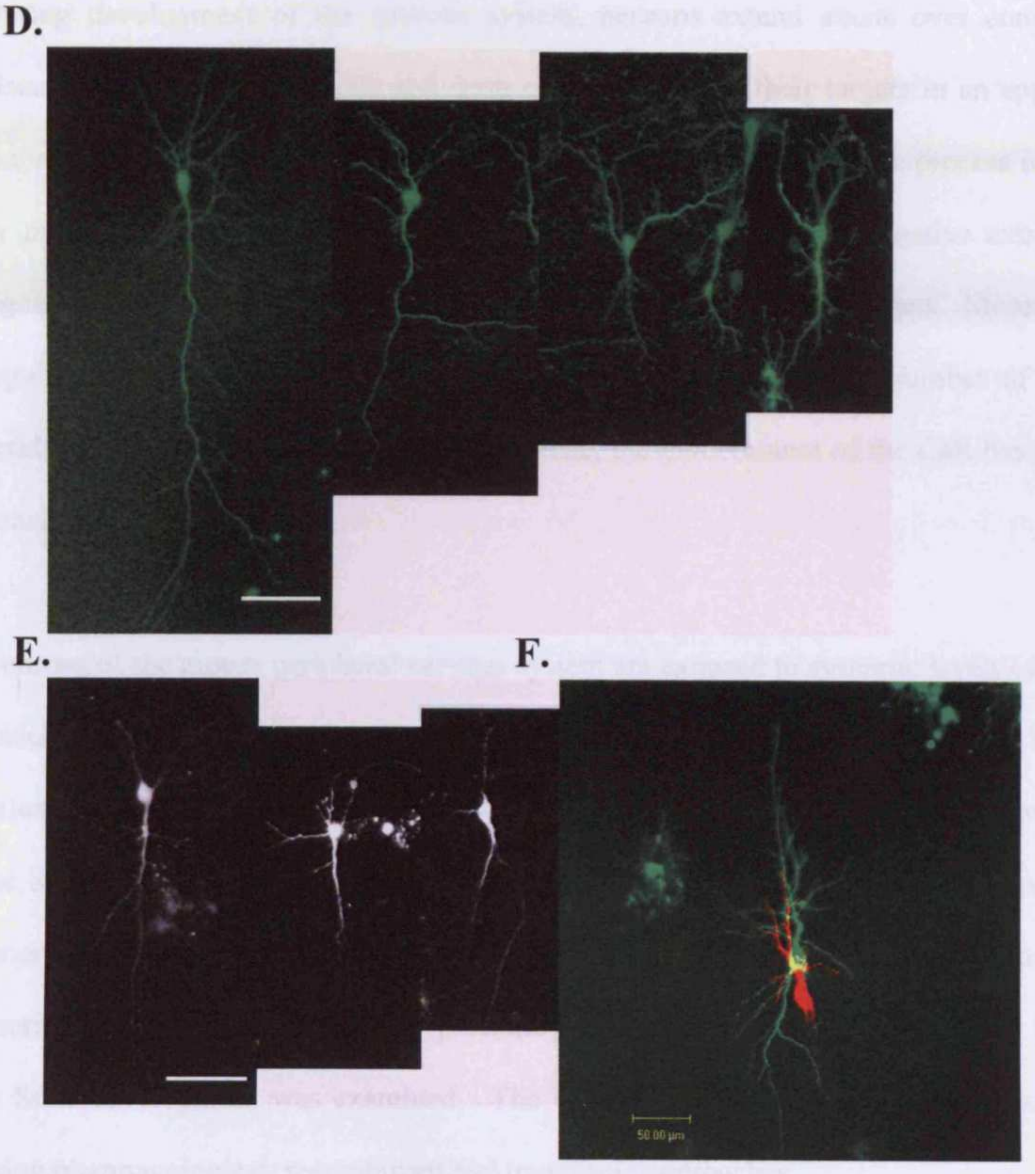

Figure 52: The Dominant Negative (R185Q) CaR Reduces Neurite Arborisation of Pyramidal Neurons from CA2 and CA3 Regions of P4 Hippocampal Slices. 300μm P4 hippocampal slices were transfected with two triple transfections combined in the same cartridge; pYFP, Bcl-X_L and pcDNA3.1 (control) and pRFP, Bcl-X_L and DN CaR-pcDNA3.1. The slices were cultured in 50% DMEM, 25% heat-inactivated horse serum, 25% HBSS and 6.5mg.ml^{-1} glucose and images of fluorescent CA2 and CA3 pyramidal neurons were captured 48hrs post-transfection. **D.** Representative fields of control-transfected neurons. **E.** Representative fields of DN CaR-pcDNA3.1 transfected neurons. **F.** A comparison of control (green) and DN CaR (red) transfected neurons within the same field demonstrates a visible reduction in size and complexity of neurite arborisation with DN CaR transfection. Scale bar = 50μm. Reproduced courtesy of Dr H.Gutierrez.

4.8 DISCUSSION

During development of the nervous system, neurons extend axons over considerable distances in order to innervate and form connections with their targets in an appropriate manner. The initiation and guidance of neuritic processes is a dynamic process instructed by multiple signals, including intrinsic mechanisms, positive and negative extracellular signals, and guidance cues from intermediate and final innervation targets. Moreover, the regulation of neurite outgrowth by $[Ca^{2+}]_o$ has been studied in a number of systems resulting in conflicting conclusions and, to date, the involvement of the CaR has not been considered.

Neurons of the mouse peripheral nervous system are exposed to systemic levels of $[Ca^{2+}]_o$, which are raised to approximately 1.7mM during embryonic life, compared to a maternal value of 1.3mM [133]. It has been shown in the current study that the CaR is expressed in the SCG, peaking at E18 during a period of axon extension, dendritic growth and target innervation *in vivo*. To determine a role for $[Ca^{2+}]_o$ on the outgrowth of sympathetic neurites, the effect of varying $[Ca^{2+}]_o$ on the projection of neuritic processes over key ages in SCG development was examined. The contribution of the CaR was then addressed using pharmacological, recombinant and transgenic approaches.

4.8.1 $[Ca^{2+}]_o$ Affects SCG Neurite Outgrowth at E18 but not P1

Initial experiments revealed there to be an effect of varying $[Ca^{2+}]_o$, over a range to which the CaR is sensitive, on neurite outgrowth at an age where CaR expression is at its highest (E18). Increasing $[Ca^{2+}]_o$ from 1.1mM to 2.3mM increased the size and complexity of E18 SCG neurite arbors. However, a similar experiment conducted using P1 SCG neurons demonstrated that there was no sensitivity to $[Ca^{2+}]_o$ at this age.

There have been many studies of how $[Ca^{2+}]_o$ influences neurite growth with conflicting findings. This is partly due to the different experimental systems employed, but also due to the many mechanisms that mediate the effects of $Ca^{2+}{}_o$. For example, growth in a low, or Ca^{2+}-free environment has shown to induce thinner, but elongated projections from PC-12 cells [222] and thin, branched neurites from chick sympathetic neurons [223] and blocking Ca^{2+} permeability reduced neurite outgrowth from dissociated chick neurons [85]. This is in contrast to Campenot and Draker (1989) who showed, using a compartmentalised culture system, distal neurites from newborn rat SCG neurons grew into, and elongated in Ca^{2+}-free medium providing the cell bodies were bathed in medium containing Ca^{2+} [91]. In addition, Mattson and Kater (1987), studying the regulation of neurite elongation and growth cone motility of *Helisoma trivolvis* neurons by Ca^{2+} influx revealed that Ca^{2+} channel blockade increased neurite elongation [84].

The initial experiments on neurite outgrowth at E18 and P1 also showed there to be a negative effect upon the survival of neurons cultured in lower $Ca^{2+}{}_o$ concentrations. This survival effect may have biased the final effect of $[Ca^{2+}]_o$ on neurite outgrowth by selecting examples from a population of neurons cultured in unfavourable growth conditions. The demonstration that neuronal death in low $[Ca^{2+}]_o$ could be prevented by pharmacological broad spectrum caspase inhibitors revealed that neurons in low $[Ca^{2+}]_o$ died of an apoptotic death (a controlled cell death characterised by cell shrinkage, DNA condensation and cleavage, and membrane blebbing) rather than a necrotic death (an uncontrolled death characterised by swelling, mitochondrial dysfunction, breakdown of homeostatic control and cell lysis) suggesting the CaR may play a role in the prevention of neuronal apoptosis at this age.

4.8.2 $[Ca^{2+}]_o$ Affects SCG Neurite Outgrowth During a Specific Window of Development

Using broad spectrum caspase inhibitors, the effect of $[Ca^{2+}]_o$ on neurite outgrowth was studied over developmental age from E15-P1. Embryonic day 15 nears the end of the proliferative period in the SCG where immature sympathetic neurons are beginning to respond to NGF (10-15% of neurons at E14; [16]) and have begun to extend axons towards their target fields. At this age, proximal axon extension is supported by artemin *in vitro* and *in vivo* [58, 59] and GDNF and neurturin *in vitro* [59]. However, the outgrowth of neuritic processes from E15 SCG neurons was seemingly unaffected by changes in $[Ca^{2+}]_o$, correlating with a relatively low level of CaR mRNA expression at this age.

At E18, when axons from an almost entirely NGF-dependent neuronal population [16] are reaching their targets and competing for limiting amounts of target-derived neurotrophic factor *in vivo*, high $[Ca^{2+}]_o$ increases the size and complexity of E18 neurite arbors *in vitro*. Moreover, E18 correlates with the peak of CaR expression in the SCG, suggesting that the effects of $[Ca^{2+}]_o$ seen *in vitro* are mediated through the CaR.

The sensitivity of neurite arborisation to changes in $[Ca^{2+}]_o$ *in vitro* is still present at P0, after the peak of naturally occurring cell death, during a phase of dendritic growth and refinement of synaptic contacts *in vivo*. At this age neurite arborisation is supported by NGF [224] and GDNF [59]. However, *in vivo* $[Ca^{2+}]_o$ reduces from foetal to adult values within 5-48 hours, where CaR would still be half-maximally activated [225]. At P1, my data show that the sensitivity of the projection of neuritic processes to $[Ca^{2+}]_o$ has been lost and, paradoxically, growth in low $[Ca^{2+}]_o$ increases neuronal growth.

It is clear that the effects of $[Ca^{2+}]_o$ are limited to a developmental window, E18-P0, where increasing $[Ca^{2+}]_o$ from 0.7mM to 2.3mM increased both the number of branch points and total length of neurite arbors. This window of development, where an intrinsic difference in the sensitivity of neurite growth to $[Ca^{2+}]_o$ was observed, correlated with the peak of CaR expression. Furthermore, the expression levels of the CaR were comparable at E15 and P1, where neurite outgrowth has no sensitivity to $[Ca^{2+}]_o$.

4.8.3 Bax-deficient Neurons

The effect of $[Ca^{2+}]_o$ on neurite outgrowth was also demonstrated using another system to support the survival of neurons in high and low $[Ca^{2+}]_o$. The neurite arborisation of E18 SCG neurons deficient for the pro-apoptotic protein, Bax [51], also displayed sensitivity to $[Ca^{2+}]_o$ in both branching and length parameters, consistent with those findings using broad-spectrum caspase inhibitors. However, Bax and Bcl-2 form homodimers and the ratio of Bax to Bcl-2 affects the cells susceptibility to apoptosis [226]. It is possible that the Bax deficiency modulates the effects of Bcl-2 on neuronal development; Bcl-2 can accelerate the maturation of early sensory neurons and enhance the growth of their axons, for example [227, 228].

Both caspase inhibitors and neurons deficient in Bax gave very similar results in terms of neurite outgrowth, therefore, neurite outgrowth experiments were then performed in the presence of pharmacological caspase inhibitors.

4.8.4 Effects of NPS-467R on E18 SCG Neurite Outgrowth

To determine whether the effect of $[Ca^{2+}]_o$ on neurite outgrowth in the present study was mediated by the CaR, the selective allosteric agonist, or calcimimetic, NPS-467R was

used to manipulate CaR function. This hydrophobic, low molecular weight phenylalkylamine compound acts by an allosteric mode of action (i.e. it's ineffective in the absence of $[Ca^{2+}]_o$), potentiating the effect of $Ca^{2+}{}_o$ on the CaR within a narrow concentration range and with a saturable effect [144].

At concentrations that maximally activate the CaR, NPS-467R can block a variety of ion channels [143]. These non-selective biological actions are characterised by a loss of stereoselectivity, where both R- and S- enantiomers are equipotent at Ca^{2+} channel blockade [143]. Therefore, I used NPS-467R at pharmacologically relevant concentrations, 10 and 100nM, [144] in the presence of low $[Ca^{2+}]_o$ (0.7mM) to modulate the neurite outgrowth from dissociated E18 SCG neurons. Despite observing unusually poor neuronal survival in the pilot experiment, 10nM NPS-467R evoked a significant increase in the size and complexity of E18 SCG neurite arbors despite 100nM having no effect. Nevertheless, 10nM NPS-467R genuinely increased neurite arborisation of E18 SCG neurons grown in low $[Ca^{2+}]_o$.

Moreover, the stereo-specificity of this response would need to be tested with the S-enantiomer, and a second generation, more sensitive and more specific calcimimetic to demonstrate selective modulation of the CaR.

4.8.5 Effects of NPS-89636 on E18 and P1 SCG Neurite Outgrowth

Calcilytic compounds, including NPS-89636, do not exhibit the phenotypic pharmacology (a phenomenon where an identical receptor may display a different pharmacology in two different tissues) that is associated with calcimimetic agents, making them a more reliable tool to discriminate CaR-specific effects from non-specific effects of $[Ca^{2+}]_o$ [143]. When

used at concentrations similar to those used to manipulate the CaR in parathyroid cells [150], the allosteric antagonist NPS-89636 decreased the size and complexity of both E18 and P0 SCG neurite arbors grown in high $[Ca^{2+}]_o$, affecting branching and length parameters at both ages. Moreover, when used at the same concentrations, NPS-89636 had no effect on the arborisation of P1 SCG neurons, an age where neurite outgrowth is not sensitive to changes in $[Ca^{2+}]_o$. This is an important and interesting observation as the lack of effect of NPS-89636 at P1 would suggest that its effect on E18 neurite arborisation was through selective antagonism of the CaR.

4.8.6 Effects of Overexpressing a Dominant Negative (R185Q) CaR

Bai *et al* (1997) [229] characterised a heterozygous inactivating mutation, R185Q, in the extracellular domain of the CaR from a patient who presented with neonatal severe hyperparathyroidism, a syndrome normally associated with a homozygous genotype. The mutant CaR exerted a dominant negative effect when co-expressed with the wild-type receptor, increasing the EC_{50} for Ca^{2+} by 37% [229]. The dominant negative (R185Q) CaR has since been used in numerous studies as a tool to specifically knock down CaR function in cells expressing the wild-type CaR, including; H-500 Leydig cancer cells [230], rat calvarial osteoblasts [111], osteoblastic MC3T3-E1 cells [231] and U87 astrocytoma cells [232].

4.8.7 Effects of Over-Expressing the Wild-type CaR

In this study, the role for the CaR in regulating SCG neurite outgrowth was further supported by data obtained from experiments using over-expression of the dominant negative CaR. These experiments resulted in a reduction of both branching and total length of E18 SCG neurite arbors grown in high $[Ca^{2+}]_o$. Furthermore, this effect of the

dominant negative CaR was lost at P1, an age where neurite arborisation is insensitive to changes in $[Ca^{2+}]_o$, demonstrating a specific effect on the CaR endogenously expressed at E18, rather than an artefact of over-expression.

To determine whether sensitivity to $[Ca^{2+}]_o$ could be restored at an age where neurite arborisation is insensitive to changes in $[Ca^{2+}]_o$, the wild-type human parathyroid CaR was over-expressed in P1 SCG neurons. Expression of the wild-type CaR at this age increased neurite arborisation of neurons grown in high $[Ca^{2+}]_o$ when compared to the control group and, therefore, re-introduced the sensitivity to $[Ca^{2+}]_o$. Interestingly, over-expression of the wild-type CaR failed to induce a further increase in E18 SCG arborisation at high $[Ca^{2+}]_o$ when compared to the control group. This suggests the effect of endogenous SCG CaR is already maximal at this age and also, as there is no effect of over-expressing the wild-type construct, there is no artefact of over-expression.

4.8.8 Effect of Genetic CaR-deficiency

The role of the CaR in mediating the effects of $[Ca^{2+}]_o$ on SCG neurite outgrowth was conclusively demonstrated using E18 SCG neurons deficient for the CaR. When grown in high $[Ca^{2+}]_o$ to significantly activate the receptor, $Car^{-/-}$ neurons showed a decrease in both branching and total neurite length when compared to $Car^{+/-}$ or $Car^{+/+}$ neurons.

Although the Sholl analysis suggested that the CaR-deficiency may have had a gene dosage effect, there was no difference between branching and length parameters of $Car^{+/-}$ and $Car^{+/+}$ neurons. The expression and upregulation of a functional exon 5-missing CaR [$^{(exon\ 5(-))}$CaR] splice variant in $Car^{-/-}$ mice [199, 233] may have a role in supporting full-length CaR function in $Car^{+/-}$ neurons, thereby eliminating any possible gene dose effect.

$^{(exon\ 5(-))}$CaR expression data may be required to definitively demonstrate that there is no gene dosage effect in the $Car^{+/-}$ neurons.

4.8.9 Effect of Genetic CaR-Deficiency on Sympathetic Innervation in Vivo

To determine whether the effects of CaR-deficiency *in vitro* could also be seen *in vivo*, sympathetic innervation of an SCG target organ from $Car^{+/-}$ and $Car^{-/-}$ mice were compared. Staining for the marker of sympathetic nerve fibres, tyrosine hydroxylase, revealed sympathetic innervation of $Car^{-/-}$ irides were reduced when compared to irides from $Car^{+/-}$ at P2 and when compared to $Car^{+/+}$ and $Car^{+/-}$ irides at P1.

The reduction of innervation in $Car^{-/-}$ mice poses several questions about the mechanism of loss. Firstly, the comparison of sympathetic innervation was carried out at P1 and P2, as at earlier ages SCG targets show only slight sympathetic innervation [234]. In theory, shortly after birth high serum PTH levels induce hypercalcaemia in the CaR-null mouse, which has been associated with impaired brain development [235], potentially inducing some confounding and misleading results. However, the $Car^{-/-}$ mice maybe reliably used within 72hrs of birth, but beyond this age these animals have reduced growth, become hypercalcaemic and die within 7-10 days [130, 236]. Secondly, a possible role for the CaR in the target field could be indirect. The CaR is expressed in many tissues, including the eye [114] where ectopic calcification is observed in an activating CaR mouse model [136]. Furthermore, the CaR mediates the secretion of numerous peptide hormones, including PTH-related peptide (PTHrP) which has been shown to promote sciatic nerve regeneration [237] and to be required for the activity-dependent survival of cerebellar granule neurons [238]. For example, if the CaR were to mediate PTHrP secretion in SCG

neurons, their target fields or in tissues en route to their target fields, CaR-deficiency and loss of CaR-mediated PTHrP secretion may have a negative effect on iris innervation.

A third question concerns the age over which the innervation is lost; we can presume that innervation is lost over the period that CaR appears to be functional *in vivo*. However, the effect of CaR loss has not been addressed in terms of earlier events in SCG development, including neuroblast proliferation and neuronal survival and, therefore, may affect innervation indirectly by affecting early SCG development.

Moreover, the innervation of other SCG target organs which have not been investigated in this study may show an even clearer loss of innervation. For example, Elshamy *et al* (1996) found that in *nt3*$^{-/-}$ mice sympathetic nerve fibres failed to innervate the pineal gland and external ear postnally, whereas the submandibular gland and the iris displayed normal innervation [234]. Whether directly or indirectly, here we demonstrate that loss of CaR function significantly impairs iris innervation *in vivo*.

4.8.10 CaR Mediates Neurite Outgrowth of Hippocampal Pyramidal Neurons

To test whether the role of the CaR in regulating the effects of $[Ca^{2+}]_o$ on neurite outgrowth goes beyond sympathetic neurons of the PNS, organotypic hippocampal cultures were transfected with the dominant negative CaR, at a time when the CaR is expressed. The size and complexity of neuritic processes projected from pyramidal neurons in CA2 and CA3 hippocampal regions were reduced when transfected with the dominant negative construct. This indicates that the CaR plays a similar functional role in the growth of processes from postnatal hippocampal neurons to its role in the outgrowth of processes from perinatal sympathetic neurons.

Currently, little is known about the functional role of the CaR in the hippocampus, yet it is known to be expressed during the postnatal development of the rat. Indeed, Chattopadhyay *et al* (1997) did not consider embryonic time-points in their developmental expression analyses, where a role for the CaR in hippocampal formation and development may have been ascertained [173]. However, a functional CaR is known to be expressed in the rat hippocampus at P0, where it modulates the activity of non-selective cation channels (NCC) in response to activation by neomycin, elevated Ca^{2+}_o or spermine [175]. In the current study we have shown the receptor may have a key role in the formation of the early postnatal hippocampus by regulating neurite growth. Moreover, Chattopadhyay *et al* (1997) show that CaR expression in the rat hippocampus peaks at P10, a level which is sustained until P30 and then drops to a significant level at P45-P60 [173]. Considering that the functional SCG CaR is dependent upon expression levels, this suggests that the receptor may have a functional role in the developing hippocampus in long-term potentiation (LTP) and later, in synaptic plasticity in the adult, for example.

4.8.11 Summary

Neurite outgrowth from sympathetic neurons is sensitive to changes in $[Ca^{2+}]_o$ over a specific, narrow window around the perinatal period of development. By using three unrelated approaches, I have conclusively demonstrated that the CaR mediates the neurite growth-promoting effects of high $[Ca^{2+}]_o$ *in vitro*. Furthermore, comparison of sympathetic innervation between mice that are heterozygous and null for the CaR reveals that the effect of the CaR also occurs *in vivo*. In addition, use of the dominant negative CaR in organotypic hippocampal cultures demonstrated that the CaR also regulates neurite growth not only in the PNS but also in the developing CNS.

CHAPTER 5

DETERMINING A ROLE FOR THE CaR IN THE REGULATION OF NEURONAL SURVIVAL DURING A PERIOD OF NATURALLY OCCURING CELL DEATH

5.1 Determining the Effect of $[Ca^{2+}]_o$ on Neuronal Survival

Due to the peak of CaR expression at E18 in the SCG, correlating with a period of naturally occurring neuronal death *in vivo*, the effect of $[Ca^{2+}]_o$ on neuronal survival and the involvement of the CaR was studied.

5.1.1 E18 SCG Neuron Survival is Dependent on $[Ca^{2+}]_o$ (I)

A pilot Ca^{2+} dose response was carried out using values for $[Ca^{2+}]_o$ over a broad millimolar range, in the presence of 0.4ng.ml^{-1} NGF. Increasing $[Ca^{2+}]_o$ from 0.7mM (19.1±0.9%; n=1 culture) to 2mM (24.4±6.6%; n=1 culture) marginally increases neuronal survival (Fig. 53). However, increasing $[Ca^{2+}]_o$ from 2 to 2.6mM (71.9±1.0%; n=1 culture) dramatically increased survival by 48%.

5.1.2 E18 SCG Neuron Survival is Dependent on $[Ca^{2+}]_o$ (II)

The $[Ca^{2+}]_o$ was reduced to a narrower range, 0.7-2.6mM, having determined that the effect of increasing $[Ca^{2+}]_o$ was maximal at 2.6mM and that $Ca^{2+}{}_o$ levels near 4mM were neither physiological nor reliably measured using the current method. Increasing $[Ca^{2+}]_o$ from 0.7 to 2.6mM had a profound effect on the survival of dissociated E18 SCG neurons. The relationship between $[Ca^{2+}]_o$ and neuronal survival was a steep sigmoidal one with an EC_{50} for $Ca^{2+}{}_o$ of 1.38mM after 24hrs (Fig. 54A) and 1.45mM after 48hrs (Fig. 54B) in culture (n=3 separate cultures).

5.1.3 P1 SCG Neuron Survival is Dependent on $[Ca^{2+}]_o$

Extracellular $[Ca^{2+}]$ decreases to a postnatal level of ~1.2mM within 5-58hrs of birth [225]. When an identical Ca^{2+} dose response was carried out using P1 SCG neurons, a steep sigmoidal curve emerged at 24hrs (Fig. 55A) but was more apparent at 48hrs (Fig.

55B) generating EC_{50} values for $[Ca^{2+}]_o$ (1.59-1.52mM; n=1 culture) comparable to those at E18.

5.1.4 $[Ca^{2+}]_o$ Potentiates the Survival Effect of NGF on E18 SCG Neurons

To study the relationship between $Ca^{2+}{}_o$-dependent and NGF-dependent survival, an NGF dose response (from 0.0032ng.ml^{-1} to 2ng.ml^{-1} NGF) was carried out using high (2.3mM), low (0.7mM) and EC_{50} (1.3mM) $[Ca^{2+}]_o$; values taken from the E18 SCG Ca^{2+} dose response (Fig. 56A-B).

Increasing $[Ca^{2+}]_o$ from 0.7mM to 1.3mM induced a upward shift in the NGF dose response after 24hrs (Fig. 56A), which was still evident after 48hrs (Fig. 56B) (n=1 culture). Furthermore, increasing $[Ca^{2+}]_o$ from 0.7mM to 2.3mM induced a much larger upward shift in the NGF dose response (n=1 culture). Importantly, Fig. 56 also shows that increases in $[Ca^{2+}]_o$ could only potentiate survival of E18 SCG neurons in the presence of NGF. Neurons cultured in lower NGF concentrations ($\leq$0.016ng.ml^{-1} NGF) died even in the presence of high (2.3mM) $[Ca^{2+}]_o$, indicating that a high $[Ca^{2+}]_o$ solution cannot compensate for the lack of NGF and, vice versa, supramaximal NGF concentrations cannot sustain neuronal survival in low (0.7mM) $[Ca^{2+}]_o$.

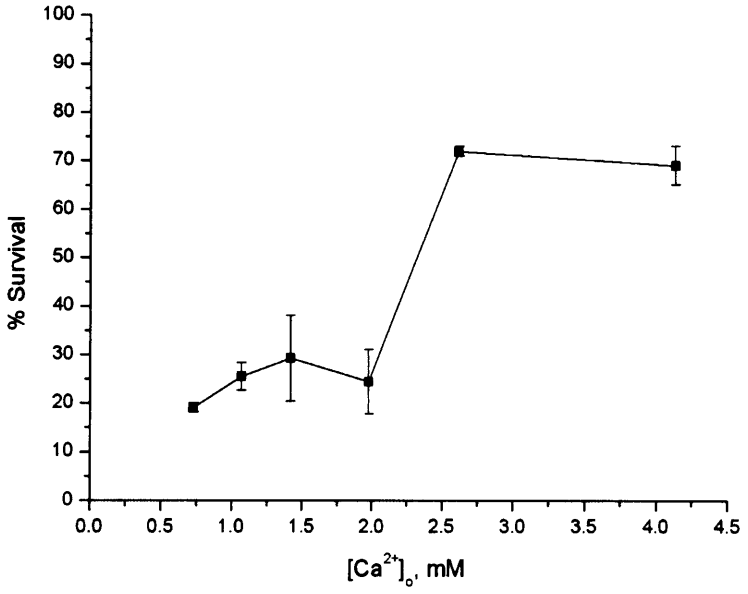

Figure 53: E18 SCG Neuron Survival is Dependent on $[Ca^{2+}]_0$ (I). The effect of extracellular Ca^{2+} on SCG neuron survival was assessed by a pilot Ca^{2+} dose response. E18 SCG neurons were cultured in 35mm dishes in the presence of 0.4ng.ml^{-1} NGF over a range of $[Ca^{2+}]_0$, from 0.7-4.15mM Ca^{2+} and percentage survival was assessed after 24hrs in culture (n=1 culture). Data are presented as the mean ± SEM.

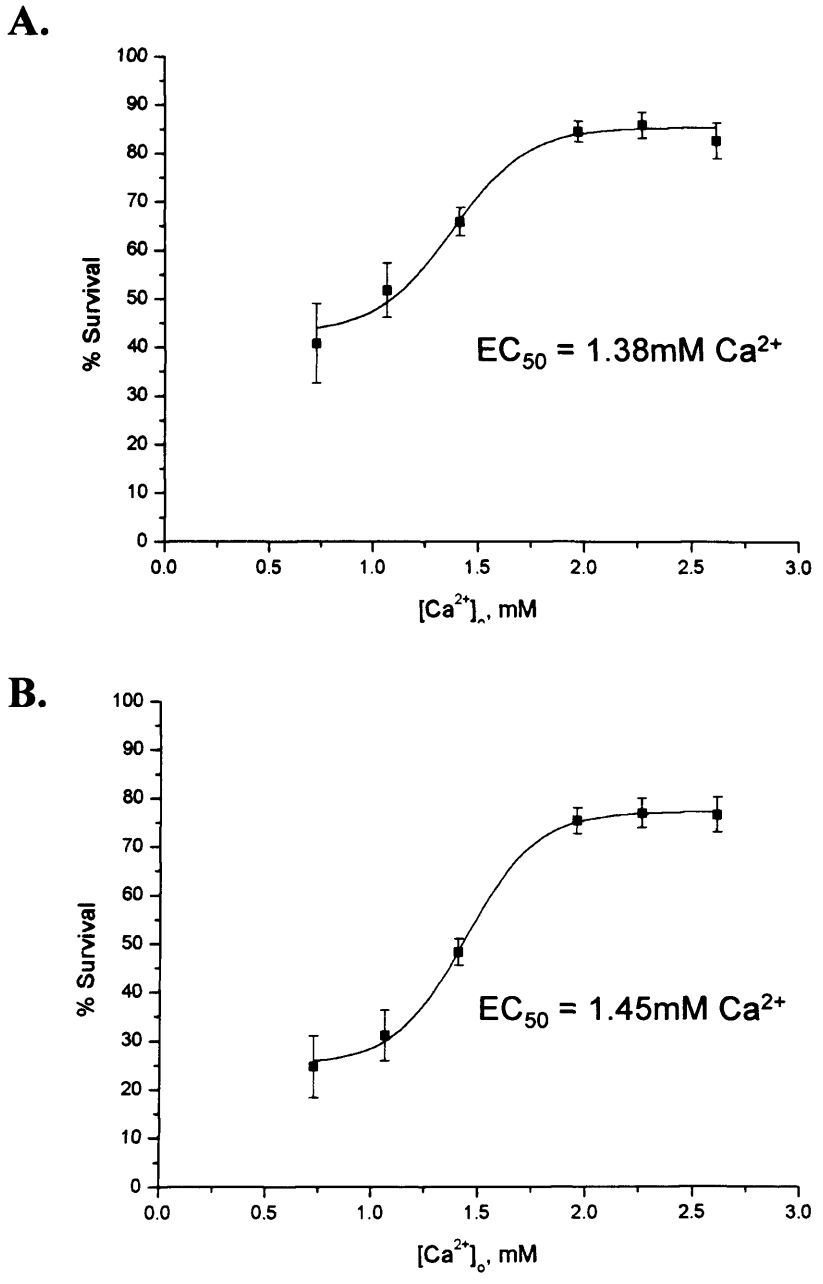

Figure 54: E18 SCG Survival is Dependent on $[Ca^{2+}]_0$ (II). The effect of $[Ca^{2+}]_0$ on SCG neuron survival was further assessed by a Ca^{2+} dose response over a narrower range. E18 SCG neurons were cultured in 35mm dishes in the presence of 0.4ng.ml^{-1} NGF over a range of $[Ca^{2+}]_0$ spanning the embryonic plasma $[Ca^{2+}]_0$ (1.69mM), from 0.7-2.5mM $[Ca^{2+}]_0$. The percentage survival was assessed after **A.** 24hrs and **B.** 48hrs in culture. The effective concentration (EC_{50}) for $[Ca^{2+}]_0$ for each curve is shown (n=3 separate cultures). Data are presented as the mean ± SEM.

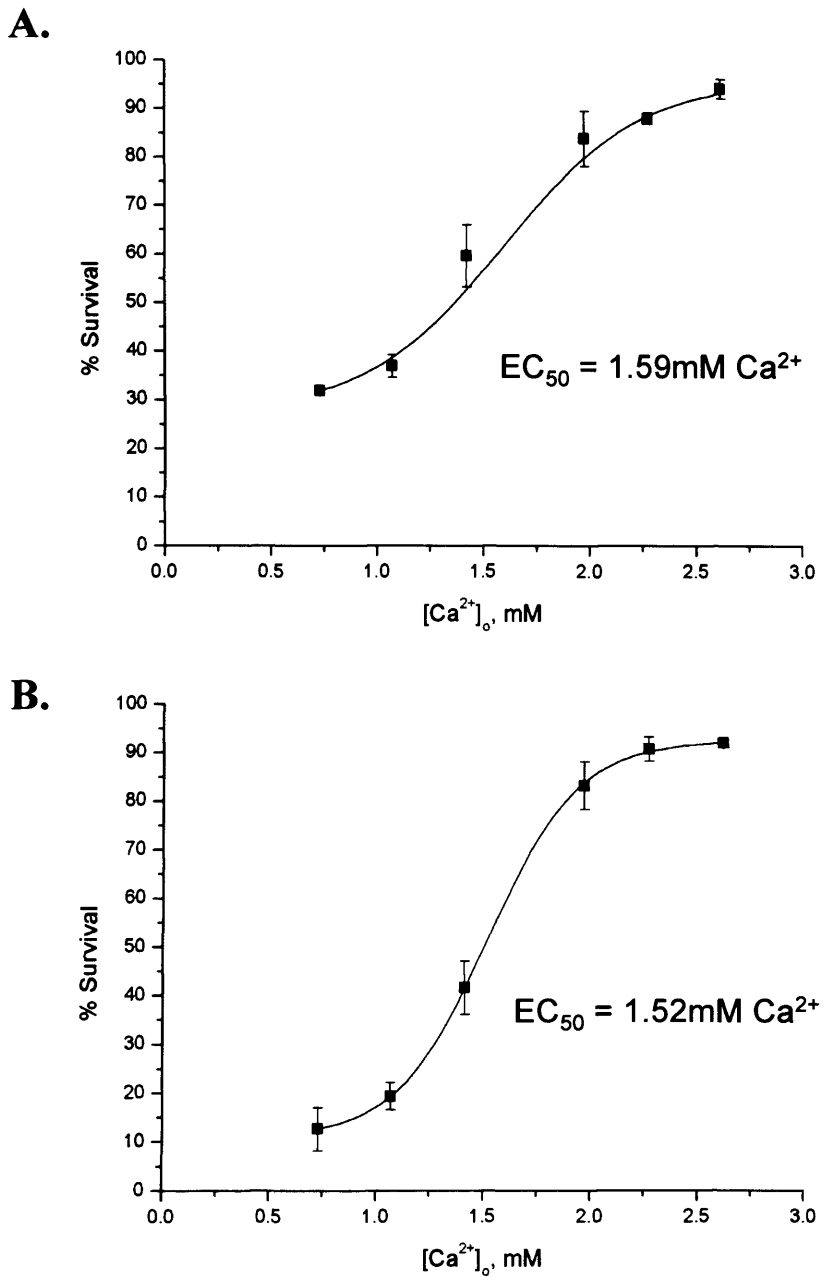

Figure 55: P1 SCG Survival is Dependent on $[Ca^{2+}]_o$. P1 SCG neurons were cultured in 35mm dishes in the presence of 0.4ng.ml^{-1} NGF over a range of $[Ca^{2+}]_o$ from 0.7-2.5mM $[Ca^{2+}]_o$. The percentage survival was assessed after **A.** 24hrs and **B.** 48hrs in culture. The EC_{50} for $[Ca^{2+}]_o$ for each curve is shown (n=1 culture). Data are presented as the mean ± SEM.

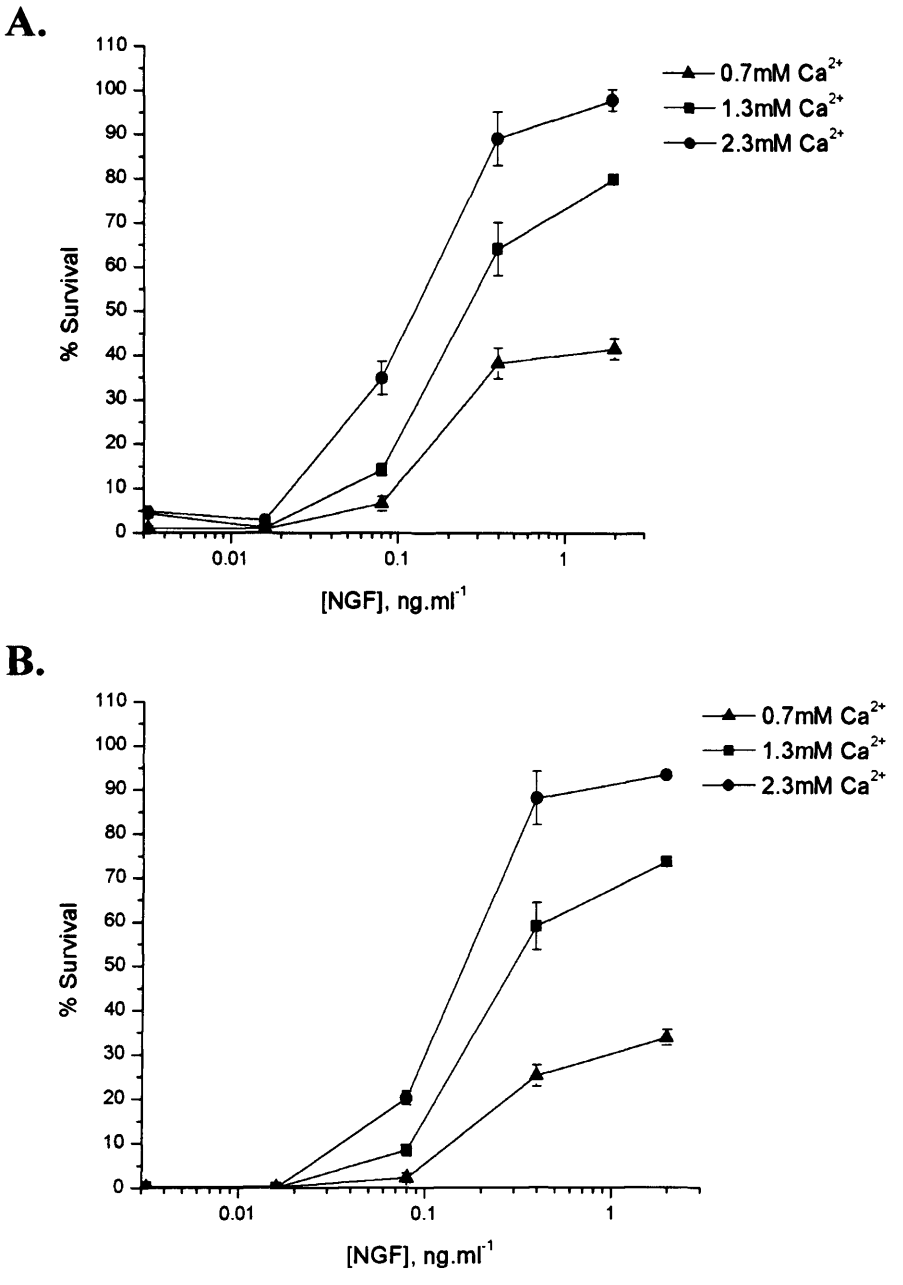

Figure 56: $[Ca^{2+}]_o$ Potentiates the Survival Effect of NGF on E18 SCG Neurons. To assess the relationship between Ca^{2+} and NGF-dependent survival an NGF dose response was carried out at high (2.3mM), low (0.7mM) and EC_{50} (1.3mM) values for $[Ca^{2+}]_o$ taken from the E18 Ca^{2+} dose response curve (see Fig. 54). E18 SCG neurons were cultured in the presence of concentrations of NGF which had been serially diluted 1:5 from 2ng.ml^{-1} to 0.0032ng.ml^{-1}. Percentage neuronal survival was then calculated at **A.** 24hrs in culture and **B.** 48hrs in culture revealing a leftward shift in the NGF dose response with increasing $[Ca^{2+}]_o$ (n=1 culture). Data are presented as the mean ± SEM.

5.2 Determining the Contribution of CaR on the Survival Effect of $[Ca^{2+}]_o$

5.2.1 NPS-467R and NPS-89636 Affect the E18 SCG Survival in a Dose Dependent Manner at EC_{50} (1.3mM) $[Ca^{2+}]_o$

To determine whether the CaR mediated the survival effects of $[Ca^{2+}]_o$ on the NGF dose response, a drug dose response was carried out using the pharmacological compounds NPS-467R (a calcimimetic) and NPS-89636 (a calcilytic) at EC_{50} (1.3mM) $[Ca^{2+}]_o$ (Fig. 57A and B). Concentrations of NPS-467R as low as 0.1nM (68.4±5.6%; n=1 culture), 1nM (60.1±9.2%; n=1 culture) and 10nM (56.2±5.3%; n=1 culture) significantly increased neuronal survival when compared to the 0nM control medium (28.2±3.4%) after 24hrs in culture (Fig. 57A). NPS-89636, however, had a less dramatic effect on neuronal survival at 1.3mM $[Ca^{2+}]_o$ but still significantly decreased the percentage of neuronal survival at the pharmacologically relevant concentration of 1nM (17.9±1.2%; n=1 culture) and 10nM (17.2±0.8%; n=1 culture) and more so at higher concentrations of 100 (14.5±1.7%; n=1 culture) and 1000nM (15.6±1.7%; n=1 culture) when compared to the 0nM control (28.3±3.4%) after 24hrs in culture (Fig. 57A).

5.2.2 10nM NPS-89636 Shifts the E18 SCG Survival NGF Dose Response in a Downward Direction in the Presence of 2.3mM $Ca^{2+}{}_o$

As 1-10nM NPS-89636 had little effect on the NGF dose response at 1.3mM $[Ca^{2+}]_o$, neurons were cultured in the presence or absence of 10nM NPS-89636 at 2.3mM $[Ca^{2+}]_o$ to modulate the $Ca^{2+}{}_o$ response further, with the intention of exploring the possibility for allosteric modulation. Fig. 58A shows that 10nM NPS-89636 shifts the NGF dose response modestly in a downward direction after 24hrs in culture (10 and 0.08ng.ml^{-1} NGF; n=1) compared to the control (n=1), which is ablated after 48hrs (Fig. 58B).

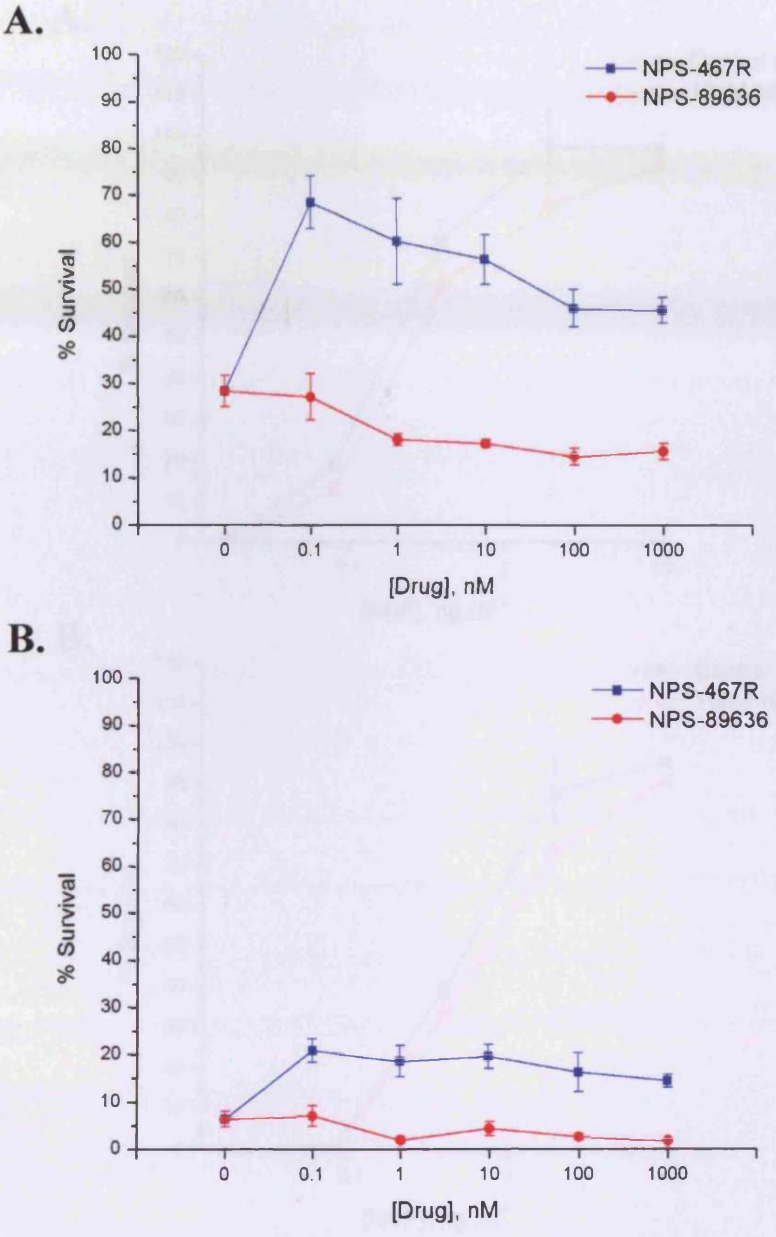

Figure 57: NPS-467R and NPS-89636 Affect E18 SCG Neuronal Survival in a Concentration-dependent Manner at EC_{50} (1.3mM) $[Ca^{2+}]_o$. E18 SCG neurons were cultured in the presence of 0.4ng.ml^{-1} NGF and 1.3mM $[Ca^{2+}]_o$ with the addition of NPS-467R (a calcimimetic) or NPS-89636 (a calcilytic), serially diluted 1:10 from 1000nM to 0.1nM in both cases (0nM acts as a control). Neuronal survival was assessed at **A.** 24hrs in culture, and **B.** 48hrs in culture (n=1 culture). Data are presented as mean ± SEM.

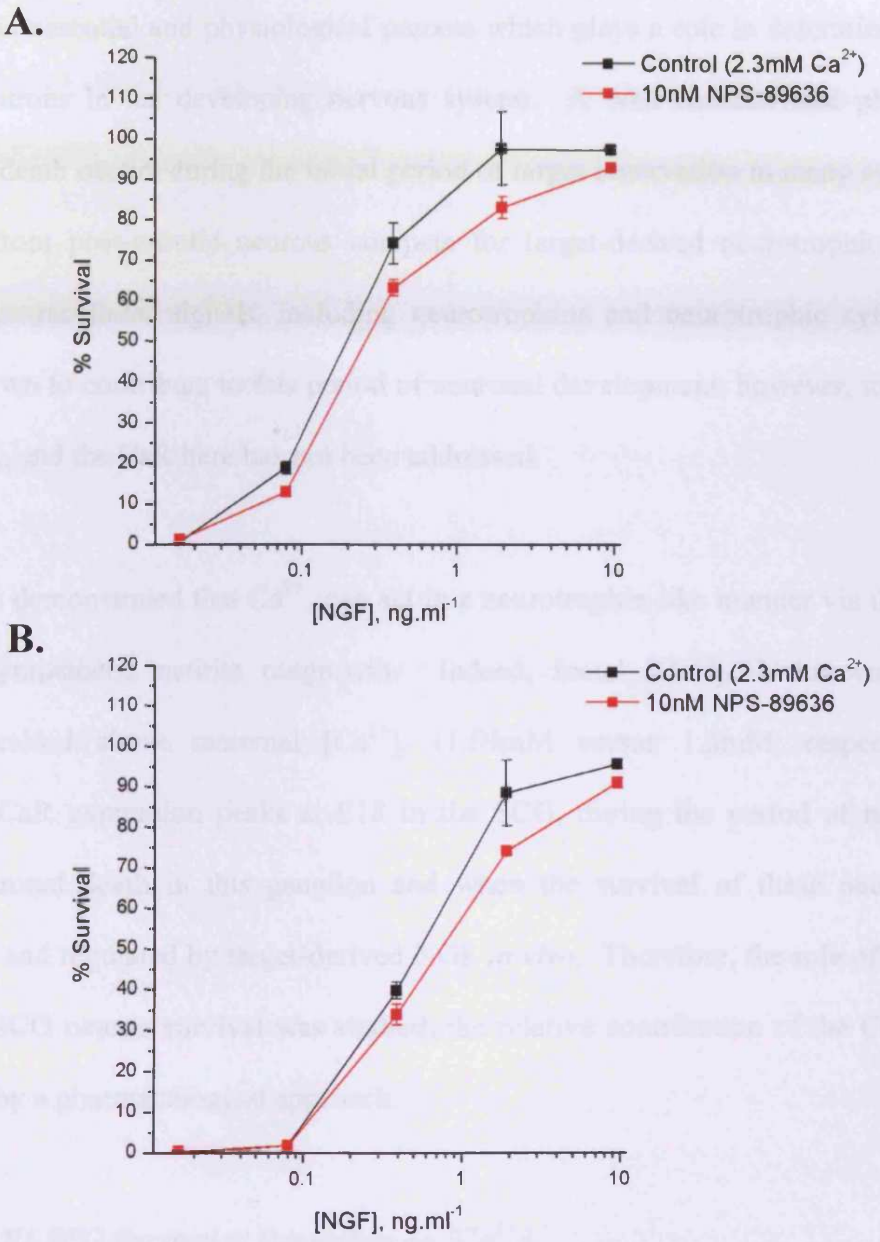

Figure 58: 10nM NPS-89636 Shifts the E18 SCG Survival NGF Dose Response In a Downward Direction at 2.3mM $[Ca^{2+}]_o$. E18 SCG Neurons were cultured in the presence of 2.3mM $[Ca^{2+}]_o$ and NGF, which was serially diluted 1:5 from 10ng.ml^{-1} to 0.016ng.ml^{-1}. NPS-89636 was added to a final concentration of 10nM. Neuronal survival was assessed at **A.** 24hrs and **B.** 48hrs in culture (n=1 culture). Data are presented as the mean ± SEM.

5.3 Discussion

Cell death is an essential and physiological process which plays a role in determining the number of neurons in the developing nervous system. A well characterised phase of apoptotic cell death occurs during the initial period of target innervation in many systems, when axons from post-mitotic neurons compete for target-derived neurotrophic factor [27]. Many extracellular signals, including neurotrophins and neurotrophic cytokines, have been shown to contribute to this period of neuronal development, however, to date a role for $[Ca^{2+}]_o$ and the CaR here has not been addressed.

This study has demonstrated that Ca^{2+}_o can act in a neurotrophin-like manner via the CaR to increase sympathetic neurite outgrowth. Indeed, foetal $[Ca^{2+}]_o$ is known to be significantly raised above maternal $[Ca^{2+}]_o$ (1.69mM versus 1.3mM, respectively). Furthermore, CaR expression peaks at E18 in the SCG, during the period of naturally occurring neuronal death in this ganglion and when the survival of these neurons is dependent on, and regulated by target-derived NGF *in vivo*. Therefore, the role of $[Ca^{2+}]_o$ in regulating SCG neuron survival was studied, the relative contribution of the CaR was then assessed by a pharmacological approach.

5.3.1 E18 and P1 SCG Survival is Dependent on $[Ca^{2+}]_o$

Initial experiments using maximal, but non-saturating [NGF] and predicted values for $[Ca^{2+}]_o$ showed that E18 SCG survival was modulated by changes in $[Ca^{2+}]_o$, with a trend towards increased neuronal survival at higher levels of Ca^{2+}_o. The effect of varying $[Ca^{2+}]_o$ on E18 SCG neuron survival was established by Ca^{2+}-dose response using measured values for $[Ca^{2+}]_o$. The number of neurons that survive in the presence of NGF was steeply and dose-dependently regulated by changes in $[Ca^{2+}]_o$. Furthermore, the steep

sigmoidal curve and the EC_{50} generated for $[Ca^{2+}]_o$ from the Ca^{2+}-dose response were reminiscent of the relationship between PTH release from parathyroid C-cells and $[Ca^{2+}]_o$ [100], suggesting a CaR-mediated process.

In the parathyroid, the CaR is half-maximally activated at 1.2-1.3mM Ca^{2+}; its activation inhibiting the secretion of PTH, a relationship which is manifested as a steep inverse sigmoidal curve [100]. In the current study, increasing $[Ca^{2+}]_o$ over a narrow range to which the CaR is sensitive increases percentage neuronal survival in a sigmoidal fashion, with a comparable EC_{50} for $[Ca^{2+}]_o$ (1.38-1.45mM) to that of the parathyroid CaR (1.3mM) [100]. Furthermore, in the current study experiments on SCG neuronal morphology showed that the use of a broad-spectrum caspase inhibitor could prevent the death of neurons cultured at low (0.7mM) $[Ca^{2+}]_o$. This indicates these neurons die an apoptotic death rather than a necrotic one, implying a role for the CaR in the prevention of neuronal apoptosis during the period of naturally occurring cell death.

In some systems, however, it has been shown that only a relatively low $[Ca^{2+}]_o$ needs to be present to support neuronal survival. Wakade *et al* (1995) demonstrated that only complete $Ca^{2+}{}_o$ deprivation could induce the death of paravertebral sympathetic neurons from 10-12 day old chick embryos, and these neurons could be rescued if as little as 0.1mM Ca^{2+} was added within 24hrs of plating [223]. Moreover, the pro-survival effect of increasing $[Ca^{2+}]_o$ observed in current study maybe either a consequence of CaR activation or potentially Ca^{2+}-influx via L-type Ca^{2+} channels. The latter is known to promote the survival of NGF-dependent rat SCG neurons in the absence of neurotrophic factors [25].

The Ca^{2+}-dose response was also carried out at P1, to determine whether changes in systemic $[Ca^{2+}]_o$, decreasing from foetal to postnatal levels, would affect the EC_{50} for $Ca^{2+}{}_o$. Preliminary experiments suggest that was apparent at P1 that the survival of neurons supported by NGF is also dependent upon $[Ca^{2+}]_o$ with an EC_{50} of 1.59-1.52mM. Moreover, the Ca^{2+}-dose response at P1 will need more independent replicates before a meaningful EC_{50} value can be determined.

5.3.2 $[Ca^{2+}]_o$ Potentiates the Survival-promoting Effect of NGF on E18 SCG Neurons

The relationship between NGF- and $Ca^{2+}{}_o$-dependent survival was studied by carrying out an NGF-dose response in the presence of low (0.7mM), EC_{50} (1.3mM) and high (2.3mM) values for $[Ca^{2+}]_o$, demonstrating how varying $[Ca^{2+}]_o$ markedly affects the NGF-dose response. Increasing $[Ca^{2+}]_o$ from 0.7 to 2.3mM more than doubled neuronal survival where NGF $\geq$0.08ng.ml^{-1}. However, $Ca^{2+}{}_o$ per se is not sufficient to support survival in the absence of NGF as high $[Ca^{2+}]_o$ failed to rescue neurons cultured at lower NGF concentrations ($\leq$0.016ng.ml^{-1}). This observation is in conflict with a potential role for Ca^{2+} influx in the high $[Ca^{2+}]_o$-mediated support of SCG neuronal survival, as modest $[Ca^{2+}]_i$ elevation via activity-dependent Ca^{2+} influx rescues NGF-deprived neurons from cell death [239]. Indeed, Koike and Tanaka (1991) demonstrated that an increase in $[Ca^{2+}]_i$ from 93nM to 240nM was required for complete survival of SCG neurons from newborn rats in the absence of NGF, where 50% survival was observed at 184nM $[Ca^{2+}]_i$ [239]. This hypothesis would need to be verified using Ca^{2+} channel blockers.

My preliminary set of experiments reveal that NGF needs to be present for $[Ca^{2+}]_o$ to have its pro-survival effects, whilst increasing $[Ca^{2+}]_o$ can potentiate maximal NGF-dependent survival. Both the CaR and NGF transduce their survival signals via common pathways,

involving PI_3K-Akt and MAPK/ERK [10, 161]. Activation of the CaR can prevent apoptotic cell death in numerous cell types in which it is expressed; including H-500 rat Leydig cells [230], AT-3 prostate carcinoma cells, c-myc overexpressing fibroblasts and CaR-transfected HEK cells [240]. However, as high $[Ca^{2+}]_o$ alone is not enough to prevent the death of E18 SCG neurons, the addition of NGF may induce a transcriptional change in CaR expression potentially by $p75^{NTR}$ induced NF-κB activation [241]. This hypothesis will need to be tested further.

5.3.3 Effects of NPS-467R and NPS-89636

To determine whether the effects of varying $[Ca^{2+}]_o$ on NGF-dependent survival were mediated through the CaR, the selective positive and negative allosteric modulators NPS-467R and NPS-89636, respectively, were used to manipulate CaR function. A dose response of both drugs at EC_{50} $[Ca^{2+}]_o$ (1.3mM) in the presence of NGF (0.4ng.ml^{-1}) revealed that NPS-467R and NPS-89636 act dose-dependently.

The allosteric agonist NPS-467R shifted the NGF dose response of neurons grown in 1.3mM $Ca^{2+}{}_o$ to higher survival levels at a very low concentration of the drug. However, the NPS-467R concentration is so low at 0.05nM that the effect on the NGF dose response is questionable. Furthermore, higher concentrations of the drug that had evoked CaR-mediated neurite outgrowth from E18 SCG neurons in this study, were tested for their ability to modulate the CaR in terms of survival. However, when used at 1.1mM $Ca^{2+}{}_o$, a lower $[Ca^{2+}]_o$ to enlarge the window for allosteric modulation, there was no significant shift in the NGF dose response. Similar problems were found when using the allosteric antagonist; no shift in the NGF dose response was seen using 5nM NPS-89636 at 1.3mM Ca^{2+}, yet when the drug was used at 10nM at 2.3mM Ca^{2+} a moderate rightward shift in

the NGF dose-response was seen. Therefore, further experiments exploring different $[Ca^{2+}]_o$ and [NPS-89636] are required to fully characterise this effect.

Preliminary data from experiments using the calcimimetic compound evoked a leftward shift in the NGF dose response evoked by high $[Ca^{2+}]_o$. Successful use of these compounds is dependent upon selecting a concentration of Ca^{2+} at or near the EC_{50} value and a suitable concentration of the drug. Further, second generation calcimimetics which have greater selectivity and greater potency will be used in future survival experiments. An encouraging response was found using the calcilytic compound, giving a predicted downward shift in the NGF dose response, yet this effect requires further investigation.

5.3.4 Summary

In the current study, the effect of varying $[Ca^{2+}]_o$ on SCG neuronal survival has been established at E18 and, to a lesser extent, P1 showing a $Ca^{2+}{}_o$-dependency similar to that of the parathyroid CaR. Furthermore, it was also shown that elevating $[Ca^{2+}]_o$ can increase maximal NGF-dependent survival where $Ca^{2+}{}_o$ acted, synergistically with NGF, in a neurotrophin-like manner. However, the role of the CaR in mediating these pro-survival effects of $[Ca^{2+}]_o$ has not yet been fully established. The use of both pharmacological modulators is still ongoing and requires further investigation. Further studies using CaR-deficient neurons and over-expression of the dominant negative and wild-type CaR constructs will be required to properly establish the contribution of the CaR to the pro-survival effects of increasing $[Ca^{2+}]_o$.

CHAPTER 6

GENERAL DISCUSSION

6.1 General Discussion

To date, CaR expression and function has been most successfully characterised within the systemic Ca^{2+}_o homeostatic system. Despite the identification of functional CaR in many tissues outside of this system, a biological role for the CaR here has never been ascribed. Furthermore, studies on CaR expression and function outside of Ca^{2+}_o homeostatic tissues have been restricted to established cell lines or adult tissues where, in most cases, a role for the CaR during development has not been considered.

In summary, this study has revealed, for the first time, that the CaR is developmentally expressed in sensory and sympathetic neurons. I have also demonstrated that the CaR mediates the effect of high $[Ca^{2+}]_o$ on sympathetic neurite outgrowth during a specific developmental window, a phenomenon shown also to occur in the developing postnatal hippocampus where, previously, the biological function of the CaR was unknown. Furthermore, preliminary data show sympathetic neuron survival to have a clear dependency on $[Ca^{2+}]_o$ and that the CaR may mediate these effects.

These findings have significant biological implications. For example, during sympathetic nervous system development alone, the CaR may play a key role in the establishment of appropriate connections with sympathetic target organs, including blood vessels, heart, lungs, liver, kidney, pancreas and intestines. Moreover, CaR expression has been confirmed in many of these targets [107, 109, 121, 168, 242], raising the possibility that the receptor may be required for the proper innervation, development and function of each tissue.

Indeed, the CaR may serve as a suitable drug target in tissues that have undergone dysinnervation, hyperinnervation or denervation, providing that a functional CaR is expressed in the neuronal population being considered. For example, sympathetic nerve sprouting and heterogeneous myocardial hyperinnervation occur after myocardial infarction (MI)-induced nerve injury [243]. The coupling between the sympathetic nerve sprouting and electrically remodelled myocardium may result in ventricular tachycardia, ventricular fibrillation and sudden death [243]. Therefore, administration of a calcilytic compound post-MI may provide a novel means to prevent MI-induced nerve sprouting and control ventricular arrhythmias and prevent sudden death. Furthermore, the CaR is expressed in sensory ganglia and, therefore, may also be implicated in various peripheral neuropathies. For example, pharmaceutical intervention with a calcimimetic compound may encourage the re-growth of processes from sensory neurons injured by exposure to hyperinsulaemia, hyperglycaemia or by physical insult. Moreover, it would be necessary to determine whether a functional CaR is expressed in adult neurons and whether receptor expression is modified after nerve injury.

The demonstration that the CaR mediates neurite outgrowth from CA2 and CA3 pyramidal neurons in the immature mouse hippocampus suggests that, here, the receptor may play a role in hippocampal formation and learning and memory. In line with this, certain CaR-deficient NSHPT individuals display neurological deficits such as impairment in learning and cognition [244-246]. To investigate this further, future studies in this field may involve a more detailed investigation of hippocampal circuitry in $Car^{+/+}$, $Car^{+/-}$ and $Car^{-/-}$ mice (or $Car^{-/-}$ $Pth^{-/-}$ adult mice), to determine whether there is a reduction in commissural fibers, efferents to the hypothalamus or thalamus, recurrent collaterals and Schaffer collaterals emanating from CA3 pyramidal neurons, for example. The CaR has

been shown to be uniformly distributed throughout the pyramidal and granule cell layers of the hippocampus and dentate gyrus [173], therefore, projections from the dentate gyrus to CA3 may also be considered. Further, a possible role for the CaR in the induction and maintenance of LTP may be investigated. Indeed, behavioural tests of adult $Car^{+/+}$ $Pth^{-/-}$ and $Car^{-/-}$ $Pth^{-/-}$ mice may be carried out to determine whether any deficits in seen hippocampal formation or LTP result in a deficiency of learning and memory *in vivo*. A role for the CaR in hippocampal formation and learning and memory may implicate the receptor as a valid drug target in Alzheimer's disease and re-wiring of tissue damaged by stroke or epilepsy.

The mechanism by which CaR exerts its effects on neurite outgrowth has not been examined during this study, however, Rho kinase and non-selective cation channels (NCCs) are likely candidates. For example, the CaR has been shown to mediate changes in actin stress fiber assembly and the morphology of CaR-transfected HEK293 cells via coupling to $G_{12/13}$ and the activation of Rho kinase [164]. In addition, CaR activation in CaR-transfected HEK293 cells [175], rat hippocampal pyramidal neurons [175] and neurons of the subfornical organ [171] increases the probability of opening of NCCs, suggesting that Ca^{2+} influx through NCCs may drive intracellular, Ca^{2+}-dependent mechanisms which promote neurite growth (reviewed by[89]).

Preliminary data suggest the survival of sympathetic neurons have a dependence upon $[Ca^{2+}]_o$ around the time of naturally occurring neuronal death, which can be modulated by calcimimetic and calcilytic compounds. These preliminary data need to be supported further by overexpression of recombinant CaR proteins and the use of CaR-deficient neurons. It will also be important to determine whether these effects are also present in

CNS neurons, where prevention of apoptotic neuronal death associated with neurodegeneration and ischaemic injury by CaR modulation would be of pharmaceutical interest.

6.1.1 Summary

The current findings have implications for both the study of CaR biology and the development of the nervous system. Here I have shown a specific role for the CaR during development of the PNS and, in addition, I have demonstrated that Ca^{2+}_o, acting through the CaR, has neurotrophic factor-like effects. On the basis of these findings, it will be of interest to determine whether the CaR plays a similar role in the multiple CNS regions in which it is expressed, where the clear biological role of the receptor is yet to be defined. In addition, these findings provide evidence for CaR modulation as a novel pharmaceutical strategy in tissues that have undergone dysinnervation, hyperinnervation, denervation or degeneration.

REFERENCES

REFERENCES

1. Glebova NO, Ginty DD. (2005) Growth and survival signals controlling sympathetic nervous system development. Annu Rev Neurosci, 28, 191-222.

2. http://en.wikipedia.org/wiki/Cranial_nerves.

3. Streit A. (2004) Early development of the cranial sensory nervous system: from a common field to individual placodes. Dev Biol, 276, 1-15.

4. D'Amico-Martel A, Noden DM. (1983) Contributions of placodal and neural crest cells to avian cranial peripheral ganglia. Am J Anat, 166, 445-68.

5. Narayanan CH, Narayanan Y. (1978) Determination of the embryonic origin of the mesencephalic nucleus of the trigeminal nerve in birds. J Embryol Exp Morphol, 43, 85-105.

6. Le Douarin NM. (2004) The avian embryo as a model to study the development of the neural crest: a long and still ongoing story. Mech Dev, 121, 1089-102.

7. Seidah NG, Benjannet S, Pareek S, Chretien M, Murphy RA. (1996) Cellular processing of the neurotrophin precursors of NT3 and BDNF by the mammalian proprotein convertases. FEBS Lett, 379, 247-50.

8. Lee R, Kermani P, Teng KK, Hempstead BL. (2001) Regulation of cell survival by secreted proneurotrophins. Science, 294, 1945-8.

9. Teng HK, Teng KK, Lee R, Wright S, Tevar S, Almeida RD, Kermani P, Torkin R, Chen ZY, Lee FS, Kraemer RT, Nykjaer A, Hempstead BL. (2005) ProBDNF induces neuronal apoptosis via activation of a receptor complex of p75NTR and sortilin. J Neurosci, 25, 5455-63.

10. Arevalo JC, Wu SH. (2006) Neurotrophin signaling: many exciting surprises! Cell Mol Life Sci, 63, 1523-37.

11. Davies AM. (2003) Regulation of neuronal survival and death by extracellular signals during development. EMBO J, 22, 2537-45.

12. Altman J, Bayer SA. (1982) Development of the cranial nerve ganglia and related nuclei in the rat. Adv Anat Embryol Cell Biol, 74, 1-90.

13. Buchman VL, Davies AM. (1993) Different neurotrophins are expressed and act in a developmental sequence to promote the survival of embryonic sensory neurons. Development, 118, 989-1001.

14. Morin X, Cremer H, Hirsch MR, Kapur RP, Goridis C, Brunet JF. (1997) Defects in sensory and autonomic ganglia and absence of locus coeruleus in mice deficient for the homeobox gene Phox2a. Neuron, 18, 411-23.

15. ElShamy WM, Ernfors P. (1996) A local action of neurotrophin-3 prevents the death of proliferating sensory neuron precursor cells. Neuron, 16, 963-72.

16. Wyatt S, Davies AM. (1995) Regulation of nerve growth factor receptor gene expression in sympathetic neurons during development. J Cell Biol, 130, 1435-46.

17. Andres R, Forgie A, Wyatt S, Chen Q, de Sauvage FJ, Davies AM. (2001) Multiple effects of artemin on sympathetic neurone generation, survival and growth. Development, 128, 3685-95.

18. Maina F, Hilton MC, Andres R, Wyatt S, Klein R, Davies AM. (1998) Multiple roles for hepatocyte growth factor in sympathetic neuron development. Neuron, 20, 835-46.

19. Davies AM. (1994) Intrinsic programmes of growth and survival in developing vertebrate neurons. Trends Neurosci, 17, 195-9.

20. Davies A, Lumsden A. (1984) Relation of target encounter and neuronal death to nerve growth factor responsiveness in the developing mouse trigeminal ganglion. J Comp Neurol, 223, 124-37.

21. Davies AM, Bandtlow C, Heumann R, Korsching S, Rohrer H, Thoenen H. (1987) Timing and site of nerve growth factor synthesis in developing skin in relation to innervation and expression of the receptor. Nature, 326, 353-8.

22. Rohrer H, Heumann R, Thoenen H. (1988) The synthesis of nerve growth factor (NGF) in developing skin is independent of innervation. Dev Biol, 128, 240-4.

23. Vogel KS, Davies AM. (1991) The duration of neurotrophic factor independence in early sensory neurons is matched to the time course of target field innervation. Neuron, 7, 819-30.

24. Davies AM. (1989) Intrinsic differences in the growth rate of early nerve fibres related to target distance. Nature, 337, 553-5.

25. Koike T, Martin DP, Johnson EM, Jr. (1989) Role of Ca^{2+} channels in the ability of membrane depolarization to prevent neuronal death induced by trophic-factor deprivation: evidence that levels of internal Ca^{2+} determine nerve growth factor dependence of sympathetic ganglion cells. Proc Natl Acad Sci U S A, 86, 6421-5.

26. Larmet Y, Dolphin AC, Davies AM. (1992) Intracellular calcium regulates the survival of early sensory neurons before they become dependent on neurotrophic factors. Neuron, 9, 563-74.

27. Oppenheim RW. (1991) Cell death during development of the nervous system. Annu Rev Neurosci, 14, 453-501.

28. Hamburger V, Levi-Montalcini R. (1949) Proliferation, differentiation and degeneration in the spinal ganglia of the chick embryo under normal and experimental conditions. J Exp Zool, 111, 457-501.

29. Oppenheim RW. (1989) The neurotrophic theory and naturally occurring motoneuron death. Trends Neurosci, 12, 252-5.

30. Cohen S. (1959) Purification and metabolic effects of a nerve growth-promoting protein from snake venom. J Biol Chem, 234, 1129-37.

31. Levi-Montalcini R. (1987) The nerve growth factor 35 years later. Science, 237, 1154-62.

32. Crowley C, Spencer SD, Nishimura MC, Chen KS, Pitts-Meek S, Armanini MP, Ling LH, McMahon SB, Shelton DL, Levinson AD, et al. (1994) Mice lacking nerve growth factor display perinatal loss of sensory and sympathetic neurons yet develop basal forebrain cholinergic neurons. Cell, 76, 1001-11.

33. Smeyne RJ, Klein R, Schnapp A, Long LK, Bryant S, Lewin A, Lira SA, Barbacid M. (1994) Severe sensory and sympathetic neuropathies in mice carrying a disrupted Trk/NGF receptor gene. Nature, 368, 246-9.

34. Harper S, Davies AM. (1990) NGF mRNA expression in developing cutaneous epithelium related to innervation density. Development, 110, 515-9.

35. Howe CL, Valletta JS, Rusnak AS, Mobley WC. (2001) NGF signaling from clathrin-coated vesicles: evidence that signaling endosomes serve as a platform for the Ras-MAPK pathway. Neuron, 32, 801-14.

36. Chao MV, Rajagopal R, Lee FS. (2006) Neurotrophin signalling in health and disease. Clin Sci (Lond), 110, 167-73.

37. Wilkinson GA, Farinas I, Backus C, Yoshida CK, Reichardt LF. (1996) Neurotrophin-3 is a survival factor in vivo for early mouse trigeminal neurons. J Neurosci, 16, 7661-9.

38. Pinon LG, Minichiello L, Klein R, Davies AM. (1996) Timing of neuronal death in trkA, trkB and trkC mutant embryos reveals developmental changes in sensory neuron dependence on Trk signalling. Development, 122, 3255-61.

39. Enokido Y, Wyatt S, Davies AM. (1999) Developmental changes in the response of trigeminal neurons to neurotrophins: influence of birthdate and the ganglion environment. Development, 126, 4365-73.

40. Forgie A, Wyatt S, Correll PH, Davies AM. (2003) Macrophage stimulating protein is a target-derived neurotrophic factor for developing sensory and sympathetic neurons. Development, 130, 995-1002.

41. Horton AR, Barlett PF, Pennica D, Davies AM. (1998) Cytokines promote the survival of mouse cranial sensory neurones at different developmental stages. Eur J Neurosci, 10, 673-9.

42. Davies AM. (1997) Studies of neurotrophin biology in the developing trigeminal system. J Anat, 191 (Pt 4), 483-91.

43. Forgie A, Kuehnel F, Wyatt S, Davies AM. (2000) In vivo survival requirement of a subset of nodose ganglion neurons for nerve growth factor. Eur J Neurosci, 12, 670-6.

44. Kotzbauer PT, Lampe PA, Heuckeroth RO, Golden JP, Creedon DJ, Johnson EM, Jr., Milbrandt J. (1996) Neurturin, a relative of glial-cell-line-derived neurotrophic factor. Nature, 384, 467-70.

45. Wyatt S, Pinon LG, Ernfors P, Davies AM. (1997) Sympathetic neuron survival and TrkA expression in NT3-deficient mouse embryos. EMBO J, 16, 3115-23.

46. Francis N, Farinas I, Brennan C, Rivas-Plata K, Backus C, Reichardt L, Landis S. (1999) NT-3, like NGF, is required for survival of sympathetic neurons, but not their precursors. Dev Biol, 210, 411-27.

47. Thompson J, Dolcet X, Hilton M, Tolcos M, Davies AM. (2004) HGF promotes survival and growth of maturing sympathetic neurons by PI-3 kinase- and MAP kinase-dependent mechanisms. Mol Cell Neurosci, 27, 441-52.

48. Edwards RH, Rutter WJ, Hanahan D. (1989) Directed expression of NGF to pancreatic beta cells in transgenic mice leads to selective hyperinnervation of the islets. Cell, 58, 161-70.

49. Purves D, Snider WD, Voyvodic JT. (1988) Trophic regulation of nerve cell morphology and innervation in the autonomic nervous system. Nature, 336, 123-8.

50. Deckwerth TL, Elliott JL, Knudson CM, Johnson EM, Jr., Snider WD, Korsmeyer SJ. (1996) BAX is required for neuronal death after trophic factor deprivation and during development. Neuron, 17, 401-11.

51. White FA, Keller-Peck CR, Knudson CM, Korsmeyer SJ, Snider WD. (1998) Widespread elimination of naturally occurring neuronal death in Bax-deficient mice. J Neurosci, 18, 1428-39.

52. Patel TD, Jackman A, Rice FL, Kucera J, Snider WD. (2000) Development of sensory neurons in the absence of NGF/TrkA signaling in vivo. Neuron, 25, 345-57.

53. Gillespie LN. (2003) Regulation of axonal growth and guidance by the neurotrophin family of neurotrophic factors. Clin Exp Pharmacol Physiol, 30, 724-33.

54. Lentz SI, Knudson CM, Korsmeyer SJ, Snider WD. (1999) Neurotrophins support the development of diverse sensory axon morphologies. J Neurosci, 19, 1038-48.

55. Tucker KL, Meyer M, Barde YA. (2001) Neurotrophins are required for nerve growth during development. Nat Neurosci, 4, 29-37.

56. Paves H, Saarma M. (1997) Neurotrophins as in vitro growth cone guidance molecules for embryonic sensory neurons. Cell Tissue Res, 290, 285-97.

57. Maina F, Klein R. (1999) Hepatocyte growth factor, a versatile signal for developing neurons. Nat Neurosci, 2, 213-7.

58. Enomoto H, Crawford PA, Gorodinsky A, Heuckeroth RO, Johnson EM, Jr., Milbrandt J. (2001) RET signaling is essential for migration, axonal growth and axon guidance of developing sympathetic neurons. Development, 128, 3963-74.

59. Yan H, Newgreen DF, Young HM. (2003) Developmental changes in neurite outgrowth responses of dorsal root and sympathetic ganglia to GDNF, neurturin, and artemin. Dev Dyn, 227, 395-401.

60. Scarisbrick IA, Jones EG, Isackson PJ. (1993) Coexpression of mRNAs for NGF, BDNF, and NT-3 in the cardiovascular system of the pre- and postnatal rat. J Neurosci, 13, 875-93.

61. Kuruvilla R, Zweifel LS, Glebova NO, Lonze BE, Valdez G, Ye H, Ginty DD. (2004) A neurotrophin signaling cascade coordinates sympathetic neuron development through differential control of TrkA trafficking and retrograde signaling. Cell, 118, 243-55.

62. Glebova NO, Ginty DD. (2004) Heterogeneous requirement of NGF for sympathetic target innervation in vivo. J Neurosci, 24, 743-51.

63. Vaillant AR, Zanassi P, Walsh GS, Aumont A, Alonso A, Miller FD. (2002) Signaling mechanisms underlying reversible, activity-dependent dendrite formation. Neuron, 34, 985-98.

64. Lein PJ, Beck HN, Chandrasekaran V, Gallagher PJ, Chen HL, Lin Y, Guo X, Kaplan PL, Tiedge H, Higgins D. (2002) Glia induce dendritic growth in cultured sympathetic neurons by modulating the balance between bone morphogenetic proteins (BMPs) and BMP antagonists. J Neurosci, 22, 10377-87.

65. Lein P, Johnson M, Guo X, Rueger D, Higgins D. (1995) Osteogenic protein-1 induces dendritic growth in rat sympathetic neurons. Neuron, 15, 597-605.

66. Beck HN, Drahushuk K, Jacoby DB, Higgins D, Lein PJ. (2001) Bone morphogenetic protein-5 (BMP-5) promotes dendritic growth in cultured sympathetic neurons. BMC Neurosci, 2, 12.

67. Fann MJ, Patterson PH. (1994) Neuropoietic cytokines and activin A differentially regulate the phenotype of cultured sympathetic neurons. Proc Natl Acad Sci U S A, 91, 43-7.

68. Snider WD. (1988) Nerve growth factor enhances dendritic arborization of sympathetic ganglion cells in developing mammals. J Neurosci, 8, 2628-34.

69. Ruit KG, Osborne PA, Schmidt RE, Johnson EM, Jr., Snider WD. (1990) Nerve growth factor regulates sympathetic ganglion cell morphology and survival in the adult mouse. J Neurosci, 10, 2412-9.

70. Bruckenstein DA, Higgins D. (1988) Morphological differentiation of embryonic rat sympathetic neurons in tissue culture. I. Conditions under which neurons form axons but not dendrites. Dev Biol, 128, 324-36.

71. Xu B, Gottschalk W, Chow A, Wilson RI, Schnell E, Zang K, Wang D, Nicoll RA, Lu B, Reichardt LF. (2000) The role of brain-derived neurotrophic factor receptors in the mature hippocampus: modulation of long-term potentiation through a presynaptic mechanism involving TrkB. J Neurosci, 20, 6888-97.

72. Gascon E, Vutskits L, Zhang H, Barral-Moran MJ, Kiss PJ, Mas C, Kiss JZ. (2005) Sequential activation of p75 and TrkB is involved in dendritic development of subventricular zone-derived neuronal progenitors in vitro. Eur J Neurosci, 21, 69-80.

73. Wirth MJ, Brun A, Grabert J, Patz S, Wahle P. (2003) Accelerated dendritic development of rat cortical pyramidal cells and interneurons after biolistic transfection with BDNF and NT4/5. Development, 130, 5827-38.

74. McAllister AK, Katz LC, Lo DC. (1997) Opposing roles for endogenous BDNF and NT-3 in regulating cortical dendritic growth. Neuron, 18, 767-78.

75. Zweifel LS, Kuruvilla R, Ginty DD. (2005) Functions and mechanisms of retrograde neurotrophin signalling. Nat Rev Neurosci, 6, 615-25.

76. Lee FS, Kim AH, Khursigara G, Chao MV. (2001) The uniqueness of being a neurotrophin receptor. Curr Opin Neurobiol, 11, 281-6.

77. Roux PP, Barker PA. (2002) Neurotrophin signaling through the p75 neurotrophin receptor. Prog Neurobiol, 67, 203-33.

78. Deshmukh M, Johnson EM, Jr. (1998) Evidence of a novel event during neuronal death: development of competence-to-die in response to cytoplasmic cytochrome c. Neuron, 21, 695-705.

79. Riccio A, Ahn S, Davenport CM, Blendy JA, Ginty DD. (1999) Mediation by a CREB family transcription factor of NGF-dependent survival of sympathetic neurons. Science, 286, 2358-61.

80. Lonze BE, Ginty DD. (2002) Function and regulation of CREB family transcription factors in the nervous system. Neuron, 35, 605-23.

81. Graef IA, Wang F, Charron F, Chen L, Neilson J, Tessier-Lavigne M, Crabtree GR. (2003) Neurotrophins and netrins require calcineurin/NFAT signaling to stimulate outgrowth of embryonic axons. Cell, 113, 657-70.

82. Patel TD, Kramer I, Kucera J, Niederkofler V, Jessell TM, Arber S, Snider WD. (2003) Peripheral NT3 signaling is required for ETS protein expression and central patterning of proprioceptive sensory afferents. Neuron, 38, 403-16.

83. Kulbatski I, Cook DJ, Tator CH. (2004) Calcium entry through L-type calcium channels is essential for neurite regeneration in cultured sympathetic neurons. J Neurotrauma, 21, 357-74.

84. Mattson MP, Kater SB. (1987) Calcium regulation of neurite elongation and growth cone motility. J Neurosci, 7, 4034-43.

85. Suarez-Isla BA, Pelto DJ, Thompson JM, Rapoport SI. (1984) Blockers of calcium permeability inhibit neurite extension and formation of neuromuscular synapses in cell culture. Brain Res, 316, 263-70.

86. Borodinsky LN, O'Leary D, Neale JH, Vicini S, Coso OA, Fiszman ML. (2003) GABA-induced neurite outgrowth of cerebellar granule cells is mediated by GABA(A) receptor activation, calcium influx and CaMKII and ERK1/2 pathways. J Neurochem, 84, 1411-20.

87. Cuppini R, Sartini S, Ambrogini P, Falcieri E, Maltarello MC, Gallo G. (1999) Control of neuron outgrowth by NMDA receptors. J Submicrosc Cytol Pathol, 31, 31-40.

88. Korkotian E, Segal M. (1999) Release of calcium from stores alters the morphology of dendritic spines in cultured hippocampal neurons. Proc Natl Acad Sci U S A, 96, 12068-72.

89. Konur S, Ghosh A. (2005) Calcium signaling and the control of dendritic development. Neuron, 46, 401-5.

90. Catsicas M, Allcorn S, Mobbs P. (2001) Early activation of $Ca^{(2+)}$-permeable AMPA receptors reduces neurite outgrowth in embryonic chick retinal neurons. J Neurobiol, 49, 200-11.

91. Campenot RB, Draker DD. (1989) Growth of sympathetic nerve fibers in culture does not require extracellular calcium. Neuron, 3, 733-43.

92. Brown EM, Gamba G, Riccardi D, Lombardi M, Butters R, Kifor O, Sun A, Hediger MA, Lytton J, Hebert SC. (1993) Cloning and characterization of an extracellular $Ca^{(2+)}$-sensing receptor from bovine parathyroid. Nature, 366, 575-80.

93. Fan GF, Ray K, Zhao XM, Goldsmith PK, Spiegel AM. (1998) Mutational analysis of the cysteines in the extracellular domain of the human Ca^{2+} receptor: effects on cell surface expression, dimerization and signal transduction. FEBS Lett, 436, 353-6.

94. Hammerland LG, Krapcho KJ, Garrett JE, Alasti N, Hung BC, Simin RT, Levinthal C, Nemeth EF, Fuller FH. (1999) Domains determining ligand specificity for Ca^{2+} receptors. Mol Pharmacol, 55, 642-8.

95. Brauner-Osborne H, Jensen AA, Sheppard PO, O'Hara P, Krogsgaard-Larsen P. (1999) The agonist-binding domain of the calcium-sensing receptor is located at the amino-terminal domain. J Biol Chem, 274, 18382-6.

96. Hu J, McLarnon SJ, Mora S, Jiang J, Thomas C, Jacobson KA, Spiegel AM. (2005) A region in the seven-transmembrane domain of the human Ca^{2+} receptor critical for response to Ca^{2+}. J Biol Chem, 280, 5113-20.

97. Ward DT, Brown EM, Harris HW. (1998) Disulfide bonds in the extracellular calcium-polyvalent cation-sensing receptor correlate with dimer formation and its response to divalent cations in vitro. J Biol Chem, 273, 14476-83.

98. Bai M, Trivedi S, Brown EM. (1998) Dimerization of the extracellular calcium-sensing receptor (CaR) on the cell surface of CaR-transfected HEK293 cells. J Biol Chem, 273, 23605-10.

99. Zhang Z, Sun S, Quinn SJ, Brown EM, Bai M. (2001) The extracellular calcium-sensing receptor dimerizes through multiple types of intermolecular interactions. J Biol Chem, 276, 5316-22.

100. Brown EM, MacLeod RJ. (2001) Extracellular calcium sensing and extracellular calcium signaling. Physiol Rev, 81, 239-297.

101. Nemeth EF, Scarpa A. (1986) Cytosolic Ca^{2+} and the regulation of secretion in parathyroid cells. FEBS Lett, 203, 15-9.

102. Brown E, Enyedi P, LeBoff M, Rotberg J, Preston J, Chen C. (1987) High extracellular Ca^{2+} and Mg^{2+} stimulate accumulation of inositol phosphates in bovine parathyroid cells. FEBS Lett, 218, 113-8.

103. Brown EM. (1999) Physiology and pathophysiology of the extracellular calcium-sensing receptor. Am J Med, 106, 238-53.

104. Chang W, Shoback D. (2004) Extracellular Ca^{2+}-sensing receptors--an overview. Cell Calcium, 35, 183-196.

105. Riccardi D, Gamba G. (1999) The many roles of the calcium-sensing receptor in health and disease. Arch Med Res, 30, 436-48.

106. Garrett JE, Tamir H, Kifor O, Simin RT, Rogers KV, Mithal A, Gagel RF, Brown EM. (1995) Calcitonin-secreting cells of the thyroid express an extracellular calcium receptor gene. Endocrinology, 136, 5202-11.

107. Riccardi D, Park J, Lee WS, Gamba G, Brown EM, Hebert SC. (1995) Cloning and functional expression of a rat kidney extracellular calcium/polyvalent cation-sensing receptor. Proc Natl Acad Sci U S A, 92, 131-5.

108. Riccardi D, Hall AE, Chattopadhyay N, Xu JZ, Brown EM, Hebert SC. (1998) Localization of the extracellular Ca^{2+}/polyvalent cation-sensing protein in rat kidney. Am J Physiol, 274, F611-22.

109. Chattopadhyay N, Cheng I, Rogers K, Riccardi D, Hall A, Diaz R, Hebert SC, Soybel DI, Brown EM. (1998) Identification and localization of extracellular $Ca^{(2+)}$-sensing receptor in rat intestine. Am J Physiol, 274, G122-30.

110. Dvorak MM, Siddiqua A, Ward DT, Carter DH, Dallas SL, Nemeth EF, Riccardi D. (2004) Physiological changes in extracellular calcium concentration directly control osteoblast function in the absence of calciotropic hormones. Proc Natl Acad Sci U S A, 101, 5140-5.

111. Chattopadhyay N, Yano S, Tfelt-Hansen J, Rooney P, Kanuparthi D, Bandyopadhyay S, Ren X, Terwilliger E, Brown EM. (2004) Mitogenic action of calcium-sensing receptor on rat calvarial osteoblasts. Endocrinology, 145, 3451-62.

112. Yano S, Brown EM, Chattopadhyay N. (2004) Calcium-sensing receptor in the brain. Cell Calcium, 35, 257-264.

113. Bouschet T, Henley JM. (2005) Calcium as an extracellular signalling molecule: perspectives on the Calcium Sensing Receptor in the brain. C R Biol, 328, 691-700.

114. Chattopadhyay N, Ye C, Singh DP, Kifor O, Vassilev PM, Shinohara T, Chylack LT, Jr., Brown EM. (1997) Expression of extracellular calcium-sensing receptor by human lens epithelial cells. Biochem Biophys Res Commun, 233, 801-5.

115. Ruat M, Molliver ME, Snowman AM, Snyder SH. (1995) Calcium sensing receptor: molecular cloning in rat and localization to nerve terminals. Proc Natl Acad Sci U S A, 92, 3161-5.

116. Emanuel RL, Adler GK, Kifor O, Quinn SJ, Fuller F, Krapcho K, Brown EM. (1996) Calcium-sensing receptor expression and regulation by extracellular calcium in the AtT-20 pituitary cell line. Mol Endocrinol, 10, 555-65.

117. House MG, Kohlmeier L, Chattopadhyay N, Kifor O, Yamaguchi T, Leboff MS, Glowacki J, Brown EM. (1997) Expression of an extracellular calcium-sensing receptor in human and mouse bone marrow cells. J Bone Miner Res, 12, 1959-70.

118. Yamaguchi T, Olozak I, Chattopadhyay N, Butters RR, Kifor O, Scadden DT, Brown EM. (1998) Expression of extracellular calcium (Ca^{2+}_o)-sensing receptor in human peripheral blood monocytes. Biochem Biophys Res Commun, 246, 501-6.

119. Cheng I, Klingensmith ME, Chattopadhyay N, Kifor O, Butters RR, Soybel DI, Brown EM. (1998) Identification and localization of the extracellular calcium-sensing receptor in human breast. J Clin Endocrinol Metab, 83, 703-7.

120. Tu C-L, Oda Y, Komuves L, Bikle DD. (2004) The role of the calcium-sensing receptor in epidermal differentiation. Cell Calcium, 35, 265-273.

121. Bruce JI, Yang X, Ferguson CJ, Elliott AC, Steward MC, Case RM, Riccardi D. (1999) Molecular and functional identification of a Ca^{2+} (polyvalent cation)-sensing receptor in rat pancreas. J Biol Chem, 274, 20561-8.

122. Garrett JE, Capuano IV, Hammerland LG, Hung BC, Brown EM, Hebert SC, Nemeth EF, Fuller F. (1995) Molecular cloning and functional expression of human parathyroid calcium receptor cDNAs. J Biol Chem, 270, 12919-25.

123. Kubo Y, Miyashita T, Murata Y. (1998) Structural basis for a Ca^{2+}-sensing function of the metabotropic glutamate receptors. Science, 279, 1722-5.

124. Cheng Z, Tu C, Rodriguez L, Dvorak MM, Margeta M, Gassmann M, Bettler B, Shoback D, Chang W. (2006) Type B gamma-aminobutyric Acid Receptors Modulate the Expression and Function of the Extracellular Ca^{2+}-sensing Receptor in Murine Growth Plate Chondrocytes. Endocrinology.

125. Gama L, Wilt SG, Breitwieser GE. (2001) Heterodimerization of calcium sensing receptors with metabotropic glutamate receptors in neurons. J Biol Chem, 276, 39053-9.

126. Pi M, Faber P, Ekema G, Jackson PD, Ting A, Wang N, Fontilla-Poole M, Mays RW, Brunden KR, Harrington JJ, Quarles LD. (2005) Identification of a novel extracellular cation-sensing G-protein-coupled receptor. J Biol Chem, 280, 40201-9.

127. Marx SJ, Attie MF, Levine MA, Spiegel AM, Downs RW, Jr., Lasker RD. (1981) The hypocalciuric or benign variant of familial hypercalcemia: clinical and biochemical features in fifteen kindreds. Medicine (Baltimore), 60, 397-412.

128. Pollak MR, Brown EM, Chou YH, Hebert SC, Marx SJ, Steinmann B, Levi T, Seidman CE, Seidman JG. (1993) Mutations in the human Ca(2+)-sensing receptor gene cause familial hypocalciuric hypercalcemia and neonatal severe hyperparathyroidism. Cell, 75, 1297-303.

129. Chattopadhyay N. (2000) Biochemistry, physiology and pathophysiology of the extracellular calcium-sensing receptor. Int J Biochem Cell Biol, 32, 789-804.

130. Ho C, Conner DA, Pollak MR, Ladd DJ, Kifor O, Warren HB, Brown EM, Seidman JG, Seidman CE. (1995) A mouse model of human familial hypocalciuric hypercalcemia and neonatal severe hyperparathyroidism. Nat Genet, 11, 389-94.

131. Kos CH, Karaplis AC, Peng JB, Hediger MA, Goltzman D, Mohammad KS, Guise TA, Pollak MR. (2003) The calcium-sensing receptor is required for normal calcium homeostasis independent of parathyroid hormone. J Clin Invest, 111, 1021-8.

132. Tu Q, Pi M, Karsenty G, Simpson L, Liu S, Quarles LD. (2003) Rescue of the skeletal phenotype in CasR-deficient mice by transfer onto the Gcm2 null background. J Clin Invest, 111, 1029-37.

133. Kovacs CS, Ho-Pao CL, Hunzelman JL, Lanske B, Fox J, Seidman JG, Seidman CE, Kronenberg HM. (1998) Regulation of murine fetal-placental calcium metabolism by the calcium-sensing receptor. J Clin Invest, 101, 2812-20.

134. Pollak MR, Brown EM, Estep HL, McLaine PN, Kifor O, Park J, Hebert SC, Seidman CE, Seidman JG. (1994) Autosomal dominant hypocalcaemia caused by a $Ca^{(2+)}$-sensing receptor gene mutation. Nat Genet, 8, 303-7.

135. Bai M, Quinn S, Trivedi S, Kifor O, Pearce SH, Pollak MR, Krapcho K, Hebert SC, Brown EM. (1996) Expression and characterization of inactivating and activating mutations in the human $Ca^{2+}{}_o$-sensing receptor. J Biol Chem, 271, 19537-45.

136. Hough TA, Bogani D, Cheeseman MT, Favor J, Nesbit MA, Thakker RV, Lyon MF. (2004) Activating calcium-sensing receptor mutation in the mouse is associated with cataracts and ectopic calcification. Proc Natl Acad Sci U S A, 101, 13566-71.

137. Urena P, Frazao JM. (2003) Calcimimetic agents: review and perspectives. Kidney Int Suppl, S91-6.

138. Quinn SJ, Ye CP, Diaz R, Kifor O, Bai M, Vassilev P, Brown E. (1997) The Ca^{2+}-sensing receptor: a target for polyamines. Am J Physiol, 273, C1315-23.

139. Ye C, Ho-Pao CL, Kanazirska M, Quinn S, Rogers K, Seidman CE, Seidman JG, Brown EM, Vassilev PM. (1997) Amyloid-beta proteins activate $Ca^{(2+)}$-permeable channels through calcium-sensing receptors. J Neurosci Res, 47, 547-54.

140. Conigrave AD, Quinn SJ, Brown EM. (2000) L-amino acid sensing by the extracellular Ca^{2+}-sensing receptor. Proc Natl Acad Sci U S A, 97, 4814-9.

141. Quinn SJ, Kifor O, Trivedi S, Diaz R, Vassilev P, Brown E. (1998) Sodium and ionic strength sensing by the calcium receptor. J Biol Chem, 273, 19579-86.

142. McLarnon S, Holden D, Ward D, Jones M, Elliott A, Riccardi D. (2002) Aminoglycoside antibiotics induce pH-sensitive activation of the calcium-sensing receptor. Biochem Biophys Res Commun, 297, 71-7.

143. Nemeth EF. (2004) Calcimimetic and calcilytic drugs: just for parathyroid cells? Cell Calcium, 35, 283-289.

144. Nemeth EF, Steffey ME, Hammerland LG, Hung BC, Van Wagenen BC, DelMar EG, Balandrin MF. (1998) Calcimimetics with potent and selective activity on the parathyroid calcium receptor. Proc Natl Acad Sci U S A, 95, 4040-5.

145. Hammerland LG, Garrett JE, Hung BC, Levinthal C, Nemeth EF. (1998) Allosteric activation of the Ca^{2+} receptor expressed in Xenopus laevis oocytes by NPS 467 or NPS 568. Mol Pharmacol, 53, 1083-8.

146. Fox J, Lowe SH, Petty BA, Nemeth EF. (1999) NPS R-568: a type II calcimimetic compound that acts on parathyroid cell calcium receptor of rats to reduce plasma levels of parathyroid hormone and calcium. J Pharmacol Exp Ther, 290, 473-9.

147. Silverberg SJ, Bone HG, 3rd, Marriott TB, Locker FG, Thys-Jacobs S, Dziem G, Kaatz S, Sanguinetti EL, Bilezikian JP. (1997) Short-term inhibition of parathyroid hormone secretion by a calcium-receptor agonist in patients with primary hyperparathyroidism. N Engl J Med, 337, 1506-10.

148. Block GA, Martin KJ, de Francisco AL, Turner SA, Avram MM, Suranyi MG, Hercz G, Cunningham J, Abu-Alfa AK, Messa P, Coyne DW, Locatelli F, Cohen RM, Evenepoel P, Moe SM, Fournier A, Braun J, McCary LC, Zani VJ, Olson KA, Drueke TB, Goodman WG. (2004) Cinacalcet for secondary hyperparathyroidism in patients receiving hemodialysis. N Engl J Med, 350, 1516-25.

149. Odenwald T, Nakagawa K, Hadtstein C, Roesch F, Gohlke P, Ritz E, Schaefer F, Schmitt CP. (2006) Acute blood pressure effects and chronic hypotensive action of calcimimetics in uremic rats. J Am Soc Nephrol, 17, 655-62.

150. Nemeth EF, Delmar EG, Heaton WL, Miller MA, Lambert LD, Conklin RL, Gowen M, Gleason JG, Bhatnagar PK, Fox J. (2001) Calcilytic compounds: potent and selective Ca^{2+} receptor antagonists that stimulate secretion of parathyroid hormone. J Pharmacol Exp Ther, 299, 323-31.

151. Shoback DM, Bilezikian JP, Turner SA, McCary LC, Guo MD, Peacock M. (2003) The calcimimetic cinacalcet normalizes serum calcium in subjects with primary hyperparathyroidism. J Clin Endocrinol Metab, 88, 5644-9.

152. Dempster DW, Cosman F, Parisien M, Shen V, Lindsay R. (1993) Anabolic actions of parathyroid hormone on bone. Endocr Rev, 14, 690-709.

153. Kimmel DB, Bozzato RP, Kronis KA, Coble T, Sindrey D, Kwong P, Recker RR. (1993) The effect of recombinant human (1-84) or synthetic human (1-34) parathyroid hormone on the skeleton of adult osteopenic ovariectomized rats. Endocrinology, 132, 1577-84.

154. Fox J, Miller MA, Stroup GB, Nemeth EF, Miller SC. (1997) Plasma levels of parathyroid hormone that induce anabolic effects in bone of ovariectomized rats can be achieved by stimulation of endogenous hormone secretion. Bone, 21, 163-9.

155. Miedlich SU, Gama L, Seuwen K, Wolf RM, Breitwieser GE. (2003) Homology modeling of the transmembrane domain of the human calcium sensing receptor and localization of an allosteric binding site. J Biol Chem.

156. Petrel C, Kessler A, Maslah F, Dauban P, Dodd RH, Rognan D, Ruat M. (2003) Modeling and mutagenesis of the binding site of Calhex 231, a novel negative allosteric modulator of the extracellular $Ca^{(2+)}$-sensing receptor. J Biol Chem, 278, 49487-94.

157. Gowen M, Stroup GB, Dodds RA, James IE, Votta BJ, Smith BR, Bhatnagar PK, Lago AM, Callahan JF, DelMar EG, Miller MA, Nemeth EF, Fox J. (2000) Antagonizing the parathyroid calcium receptor stimulates parathyroid hormone secretion and bone formation in osteopenic rats. J Clin Invest, 105, 1595-604.

158. Gama L, Breitwieser GE. (1998) A carboxyl-terminal domain controls the cooperativity for extracellular Ca^{2+} activation of the human calcium sensing receptor. A study with receptor-green fluorescent protein fusions. J Biol Chem, 273, 29712-8.

159. Kifor O, Diaz R, Butters R, Brown EM. (1997) The Ca^{2+}-sensing receptor (CaR) activates phospholipases C, A2, and D in bovine parathyroid and CaR-transfected, human embryonic kidney (HEK293) cells. J Bone Miner Res, 12, 715-25.

160. Bai M, Trivedi S, Lane CR, Yang Y, Quinn SJ, Brown EM. (1998) Protein kinase C phosphorylation of threonine at position 888 in $Ca^{2+}{}_o$-sensing receptor (CaR) inhibits coupling to Ca2+ store release. J Biol Chem, 273, 21267-75.

161. Ward DT. (2004) Calcium receptor-mediated intracellular signalling. Cell Calcium, 35, 217-228.

162. de Jesus Ferreira MC, Helies-Toussaint C, Imbert-Teboul M, Bailly C, Verbavatz JM, Bellanger AC, Chabardes D. (1998) Co-expression of a Ca^{2+}-inhibitable adenylyl cyclase and of a Ca^{2+}-sensing receptor in the cortical thick ascending limb cell of the rat kidney. Inhibition of hormone-dependent cAMP accumulation by extracellular Ca^{2+}. J Biol Chem, 273, 15192-202.

163. Huang C, Hujer KM, Wu Z, Miller RT. (2004) The Ca^{2+}-sensing receptor couples to Galpha12/13 to activate phospholipase D in Madin-Darby canine kidney cells. Am J Physiol Cell Physiol, 286, C22-30.

164. Davies SL, Gibbons CE, Vizard T, Ward DT. (2006) Calcium-Sensing Receptor Induces Rho Kinase-Mediated Actin Stress Fiber Assembly And Altered Cell Morphology Though Not In Response To Aromatic Amino Acids. Am J Physiol Cell Physiol.

165. Handlogten ME, Huang C, Shiraishi N, Awata H, Miller RT. (2001) The Ca^{2+}-sensing receptor activates cytosolic phospholipase A2 via a Gqalpha -dependent ERK-independent pathway. J Biol Chem, 276, 13941-8.

166. Kifor O, MacLeod RJ, Diaz R, Bai M, Yamaguchi T, Yao T, Kifor I, Brown EM. (2001) Regulation of MAP kinase by calcium-sensing receptor in bovine parathyroid and CaR-transfected HEK293 cells. Am J Physiol Renal Physiol, 280, F291-302.

167. Bukoski RD, Bian K, Wang Y, Mupanomunda M. (1997) Perivascular sensory nerve Ca^{2+} receptor and Ca^{2+}-induced relaxation of isolated arteries. Hypertension, 30, 1431-9.

168. Wang Y, Bukoski RD. (1998) Distribution of the perivascular nerve Ca^{2+} receptor in rat arteries. Br J Pharmacol, 125, 1397-404.

169. Weston AH, Absi M, Ward DT, Ohanian J, Dodd RH, Dauban P, Petrel C, Ruat M, Edwards G. (2005) Evidence in favor of a calcium-sensing receptor in arterial endothelial cells: studies with calindol and Calhex 231. Circ Res, 97, 391-8.

170. Ruat M, Snowman AM, Hester LD, Snyder SH. (1996) Cloned and expressed rat Ca^{2+}-sensing receptor. J Biol Chem, 271, 5972-5.

171. Washburn DL, Smith PM, Ferguson AV. (1999) Control of neuronal excitability by an ion-sensing receptor (correction of anion-sensing). Eur J Neurosci, 11, 1947-54.

172. Washburn DL, Anderson JW, Ferguson AV. (2000) The calcium receptor modulates the hyperpolarization-activated current in subfornical organ neurons. Neuroreport, 11, 3231-5.

173. Chattopadhyay N, Legradi G, Bai M, Kifor O, Ye C, Vassilev PM, Brown EM, Lechan RM. (1997) Calcium-sensing receptor in the rat hippocampus: a developmental study. Brain Res Dev Brain Res, 100, 13-21.

174. Chattopadhyay N, Jeong KH, Yano S, Huang S, Pang JL, Ren X, Terwilliger E, Kaiser UB, Vassilev PM, Pollak MR, Brown EM. (2006) Calcium receptor

stimulates chemotaxis and secretion of MCP-1 in GnRH neurons in vitro: Potential impact on reduced GnRH neuron population in CaR-null mice. Am J Physiol Endocrinol Metab.

175. Ye C, Kanazirska M, Quinn S, Brown EM, Vassilev PM. (1996) Modulation by polycationic $Ca^{(2+)}$-sensing receptor agonists of nonselective cation channels in rat hippocampal neurons. Biochem Biophys Res Commun, 224, 271-80.

176. Vassilev PM, Ho-Pao CL, Kanazirska MP, Ye C, Hong K, Seidman CE, Seidman JG, Brown EM. (1997) Cao-sensing receptor (CaR)-mediated activation of K^+ channels is blunted in CaR gene-deficient mouse neurons. Neuroreport, 8, 1411-6.

177. Vassilev PM, Mitchel J, Vassilev M, Kanazirska M, Brown EM. (1997) Assessment of frequency-dependent alterations in the level of extracellular Ca^{2+} in the synaptic cleft. Biophys J, 72, 2103-16.

178. Rusakov DA, Fine A. (2003) Extracellular Ca^{2+} depletion contributes to fast activity-dependent modulation of synaptic transmission in the brain. Neuron, 37, 287-97.

179. Smith SM, Bergsman JB, Harata NC, Scheller RH, Tsien RW. (2004) Recordings from single neocortical nerve terminals reveal a nonselective cation channel activated by decreases in extracellular calcium. Neuron, 41, 243-56.

180. Chattopadhyay N, Ye CP, Yamaguchi T, Kifor O, Vassilev PM, Nishimura R, Brown EM. (1998) Extracellular calcium-sensing receptor in rat oligodendrocytes: expression and potential role in regulation of cellular proliferation and an outward K^+ channel. Glia, 24, 449-58.

181. Chattopadhyay N, Evliyaoglu C, Heese O, Carroll R, Sanders J, Black P, Brown EM. (2000) Regulation of secretion of PTHrP by $Ca^{(2+)}$-sensing receptor in human astrocytes, astrocytomas, and meningiomas. Am J Physiol Cell Physiol, 279, C691-9.

182. Shankar PP, Wei H, Davee SM, Funk JL. (2000) Parathyroid hormone-related protein is expressed by transformed and fetal human astrocytes and inhibits cell proliferation. Brain Res, 868, 230-40.

183. Ilschner S, Ohlemeyer C, Gimpl G, Kettenmann H. (1995) Modulation of potassium currents in cultured murine microglial cells by receptor activation and intracellular pathways. Neuroscience, 66, 983-1000.

184. Davies AM. (1995) Cranial Sensory Neurons. Neural Cell Cultures: A Practical Approach. Ed. Cohen, J. and Wilkin, G. Oxford University Press., 153-176.

185. Theiler K. (1989) The House Mouse: Atlas of Embryonic Development. Springer-Verlag, New York.

186. http://www.informatics.jax.org/cookbook/.

187. Stratagene. (2005) Introduction to Quantitative PCR. www.stratagene.com, 1-49.

188. Wullner U, Isenmann S, Gleichmann M, Klockgether T, Bahr M. (1998) Expression of neurotrophins and neurotrophin receptors in the cerebellum of mutant weaver and lurcher mice. Brain Res Dev Brain Res, 110, 1-6.

189. Meldgaard M, Fenger C, Lambertsen KL, Pedersen MD, Ladeby R, Finsen B. (2006) Validation of two reference genes for mRNA level studies of murine disease models in neurobiology. J Neurosci Methods, 156, 101-10.

190. Liu W, Yasui K, Opthof T, Ishiki R, Lee JK, Kamiya K, Yokota M, Kodama I. (2002) Developmental changes of $Ca^{(2+)}$ handling in mouse ventricular cells from early embryo to adulthood. Life Sci, 71, 1279-92.

191. Bax B, Blundell TL, Murray-Rust J, McDonald NQ. (1997) Structure of mouse 7S NGF: a complex of nerve growth factor with four binding proteins. Structure, 5, 1275-85.

192. Calbiochem. Inhibitor SourceBook. Second Edition.

193. Er E, Oliver L, Cartron PF, Juin P, Manon S, Vallette FM. (2006) Mitochondria as the target of the pro-apoptotic protein Bax. Biochim Biophys Acta, 1757, 1301-11.

194. Yuan J, Yankner BA. (2000) Apoptosis in the nervous system. Nature, 407, 802-9.

195. Sholl DA. (1953) Dendritic organization in the neurons of the visual and motor cortices of the cat. J Anat, 87, 387-406.

196. Stratagene. QuikChange II XL Site Directed Mutagenesis Kit Instruction Manual.

197. Black IB, Mytilineou C. (1976) Trans-synaptic regulation of the development of end organ innervation by sympathetic neurons. Brain Res, 101, 503-21.

198. Rittenhouse AR, Zigmond RE. (1990) Nerve stimulation in vivo acutely increases tyrosine hydroxylase activity in the superior cervical ganglion and its end organs. Brain Res, 524, 156-9.

199. Oda Y, Tu CL, Pillai S, Bikle DD. (1998) The calcium sensing receptor and its alternatively spliced form in keratinocyte differentiation. J Biol Chem, 273, 23344-52.

200. ElShamy WM, Ernfors P. (1997) Brain-derived neurotrophic factor, neurotrophin-3, and neurotrophin-4 complement and cooperate with each other sequentially during visceral neuron development. J Neurosci, 17, 8667-75.

201. Jones KR, Farinas I, Backus C, Reichardt LF. (1994) Targeted disruption of the BDNF gene perturbs brain and sensory neuron development but not motor neuron development. Cell, 76, 989-99.

202. Ernfors P, Lee KF, Jaenisch R. (1994) Mice lacking brain-derived neurotrophic factor develop with sensory deficits. Nature, 368, 147-50.

203. Sang Q, Young HM. (1998) The origin and development of the vagal and spinal innervation of the external muscle of the mouse esophagus. Brain Res, 809, 253-68.

204. Moore MW, Klein RD, Farinas I, Sauer H, Armanini M, Phillips H, Reichardt LF, Ryan AM, Carver-Moore K, Rosenthal A. (1996) Renal and neuronal abnormalities in mice lacking GDNF. Nature, 382, 76-9.

205. Mohamed SS, Atkinson ME. (1983) A histological study of the innervation of developing mouse teeth. J Anat, 136, 735-49.

206. Canaff L, Hendy GN. (2002) Human calcium-sensing receptor gene. Vitamin D response elements in promoters P1 and P2 confer transcriptional responsiveness to 1,25-dihydroxyvitamin D. J Biol Chem, 277, 30337-50.

207. Brown AJ, Zhong M, Finch J, Ritter C, McCracken R, Morrissey J, Slatopolsky E. (1996) Rat calcium-sensing receptor is regulated by vitamin D but not by calcium. Am J Physiol, 270, F454-60.

208. Delvin EE, Gilbert M, Pere MC, Garel JM. (1988) In vivo metabolism of calcitriol in the pregnant rabbit doe. J Dev Physiol, 10, 451-9.

209. Clark SA, Boass A, Toverud SU. (1986) Development-related regulation of plasma $1,25(OH)_2D_3$ concentration by calcium intake in rat pups. Bone Miner, 1, 193-203.

210. Canaff L, Hendy GN. (2005) Calcium-sensing receptor gene transcription is up-regulated by the proinflammatory cytokine, interleukin-1beta. Role of the NF-kappaB PATHWAY and kappaB elements. J Biol Chem, 280, 14177-88.

211. Mentaverri R, Yano S, Chattopadhyay N, Petit L, Kifor O, Kamel S, Terwilliger EF, Brazier M, Brown EM. (2006) The calcium sensing receptor is directly involved in both osteoclast differentiation and apoptosis. FASEB J, 20, 2562-4.

212. Rodriguez L, Tu C, Cheng Z, Chen TH, Bikle D, Shoback D, Chang W. (2005) Expression and Functional Assessment of an Alternatively Spliced Extracellular Ca^{2+}-sensing Receptor in Growth Plate Chondrocytes. Endocrinology.

213. Wellendorph P, Brauner-Osborne H. (2004) Molecular cloning, expression, and sequence analysis of GPRC6A, a novel family C G-protein-coupled receptor. Gene, 335, 37-46.

214. Chattopadhyay N, Ye C, Yamaguchi T, Nakai M, Kifor O, Vassilev PM, Nishimura RN, Brown EM. (1999) The extracellular calcium-sensing receptor is expressed in rat microglia and modulates an outward K^+ channel. J Neurochem, 72, 1915-22.

215. Chattopadhyay N, Ye CP, Yamaguchi T, Vassilev PM, Brown EM. (1999) Evidence for extracellular calcium-sensing receptor mediated opening of an outward K+ channel in a human astrocytoma cell line (U87). Glia, 26, 64-72.

216. Ferry S, Traiffort E, Stinnakre J, Ruat M. (2000) Developmental and adult expression of rat calcium-sensing receptor transcripts in neurons and oligodendrocytes. Eur J Neurosci, 12, 872-84.

217. Wang Y, Awumey EK, Chatterjee PK, Somasundaram C, Bian K, Rogers KV, Dunn C, Bukoski RD. (2003) Molecular cloning and characterization of a rat sensory nerve Ca^{2+}-sensing receptor. Am J Physiol Cell Physiol, 285, C64-75.

218. Pidasheva S, Canaff L, Simonds WF, Marx SJ, Hendy GN. (2005) Impaired cotranslational processing of the calcium-sensing receptor due to signal peptide missense mutations in familial hypocalciuric hypercalcemia. Hum Mol Genet, 14, 1679-90.

219. Ward DT, McLarnon SJ, Riccardi D. (2002) Aminoglycosides increase intracellular calcium levels and ERK activity in proximal tubular OK cells expressing the extracellular calcium-sensing receptor. J Am Soc Nephrol, 13, 1481-9.

220. Chang W, Tu C, Bajra R, Komuves L, Miller S, Strewler G, Shoback D. (1999) Calcium sensing in cultured chondrogenic RCJ3.1C5.18 cells. Endocrinology, 140, 1911-9.

221. Tu CL, Chang W, Bikle DD. (2001) The extracellular calcium-sensing receptor is required for calcium-induced differentiation in human keratinocytes. J Biol Chem, 276, 41079-85.

222. Koike T. (1983) Nerve growth factor-induced neurite outgrowth of rat pheochromocytoma PC 12 cells: dependence on extracellular Mg^{2+} and Ca^{2+}. Brain Res, 289, 293-303.

223. Wakade TD, Przywara DA, Kulkarni JS, Wakade AR. (1995) Morphological and transmitter release properties are changed when sympathetic neurons are cultured in low Ca^{2+} culture medium. Neuroscience, 67, 967-76.

224. Campenot RB. (1987) Local control of neurite sprouting in cultured sympathetic neurons by nerve growth factor. Brain Res, 465, 293-301.

225. Wandrup J, Kancir C, Norgaard-Pedersen B. (1984) The concentration of free calcium ions in capillary blood from neonates on a routine basis using the ICA 1. Scand J Clin Lab Invest, 44, 19-24.

226. Korsmeyer SJ. (1999) BCL-2 gene family and the regulation of programmed cell death. Cancer Res, 59, 1693s-1700s.

227. Middleton G, Pinon LG, Wyatt S, Davies AM. (1998) Bcl-2 accelerates the maturation of early sensory neurons. J Neurosci, 18, 3344-50.

228. Hilton M, Middleton G, Davies AM. (1997) Bcl-2 influences axonal growth rate in embryonic sensory neurons. Curr Biol, 7, 798-800.

229. Bai M, Pearce SH, Kifor O, Trivedi S, Stauffer UG, Thakker RV, Brown EM, Steinmann B. (1997) In vivo and in vitro characterization of neonatal

hyperparathyroidism resulting from a de novo, heterozygous mutation in the Ca2+-sensing receptor gene: normal maternal calcium homeostasis as a cause of secondary hyperparathyroidism in familial benign hypocalciuric hypercalcemia. J Clin Invest, 99, 88-96.

230. Tfelt-Hansen J, Ferreira A, Yano S, Kanuparthi D, Romero JR, Brown EM, Chattopadhyay N. (2005) Calcium-sensing receptor activation induces nitric oxide production in H-500 Leydig cancer cells. Am J Physiol Endocrinol Metab, 288, E1206-13.

231. Yamauchi M, Yamaguchi T, Kaji H, Sugimoto T, Chihara K. (2004) Involvement of calcium-sensing receptor (CaR) in osteoblastic differentiation of mouse MC3T3-E1 cells. Am J Physiol Endocrinol Metab.

232. Ye CP, Yano S, Tfelt-Hansen J, MacLeod RJ, Ren X, Terwilliger E, Brown EM, Chattopadhyay N. (2004) Regulation of a Ca^{2+}-activated K^{+} channel by calcium-sensing receptor involves p38 MAP kinase. J Neurosci Res, 75, 491-8.

233. Komuves L, Oda Y, Tu CL, Chang WH, Ho-Pao CL, Mauro T, Bikle DD. (2002) Epidermal expression of the full-length extracellular calcium-sensing receptor is required for normal keratinocyte differentiation. J Cell Physiol, 192, 45-54.

234. ElShamy WM, Linnarsson S, Lee KF, Jaenisch R, Ernfors P. (1996) Prenatal and postnatal requirements of NT-3 for sympathetic neuroblast survival and innervation of specific targets. Development, 122, 491-500.

235. Ward BK, Magno AL, Davis EA, Hanyaloglu AC, Stuckey BG, Burrows M, Eidne KA, Charles AK, Ratajczak T. (2004) Functional deletion of the calcium-sensing receptor in a case of neonatal severe hyperparathyroidism. J Clin Endocrinol Metab, 89, 3721-30.

236. Adams GB, Chabner KT, Alley IR, Olson DP, Szczepiorkowski ZM, Poznansky MC, Kos CH, Pollak MR, Brown EM, Scadden DT. (2006) Stem cell engraftment at the endosteal niche is specified by the calcium-sensing receptor. Nature, 439, 599-603.

237. Macica CM, Liang G, Lankford KL, Broadus AE. (2006) Induction of parathyroid hormone-related peptide following peripheral nerve injury: role as a modulator of Schwann cell phenotype. Glia, 53, 637-48.

238. Ono T, Inokuchi K, Ogura A, Ikawa Y, Kudo Y, Kawashima S. (1997) Activity-dependent expression of parathyroid hormone-related protein (PTHrP) in rat cerebellar granule neurons. Requirement of PTHrP for the activity-dependent survival of granule neurons. J Biol Chem, 272, 14404-11.

239. Koike T, Tanaka S. (1991) Evidence that nerve growth factor dependence of sympathetic neurons for survival in vitro may be determined by levels of cytoplasmic free Ca^{2+}. Proc Natl Acad Sci U S A, 88, 3892-6.

240. Lin KI, Chattopadhyay N, Bai M, Alvarez R, Dang CV, Baraban JM, Brown EM, Ratan RR. (1998) Elevated extracellular calcium can prevent apoptosis via the calcium-sensing receptor. Biochem Biophys Res Commun, 249, 325-31.

241. Carter BD, Kaltschmidt C, Kaltschmidt B, Offenhauser N, Bohm-Matthaei R, Baeuerle PA, Barde YA. (1996) Selective activation of NF-kappa B by nerve growth factor through the neurotrophin receptor p75. Science, 272, 542-5.

242. Wang R, Xu C, Zhao W, Zhang J, Cao K, Yang B, Wu L. (2003) Calcium and polyamine regulated calcium-sensing receptors in cardiac tissues. Eur J Biochem, 270, 2680-8.

243. Chen PS, Chen LS, Cao JM, Sharifi B, Karagueuzian HS, Fishbein MC. (2001) Sympathetic nerve sprouting, electrical remodeling and the mechanisms of sudden cardiac death. Cardiovasc Res, 50, 409-16.

244. Aida K, Koishi S, Inoue M, Nakazato M, Tawata M, Onaya T. (1995) Familial hypocalciuric hypercalcemia associated with mutation in the human $Ca^{(2+)}$-sensing receptor gene. J Clin Endocrinol Metab, 80, 2594-8.

245. Chikatsu N, Fukumoto S, Suzawa M, Tanaka Y, Takeuchi Y, Takeda S, Tamura Y, Matsumoto T, Fujita T. (1999) An adult patient with severe hypercalcaemia and hypocalciuria due to a novel homozygous inactivating mutation of calcium-sensing receptor. Clin Endocrinol (Oxf), 50, 537-43.

246. Cole D, Forsythe CR, Dooley JM, Grantmyre EB, Salisbury SR. (1990) Primary neonatal hyperparathyroidism: a devastating neurodevelopmental disorder if left untreated. J Craniofac Genet Dev Biol, 10, 205-14.

APPENDICES

APPENDIX 1

Tris-Acetate EDTA (TAE) Buffer (20X)

96.8g Tris

14.8g EDTA.$2H_2O$

32.8g Sodium Acetate

34ml Acetic Acid

to 1L with dH_2O and pH 7.8-7.9

Poly-ornithine Solution

9.2g boric acid (Sigma) was dissolved in 1L dH_2O and adjusted to pH 8.4 with NaOH. 500mg poly-DL-ornithine hydrobromide (Sigma) was dissolved in the borate solution and filter sterilised using a 0.2µm Acrocap filter unit (Pall Corporation). The poly-ornithine solution was stored in two 500ml bottles at 4°C for up to 2 weeks.

Albumax I

20g Albumax I (Gibco, Invitrogen) was slowly dissolved in 100ml cell culture grade dH_2O (Gibco, Invitrogen) over 45mins to 1hr. To this the following was added:-

Amount to add	Reagent	Stock Solution
160mg	Putrescine (Sigma)	
1ml	Progesterone (Sigma)	0.625mg.ml^{-1} in ethanol
10ml	L-thyroxine (Sigma)	0.4mg.ml^{-1} in ethanol
10ml	Sodium selenite (Sigma)	0.4mg.ml^{-1} in PBS
10ml	Tri-Iodothyronine (Sigma)	0.34mg.ml^{-1} in ethanol

Table 7: Reagents required to supplement the albumax I solution.

The albumax solution was then aliquoted into 5.5ml volumes and stored at -20°C.

Trypsin

50mg Trypsin (Worthington) was dissolved in 5ml Ca^{2+}/Mg^{2+} free PBS (Gibco, Invitrogen), filter sterilised and stored as 50µl aliquots at -20°C.

Siliconised Pipettes

Glass Pasteur pipettes (Fisher Scientific) were placed in a large beaker which was filled with dH_2O upto ¾ length of the pipettes and left for 2mins. The dH_2O was removed and replaced with dichlorodimethylsaline (BDH) and left for 30mins. The pipettes were then washed 5 times with dH_2O, a further 2 times with sterile PBS then placed in pipette boxes and autoclaved.

APPENDIX 2

Scan Mode	Plane, multitrack, 8 bit
Stack size	512 x 512, 230.3μm x 230.3μm
Scaling	0.45μm x 0.45μm
Position	X: 0.0μm Y:-52.1μm Z: 0.0μm
Pixel time	2.56μs
Objective	40X/0.75 W Ph2
Beam splitters	MBS: HFT 488/543, DBS1: NFT 545, DBS2: mirror, DB3: plate
Wavelength	T1: 543nm, 100% T2: 488nm, 4%
Filters	Ch1-1: LP 560, Ch2-2: BP500-550 IR
Pinhole	Ch1-1: 78μm, Ch2-2: 317μm

Table 8: Leica LSM510 confocal microscope settings used in the immunodetection of CaR in E18 SCG neurons.

APPENDIX 3

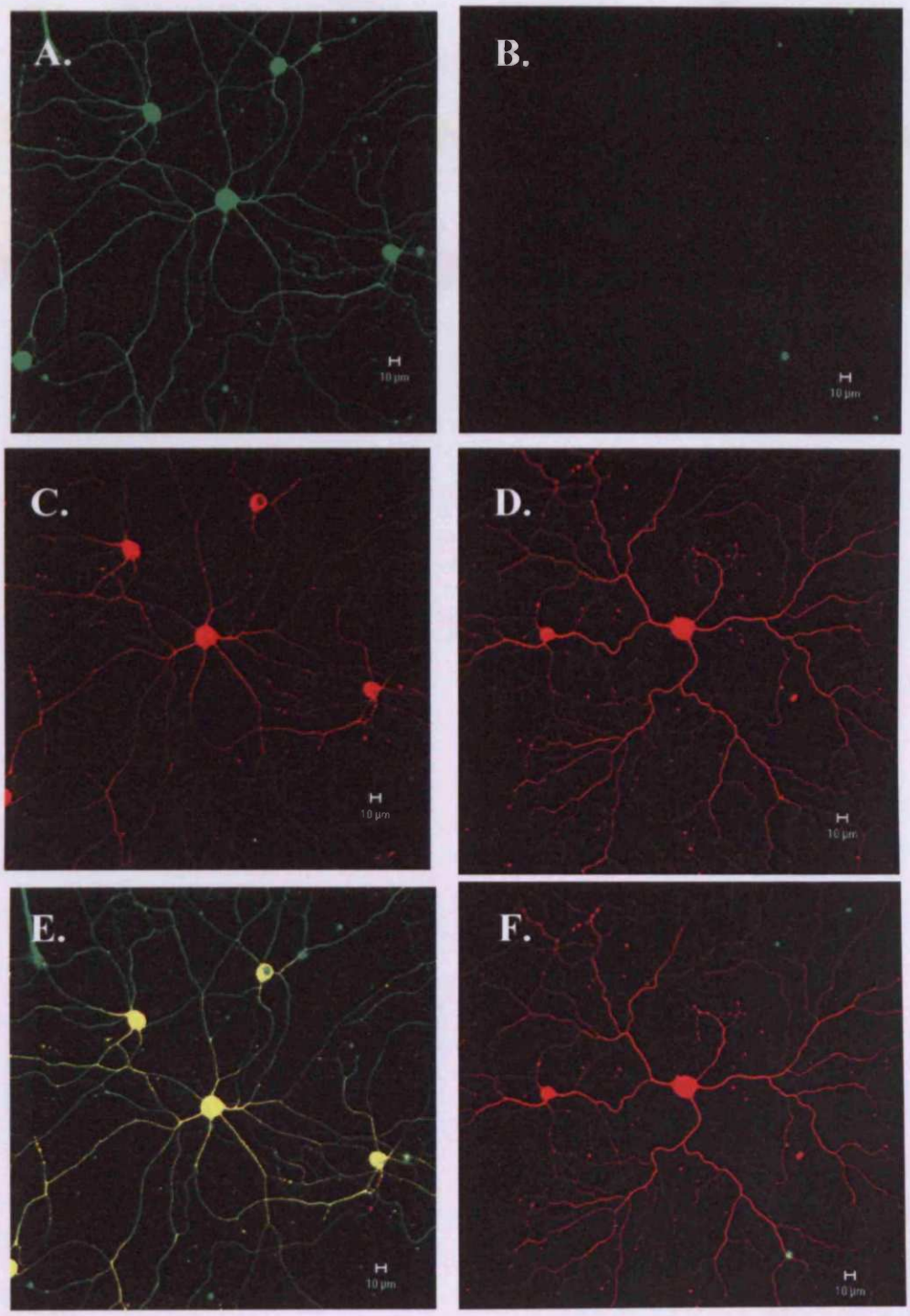

Figure 59: CaR Immunolocalisation in Dissociated E18 SCG Neurons. E18 SCG neurons were dissociated and cultured in 4 well dishes in the presence of 0.4ng.ml^{-1} NGF using F-14 medium at the standard $[Ca^{2+}]_o$ (1.4mM) for 24hrs. **A.** Anti-CaR polyclonal antibody (Imgenex; IMG-71168) raised to the CaR N-terminus, **B.** Negative control (anti-CaR antibody omitted), **C.** and **D.** β-III tubulin, **E.** and **F.** Merge.